MANDELATE RACEMASE: INSIGHTS INTO SUBSTRATE TOLERANCE, NOVEL INHIBITOR-BINDING MODES, AND THE ROLE OF BINDING DETERMINANTS

by

Mitesh Nagar

Submitted in partial fulfilment of the requirements
for the degree of Doctor of Philosophy

at

Dalhousie University
Halifax, Nova Scotia
June 2015

TABLE OF CONTENTS

LIST OF SCHEMES

LIST OF FIGURES

LIST OF TABLES

ABSTRACT

Mandelate racemase (MR) is a useful model for studying the enzyme-catalyzed abstraction of an α-proton from carbon acid substrates with high pK_a values. MR, an archetype of enolase superfamily, uses the Brønsted acid-base catalysts Lys 166 and His 297 in a two-base mechanism to catalyze the interconversion of the enantiomers of mandelic acid via an *aci*-carboxylate (enolate) intermediate.

Based on the broad substrate spectrum of MR, it has been proposed that β,γ-unsaturation is a requisite feature of substrates. However, this thesis shows that MR can catalyze the interconversion of enantiomers of trifluorolactate with the chemical step being fully rate-limiting, suggesting that the presence of electron withdrawing groups such as the trifluoromethyl group on the α-carbon can stabilize the enolic intermediate through inductive effects. Thus, β,γ-unsaturation is not an absolute requirement for MR catalysis.

A rather surprising finding was that the substrate-product analogue of trifluorolactate, 3,3,3-trifluoro-2-hydroxy-2-(trifluoromethyl)-propanoate (TFHTP), bound to MR with an affinity similar to that observed for transition state (TS) analogue inhibitors. Based on the x-ray crystal structure of the MR–TFHTP complex, the high binding affinity of TFHTP could be partly attributed to a novel binding-mode in which the carboxylate is involved in a salt-bridge with Lys 166 and His 297. Tartronate and mesoxalate were identified as reversible competitive inhibitors, which also form similar salt bridges, and 3-hydroxypyruvate acted as an irreversible, time-dependent inhibitor that undergoes Schiff-base formation with Lys 166 to form an aldehyde/enol(ate) adduct. Such an unprecedented reaction catalyzed by MR suggests a possible mechanistic link between the metal-dependent enolase superfamily and other α/β-barrel enzymes utilizing Schiff-base chemistry.

The x-ray crystal structure of the MR-benzohydroxamate (BzH) complex suggested that Lys 166, His 297, and Tyr 54 play a role in BzH binding, and may afford TS stabilization. Tyr 54 mutants revealed that the role of Tyr 54 is relatively minor; however, isothermal titration calorimetry studies with the Lys 166- and/or His 297-MR mutants revealed that the Brønsted acid-base catalysts, especially Lys 166, interact with the hydroxamate moiety as well as the phenyl ring of BzH, possibly via cation-π/NH-π interactions. The work presented in this thesis suggests that the Brønsted acid-base catalysts can act as binding determinants and stabilize the enolate moiety of the altered substrate in the TS, a role that was previously overlooked.

LIST OF ABBREVIATIONS USED

ATCC	American type culture collection
BSA	bovine serum albumin
BzH	benzohydroxamate
BzF	benzoylformate
CoA	coenzyme A
CD	circular dichroism
CHCHA	cyclohexanecarbohydroxamic acid
CHES	*N*-cyclohexyl-2-aminoethanesulfonic acid
CHAPS	3-[(3-cholamidopropyl)dimethylammonio]-1-propanesulfonate
CfN	cupferron
DCPIP	2,6-dicholophenolindophenol
DHDPS	dihydrodipicolinate synthase
dmMR	double mutant mandelate racemase
DTT	dithiothreitol
E.C.	enzyme commission number
EDTA	ethylenediaminetetraacetic acid
ESI	electron spray ionization
3-FP	3-fluoropyruvate
FPLC	fast protein liquid chromatography
α-HIB	α-hydroxyisobutyrate
HEPES	4-(2-hydroxyethyl)-1-piperazineethanesulfonic acid
1-HEP	1-hydroxyethylphosphonate
3-HP	3-hydroxypyruvate
HPLC	high-performance liquid chromatography
IEF	isoelectric focusing
IPTG	isopropyl β-D-1-thiogalactopyranoside
ITC	isothermal titration calorimetry
KIE	kinetic isotope effect
LB	lysogeny broth

LC-MS	liquid chromatography-mass spectrometry
MES	2-(*N*-morpholino)ethanesulfonic acid
MLE	muconoate lactonizing enzyme
MS	mass spectrometry
Mox	mesoxalate
MOPS	3-morpholinopropane-1-sulfonic acid
MR	mandelate racemase
Mw	molecular weight
NAL	*N*-acetylneuraminate lyase
NMR	nuclear magnetic resonance
OD	optical density
OSBS	*o*-succinylbenzoate synthase
PAGE	polyacrylamide gel
PIPES	piperazine-*N*,*N*'-bis[2-ethanesulfonic acid]
Pyr	pyruvate
(*R*)-α-PGH	(*R*)-α-phenylgycidate
(*R*)-atro	(*R*)-atrolactate
(*R*)-man	(*R*)-mandelate
(*S*)-atro	(*S*)-atrolactate
SCOP	structural classification of proteins
SDS	sodium dodecyl sulfate
SHCHC	2-succinyl-6-hydroxy-2,4-cyclohexadiene-1-carboxylate
SSHB	short, strong hydrogen-bonds
TAPS	3-[[1,3-dihydroxy-2-(hydroxymethyl)propan-2-yl]amino]propane-1-sulfonic acid
TFHEP	2,2,2-trifluoro-1-hydroxyethylphosphonate
TFHTP	3,3,3-trifluoro-2-hydroxy-2-(trifluoro-methyl)propanoate
TFL	trifluorolactate
TIM	triosephosphate isomerase
TOF	time of flight
tmMR	triple mutant mandelate racemase

TS	transition state
UV	ultra-violet
wt	wild-type

ACKNOWLEDGEMENTS

Great teacher, insightful PI, and a supportive mentor – yes, I can relate these qualities to my supervisor Dr. Stephen L. Bearne. It has been my privilege to work with him, and I thank Dr. Bearne for providing me with the opportunity to watch and learn a lot from his knowledge and experience. His passion for research has been an inspiration for me since the day I joined his lab. Dr. Bearne's contributions towards my thesis are not just intellectual, he also contributed through his lab work by synthesizing one of the compounds that I used in my studies. He has been always encouraging me and pushing me to develop into a better researcher. Special thanks to him for being very patient during the thesis writing, and for helping me in rectifying lab-related or other issues with his critical advice.

I would also like to thank my thesis committee members: Dr. Jan Rainey, Dr. Carmichael Wallace, and Dr. Ray Syvitski for sharing their time and expertise over the past few years. I am also thankful to Dr. David Jakeman who agreed to serve on my committee when Dr. Syvitski was not available. I would like thanking Dr. Martin St. Maurice and his graduate students Adam Lietzan and Britney Wyatt from Department of Biological Sciences, Marquette University, USA, for solving mandelate racemase x-ray crystal structures with various ligands that supported my studies and without which my conclusions would not have been complete. I would like to acknowledge expert-assistance from Dr. Nadine Merkley at the National Research Council, Halifax, for the NMR experiments and from Dr. Alejandro Cohen of the Proteomic and Mass Spectrometry Core Facility, Dalhousie University, Halifax, for conducting mass spectrometry experiments and aiding in the data analysis. I would also like to thank co-authors of my publications for their contributions, especially Dr. Ariun Narmandakh who did the ground work for trifluorolactate story.

I would like to acknowledge and thank Dr. Bearne and the funding sources of the Bearne lab (especially NSERC) for the financial support during my thesis work. In addition, I would also like to thank the Department of Biochemistry and Molecular Biology for covering my international differential fee, and for additional funding through teaching assistantships.

Now that I mentioned being a teaching assistant (TA), I must thank Paul and Heidi who work hard conducting the undergraduate labs and make a TA's life much easier. I would also like to extend my thanks to the department's office staff: Roisin, Melissa, and Barb for their continuous assistance in administrative as well as non-administrative matters. Roisin is very special to me and will always be; so thank you for taking good care of me.

I would also like to thank present and past members of the Bearne Lab for their help and thoughtful discussions during group meetings: Sander, Craig, Yuriy, Mandar, Matt, Greg, Sarah, Mohan, and Palash. I wish to thank friends in Halifax, who made sure that I didn't miss my family and friends from India: Hiren, Arun, Aditya, Jay, and families of Gerard and Naval.

Lastly, I would like to take this opportunity to thank my high school buddies and extended family for their constant encouragement during my thesis work. I am grateful to my parents for their continuous unconditional love and support. I am indebted to my brother, Nivedan, who has sacrificed a lot for me. Special thanks to my wife Jyoti; I am lucky to have her in my life. She has been very patient, understanding, and has always stood by me to make my graduate-school journey easier.

CHAPTER 1

INTRODUCTION

1.1 MANDELATE RACEMASE

Mandelate racemase (MR, E.C. 5.1.2.2) from *Pseudomonas putida* A.3.12 (ATCC 12633) is a member of the enolase superfamily and catalyzes Mg^{2+}-dependent 1,1-proton transfer that interconverts enantiomers of mandelate **(Scheme 1.1)** with similar kinetic parameters for both substrate enantiomers.

1.1.1 Expression and Characterization of MR

Mandelic acid (phenylglycolic acid or 2-phenyl-2-hydroxyacetic acid) is an α-hydroxycarboxylic acid of plant origin (Bhat & Vaidyanathan, 1976). Both enantiomers (*R*)- and (*S*)-mandelate occur in nature. A variety of microorganisms including bacteria (both Gram positive and negative), yeast, and *Aspergillus niger* can utilize mandelic acid as a sole source of carbon (Bhat & Vaidyanathan, 1976; Hegeman *et al*., 1970). Most of these microorganisms can utilize only (*R*)-mandelate or (*S*)-mandelate as a carbon source due to the presence of either an (*R*)- or (*S*)-stereospecific mandelate dehydrogenase. Others that can use both enantiomers of mandelate contain both (*R*)- and (*S*)-stereospecific mandelate dehydrogenases. The only known exception is *Pseudomonas putida* A.3.12 (ATCC 12633), in which Gunsalus and coworkers identified the metabolic pathway responsible for mandelic acid catabolism and showed that this organism can utilize both enantiomers of mandelate despite having only an (*S*)-stereospecific mandelate dehydrogenase. This unique ability to utilize both enantiomers of mandelate in absence of

Scheme 1.1 Reaction catalyzed by mandelate racemase (MR)

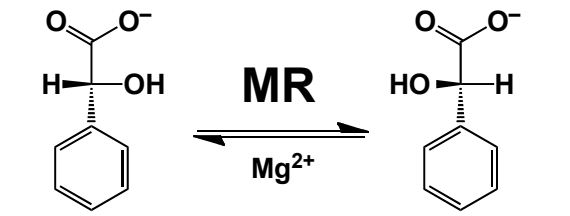

(*R*)-mandelate (*S*)-mandelate

an (*R*)-stereospecific mandelate dehydrogenase is due to the presence of a racemase that interconverts the (*R*)- and (*S*)-enantiomers of mandelate (Gunsalus *et al*., 1953a; Gunsalus *et al*., 1953b; Stanier *et al*., 1953). *Pseudomonas putida* A.3.12 (ATCC 12633) catabolizes mandelate via a pathway containing at least 11 inducible enzymes **(Figure 1.1)** (Hegeman *et al*., 1970). The enzymes of this pathway are divided into two groups: the mandelate group and the β-ketoadipate group. The mandelate group of enzymes converts mandelate to benzoate (Gunsalus *et al*., 1953a; Gunsalus *et al*., 1953b; Stanier *et al*., 1953), and the β-ketoadipate group of enzymes subsequently metabolize benzoate to succinate and acetyl-CoA (Ornston, 1971; Reiner, 1971; Reiner & Hegeman, 1971). These end products then enter the Krebs cycle to generate energy for cellular metabolism.

Genes encoding the mandelate group of enzymes constitute an operon that can be induced equally by any of the first three compounds of the catabolic pathway, i.e., (*R*)-mandelate, (*S*)-mandelate, and benzoylformate (Hegeman, 1966a). According to Hegeman, analogues of these compounds should have certain features to be an inducer of expression of the mandelate group of enzymes. First, the aromatic ring of an analogue should be a phenyl ring or substituted phenyl ring, e.g., *p*-chloro, *p*-bromo, *m*- and *p*-hydroxymandelate are found to be inducers; heteroaryl analogues of mandelate having pyridine and thiophene rings do not induce. Second, a carboxyl group is important, as mandelate or benzoylformate analogues with a carboxyl replaced by methyl or hydroxymethyl do not induce enzyme expression. And third, compounds should have an electronegative functional group on the α-carbon such as hydroxyl (e.g., mandelate), carbonyl (e.g., benzoylformate), thioether (e.g., phenylthioacetate), or an ether (e.g., phenoxyacetate) to cause induction.

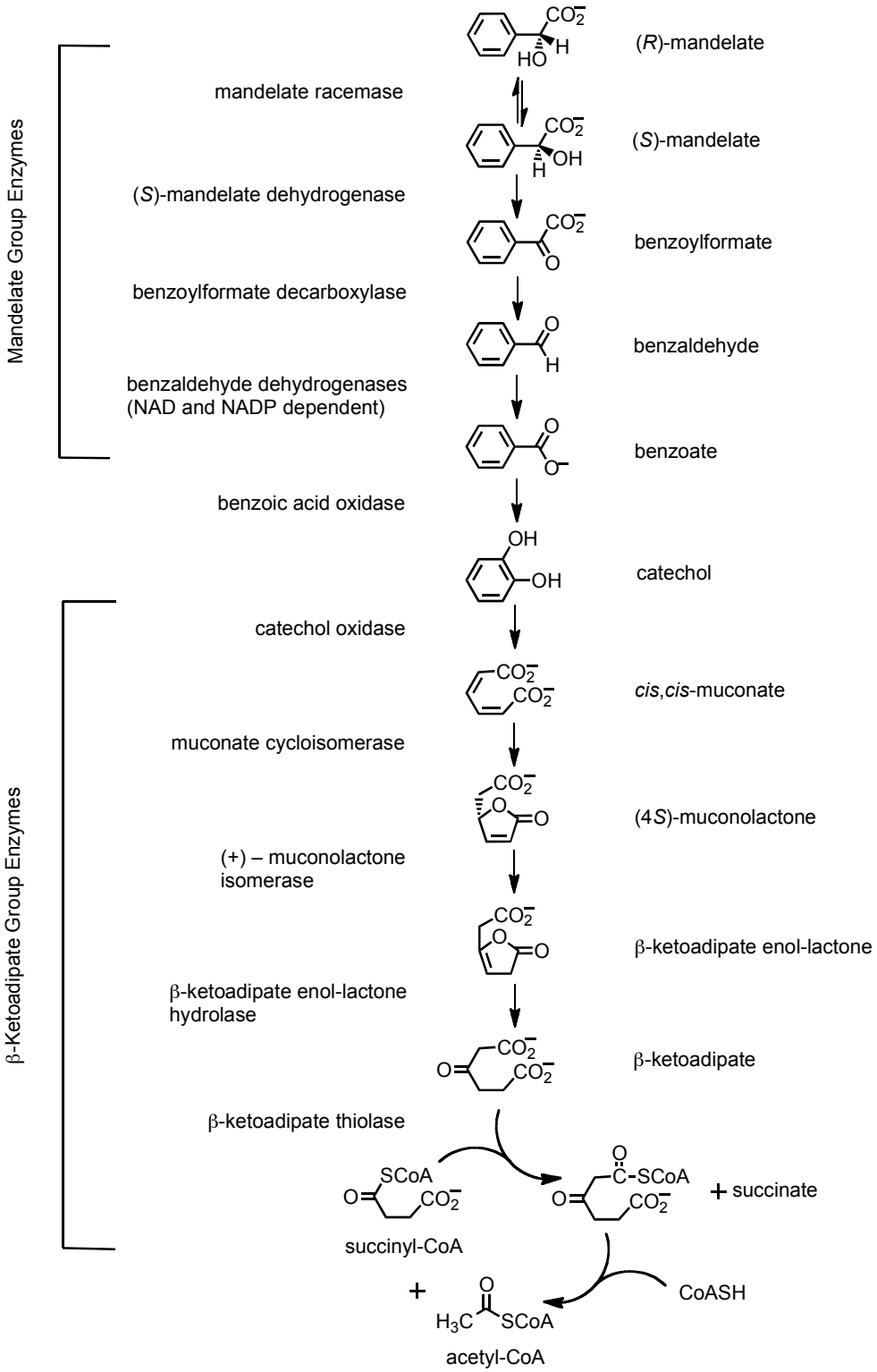

Figure 1.1 Catabolic pathway of (*R*)- and (*S*)-mandelic acid in *Pseudomonas putida* A.13.12 (adapted from Hegeman *et al*., 1970)

The mandelate operon is among the earliest described operons (Hegeman, 1966b). Genetic experiments by Wheelis and Stainer showed that the genes of mandelate pathway operon are linked and closely clustered on the bacterial chromosome (Wheelis & Stanier, 1970), but no further work on the operon structure was conducted over the next two decades. In the late 1980s, however, cloning and sequencing revealed that the gene encoding MR, from *P. putida*, is located immediately downstream of the promoter and is the first gene in the mandelate operon (Ransom *et al*., 1988). Later, it was found that the genes encoding MR (*mdlA*), mandelate dehydrogenase (*mdlB*), and benzoylformate decarboxylase (*mdlC*) lie on a single 10.5 kb restriction fragment and are arranged in an operon (Tsou *et al*., 1990).

Using a crude preparation from *P. putida*, Gunsalas *et al*. (1953a) were the first to characterize MR showing that the enzyme was soluble and does not require any cofactor for activity. Weil-Malherbe (1966) assayed partially purified MR using a coupled assay with L-mandelate dehydrogenase to determine the rates of racemization for the D- and L-enantiomers of mandelate (i.e., (*R*)-mandelate or (*S*)-mandelate, respectively). Weil-Malherbe showed that the optimum pH for MR activity is ~7.8 and that Mg^{2+} acts as an activator (Weil-Malherbe, 1966). Studies conducted by Fee *et al*. (1974) suggested that the divalent metal ion is an absolute requirement for MR activity, and that the activity of demetalized MR can be restored by various divalent metal ions such as Mg^{2+}, Co^{2+}, Ni^{2+}, Mn^{2+}, and Fe^{2+}, with Mg^{2+} being the most effective activator. The order of addition of mandelate and Mg^{2+} made a difference in the time needed for reactivation of the enzyme, indicating that free Mg^{2+}, rather than an Mg^{2+}–mandelate complex reactivates the enzyme (Fee *et al*., 1974). Hegeman *et al*. (1970) purified MR from *P. putida* to homogeneity and

confirmed the properties of MR previously determined using either crude or partially purified preparations. In addition, Hammett plot analysis ($\rho = +2$) of the kinetic data with *para*-substituted mandelic acid analogues bearing either electron donating or electron withdrawing groups indicated the involvement of a carbanion intermediate in the reaction mechanism of MR (Hegeman *et al*., 1970). In a parallel study, Kenyon and Hegeman (1970) examined the MR-catalyzed exchange between the solvent and the α-deuterated substrate, and reported a significant primary kinetic isotope effect ($V_H/V_D = 5.1–5.6$) that was consistent with the cleavage of the α-carbon–hydrogen bond to generate an intermediate. The possibility of a carbonium ion intermediate was ruled out due to the absence of MR-catalyzed exchange of ^{18}O from 55% ^{18}O-enriched water into mandelic acid (Kenyon & Hegeman, 1970). Overall, these studies suggested that α-carbon–hydrogen bond cleavage occurs to form a carbanion intermediate and stabilization of the negative charge on α-carbon in the transition state favors the MR-catalyzed racemization reaction. Kenyon and Hegeman (1970) also showed that MR is capable of acting on both the substrate enantiomers with almost equal efficiency (i.e., $k_{cat}^{R\rightarrow S} \approx k_{cat}^{S\rightarrow R}$, $K_m^{S\rightarrow R} \approx K_m^{S\rightarrow R}$; and for MR $K_m \approx K_S$ (Fee *et al*., 1974; Maggio *et al*., 1975; St. Maurice & Bearne, 2002)).

1.1.2 Mechanism of the Reaction Catalyzed by MR

Hegeman *et al*. proposed that the cleavage of the α-carbon-hydrogen bond occurs during the course of racemization to generate a carbanion intermediate. The question was, how precisely does the inversion of configuration occur? Two mechanisms have been proposed for the enzyme-catalyzed hydrogen transfer without the assistance of a

coenzyme: a one-base mechanism and a two-base mechanism (Cardinale & Abeles, 1968; Rose, 1966). In the one-base mechanism, an enzymatic Brønsted base (proton acceptor) abstracts the α-hydrogen from a substrate generating a carbanion and then the conjugate Brønsted acid reprotonates either face of this intermediate in a stereo-random fashion to yield either the substrate enantiomer or the product enantiomer. Cardinale and Abeles (1968) suggested that during a one-base mechanism, either the enzymatic Brønsted base should be flexible enough to interact with the α-hydrogen of both enantiomers or it must change position relative to the hydrogen acceptor during the course of racemization. In the case of the alternative two-base mechanism, two enantiospecific Brønsted bases (proton acceptors) are located on either face of the chiral center. One base abstracts the α-proton from the substrate enantiomer to generate an intermediate, and the conjugate acid of the second base protonates the intermediate from opposite side to generate the product enantiomer. The roles of these Brønsted bases are reversed when the reaction occurs in the opposite direction (Cardinale & Abeles, 1968; Rose, 1966).

These two mechanisms can be distinguished on the basis of the extent of substrate-derived proton exchange with solvent (Rose, 1966). In the one-base mechanism, there is a substantial amount of 'internal return' (product enantiomer retains the substrate derived proton) or in the case when there is a negligible amount of internal return, the ratio of the rates of solvent exchange into product and substrate is same, regardless of which enantiomer is used as the substrate (Cardinale & Abeles, 1968; Rose, 1966). However, in the two-base mechanism, there is minimal 'internal return' because the base that protonates the intermediate to form the product usually rapidly exchanges its proton with the solvent. In addition, if the bases are monoprotic and the exchange of the

substrate derived proton at the stage of the intermediate is minimal, little or no solvent deuterium should appear in the remaining substrate pool, regardless of substrate chirality (Cardinale & Abeles, 1968; Rose, 1966).

Isotope exchange experiments by Sharp *et al*. (1977) provided additional insight into the mechanism of MR. The absence of MR-catalyzed intermolecular proton transfer indicated a one-base mechanism (Sharp *et al*., 1977), which was later supported by studies conducted by other investigators (Kenyon & Hegeman, 1979; Whitman *et al*., 1985). However, the limitations of these experiments to distinguish between a one-base mechanism and a two-base mechanism in which there is rapid and direct proton transfer between two acceptors led Powers *et al*. (1991) to reinvestigate the mechanism. They used high resolution gas-chromatography/mass-spectrometry to examine the deuterium/hydrogen exchange of the α-hydrogen at early time-points during MR-catalyzed racemization of (*R*)- and (*S*)-[α-^{1}H]mandelate in D_2O. The α-proton in the product was found to be solvent derived regardless of the direction of the reaction, indicating a two-base mechanism. Solvent exchange was also studied in the remaining substrate pools. In the (*R*)→(*S*) direction, a lack of solvent exchange in the remaining (*R*)-mandelate indicated a monoprotic (*R*)-specific base, but in the (*S*)→(*R*) direction significant solvent exchange occurred in the remaining (*S*)-mandelate consistent with a polyprotic (*S*)-specific base. In order to avoid a false positive result arising from the internal return of a proton (one-base mechanism) due to contamination by H_2O in D_2O, analogous experiments were conducted with (*R*)- and (*S*)-[α-^{2}H]mandelate in H_2O where the substrate constituted the sole source of deuterium (Powers *et al*., 1991). Results from these experiments provided compelling kinetic evidence for a two-base mechanism

Scheme 1.2 Two-base mechanism of MR-catalyzed reaction

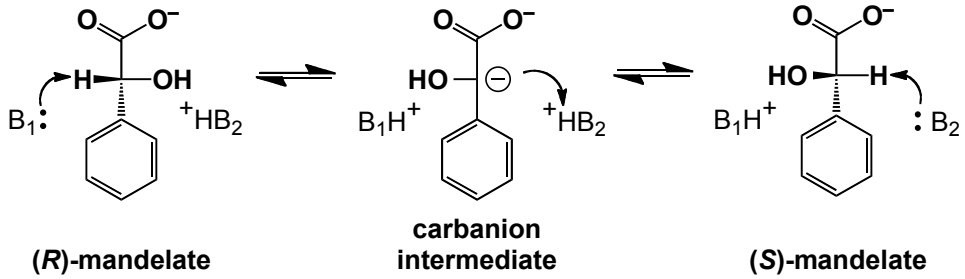

(Scheme 1.2). Although mechanistic studies of the MR-catalyzed reaction strongly suggested formation of carbanion intermediate (Hegeman *et al*., 1970; Kallarakal *et al*., 1995; Kenyon & Hegeman, 1970; Landro *et al*., 1991; Lin *et al*., 1988; Neidhart *et al*., 1991), the existence/stability of such a high energy species during an enzymatic reaction is questionable (Thibblin & Jencks, 1979). Thibblin and Jencks suggested that, in order to catalyze difficult reactions such as proton abstraction from carbon acids, an enzyme should either stabilize the carbanion intermediate generated via a stepwise mechanism or avoid its formation via a concerted mechanism.

Studies with the H297N mutant (one of the active site bases – see section 1.1.5) of MR provided convincing evidence for a step-wise mechanism (Landro *et al*., 1991). Interestingly, the H297N mutant had no detectable racemization activity with either of the substrate enantiomers, but it catalyzed the stereospecific elimination of bromide from racemic *p*-(bromomethyl)mandelate yielding *p*-(methyl)benzoylformate **(Scheme 1.3)**, and the exchange of the α-proton of (*S*)-mandelate in D_2O at rate nearly identical to that measured for the wild-type enzyme (Landro *et al*., 1991). Both of these studies are consistent with the formation of an intermediate during the H297N-MR-catalyzed reaction and the exchange of the α-proton of (*S*)-mandelate suggests that the intermediate was stabilized for long enough to allow time for rotation about the $^{\varepsilon}C$–$^{\zeta}N$ bond of the polyprotic conjugate acid of the (*S*)-specific Brønsted base. Therefore, MR catalyzes the racemization of (*R*)- and (*S*)-mandelate using a two-base mechanism in a stepwise manner, in which an enantiospecific base abstracts the α-proton from a single enantiomer to generate a carbanion intermediate that is protonated by the conjugate acid of either Brønsted base to generate either the product or regenerate the substrate.

Scheme 1.3 MR-catalyzed elimination of bromide from *p*-(bromomethyl)mandelate

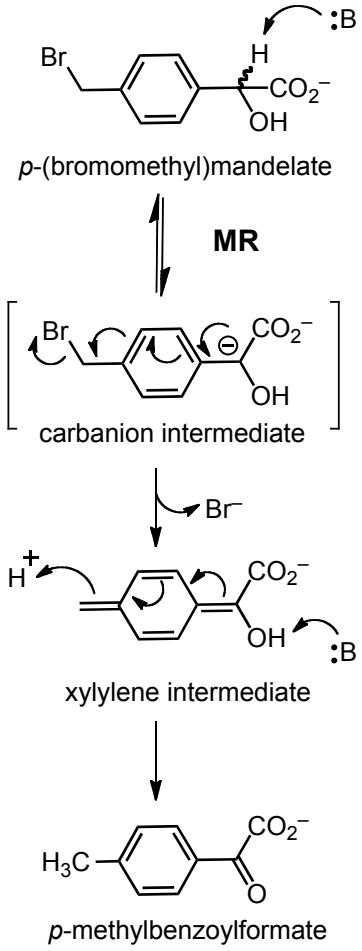

1.1.3 The Structure of MR

Initial characterization of MR from *Pseudomonas putida* A.3.12 (ATCC 12633) using SDS-PAGE revealed a subunit molecular mass of approximately 69 500 Da (Fee *et al*., 1974). Cross-linking studies with dimethyl suberimidate showed that the quaternary structure of MR is composed of four identical subunits with a total molecular mass of approximately 280 000 Da (Fee *et al*., 1974). Later, SDS-PAGE using a highly purified enzyme, obtained after the cloning and over-expression of the gene encoding MR in *E. coli*, showed a subunit molecular weight of 41 000 Da that differed significantly from the earlier results (Ransom *et al*., 1988). In agreement with this observation, a molecular weight of 38 570 Da was reported based on the amino acid sequence (359 amino acid residues) deduced from the DNA sequence (Tsou *et al*., 1989), suggesting that the 280 kDa species observed by Fee *et al*. was likely an octamer.

Development of a high-yield expression system and purification procedure for MR enabled Neidhart *et al*. to grow the first crystals of MR for x-ray crystallographic studies (Neidhart *et al*., 1988). The first x-ray crystal structure of MR, solved at 2.5-Å resolution, revealed that the quaternary structure is a tightly packed octamer with identical subunits (Neidhart *et al*., 1991). This octameric structure is described as a 'tetramer of dimers' based on the high intimacy of the interface between two-fold related subunits compared to the four-fold interface, and the observation that the active site includes residues from two-fold related subunits (functional dimer) (Neidhart *et al*., 1991). The high intimacy between the two-fold related subunits could be attributed to the interaction of an interdigitating loop (residues 88-95) with the adjoining monomer in such a way that the tip of the loop, i.e., Leu 93, forms a part of the hydrophobic pocket within

the active site of the adjacent monomer **(Figure 1.2 A)**. This tight association of subunits in a dimer may explain the discrepancy in the subunit molecular weights reported by Fee *et al*. (1974).

The MR monomer is composed of three distinct domains: the N-terminal domain (residues 5–126), the central domain (residues 134–319), and a smaller C-terminal domain (residues 331–359) **(Figure 1.2 B)** (Neidhart *et al*., 1991). The N-terminal domain, also known as the capping domain, consists of a three-stranded antiparallel β-sheet and an antiparallel four α-helix bundle. The central domain consists of an α/β barrel similar to that of triosephosphate isomerase (α_8/β_8) barrel (i.e., TIM barrel) (Banner *et al*., 1975), with an exception of the missing the eighth α-helix. In MR, a small irregular C-terminal domain composed of extended strands fills the space normally occupied by the eighth α-helix present in other TIM barrel proteins.

1.1.4 Active Site Architecture

The location of the active site was determined from the position of the metal ions europium and manganese in the native structure and the position of electron dense iodine in the structure of MR complexed with *p*-iodomandelate (Neidhart *et al*., 1991). The side chain carboxyl groups of Asp 195, Glu 221, and Glu 247, located at the C-terminal end of the third, fourth, and fifth β-strands of the central domain, ligate the metal ion **(Figure 1.3 A)**. Therefore, like all known parallel α/β barrels, the active site of MR is located at the mouth of β-barrel towards the C-terminal ends of the core β-strands, at the interface of N-terminal domain and the central domain **(Figure 1.2 B & 1.3 A)**. Despite the participation of two subunits forming an active site, as discussed in the previous section,

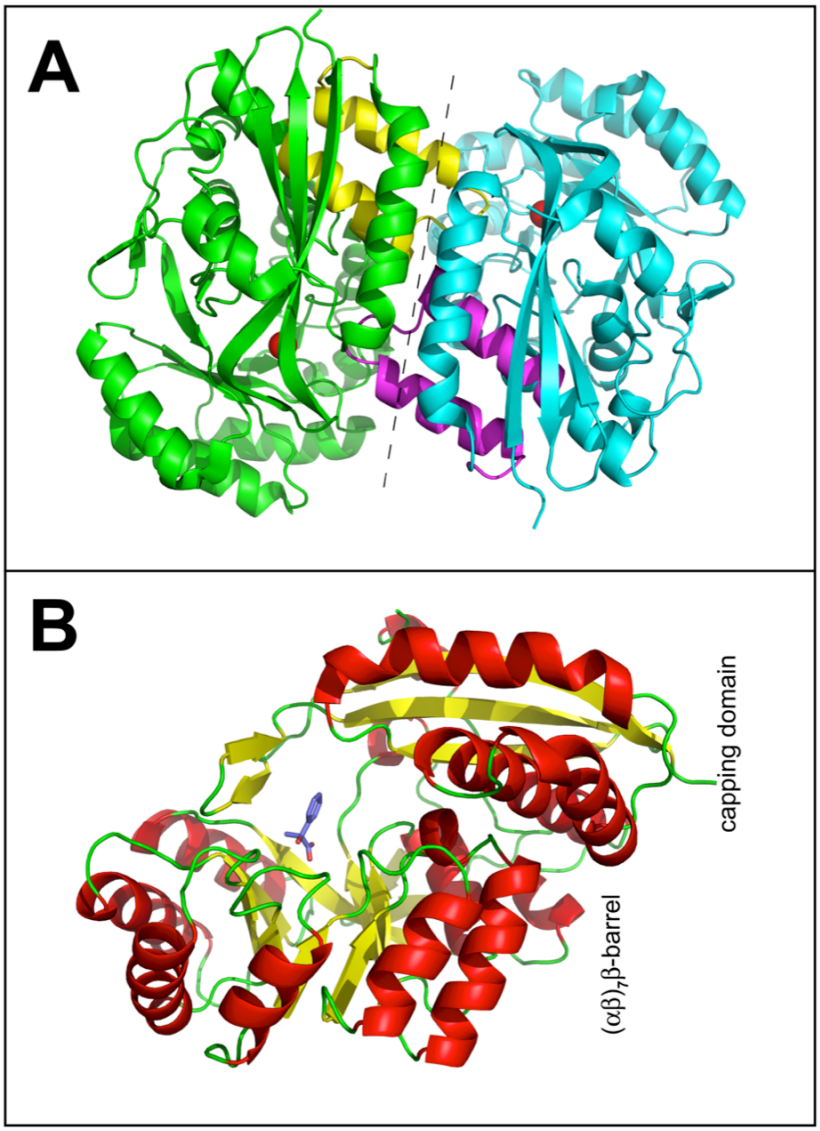

Figure 1.2 X-ray crystal structure of MR. (A) Dimeric structure of MR [PDB entry 3UXK (Lietzan *et al*., 2012)]. Two monomers, green and cyan, interact with each other with inter-digitating loops shown as yellow and magenta. The dimer interface is indicated by a dashed line and Mg^{2+} ions (shown in red) indicate the location of active sites in each monomer. **(B)** Domain structure of the MR monomer [PDB entry 1MDR (Landro *et al*., 1994)]. The location of active site at the mouth of β-barrel is indicated by the bound (*S*)-atrolactate, a subsatrate analogue (shown in purple and as stick representation).

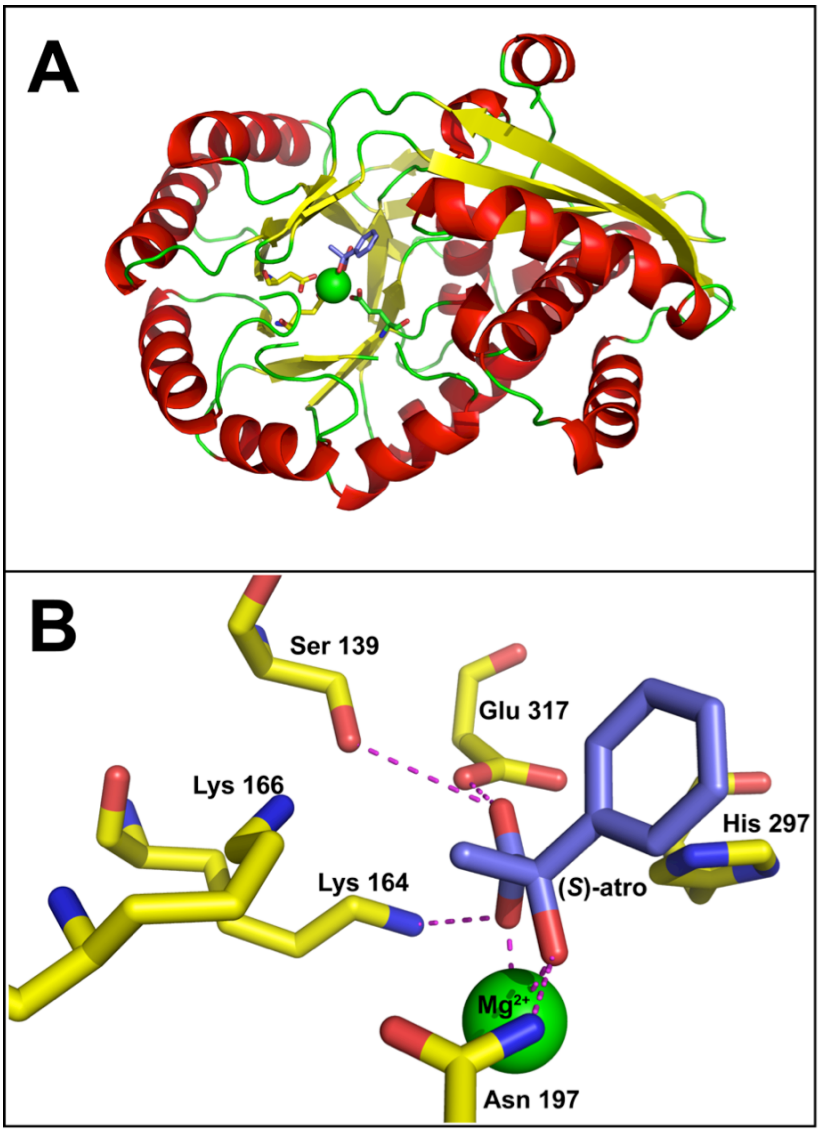

Figure 1.3 Active site architecture of MR with bound (*S*)-atrolactate [PDB entry 1MDR (Landro *et al*., 1994)]. **(A)** Side-chain carboxyls of Asp 195, Glu 221, and Glu 247 hold the essential Mg^{2+} ion (green) in the active site. **(B)** The bound substrate analogue, (*S*)-atrolactate (purple) mimicks the productive orientation of the substrate. Various electrostatic and H-bonding interactions involved in substrate binding as well as in TS stabilization are shown as dashed lines.

there is one independent active sites per monomer. A model of the structure of MR complexed with *p*-iodomandelate permitted identification of the substrate binding site and the residues participating in substrate binding and catalysis (Neidhart *et al*., 1991). The productive orientation of the substrate in the active site has been confirmed by a number of crystal structures of wild-type and mutant MR enzyme complexes with various substrates and inhibitors, e.g., see **Figure 1.3 B** (Kallarakal *et al*., 1995; Landro *et al*., 1994; Mitra *et al*., 1995; Schafer *et al*., 1996). In the productive orientation, the α-hydroxyl group and one of the carboxylate oxygens of the substrate chelate the essential Mg^{2+}, Lys 164 forms a hydrogen bond with the metal-coordinated carboxylate oxygen, and Glu 317 interacts with the other carboxylate oxygen. Based on the accessibility of the α-H of the specific substrate enantiomers, His 297 and Lys 166 were assigned as the (*R*)- and (*S*)-specific bases, respectively (Neidhart *et al*., 1991). These assignments were in agreement with the previously predicted monoprotic and polyprotic nature of the (*R*)-specific and (*S*)-specific bases, respectively (Powers *et al*., 1991). Asn 197 interacts with the α-hydroxyl group of the substrate and Ser 139 forms a hydrogen bond with the oxygen of the carboxylate that interacts with Glu 317 **(Figure 1.3 B)**; both interactions help to stabilize the intermediate in the transition state (Gu & Yu, 2012; St. Maurice & Bearne, 2000). Due to the presence of these multiple electrostatic and/or hydrogen bond interactions between the substrate and the MR active site, it was anticipated that the α-hydroxyl and the carboxylate group of the substrate would remain relatively fixed during the catalysis and that the phenyl ring might move during catalysis (Siddiqi *et al*., 2005).

An important feature of the MR active site is the presence of a large hydrophobic pocket that facilitates binding of phenyl group of the substrate. This hydrophobic pocket

is composed of residues from the N-terminal domain (Leu 18, Val 22, Val 29, Phe 52, and Tyr 54) and the barrel domain (Leu 298, Leu 319, and Leu 321) (Neidhart *et al*., 1991). In addition, the hydrophobic domain also includes residues 19-30 from the mobile flap and Leu 93 from the adjacent subunit. The broad range of substrate specificity exhibited by MR, and tolerance for binding bulky substrates and substrate analogues, suggests that the hydrophobic pocket is flexible and accommodating in nature (Burley & Bearne, 2005; Felfer *et al*., 2001; St. Maurice & Bearne, 2004). This hydrophobic pocket can be divided into two binding pockets, one specific for the phenyl ring of (*R*)-mandelate and the other for the phenyl ring of (*S*)-mandelate (Bourque & Bearne, 2008; Siddiqi *et al*., 2005) **(Figure 1.4 A)**. During catalysis, the phenyl group of (*R*)-mandelate or (*S*)-mandelate is initially bound in its corresponding pocket, but upon proton abstraction by the enantiospecific Brønsted base, the phenyl ring moves through the hydrophobic pocket to form a planar intermediate and comes to rest in the pocket for the product enantiomer (Siddiqi *et al*., 2005). Indeed, structural overlays of crystal structures of MR complexed with benzohydroxamate (a transition state analogue inhibitor) and (*S*)-atrolactate (a ground state analogue inhibitor) revealed that the *para* carbon of the phenyl ring moves ~1.2 Å upon going from the substrate state to the intermediate state, consistent with the proposed motion (Lietzan *et al*., 2012) **(Figure 1.4 B)**.

1.1.5 Brønsted Acid-Base Catalysts: Lys 166 and His 297

Studies by Powers *et al*. (1991) and Neidhart *et al*. (1991) suggested that His 297 and Lys 166 are the two Brønsted acid-base catalysts that abstract the α-proton exclusively from (*R*)-mandelate or (*S*)-mandelate, respectively. But the most definitive

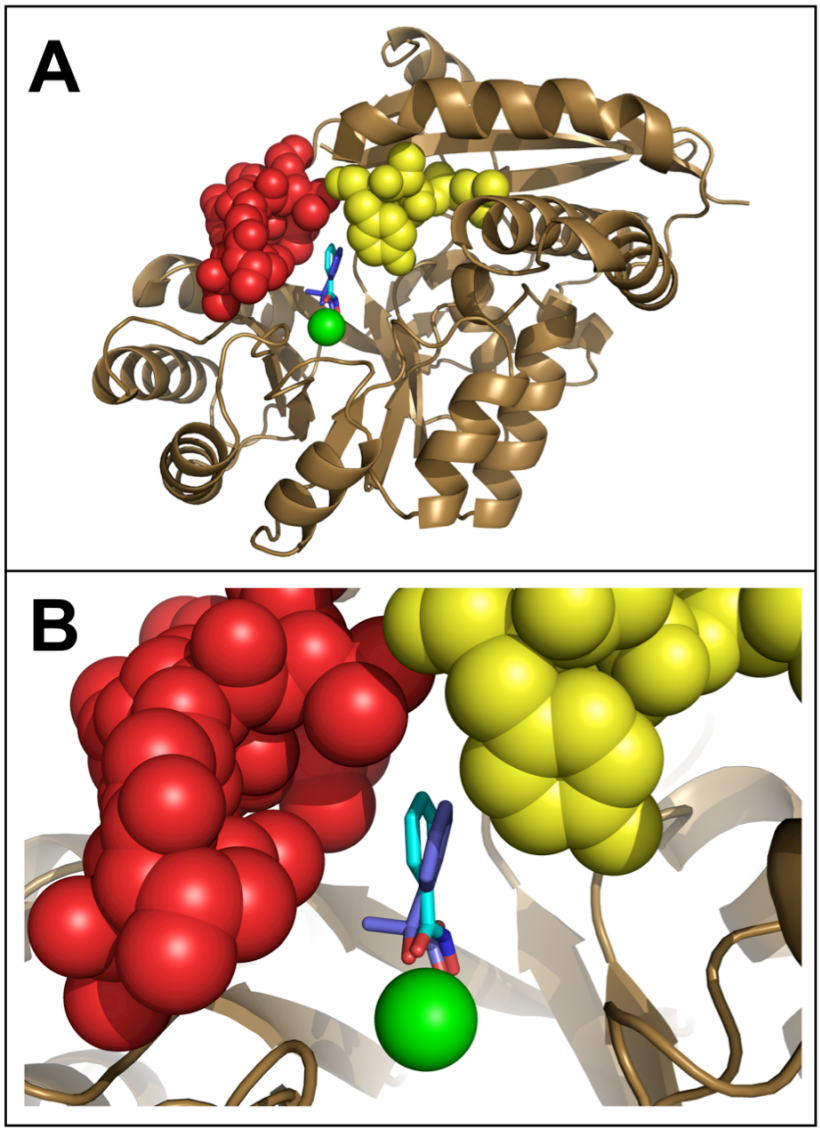

Figure 1.4 Hydrophobic cavity of MR. (A) Residues of the putative *R*-pocket (red) and *S*-pocket (yellow) are shown in space filling representation. The phenyl ring of bound (*S*)-atrolactate [purple; PDB entry 1MDR (Landro *et al*., 1994)], and benzohydroxamate [sky blue; PDB entry 3UXK (Lietzan *et al*., 2012)] interacts with residues of the hydrophobic pocket via van der Waals interactions. The Mg^{2+} ion is shown in green. **(B)** Enlarged view of superposed (*S*)-atrolactate and BzH structures show that the *para*-carbon of the phenyl ring moves while the β-carbon remains fixed.

evidence for their roles came from site-directed mutagenesis experiments, solvent exchange studies with mutants, and affinity-labeling studies.

Landro *et al*. (1991) created the H297N mutant and studied the kinetic and structural properties of this mutant. The x-ray structure of the H297N mutant (at 2.2-Å resolution) showed no conformational alterations compared to the structure of wild-type MR but the mutant was unable to racemize either of the substrate enantiomers. Interestingly, the H297N mutant catalyzed the elimination of bromide from (*S*)- but not (*R*)-*p*-(bromomethyl)mandelate **(Scheme 1.3)** and the exchange of the α-proton of (*S*)- but not (*R*)-mandelate with solvent derived deuterium (Landro *et al*., 1991). It is evident from these studies that the H297N mutation abolished the catalytic properties of the (*R*)-specific base but not the (*S*)-specific base. Thus, His 297 functions as the (*R*)-specific Brønsted base catalyst in the MR-catalyzed reaction **(Scheme 1.4)**.

The identity of the (*S*)-specific base was established using an affinity label, (*R*)-α-phenylglycidate (an epoxide-containing derivative of mandelate) (Landro *et al*., 1994). It was shown that (*R*)-α-phenylglycidate, and not the (*S*)-enantiomer, inactivates MR in a stereospecific and stoichiometric manner **(Scheme 1.5)**. The x-ray crystal structure of the inactivated MR revealed that the covalent adduct is formed by nucleophilic attack of the ε-amino group of Lys 166 on the distal carbon of (*R*)-α-phenylglycidate **(Figure 1.5)**. The position of this carbon is equivalent to the α-proton on (*S*)-mandelate, indicating that the side chain of Lys 166 is ideally positioned to abstract the α-proton from the (*S*)-mandelate (Landro *et al*., 1994). Another piece of evidence indicating that Lys 166 is the (*S*)-specific base came from kinetic studies of the K166R mutant. The x-ray crystal

Scheme 1.4 Mechanism of MR-catalyzed inter-conversion of mandelate enantiomers

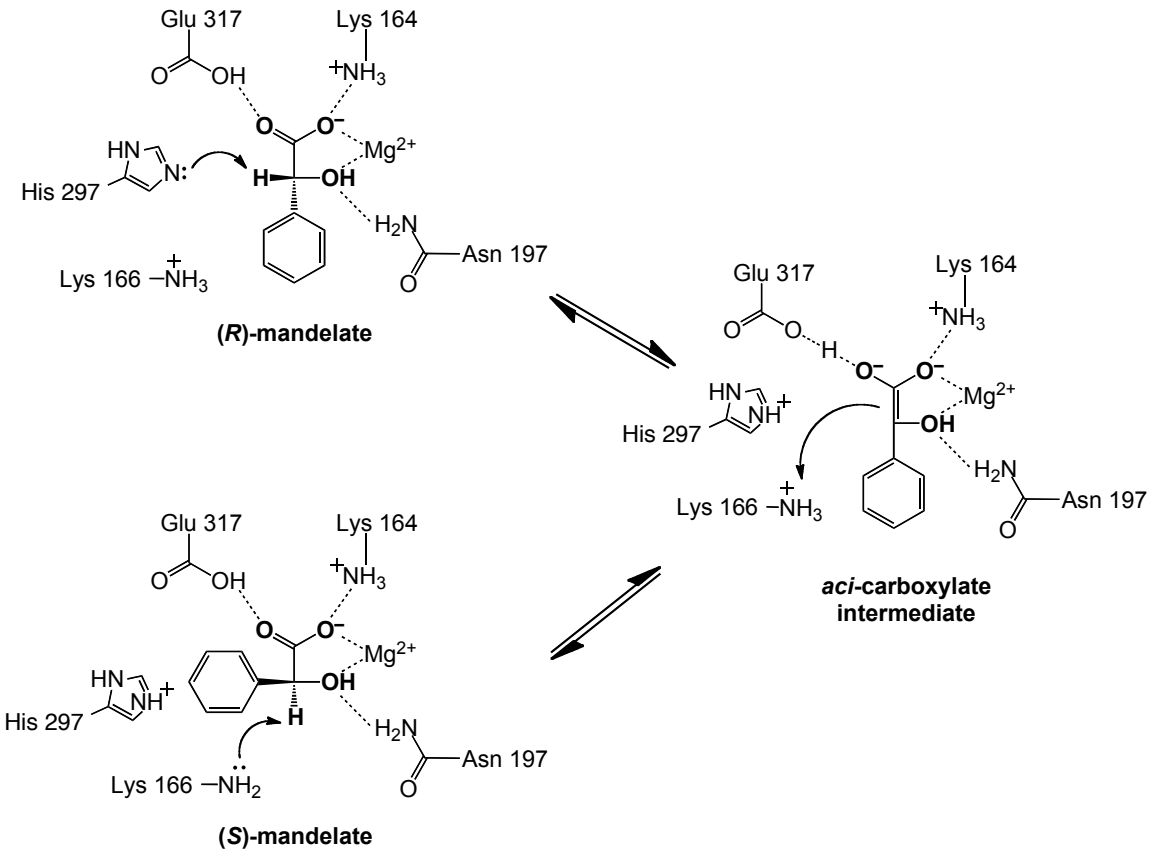

Scheme 1.5 Mechanism of inactivation of MR by (*R*)-α-phenylglycidate

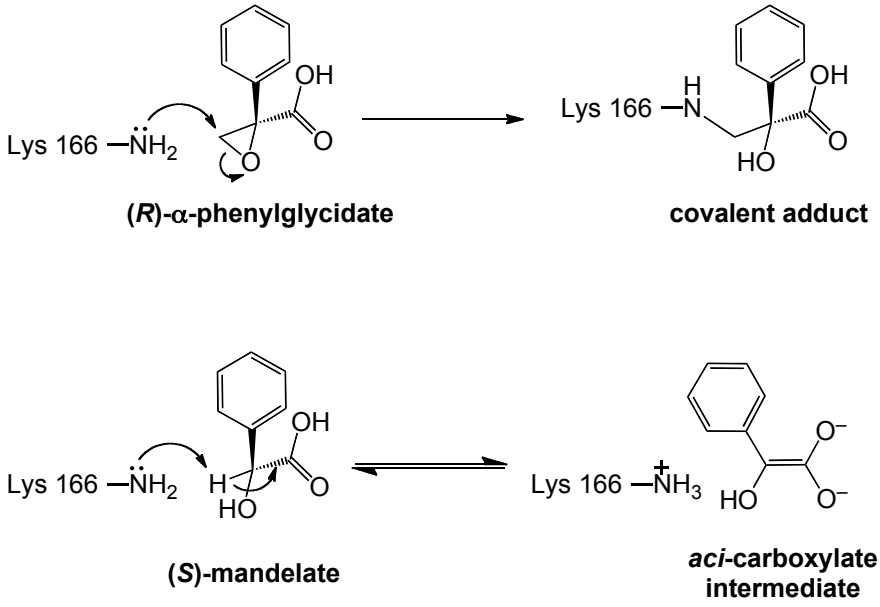

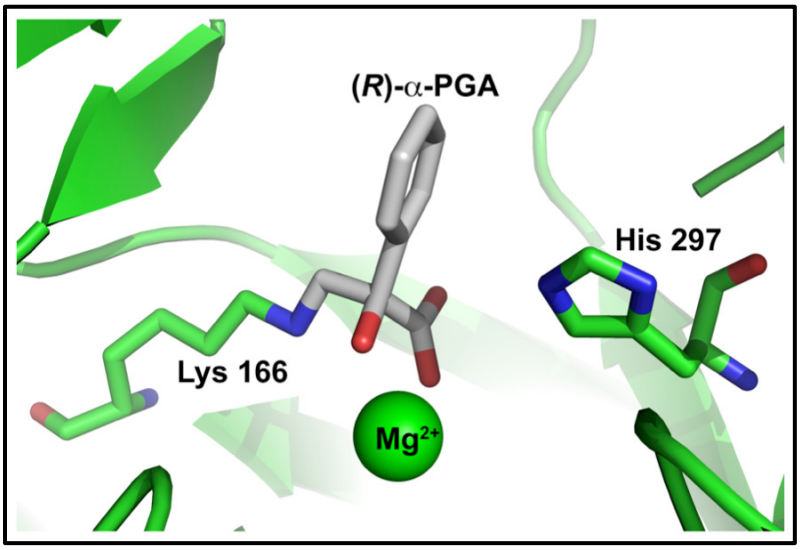

Figure 1.5 X-ray crystal structure of MR inactivated with (*R*)-α-phenylglycidate ((*R*)-α-PGA) [PDB entry 1MNS (Landro *et al*., 1994)].

structure of K166R-MR (1.8-Å resolution) did not show any major structural alterations compared to wild-type MR except for a minimal perturbation in the position of the side chain of residue 166 due to the Lys→Arg mutation (Kallarakal *et al*., 1995). Although the K166R mutant retained low levels of racemase activity (k_{cat} reduced by ~10^3–fold) in both reaction directions, it was able to catalyze stereoselective elimination of bromide from (*R*)- but not (*S*)-*p*-(bromomethyl)mandelate **(Scheme 1.3)** at a rate similar to that of the wild-type enzyme (Kallarakal *et al*., 1995). Together, these results provide convincing evidence that Lys 166 is the (*S*)-specific Brønsted base catalyst in the MR-catalyzed reaction **(Scheme 1.4)**.

The pH-rate profile of wild-type MR revealed similar pK_a values for both the basic catalyst (pK_a = 6.4) and the acidic catalyst (pK_a = 10.0) in both reaction directions (Landro *et al*., 1991). These pK_a values were deduced from the ascending and descending limbs of the Dixon-Webb log plots for the dependencies of k_{cat} on pH. In the (*R*)→(*S*) reaction direction, the pK_a of 6.4 corresponds to the pK_a of the conjugate acid of His 297, the (*R*)-specific base, while the pK_a of 10 corresponds to the pK_a of the conjugate acid Lys 166, that reprotonates the intermediate to generate (*S*)-mandelate. In the (*S*)→(*R*) reaction direction, the pK_a values and the roles of His 297 and Lys 166 are interchanged. In fact, the pD dependence of the rate of exchange of solvent deuterium in (*S*)-mandelate catalyzed by the H297N mutant confirmed the pK_a value (6.4) of the Brønsted base catalyst, Lys 166 (Landro *et al*., 1991). The pH-rate profiles of the K166R mutant showed that pK_a values deduced from the ascending limb of the pH plot were in agreement with the expected pK_a values for His 297 (6.4, in the (*R*)→(*S*) reaction direction) and Arg 166 (7.9, (*S*)→(*R*) reaction direction) for the Brønsted base catalyst,

while the pK_a values deduced from the descending limb remained unaltered in both directions, suggesting that assignment of the pK_a values deduced from the descending limb to the Brønsted acid catalysts is questionable (Gerlt, 1998; Kallarakal *et al*., 1995). Therefore, only the pK_a values of the conjugate acids of His 297 and Lys 166 (i.e., the Brønsted base catalysts) are well established (6.4) (Kallarakal *et al*., 1995; Landro *et al*., 1994). This pK_a value is consistent with the normal pK_a of the imidazole side chain of His (~6), but the pK_a of the Lys side chain is highly perturbed relative to the normal pK_a (~10). The depressed pK_a of Lys 166 could be explained by the destabilization of the positive charge on Lys 166 due to the close proximity of positive electrostatic potential provided by Lys 164 and the Mg^{2+} ion (Neidhart *et al*., 1991). Although His 297 is also located in close proximity and equidistant (*cf*. Lys 166) to the Lys 164 and the Mg^{2+}, it maintains a normal pK_a value possibly due to the hydrogen-bonding interaction with Asp 270. Together His 297 and Asp 270 function as a catalytic dyad in the active site of MR (Schafer *et al*., 1996).

Although estimating the pK_a of the Brønsted acid catalyst is problematic (Kallarakal *et al*., 1995), it is clear that His 297 and Lys 166 act as the Brønsted acid catalysts and the pK_a values of these residues must therefore be perturbed to catalyze the reaction in both directions (Landro *et al*., 1994; Neidhart *et al*., 1991; Schafer *et al*., 1996). This shift in pK_a values seems to be enantioselective and likely originates via conformational changes induced by the stereochemistry of the substrate, which likely change the distribution of charged residues in the active site. In fact, the change of a single H-bond interaction due to the binding of different enantiomers could lead to a change in the pK_a value by ~1-2 units within the protein environment (Ishikita & Saito,

2014). But, in the absence a crystal structure of MR with bound (*R*)-mandelate, these conformational changes remain unknown.

1.1.6 Brønsted Acid Catalyst: Glu 317

The mechanism of the reaction catalyzed by MR involves formation of a transiently stable carbanion intermediate (Hegeman *et al*., 1970; Kenyon & Hegeman, 1970; Landro *et al*., 1991; Lin *et al*., 1988; Mitra *et al*., 1995; Neidhart *et al*., 1991), but the life span of such an unstable enolate anion intermediate (~10^{-13} s) would be too short to account for the rate of reaction catalyzed by MR (Thibblin & Jencks, 1979). In order to explain the rates of enzyme-catalyzed proton abstractions, Gerlt and Gassman proposed a concerted general acid-general base catalysis mechanism where abstraction of the α-proton by a Brønsted base is concerted with protonation (complete or partial) of the carboxyl group by a Brønsted acid catalyst to generate a more stable enol intermediate rather than enolate anion intermediate (Gerlt & Gassman, 1993a; Gerlt & Gassman, 1993b). The crystal structures of MR with bound (*S*)-atrolactate showed that one of the carboxylate oxygens of this mandelate analogue is hydrogen bonded to the carboxylate of Glu 317, suggesting that this residue could act as a Brønsted acid catalyst (Landro *et al*., 1994). Mitra *et al*. (1995) tested this proposal by characterizing E317Q mutant. Changing Glu 317 to a Gln residue would maintain the hydrogen bonding interaction with the carboxylate of substrate while affecting the rate of proton transfer due to the much higher pK_a of Gln (pK_a ~15) relative to Glu (pK_a ~6). Indeed, the crystal structure of the E317Q mutant with (*S*)-atrolactate bound revealed hydrogen-bonding interactions between the carboxylate of atrolactate and the Gln side chain, and the kinetic studies showed a

substantial decrease (by a factor of ~10^4) in k_{cat} in both reaction directions while not altering the affinities (K_m) for (*R*)- and (*S*)-mandelate (Mitra *et al*., 1995). The E317Q mutation also impaired MR's capability to catalyze the elimination of bromide from either of the enantiomers of *p*-(bromomethyl)mandelate **(Scheme 1.3)**. These results suggested that Glu 317 acts a Brønsted acid catalyst and that the proton transfer by Glu 317 helps to stabilize the enolic intermediate (Mitra *et al*., 1995). In addition to Glu 317, Lys 164 and Mg^{2+} also play an important role in neutralizing the negative charge of the carboxylate of bound mandelate **(Scheme 1.4)** thus lowering the pK_a of the α-proton by ~7 units to facilitate proton abstraction (Landro *et al*., 1994; Mitra *et al*., 1995). Refer to section 2.1 for a detailed discussion.

1.1.7 Assay of MR activity

Over the years various techniques have been developed to assay MR activity. Hegeman *et al*. developed a coupled kinetic assay that utilized an (*S*)-specific dehydrogenase and 2,6-dichlorophenolindophenol (DCPIP, λ_{max} = 600 nm) (Hegeman, 1970). The conversion of (*R*)-mandelate to (*S*)-mandelate by MR, and further oxidation of (*S*)-mandelate to benzoylformate and concomitant reduction of DCPIP by (*S*)-mandelate dehydrogenase can be monitored spectrophotometrically by following the color change due to the conversion of oxidized DCPIP (blue) to reduced DCPIP (colorless). However, this coupled assay has a few shortcomings. First, (*S*)-mandelate dehydrogenase, a membrane bound enzyme linked to the electron transporter system, is used in vesicular form that leads to high turbidity and re-oxidation of DCPIP. Second, the

rates can be monitored only in one reaction direction, i.e., (*R*)→(*S*) due to the specificity of (*S*)-mandelate dehydrogenase (Kenyon & Hegeman, 1979; Sharp *et al*., 1979).

To overcome these disadvantages, Sharp *et al*. (1979) developed a circular dichroism (CD)-based assay. A relation similar to the Beer-Lambert law for optical absorption relates the circular dichroic intensity to concentration of an optically active compound ($\theta = [\theta]_e c l$, where θ is observed ellipticity, $[\theta]_e$ is the molar ellipticity, c is molar concentration of a chiral molecule, and l is the path-length). Because the magnitudes of molar ellipticity for both enantiomers of mandelic acid are equal and have opposite signs at 262 nm, the rate of conversion of one enantiomer into the other can be monitored by following the rate of change in ellipticity and using equation 1.1 (e.g., (*R*)- to (*S*)-mandelate).

$$\frac{d\theta}{dt} = [\theta]_R l \left(\frac{d[R]}{dt} - \frac{d[S]}{dt}\right) \tag{1.1}$$

where θ is the observed ellipticity for a given sample concentration (degree), [*R*] and [*S*] are the molar concentrations of the (*R*)- and (*S*)-enantiomers, respectively, and $[\theta]_R$ (units of deg $M^{-1}cm^{-1}$) is the molar ellipticity of (*R*)-mandelate. The initial velocity (v_i) of the racemization reaction can be calculated using equation 1.2 (derived from equation 1.1).

$$v_i = \frac{1}{2[\theta]_R l}\left(\frac{d\theta}{dt}\right) \tag{1.2}$$

Unlike the coupled assay, this direct kinetic assay may be employed to follow MR activity in both (*R*)→(*S*) and (*S*)→(*R*) reaction directions.

Alternatively, polarimetry has also been used to monitor the MR-catalyzed reaction (Hegeman *et al*., 1970; Landro *et al*., 1991; Mitra *et al*., 1995; Stecher *et al*.,

1998; Weil-Malherbe, 1966). However, both the polarimetry-based and CD-based assays lack sensitivity to measure accurate velocities at substrate concentrations near or below the K_m value (Landro *et al*., 1991; Stecher *et al*., 1998).

Bearne *et al*. (1999) developed a facile and sensitive HPLC-based assay. This fixed-time assay involves enzymatic conversion of (*R*)- to (*S*)-mandelate (or the reverse direction) followed by the separation and detection of the substrate and product using isocratic reversed-phase HPLC on a Sumichiral OA-0166 column and absorbance detection (Bearne *et al*., 1999). Although the HPLC-based assay is more sensitive at low substrate concentrations, it is more labour-intensive. Therefore, the CD-based assay was preferred for the present studies.

1.1.8 The Enolase Superfamily

The discovery of structural similarities between MR and muconoate lactonizing enzyme (MLE) was the stepping-stone to classify enzymes into superfamilies (Gerlt *et al*., 2005; Neidhart *et al*., 1990). Both enzymes share (i) a $(\alpha/\beta)_7\beta$-barrel domain containing the active site comprised of highly conserved residues that bind the essential Mg^{2+}, and (ii) an $\alpha + \beta$-capping domain (formed from the polypeptide segments at N and C termini) that provides substrate specificity (Gerlt *et al*., 2012) **(Figure 1.6)**. Later, recognition of the same domain architecture in the structure of yeast enolase established the 'enolase superfamily' (Babbitt *et al*., 1996; Babbitt *et al*., 1995; Hasson *et al*., 1998), named after enolase, a member that is present in all living systems (Richard & Amyes, 2001). The conserved bi-domain structure in the enolase superfamily provides compelling evidence that the members might have evolved from a common ancestor by

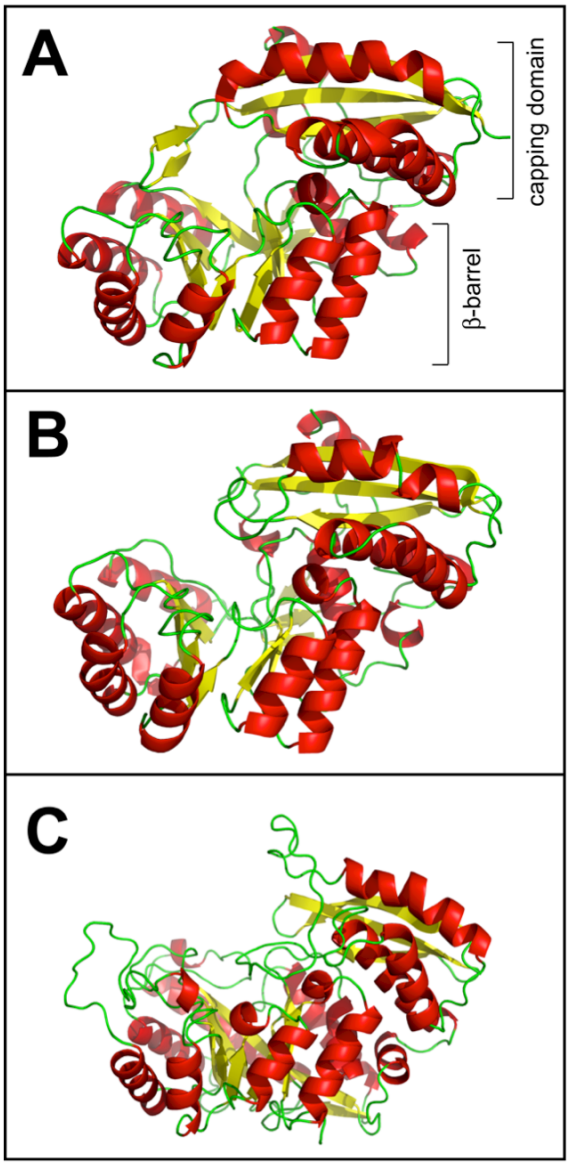

Figure 1.6 X-ray crystal structures of enolase superfamily members showing similar bidomain architecture. (A) MR [PDB entry 1MDR (Landro *et al*., 1994], (B) MLE [PDB entry 1BKH (Hasson *et al*., 1998)], and (C) enolase [PDB entry 1ELS (Zhang *et al*., 1994)].

divergent evolution (Gerlt & Raushel, 2003). Therefore, by definition, a superfamily is a group of enzymes that share a common structural scaffold but catalyze different overall reactions (Babbitt & Gerlt, 1997). At present, the enolase superfamily includes more than 8000 members that are classified into seven sub-groups based on the location of the acid/base catalysts: MR, MLE, enolase, D-glucarate dehydratase, D-mannonate dehydrtase, β-methylaspartate ammonia lyase, and galactarate dehydratase (Gerlt *et al*., 2012). The MR subgroup includes MR and ten acid sugar dehydratases. The members of this mechanistically diverse superfamily catalyze a variety of different reactions, including racemization, epimerization, cycloisomerization, and both *syn* and *anti* β-elimination reactions. However, all of these reactions start with a thermodynamically difficult common partial reaction in which an active site Brønsted base (pK_a ~7) abstracts the α-proton from a carbon acid substrate (pK_a 29–32) to generate an enolic intermediate that is stabilized by coordination to a divalent metal ion **(Scheme 1.6)**. This stabilized intermediate is then converted into a product depending on the residues involved in catalysis and the overall active site structure of the specific enolase superfamily member. Structure/function studies of the enolase superfamily have provided a basis for predicting the functions of unknown members such as *cis*-3-hydroxy-L-proline dehydratases (Zhang *et al*., 2015), galactarate dehydratase III (Groninger-Poe *et al*., 2014), D-mannonate and D-gluconate dehydratases (Wichelecki *et al*., 2014), 3′,5′-nucleotide bisphosphate phosphatase (Cummings *et al*., 2014), 4-hydroxy-L-proline betaine epimerase (Zhao *et al*., 2013), and engineering known members so that novel reactions can be catalyzed (Schmidt *et al*., 2003; Vick & Gerlt, 2007).

Scheme 1.6 Reaction mechanisms of enolase superfamily members

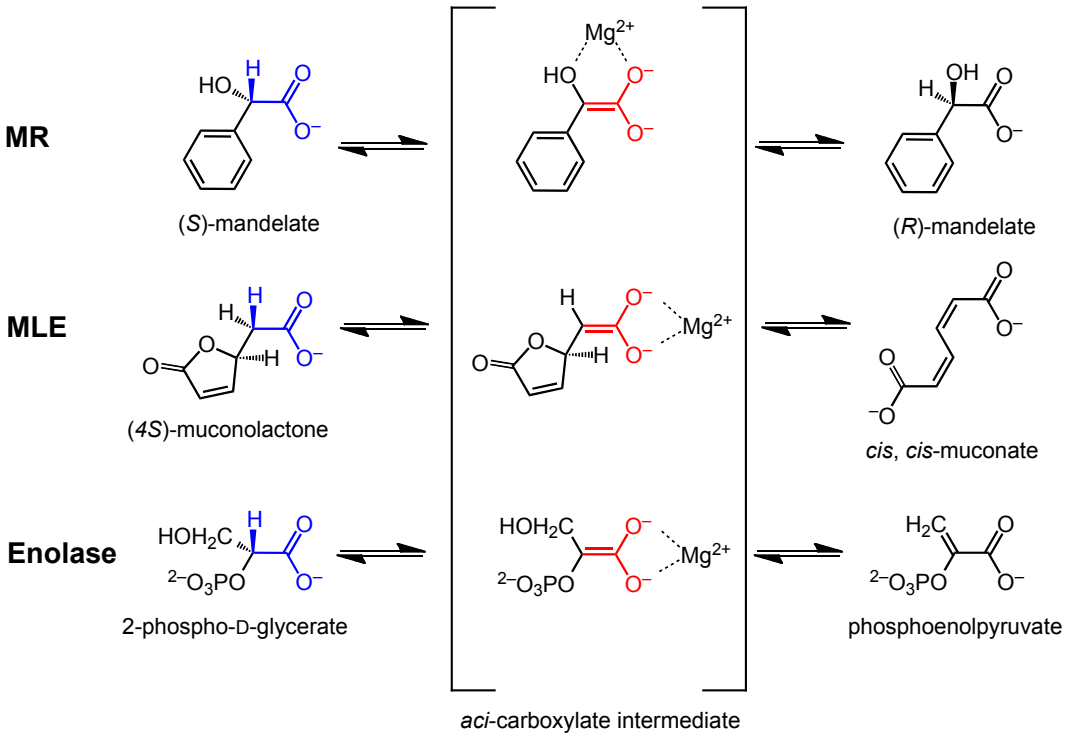

1.2 Enzyme-Catalyzed Proton Abstraction from Carbon Acids

1.2.1 The Mechanistic Problems

Proton abstraction reactions are ubiquitous in nature. Many enzymes involved in various catabolic and anabolic pathways catalyze the abstraction of a proton from a carbon acid adjacent to a carbonyl or a carboxylate group (α-proton of a carbon acid) (Gerlt, 2007). Some enzymes, such as amino acid racemases and transaminases, and acyl-CoA dehydrogenases, require pyridoxal phosphate or flavin derivatives, respectively, as cofactors (Gerlt, 2007; Richard & Amyes, 2001); others, like MR, require either metal-ion assistance, or like glutamate racemase, require no cofactor (Tanner, 2002). Further discussion focuses on the organic-cofactor-independent enzyme-catalyzed proton abstraction reactions such as 1,1-, 1,2-, and 1,3-proton transfers, β-elimination/dehydration, and Claisen condensation reactions. Each of these reactions is initiated by abstraction of the α-proton of the carbon acid substrate, in most cases via a step-wise mechanism resulting in generation of a transiently stable enolate intermediate (Gerlt, 1998; Tanner, 2002). Based on the Marcus formalism, the activation energy barrier for a proton abstraction reaction can be portioned into (i) a thermodynamic barrier ($\Delta G°$), and (ii) an intrinsic barrier ($\Delta G^{\ddagger}_{int}$) (Gerlt & Gassman, 1992, 1993a; Gerlt & Gassman, 1993b).

The thermodynamic barrier ($\Delta G°$) is associated with both the transfer of α-proton from the carbon acid to the Brønsted base catalyst and the conversion of the keto tautomer of the carbon acid into its enol tautomer (Gerlt & Gassman, 1993a). The α-proton of carbon acids is relatively acidic (pK_a of carbon acid adjacent to aldehyde, ketone, and thioester, 18–20; carboxylic acid, 22–25; and carboxylate anion, 29–32)

compared to the acidity of hydrocarbons ($pK_a > 50$ for alkanes) due to the resonance stabilization provided by the adjoining carbonyl containing group (Gerlt & Gassman, 1992; Richard & Amyes, 2001). Still, the pK_a difference between the α-proton of carbon acids (pK_a ~18–32) and the conjugate acids of the Brønsted acid-base catalysts (pK_a ~7) in the active site is too high to account for the rapid rates of enzyme catalyzed proton transfers (Gerlt & Gassman, 1993a; Gerlt & Gassman, 1993b; Thibblin & Jencks, 1979). For example, the estimated pK_a of mandelate anion is ~29 (Renaud & Fox, 1988), and the pK_a of the conjugate acids of the Brønsted acid-base catalysts Lys 166 and His 297 is 6.4 in the MR-catalyzed reaction (Kallarakal *et al*., 1995; Landro *et al*., 1991). Assuming that the free energy of activation ($\Delta G^{\ddagger}$) to generate an intermediate is solely determined by the thermodynamic barrier ($\Delta G°$) associated with the proton transfer from the carbon acid substrate to the Brønsted base catalyst, $\Delta G^{\ddagger}$ can be related to the difference in pK_a values between the proton donor and acceptor ($\Delta G^{\ddagger} \approx \Delta G° = -2.303RT\Delta pK_a$) (Gerlt, 1998, 2007; Gerlt & Gassman, 1992). Using this correlation, the calculated $\Delta G^{\ddagger}$ for the MR-catalyzed proton abstraction would be 31 kcal/mol, which is 17 kcal/mol greater than the observed value on the enzyme (14 kcal/mol (Mitra *et al*., 1995)), suggesting that MR must stabilize this transiently stable intermediate to reduce the thermodynamic barrier ($\Delta G°$). Sections 1.2.2 & 1.2.3 discuss the proposed strategies for stabilization of the intermediate.

The intrinsic barrier ($\Delta G^{\ddagger}_{int}$) is defined as the activation energy barrier in absence of a thermodynamic barrier, i.e., if the proton transfer reaction were isoenergetic (Gerlt & Gassman, 1993a). The $\Delta G^{\ddagger}_{int}$ for a non-enzymatic abstraction of the α-proton from carbon acid (~12 kcal/mol) is much greater than that for abstraction of the proton from a

heteroatom or normal acid (~3 kcal/mol) (Gerlt & Gassman, 1993a). This difference can be explained by the need for re-organization of solvent that occurs when charge is localized on carbonyl/carboxyl oxygen and rehybridization of the tetrahedral α-carbon occurs after proton abstraction. Preorganization of functional groups ($\Delta S^{\ddagger}_{int}$) in active sites may reduce $\Delta G^{\ddagger}_{int}$ of enzyme-catalyzed proton abstraction reactions (Gerlt & Gassman, 1993a; Gerlt & Gassman, 1993b; Warshel, 1998).

1.2.2 Electrophilic Catalysis

The pK_a of the α-proton of mandelic acid is ~22, whereas the pK_a of the neutral enol of mandelic acid is ~6.6 (Chiang *et al*., 1997; Chiang *et al*., 1990); and the difference between these pK_a values yields a pK_E value 15.4 (where K_E is the equilibrium constant of the keto-enol equilibrium of the neutral carbon acid) **(Scheme 1.7)** (Chiang & Kresge, 1991; Chiang *et al*., 1990). Gerlt *et al*. (1991) suggested that this pK_E value (~15.4) also reflects a combination of the pK_a values of the α-proton and the protonated carbonyl group (~ –8, based on the pK_a of phenylacetic acid (Flexser *et al*., 1935)), and therefore, the pK_a of the α-proton must be ~7.4 in the active site **(Scheme 1.7)** (Gerlt *et al*., 1991). This value is similar to the pK_a values reported for the conjugate acids of His 297 and Lys 166 (both ~6.4). A similar increase in the acidity of the α-proton of a carbon acid substrate can be achieved within the active site of enzymes by either hydrogen bonding or metal coordination. In fact, crystal structures of the enzymes catalyzing proton abstraction from carbon acids reveal the presence of a potential electrophilic catalyst proximal to the carbonyl/carboxylate group of substrate (Gerlt *et al*., 1991). This proper positioning of the electrophilic catalyst may help in reducing the intrinsic barrier,

Scheme 1.7 Keto-enol equilibrium of mandelic acid (adapted from Gerlt *et al*., 1991)

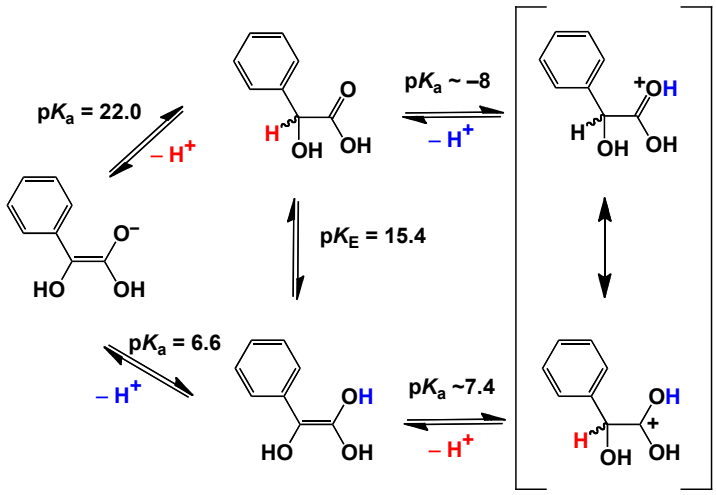

$\Delta G^{\ddagger}_{int}$. To explain the observed rates of enzymatic proton abstraction reactions, Gerlt and Gassman (1993) proposed that concerted general acid-base catalysis occurs and that Glu 317, which is located 2.6 Å from the carboxylate oxygen of the substrate (Landro *et al*., 1994; Mitra *et al*., 1995), acts as the electrophilic catalyst (Gerlt & Gassman, 1993a; Gerlt & Gassman, 1993b). The estimated pK_a of Glu 317 in the MR active site is ~6 (Gerlt, 1998). This value matches with the pK_a of the neutral enol of mandelic acid (6.4-6.6) allowing rapid proton transfer between the two groups (Gerlt, 2007; Gerlt & Gassman, 1993a). Computer simulation studies on the MR-catalyzed racemization of vinylglycolate also support the role of Glu 317 in concerted general acid catalysis (Garcia-Viloca *et al*., 2001).

Alternatively, similar pK_a values may promote the formation of a short, strong hydrogen bond (SSHB) between the Brønsted acid catalyst and the enolic intermediate, which could facilitate the reduction of the pK_a of the α-proton in the transition state (Gerlt & Gassman, 1993a; Gerlt & Gassman, 1993b). SSHBs or "low barrier hydrogen bonds" are formed when the two heteroatoms having approximately same pK_a values come closer than the sum of their van der Waals radii (< 2.55 Å for O–H–O) and the barrier between the two potential energy wells for each H-bond reduces to an extent that proton is equally shared between the two heteroatoms (Cleland & Kreevoy, 1994; Frey *et al*., 1994; Gerlt & Gassman, 1993a). Cleland and Kreevoy (1994) proposed that a weak hydrogen bond between the enzyme and the substrate could subsequently become a SSHB as the proton is abstracted from the carbon acid, and the formation of SSHBs can contribute 10-20 kcal/mol to facilitate transition state stabilization during the catalysis. Therefore, this hypothesis has been invoked to explain energetics of several other enzyme

systems including serine proteases like chymotrypsin (Frey *et al*., 1994) and trypsin (Ishida, 2006), triosephosphate isomerase (TIM) and MR (Gerlt & Gassman, 1993a), and acetylcholinesterase (Massiah *et al*., 2001). Over time, many enzymologists have debated the existence, chemical properties, and role of SSHBs in enzyme catalysis (Ash *et al*., 1997; Guthrie, 1996; Guthrie & Kluger, 1993; Scheiner & Kar, 1995; Schutz & Warshel, 2004; Warshel *et al*., 1995). Although, neutron diffraction studies have shown the existence of the SSHBs in crystals, their existence in solution still remains a controversial issue (Graham *et al*., 2013; Nadal-Ferret *et al*., 2014).

1.2.3 Electrostatic Stabilization

Guthrie and Kluger (1993) challenged the proposal of electrophilic catalysis and considered it to be insufficient to explain the rates of enzyme-catalyzed proton abstraction reactions. They showed that the *O*-protonated acid, the enol, and the enolate of the mandelic acid have similar energies. Since both the proposed enol or enolate intermediates were higher in energy than the observed transition state in the MR-catalyzed reaction, Guthrie and Kluger proposed that MR must primarily stabilize the intermediate to overcome the thermodynamic problem (Guthrie & Kluger, 1993). According to Guthrie and Kluger, formation of the enolate would be favored in the active site because the negative charge on the enolate increases the possibility of electrostatic stabilization and thus eliminates the need for concerted general acid (electrophilic) catalysis. On the contrary, formation of the enol would be counterproductive owing to the difficulties an enzyme would face to stabilize such a neutral intermediate (Guthrie & Kluger, 1993). Electrostatic/Coulombic interactions between the dianionic (enolate)

intermediate and the divalent metal ion in the apolar (low dielectric) environment of the enzyme active site could provide significant (up to 18 kcal/mol) energy for TS stabilization. In fact, Warshel *et al*. (1995) advocated that this electrostatic stabilization is sufficient to account for the observed catalysis without the need to invoke a SSHB. Although the presence of SSHBs in MR have not yet been demonstrated by the characteristic deuterium fractionation factors and/or large downfield ^{1}H NMR chemical shifts (17-19 ppm) (Nadal-Ferret *et al*., 2014), studies with the E317Q (Mitra *et al*., 1995) and K166R mutants (Kallarakal *et al*., 1995) (discussed in earlier sections), along with the calculations of the effective molarities of Lys 166, His 297, and Glu 317 (Bearne & Wolfenden, 1997), have suggested that Glu 317 interacts more strongly with the altered substrate in transition state. In addition, formation of the enolate anion intermediate from mandelate increases the charge densities on the carboxylate oxygens from -0.5 to -1.0 (Cleland *et al*., 1998). This could, very well, enhance the electrostatic interactions between Mg^{2+} and the carboxylate as well as the hydrogen bond strength between Glu 317 and the carboxylate of the substrate. Therefore, despite the debate over the role of SSBHs in enzyme catalysis, in case of MR, both the electrophilic catalysis and the electrostatic stabilization could contribute towards stabilization of intermediate.

1.3 Enzyme Catalysis: Crossing the Barrier

1.3.1 Transition State Stabilization

Like any catalyst, enzymes accelerate the rates of reactions by lowering the activation energy. Pauling (1948) proposed that the large rate enhancements afforded by enzymes stem from the enhanced binding affinity of enzymes for the activated complex

or transition state (TS) (Pauling, 1948). Over the years, this proposal has been supported by abundant evidence and applied to explain enzyme catalysis (Amyes & Richard, 2013; Lienhard, 1973; Lolis & Petsko, 1990; Schramm, 1998; Wolfenden, 1969, 1976). Wolfenden proposed that the affinity of an enzyme for the TS (i.e., TS stabilization) could be quantified using a thermodynamic cycle and TS theory **(Scheme 1.8)**, for a one-substrate reaction (Wolfenden, 1969; Wolfenden, 1972). This thermodynamic cycle is comprised of equilibria for the dissociation of ES (K_s) and ES‡ ($K^{‡}_{cat}$), the formation of the non-enzymatic TS (S‡; $K^{‡}_{non}$), and the hypothetical equilibrium constant for the binding of free enzyme to the TS (K_{tx}). The equilibrium constants for the enzyme-catalyzed and the uncatalyzed reactions can be related by equation 1.3.

$$\frac{K_{\mathrm{tx}}}{K_{\mathrm{s}}} = \frac{K^{‡}_{\mathrm{non}}}{K^{‡}_{\mathrm{cat}}} \tag{1.3}$$

The equilibrium constant between the reactant and the transition state ($K^{‡}$) can be expressed in terms of a measurable first-order rate constant (k) using equation 1.4 (transition state theory), where k_BT/h is the universal frequency factor (k_B = Boltzmann constant, h = Planck's constant, and T = absolute temperature). Using ΔG = RTln$K$ (where K is a dissociation constant), first-order rate constants (k) can also be expressed in terms of the free energy of activation (equation 1.5), $\Delta G^{‡}$.

$$k = \left(\frac{k_{\mathrm{B}}\mathrm{T}}{h}\right) K^{‡} \tag{1.4}$$

$$k = \left(\frac{k_{\mathrm{B}}\mathrm{T}}{h}\right) exp\left(\frac{-\Delta G^{‡}}{\mathrm{RT}}\right) \tag{1.5}$$

Scheme 1.8 Thermodynamic cycle depicting the enzyme-catalyzed and non-enzymatic conversion of substrate into product

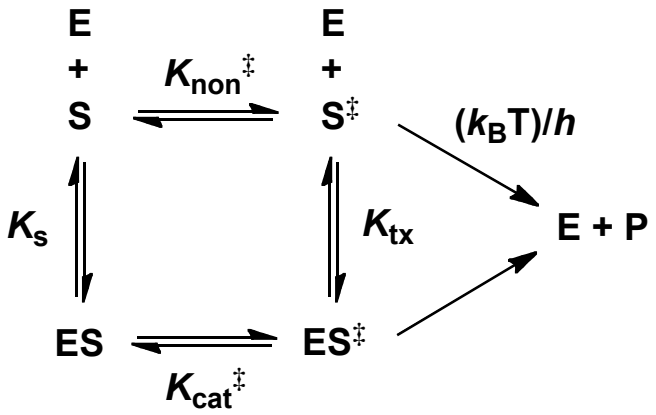

By expressing $K_{non}^{\ddagger}$ and $K_{cat}^{\ddagger}$ (in equation 1.3) in terms of k_{non} and k_{cat} (equation 1.4), respectively, K_{tx}, the virtual dissociation constant for the enzyme-substrate complex in the transition state, can be calculated using equation 1.6, where k_{non} and (k_{cat}/K_s) are the first-order and the second-order rate constants for the non-enzymatic and enzymatic reactions, respectively.

$$K_{tx} = \frac{k_{non}}{(k_{cat}/K_s)} \tag{1.6}$$

The reciprocal of K_{tx} is the proficiency of an enzyme, and is defined as the degree to which an enzyme stabilizes the altered substrate in transition state compared to the substrate in ground state (Radzicka & Wolfenden, 1995a). A similar relationship has been derived for multi-substrate enzymes (Byers, 1978; Lienhard, 1973; Stockbridge & Wolfenden, 2009). The free energy diagram in **Figure 1.7** illustrates the concept of using reaction coordinates for a hypothetical unimolecular reaction proceeding in the presence and absence of an enzyme. The reported proficiencies of various enzymes range from 10^9 (carbonic anhydrase) to 10^{29} M^{-1} (alkylsulfatase), corresponding to 10 to 39.5 kcal/mol of free energy of TS stabilization (Edwards *et al*., 2012; Miller & Wolfenden, 2002; Snider & Wolfenden, 2001). Estimation of enzyme proficiency is limited by the difficulty in measuring non-enzymatic reaction rates for very sluggish reactions. Bearne & Wolfenden determined the free energy of activation for the non-enzymatic racemization of mandelic acid (–34.6 kcal/mol, i.e., $k_{non} = 3 \times 10^{-13}$ s^{-1}) and showed that MR is a remarkably proficient enzyme, enhancing the rate by 10^{15}-fold and reducing the activation barrier for proton abstraction from mandelic acid by ~26 kcal/mol (Bearne & Wolfenden, 1997).

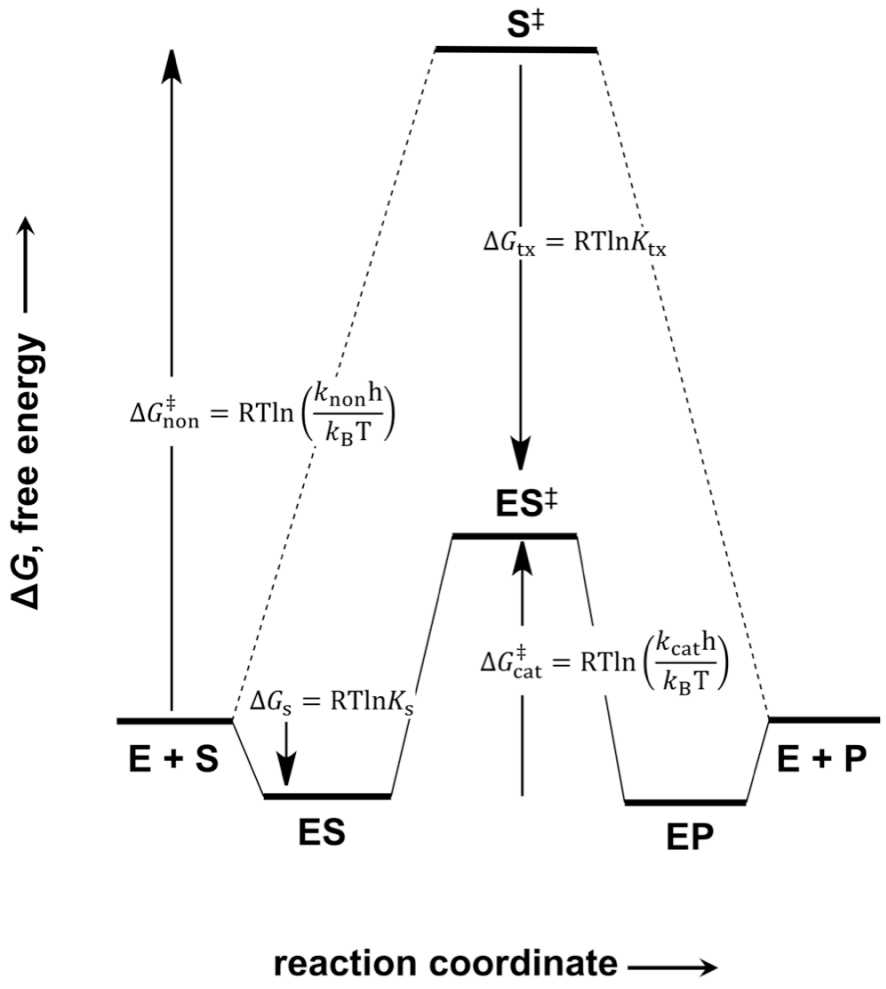

Figure 1.7 Reaction coordinate diagram for enzyme-catalyzed and a non-enzymatic conversion of substrate to product. ΔG_{tx}, represents the free energy of transition state stabilization provided by the enzyme.

The above-mentioned thermodynamic analysis is based on two assumptions (Wolfenden, 1972). First, it is assumed that both the enzymatic and non-enzymatic pathways involve identical transitions states. Thermodynamically, the non-enzymatic reaction in bulk solvent should follow a mechanism involving lowest energy path. If this mechanism differs from the corresponding enzymatic mechanism, then the actual barrier for the hypothetical non-enzymatic reaction would be higher and thus, TS stabilization would be underestimated. Second, it is assumed that the chemical step is rate-limiting for the enzyme-catalyzed reaction. However, during enzymatic reactions, observed rates (k_{cat} or k_{cat}/K_m values) could be limited by other factors including conformational changes and/or the substrate-binding/product-release step. In fact, in the case of MR, viscosity studies have shown that the chemical step is only partially rate-limiting and that the rate constant for the chemical step (k_2, 800 s^{-1}) is greater than observed rate constant (k_{cat}, 600 s^{-1}) (St. Maurice & Bearne, 2002). Thus, the affinity of the enzyme for the altered substrate in the TS, K_{tx}, calculated using k_{cat}/K_m rather than k_2/K_m would be overestimated (i.e., underestimation of TS stabilization). Therefore, in either case, K_{tx} provides only a minimum estimate of TS stabilization (Lienhard, 1973; Wolfenden, 1972).

1.3.2 Transition State Analogues

The typical lifetime of a TS is assumed to be 10^{-13} s, i.e., equivalent to the time for a bond vibration (Thibblin & Jencks, 1979). Therefore, it would be unrealistic to think that an ideal stable transition state analogue would have identical binding properties to the TS. At best, a transition analogue could be a close electronic and geometric mimic of the TS and thereby possess a portion of the total binding interaction of the true TS

(Wolfenden, 1972). Still, the observed affinity of TS analogues is much higher compared to substrates in the ground state, which is consistent with Pauling's theory (Radzicka & Wolfenden, 1995b; Schramm, 2007; Wolfenden, 1976). In some rare cases like the inhibition of adenosine deaminase by 6-hydroxy-1,6-dihydropurine ribonucleoside (Kati & Wolfenden, 1989), and cytidine deaminase by 3,4-dihydrourindine (Frick *et al*., 1989), the affinity of the enzyme for the TS analogue is almost equal to that calculated for the actual TS (i.e., observed binding affinity K_i approaches K_{tx}). Therefore, TS analogues could provide evidence for the postulated intermediates and the mechanism of enzyme reactions.

The accepted mechanism of MR-catalysis proceeds via the formation of an *aci*-carboxylate intermediate. Hydroxamates (resembling the enolate with an sp^2 hybridized α-carbon) and phosphonate analogues (resembling the dianionic character of the carboxylate of the enolate) have been used as structural mimics of the *aci*-carboxylate in the characterization of enolase superfamily members (Bearne & Kluger, 1992; Gulick *et al*., 2000; Wedekind *et al*., 1994). It has been shown that reversible competitive inhibitors of MR including benzohydroxamate (BzH, K_i = 9.3 μM), α-hydroxybenzylphosphonate (K_i = 4.7 μM) (St. Maurice & Bearne, 2000), *N*-hydroxyfomanilide (K_i = 2.8 μM), and cupferron (K_i = 2.7 μM) (Bourque *et al*., 2007) bound MR two-orders of magnitude more tightly than the substrate (K_m = 1.2 mM, (*R*)-mandelate; K_m = 1.0 mM, (*S*)-mandelate (Nagar *et al*., 2011)). However, this high binding affinity is not sufficient evidence to prove that an intermediate/TS analogue mimics the structural and electronic character of the true TS.

TS mimicry can also be assessed by demonstrating a correlation between the free energy change accompanying TS analogue binding ($1/K_i$) and the relative free energies of activation (k_{cat}/K_m) (equation 1.7) for a variety of mutants catalyzing similar reactions (Bartlett & Marlowe, 1983; Phillips *et al*., 1992).

$$\log\left(\frac{k_{\mathrm{cat}}}{K_{\mathrm{m}}}\right) = \log k_{\mathrm{non}} + \log\left(\frac{1}{K_{\mathrm{TX}}}\right) \tag{1.7}$$

Analysis of BzH binding to various MR mutants showed a slope of unity suggesting that BzH does indeed exhibit mimicry of altered substrate in TS (Lietzan *et al*., 2012). Since cupferron is isosteric and isoelectric with BzH it could also be regarded as mimic of the *aci*-carboxylate intermediate.

Schramm (2005) linked the binding of TS analogues to the dynamic protein conformational changes that occur during enzyme catalysis. When a TS analogue enters the active site, the protein structure collapses around the TS analogue to generate a more stable compressed form of the enzyme resulting in tight binding (Schramm, 1998, 2005, 2007; Schwartz & Schramm, 2009). But this protein conformation would lie off the actual normal reaction pathway because, during catalysis, the enzyme has to return to an open conformation to facilitate product release. Therefore, TS analogues could only capture a rare conformation event that accompanies generation of the transition state (Schramm, 2005).

The crystal structures of MR bound with BzH and cupferron, in accordance to Schramm's proposal, showed overall constriction of the active site including a tighter complex of these intermediates with Mg^{2+} compared to the MR structure bound with (*S*)-atrolactate, a substrate analogue (Lietzan *et al*., 2012). However, these conformational

changes were relatively minor, suggesting that the alterations in MR structure that contribute to discrimination between the altered substrate in TS and the ground state by this proficient enzyme are extremely subtle (Lietzan *et al*., 2012). However, it should be noted that BzH and cupferron only capture ~7 kcal/mol of the total 26 kcal/mol of TS stabilization energy available.

1.4 THESIS OVERVIEW

MR is an extremely proficient enzyme that binds the altered substrate in TS 10^{16}-fold better than the substrate in ground state and reduces the activation barrier by 26 kcal/mol. The broad goals of my research were to better understand the role of substituents groups on the α-carbon of the substrate in MR-catalysis and to gain insights into the binding determinants that might play role in differential binding, i.e., TS stabilization.

An extensive survey of MR substrates led Felfer *et al*. (2005) to propose that β,γ-unsaturation is a minimal requirement (i.e., vinylglycolate is the simplest substrate of MR (Li *et al*., 1995)) for a ligand to be a substrate since this moiety can stabilize the carbanion by resonance-stabilization/conjugation. However, an electron-withdrawing group such as a trifluoromethyl group could also stabilize an enolic intermediate via inductive effects. Therefore, I explored trifluorolactate as a potential substrate for the MR-catalyzed racemization reaction (Chapter 2) and designed substrate-product and TS/intermediate analogue inhibitors of MR based on this new substrate (Chapter 3) to exploit the enhanced-binding of the trifluoromethyl group within hydrophobic cavity of MR. The observed novel binding-mode of the substrate-product analogue of

trifluorolactate led me to test the binding of ligands that contained polar groups instead of the hydrophobic phenyl or trifluoromethyl groups (Chapter 4). MR-inhibitor interactions in both studies (Chapter 3 & 4) showed involvement of the Brønsted acid-base catalysts in binding.

The x-ray crystal structure of MR with BzH, a TS/intermediate analogue, shows relatively minor alterations in the overall enzyme structure suggesting that the structural changes and accompanying interactions that discriminate between the altered substrate in the TS and the ground state by MR are subtle (Lietzan *et al*., 2012). However, there are two minor changes in the active site architecture: first, the Brønsted acid-base catalysts are equidistant form the α-carbon; and, second, movement of the side-chain of Tyr 54 towards the phenyl ring of BzH is observed. Site-directed mutagenesis, kinetic, and inhibition studies using BzH were conducted to understand the role of Tyr 54 (Chapter 5). To gain insights into possible interactions between the Brønsted acid-base catalysts and BzH, I conducted binding studies of Lys 166 and/or His 297 mutants with various ligands, including BzH, using isothermal titration calorimetry (Chapter 6). Finally, I conducted ^{15}N NMR studies with MR-Lys 166 variants in presence/absence of various ligands to understand the change in protonation state of Lys 166 upon ligand binding (Chapter 7). Unfortunately, NMR studies are inconclusive and need further investigation.

CHAPTER 2

RACEMIZATION OF TRIFLUOROLACTATE : AN ALTERNATIVE SUBSTRATE OF MR

Reproduced in part with permission from – Nagar, M., Narmandakh, A., Khalak, Y., and Bearne, S. L. (2011) Redefining the Minimal Substrate Tolerance of Mandelate Racemase. Racemization of Trifluorolactate. Biochemistry ***50****, 8846–8852. Copyright 2011 American Chemical Society.*

2.1 INTRODUCTION

Almost all reported enzymes are specific for a particular type of chemical reaction and can catalyze that reaction using a specific class of compounds. MR is no exception, it catalyzes the Mg^{2+}–dependent 1,1-proton transfer reaction to interconvert the enantiomers of variety of mandelate derivatives, and thus exhibits broad range substrate specificity **(Figure 2.1)**. Derivatives of mandelate with substitutions on the phenyl ring (Felfer *et al*., 2001; Hegeman *et al*., 1970), or with the phenyl ring replaced by (a) a heterocyclic aromatic ring (i.e., furan and thiophene) (Felfer *et al*., 2001), (b) a bulkier aromatic moiety such as a naphthyl group (St. Maurice & Bearne, 2004), or (c) non-aromatic groups such as a 1,2-cyclohexenyl (Felfer *et al*., 2005), vinyl (Li *et al*., 1995), or propargyl (Landro *et al*., 1992) also serve as substrates for MR. Propargylglycolate also acts as an irreversible inhibitor of MR, but the rate of inactivation is ~10^4-fold slower than that of racemization (Landro *et al*., 1992).

To date, the simplest substrate identified is vinylglycolate. The observed rate of racemization of vinylglycolate in both reaction directions is found to be ~35% of that measured for mandelate (e.g., turnover numbers (k_{cat}) in $R \rightarrow S$ direction are 240 and 700 s^{-1} when (*R*)-vinylglycolate and (*R*)-mandelate are used as substrates, respectively)

Figure 2.1 Substrate spectrum of MR

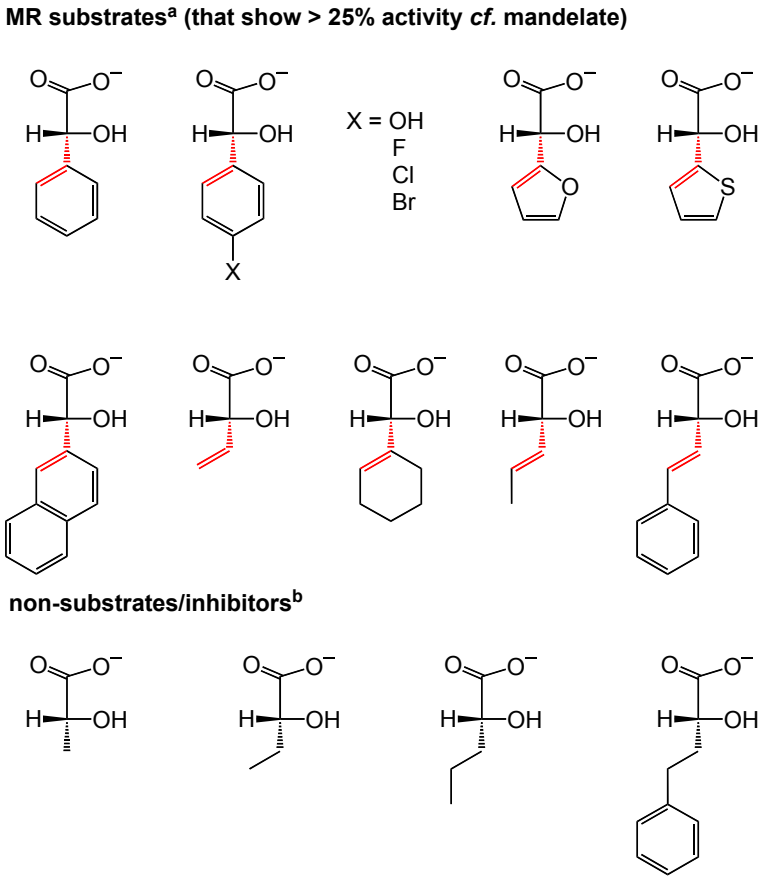

[a] (Felfer *et al*., 2005; Hegeman, 1966a; Hegeman *et al*., 1970; Li *et al*., 1995)

[b] (Felfer *et al*., 2005; Hegeman *et al*., 1970; Li *et al*., 1995; St. Maurice & Bearne, 2004)

(Li *et al*., 1995), suggesting that the vinyl group could provide a similar level of electron delocalization during the catalysis as the phenyl group of mandelate. The ability of MR to racemize this substrate and not α-hydroxyalkanoic acids such as α-hydroxybutyrate (Li *et al*., 1995) and lactate (St. Maurice & Bearne, 2004) suggests that β,γ-unsaturation is required for racemization **(Figure 2.1)**. Indeed, crystal structures with bound atrolactate reveal that this substrate analogue assumes a conformation within the active site such that proton abstraction is stereoelectronically favored (i.e., the plane of the phenyl ring is approximately perpendicular to the C_α–H bond, **Figure 2.2**). A comprehensive review of the substrate tolerance of MR conducted by Felfer *et al*. led these authors to conclude that substrates of mandelate racemase must possess β,γ-unsaturation as a minimal requirement for activity (Felfer *et al*., 2005; Felfer *et al*., 2001). The β,γ-unsaturation of aromatic groups attached to the α-carbon contributes to the resonance stabilization of the α-carbanion intermediate through their aromaticity (expressed as resonance energy). Indeed, the ability of phenyl and hetero-aromatic groups, such as furan and thiophene, to stabilize the α-carbanion is nicely paralleled to the resonance energy the group (Felfer *et al*., 2005). But the resonance energy of the allyl anion (~4 kcal/mol (Barbour & Karty, 2004)) is not sufficient to explain the 35% MR activity (relative to mandelate) observed when vinylglycolate is the substrate (*cf*. 24–38% activity with a furan analogue of mandelate that has a resonance energy of 13 kcal/mol (Felfer *et al*., 2005)). Therefore, inductive effects should also contribute for stabilization of the carbanion (Barbour & Karty, 2004). Hence, I explored trifluorolactate as an alternative substrate.

In the present chapter, it is shown that the requirement for β,γ-unsaturation is not absolute. MR accepts trifluorolactate (TFL) as a substrate and, thus, stabilization of the

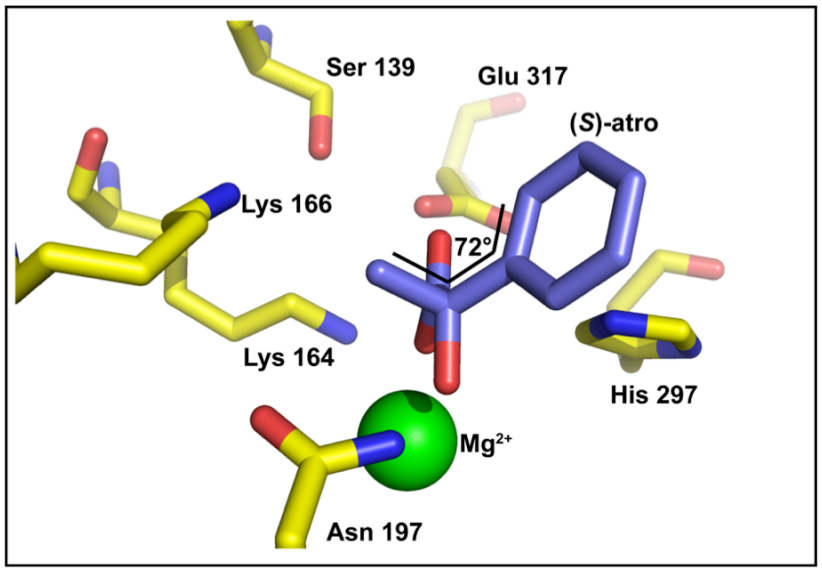

Figure 2.2 X-ray crystal structure of the active site of MR with bound (S)-atrolactate [PDB entry 1MDR (Landro *et al*., 1994)]. The phenyl ring is approximately orthogonal to the C_α–CH_3 bond (*cf*. C_α–H bond) and the dihedral angle for atoms between *ortho* carbon of the phenyl ring and the CH_3 group is 72°.

negative charge of the enolic intermediate through inductive effects is also sufficient to promote the reaction. Although MR binds TFL with an affinity similar to that exhibited for mandelate, the chemical step is completely rate-limiting during racemization of TFL. In addition, this chapter reports that the active site of the enzyme exhibits enhanced interaction with the trifluoromethyl group on the substrate relative to a methyl group.

2.2 MATERIALS AND METHODS

2.2.1 General

(*R*)- and (*S*)-Mandelic acid, (*S*)-TFL, and all other reagents, unless mentioned otherwise, were purchased from Sigma-Aldrich Canada Ltd. (Oakville, ON). (*R*)-TFL was purchased from SynQuest (Alachua, FL). Protein purifications were conducted using an ÄKTA FPLC from GE Healthcare (Baie d'Urfé, QC) with protein elution detected by monitoring the absorbance at 280 nm. Circular dichroism (CD)-based assays and spectral measurements were conducted using a JASCO J-810 spectropolarimeter. NMR spectroscopic analyses were conducted at the Nuclear Magnetic Resonance Research Resource (NMR-3) using a Bruker AV-300 spectrometer.

2.2.2 Expression and Purification of MR

Recombinant MR from *Pseudomonas putida* was overexpressed in and purified from *Escherichia coli* BL21(DE3) cells transformed with a pET-52b(+) plasmid (Novagen, Madison, WI) containing the MR open reading frame as described previously (Narmandakh & Bearne, 2010). This construct encodes the MR gene product as a fusion protein with an N-terminal StrepII-tag (MASWSHPQFEKGALEVLFQGPGYHM$_1$–MR, where M$_1$ denotes the initial Met of wild-type MR). Briefly, two 10 mL disposable sterile culture tubes containing lysogeny broth (LB, 5 mL) and ampicillin (50 μg/mL) were inoculated with glycerol stock (10 μL each) and incubated overnight at 37 °C with continuous shaking at 250 rpm. The next day, culture (10 mL) from both tubes was used to inoculate LB broth (1.0 L) containing ampicillin (50 μg/mL) in a 2 L Erlenmeyer flask. The culture was incubated for ~ 5.5 h at 37 °C with continuous shaking at 250 rpm (no

induction by IPTG was used (Narmandakh & Bearne, 2010)), the cells were then harvested by centrifugation (3000 ×*g*, 10 min, 4 °C) and the cell pellet was stored at –20 °C until further processing. The frozen pellets (2) were thawed and resuspended in ice-cold wash buffer [Tris-Cl buffer (100 mM, pH 8.0) containing NaCl (150 mM) and EDTA (1 mM)]. The cells were lysed using sonication with 5 × 10 s bursts with 1 min cooling intervals, at a constant power setting of 5.5 using a Branson Sonifier 250. The soluble cell extract was clarified by centrifugation (40,000 ×*g*, 30 min, 4 °C) and the supernatant (18–20 mL) was loaded onto a column containing Strep-Tactin Superflow affinity resin (10 mL) (IBA GmbH, Göttingen, Germany) connected to an ÄKTA FPLC. After washing the column with wash buffer (5 × column volume), the enzyme was eluted by adding wash buffer containing desthiobiotin (2.5 mM). Upon elution, the enzyme was dialyzed against storage buffer [HEPES buffer (100 mM, pH 7.5) containing $MgCl_2$ (3.3 mM), NaCl (200 mM), and glycerol (10%, v/v)] and stored at –20 °C. The purity of the enzyme was assessed using SDS-PAGE (12% acrylamide) with staining by Coomassie blue R-250 (Sambrook *et al*., 1989).

2.2.3 MR Assay

MR activity was assayed using a CD-based assay similar to that described by Sharp *et al*. (1979). All assays were conducted at 25 °C in Na^+-HEPES buffer (0.1 M, pH 7.5) containing $MgCl_2$ (3.3 mM) (i.e., assay buffer) and bovine serum albumin (BSA, ≤ 0.01%). Initial velocities were determined by following the change in ellipticity at 262 or 228 nm when mandelate or TFL was the substrate, respectively, using a quartz cuvette with a 0.2-, 0.5-, or 1-cm light path with (*R*)-TFL, (*S*)-TFL, or mandelate as the substrate,

respectively. The concentrations of mandelate (0.25–10.00 mM) and TFL (0.50–10.00 mM) were as indicated. Substrate solutions were incubated at 25 °C prior to initiation of the reaction by addition of freshly thawed enzyme solution to yield a final concentration of 0.15 or 33 μg/mL when mandelate or TFL was the substrate, respectively. The molar ellipticity for TFL at 228 nm was $[\theta]_{228}$ = 4404 deg mol^{-1} cm^2 (– for (*S*)-TFL and + for (*R*)-TFL).

2.2.4 Data Analysis and Protein Concentration

The values of V_{max} and K_m were determined from plots of the initial velocity (v_i) versus substrate concentration ([S]) by fitting equation 2.1 to the data using nonlinear regression analysis with KaleidaGraph v. 4.02 software from Synergy Software (Reading, PA). All kinetic parameters were determined in triplicate, and average values are reported. The reported errors are standard deviations. Protein concentrations were determined using either the Bio-Rad protein assay (Bio-Rad Laboratories, Mississauga, ON, Canada) with BSA standards or by measuring the absorbance at 280 nm using an extinction coefficient of 53 400 M^{-1} cm^{-1} that was calculated using the ProtParam tool available on the ExPASy server (Gasteiger *et al*., 2003). The values of k_{cat} were obtained by dividing V_{max} values by the total enzyme concentration ($[E]_t$) using Mw = 41 264 Da.

$$v_i = \frac{V_{\max}[S]}{K_m + [S]} \tag{2.1}$$

2.2.5 Product Analysis using ^{19}F NMR spectroscopy

To demonstrate that MR catalyzes the racemization of TFL and that the loss of ellipticity during the CD assay does not result from the β-elimination of fluoride, a product analysis was conducted. Two reaction mixtures (1.0 mL each) were prepared: a control containing 50 mM (*S*)-TFL in assay buffer and an MR reaction mixture containing 50 mM (*S*)-TFL and MR (59 μg/mL) in assay buffer. Each reaction mixture was incubated for 16 h at 25 °C. After 16 h, the MR reaction mixture was passed through a Microcon Ultracel YM-10 centrifugal filter (10 kDa MWCO; Millipore, Billerica, MA) to remove the protein, yielding the MR reaction solution. D_2O, containing trifluoroacetic acid (TFA; 40 mM), was then added to the MR reaction solution and control solution, as an internal standard, to bring the final concentrations of D_2O to 25% (v/v) and TFA to 10 mM. The MR reaction and control solutions were subsequently analyzed using ^{19}F NMR spectroscopy (282.40 MHz).

2.2.6 Effect of Viscosity on Racemization of Trifluorolactate

The dependence of the MR-catalyzed racemization of (*S*)-TFL on solution viscosity was measured as described previously (St. Maurice & Bearne, 2002) using sucrose as the viscosogen because sucrose does not induce major perturbations in MR structure up to a concentration of 35% (w/v) (St. Maurice, 2003). Briefly, stock solutions of varying concentrations of sucrose were prepared in assay buffer at twice the desired final concentration and subsequently diluted 1:1 with assay buffer. Reaction mixtures were prepared in rectangular quartz cuvettes with a 0.5-cm light path. Typically, 400 μL of (*S*)-TFL (0.5–20.0 mM) in Na^+-HEPES buffer (0.1 M, pH 7.5) containing $MgCl_2$ (3.3 mM) was mixed with 500 μL of the viscosogen containing stock solution (prepared at

twice the desired final concentration). The reaction was initiated by addition of 100 μL of wild-type MR (330 μg/mL) in Na^+-HEPES buffer (0.1 M, pH 7.5) containing $MgCl_2$ (3.3 mM) and BSA (0.1%).

2.3 RESULTS

2.3.1 Product Analysis using ^{19}F NMR Spectroscopy

The MR-catalyzed reaction with either (*R*)-TFL or (*S*)-TFL (10 mM) showed a change in ellipticity over time during the CD assay **(Figure 2.3)**. Such a loss in ellipticity could arise because of either the racemization of the TFL enantiomers or β-elimination of fluoride generating 3,3-difluoropyruvate **(Scheme 2.1)**. Although the strong electron-withdrawing effect of the trifluoromethyl group may stabilize the carbanion species inductively to favour racemization, trifluoromethyl carbanions have a higher tendency to release fluoride spontaneously to yield the corresponding difluoro compound (Uneyama *et al*., 2008). In order to demonstrate that MR was catalyzing racemization, ^{19}F NMR spectra were recorded for both a reaction solution containing MR and (*S*)-TFL and for a control solution which lacked MR after each solution had been incubated for 16 h at 25 °C. During this time, the ellipticity of the reaction solution containing MR increased from −200.0 to −92.0 mdeg (at 228 nm), while the ellipticity of the control solution remained unchanged at −118.0 mdeg. (The observed ellipticity of the reaction solution does not go to zero upon completion of the reaction but attains a value of −92 mdeg due to the presence of MR and BSA in the solution.) The signal corresponding to the trifluoromethyl group appeared as a doublet at 0.08 ppm (J_{H-F} = 8.1 Hz, vicinal coupling), relative to the TFA internal standard, in the spectra of both the control and MR reaction

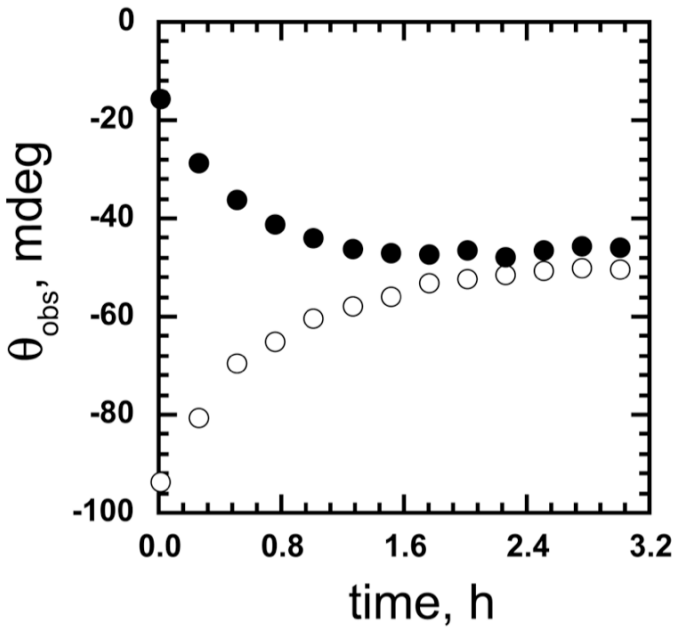

Figure 2.3 Change in CD signal due to the MR-catalyzed reaction with (*R*)-TFL and (*S*)-TFL. The change in ellipticity was followed over time starting with either (*R*)-TFL (●, 10 mM) or (*S*)-TFL (○, 10 mM) as the substrate. The CD signals do not converge at an ellipticity value of zero because the total ellipticity at 228 nm is offset by the presence of MR (1.8 μg/mL) and BSA (80 μg/mL).

Scheme 2.1 Possible reactions that could lead to a reduction in the observed ellipticity.

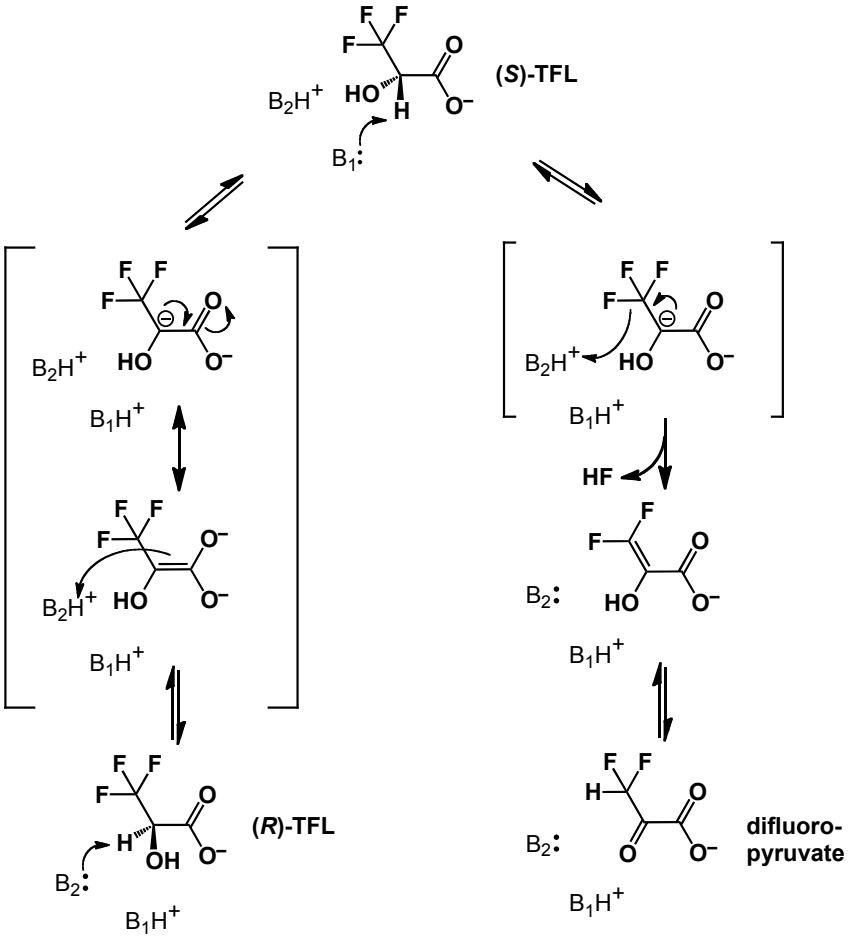

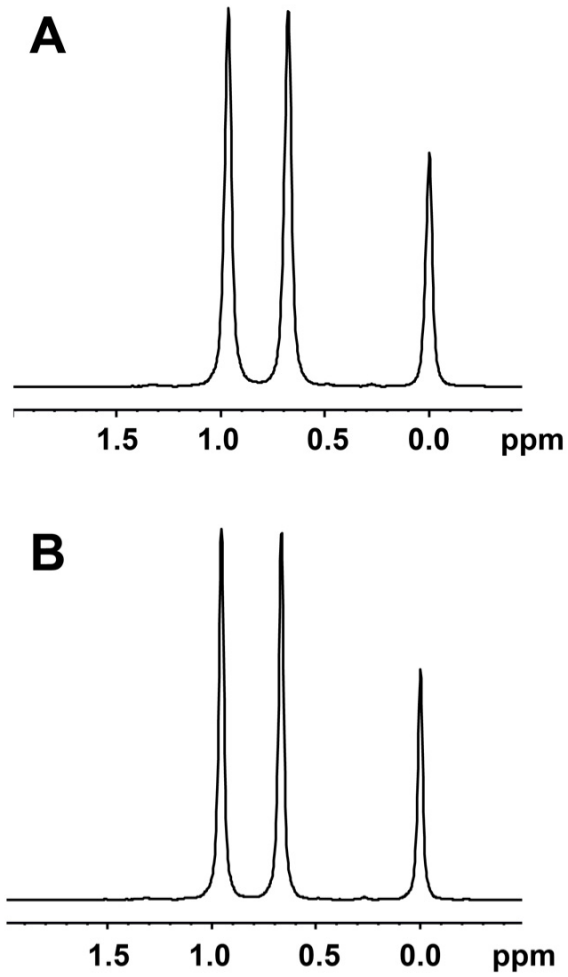

Figure 2.4 Analysis of products after MR reaction with (*S*)-TFL using ^{19}F NMR spectroscopy. ^{19}F NMR spectra of the protein-free MR reaction solution obtained from the reaction of (*S*)-TFL (50 mM) (A) in the absence of MR (i.e., control) and (B) in the presence of MR (59 μg/mL). Chemical shifts are reported relative to trifluoroacetic acid, which was used as internal standard (i.e., $\delta = 0.0$).

samples **(Figure 2.4)**. No fluorine signals corresponding to the $CH\mathbf{F}_2$ group of 3,3-difluoropyruvate (d, J_{H-F} = 53 Hz (Alberg *et al*., 1992), geminal coupling) or fluoride were detected in either spectrum. Hence, there was no evidence that MR catalyzed β-elimination when TFL was the substrate. Apparently, the inductive effects provided by the trifluoromethyl group are sufficient to favor racemization.

2.3.2 Kinetic Characterization

The kinetics of the MR-catalyzed racemization of (*R*)- and (*S*)-TFL obeyed Michaelis-Menten kinetics **(Figure 2.5)**. For (*R*)-TFL, the measured k_{cat} and K_m values were 2.0 ± 0.2 s^{-1} and 1.2 ± 0.2 mM, respectively. In the reverse direction, i.e., for (*S*)-TFL, the values were 2.5 ± 0.3 s^{-1} and 1.74 ± 0.08 mM **(Table 2.1)**, respectively. The K_m values for (*R*)- and (*S*)-TFL were similar to those observed for mandelate (~1 mM) **(Table 2.1)**; but, the turnover numbers (k_{cat}) for the TFL enantiomers were markedly reduced compared to (*R*)-mandelate (792 ± 19 s^{-1}) and (*S*)-mandelate (637 ± 31 s^{-1}) **(Table 2.1)**. To compare the turnover of TFL with mandelate, it is important to bear in mind that superimposition of the carboxyl, hydroxyl, and α-proton of (*R*)-mandelate and (*S*)-TFL places the phenyl group of (*R*)-mandelate in the same spatial orientation as the CF_3 group of (*S*)-TFL (and vice versa). MR catalyzes the racemization of (*R*)-mandelate and (*S*)-mandelate with almost identical kinetic constants **(Table 2.1)**; however, in general, MR catalyzes the racemization of (*R*)-mandelate with a slightly greater turnover number than exhibited for (*S*)-mandelate but binds the latter enantiomer slightly better (St. Maurice & Bearne, 2000, 2002). MR exhibits similar enantioselectivity with TFL, catalyzing the racemization of (*S*)-TFL (*cf*. (*R*)-mandelate) with a greater turnover

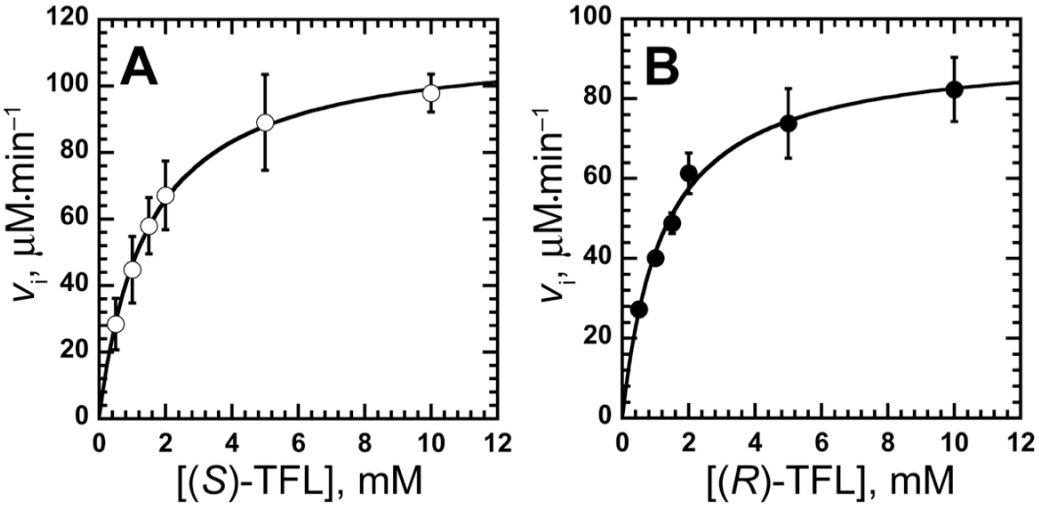

Figure 2.5 Representative Michaelis–Menten plots for MR-catalyzed racemization of (A) (*S*)-TFL and (B) (*R*)-TFL

Table 2.1 Kinetic parameters for the racemization of mandelate and trifluorolactate by MR

substrate	K_m (mM)	k_{cat} (s^{-1})	k_{cat}/K_m ($M^{-1}s^{-1}$)
(*R*)-mandelate	1.2 ± 0.2	792 ± 19	6.5 (± 0.8) × 10^5
(*S*)-mandelate	1.0 ± 0.1	637 ± 31	6.2 (± 0.8) × 10^5
(*R*)-trifluorolactate	1.2 ± 0.2	2.0 ± 0.2	1.6 (± 0.3) × 10^3
(*S*)-trifluorolactate	1.7 ± 0.1	2.5 ± 0.3	1.4 (± 0.2) × 10^3

number than exhibited for (*R*)-TFL but binds the latter enantiomer slightly better.

2.3.3 Viscosity Effects

For many enzymes, the rate-determining step is the chemical conversion of substrate into product within the active site. But some proficient enzymes including acetylcholinesterase (Bazelyansky *et al*., 1986), β-lactamase (Hardy & Kirsch, 1984), carbonic anhydrase (Pocker & Janjic, 1987), triosephosphate isomerase (Blacklow *et al*., 1988), fumarase (Sweet & Blanchard, 1990), and alkaline phosphatase (Simopoulos & Jencks, 1994) have evolved to optimize the chemical step so that it is no longer completely rate-limiting. Instead, external steps such as substrate association and/or product dissociation become partially or fully rate-limiting. Unlike internal processes (i.e., those occuring within the enzyme substrate complex(es)), the rates of these external steps depend on the microviscosity of the solvent (Brouwer & Kirsch, 1982; Mattei *et al*., 1999). MR catalysis with mandelate as the substrate showed partial viscosity dependence (St. Maurice & Bearne, 2002). Because the catalytic efficiency of MR with TFL is reduced by ~ 400-fold **(Table 2.1)**, we examined the effects of solvent viscosity on the steady-state kinetic parameters of MR catalysis with (*S*)-TFL as the substrate using sucrose as the viscosogen **(Table 2.2)**. The values of the relative solvent viscosities ($\eta_{rel} = \eta/\eta°$, where $\eta°$ is the viscosity of the HEPES buffer in absence of added viscosogen) were determined under similar conditions as employed previously using mandelate as the substrate (St. Maurice & Bearne, 2002). The relative values of k_{cat} (i.e., $k_{cat}^{o}/k_{cat}^{\eta}$) and k_{cat}/K_m (i.e., $(k_{cat}/K_m)^{o}/(k_{cat}/K_m)^{\eta}$) showed no dependence on the microviscosity of the solvent **(Figure 2.6)**, suggesting that neither product release nor substrate binding were

Table 2.2 Effect of viscosity on the kinetic parameters for the MR-catalyzed racemization of (*S*)-TFL

sucrose (%)	η/η°	k_{cat} (s^{-1})	K_m (mM)	$k_{cat}^{o}/k_{cat}^{\eta}$	$(k_{cat}/K_m)^{o}/(k_{cat}/K_m)^{\eta}$
0.00	1.00	2.45 ± 0.25	1.74 ± 0.08	1.00 ± 0.14	1.00 ± 0.16
10.0	1.32	2.21 ± 0.43	1.71 ± 0.45	1.11 ± 0.24	1.09 ± 0.38
20.0	1.88	2.53 ± 0.46	1.64 ± 0.51	0.97 ± 0.20	0.92 ± 0.34
27.5	2.48	2.61 ± 0.19	1.49 ± 0.09	0.94 ± 0.12	0.80 ± 0.12
32.5	3.06	2.40 ± 0.05	1.53 ± 0.12	1.02 ± 0.11	0.90 ± 0.13
35.0	3.42	2.04 ± 0.26	1.42 ± 0.36	1.20 ± 0.19	0.98 ± 0.30

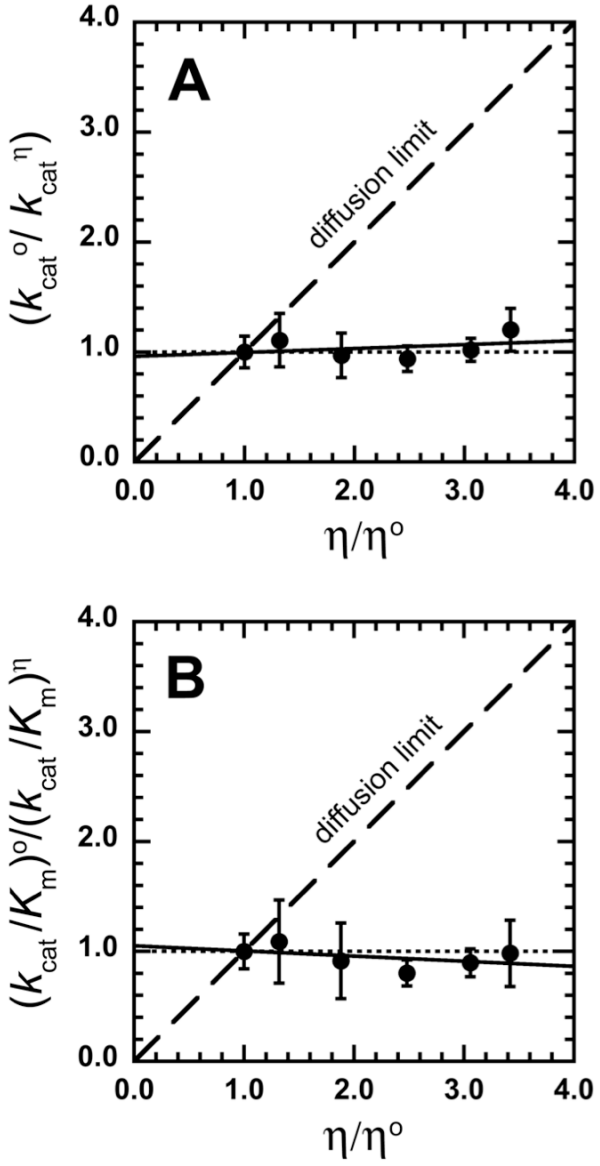

Figure 2.6 Dependence of the relative kinetic parameters for the racemization of (*S*)-TFL on the relative solvent viscosity. The (A) relative k_{cat} (i.e., $k_{cat}^{o}/k_{cat}^{\eta}$) and (B) relative k_{cat}/K_m (i.e., $(k_{cat}/K_m)^{o}/(k_{cat}/K_m)^{\eta}$) values were determined at varying values of η_{rel} using sucrose as the viscosogen. The values of used η_{rel} were from St. Maurice & Bearne (2002). The long dashed line (slope = 1) corresponds to the situation when the rate of the reaction is fully limited by diffusion.

rate-limiting. These results are consistent with the chemical step being rate-limiting (Brouwer & Kirsch, 1982) during the MR-catalyzed racemization of TFL.

2.4 DISCUSSION

2.4.1 TFL as a Substrate

All substrates of MR reported to date have β,γ-unsaturation leading to the notion that delocalization of the negative charge generated upon general base-catalyzed deprotonation of the α-carbon acid is required for catalysis (Felfer *et al*., 2005; Felfer *et al*., 2001; Kenyon & Hegeman, 1970; Li *et al*., 1995; Lin *et al*., 1988; St. Maurice & Bearne, 2002, 2004). However, a suitable electron-withdrawing group, such as the trifluoromethyl group (Bégué & Bonnet-Delpon, 2008; True *et al*., 2003), adjacent to the α-carbon, might also be expected to promote catalysis. For example, the replacement of the methyl group of acetophenone by the trifluoromethyl group favors hydride transfer such that reduction of 2,2,2-trifluoroacetophenone is catalyzed by alcohol dehydrogenase from *Thermus thermophilus* HB27 while acetophenone is not a substrate (Pennacchio *et al*., 2008). Hence, the possibility that TFL could serve as a substrate for the MR-catalyzed racemization reaction was investigated.

MR-catalyzed interconversion of mandelate enantiomers proceeds via formation of carbanion intermediate (Kenyon & Hegeman, 1970; Lin *et al*., 1988). Formation of such an intermediate when TFL is substrate can have two fates **(Scheme 2.1)**: either it can accept a proton from the conjugate acid of an active site Brønsted base to either invert or retain the stereochemistry, or it can undergo defluorination to yield difluoropyruvate. ^{19}F NMR spectroscopic analysis of the products of the MR-catalyzed

reaction with TFL was consistent with the absence of the β-elimination product, difluoropyruvate. When TFL is the substrate, the negative charge of the resulting carbanion could delocalize into the π-system of the α-carboxyl group to prevent accumulation of negative charge on the fluorine atoms and thus avoid fluoride elimination (Uneyama *et al*., 2008). These results are consistent with earlier reports that show that the α-trifluoromethyl carbanions are stabilized by the electron withdrawing groups such as esters (Fuchigami & Nakagawa, 1987), nitro groups (Seebach *et al*., 1986), or carbonyl groups (Itoh *et al*., 2003). Thus, the observed reduction of the ellipticity **(Figure 2.3)** and the absence of β-elimination product **(Figure 2.4)** indicate that MR catalyzes the racemization of (*R*)- and (*S*)-TFL. These results are further supported by the observation that MR catalyzed the exchange of the α-proton with deuterium when the reaction was conducted in buffered D_2O (Nagar *et al*., 2011), consistent with deprotonation-reprotonation events.

Although the inductive stabilization afforded by the trifluoromethyl group favored enzymatic proton abstraction as expected, the fact that MR exhibits very low affinity for lactate ($K_i \approx 30$ mM) (St. Maurice & Bearne, 2004) suggested that it might also exhibit low affinity for TFL. Surprisingly, this was not the case. Indeed, the K_m values for (*R*)- and (*S*)-TFL are ~ 1–2 mM, similar to those for mandelate **(Table 2.1)**. Previous studies have shown that the dependence of binding free energies for glycolate analogues on π (π being the hydrophobicity substituent constant based on partitioning coefficients between octanol and water (Hansch & Leo, 1979)) follows the equation $\log(K_m \text{ or } K_i) = (-0.72\ (\pm 0.08) \times \pi) - 1.4\ (\pm 0.1)$ (St. Maurice & Bearne, 2004). The steric volume of a CF_3 group is much larger than that of a methyl group, approximating that of an isopropyl group

(Bégué & Bonnet-Delpon, 2008; Yamazaki *et al*., 2009). The value of π for the CF_3 group is 0.88 (Hansch & Leo, 1979), indicating that the value of K_m for TFL should be ~10 mM (i.e., 10 ± 6 mM). Hence, MR appears to bind the CF_3 group of TFL with an affinity that exceeds that predicted from hydrophobic effects alone by about 5–10-fold. These calculations suggest that additional binding interactions may be involved in recognition of the CF_3 group.

DiMagno suggested that "polar hydrophobicity" of trifluoromethyl group in ligands might provide unique opportunities that enhance binding within a protein target (Biffinger *et al*., 2004; Kim *et al*., 1998). Although C–F bonds have rather limited H-bond acceptor ability (Bégué & Bonnet-Delpon, 2008; Dunitz, 2004), weak H-bond interactions with the conjugate acid of one of the active site Brønsted base catalysts and optimally aligned F--H-N-amide interactions could contribute to binding. In addition, orthogonal dipolar interactions with polarizable bonds on the protein (Fischer *et al*., 2007; Olsen *et al*., 2004; Paulini *et al*., 2005; Yamazaki *et al*., 2009), i.e., interactions of C–F with amide carbonyls in a specific orientation, reminiscent of trajectory-dependent n-π* (amine-carbonyl) interactions (Berkowitz *et al*., 2008; Burgi *et al*., 1973), could also enhance the binding of the trifluoromethyl group in the active site. Replacement of the methyl group of lactic acid by the trifluoromethyl group reduces the pK_a value of the carboxylic acid group from 3.86 in lactic acid (Jencks & Regenstein, 1968) to 2.75 in racemic TFL (Götzö & Seebach, 1996). Although this reduction in pK_a of the carboxylic acid likely has little effect on binding, the accompanying reduction in the pK_a value of the α-hydroxyl group (Yamazaki *et al*., 2009) could result in stronger interactions with the magnesium ion within the active site. It is surprising that MR, as a member of the enolase

superfamily, exhibits enhanced affinity for TFL relative to lactate. Conversely, yeast and muscle enolase have been shown to bind the 2-phosphoglycolate analogue $\mathbf{CH_3}CH(OPO_3H^-)COO^-$ with a dissociation constant of ~0.4 mM but do not bind $\mathbf{CF_3}CH(OPO_3H^-)COO^-$ (Stubbe & Abeles, 1980).

Although MR binds TFL with an affinity similar to that exhibited for mandelate, MR catalyzes the racemization of TFL with efficiencies that are ~400-fold lower than those observed for mandelate **(Table 2.1)**. This reduction in catalytic efficiency arises mainly from the reduction in the k_{cat} values by ~318-fold **(Table 2.1)**. The value of K_{eq} (treating (*S*)-TFL as the product) calculated using the Haldane relation (Segel, 1975) is 0.9 ± 0.2, which is experimentally equal to unity, as expected for a racemase.

2.4.2 Transition State Stabilization

The efficiency (k_{cat}/K_m) of an enzyme-catalyzed reaction and the rate constant for the corresponding non-enzymatic reaction (k_{non}) may be used to estimate an upper limit for the virtual dissociation constant ($K_{tx} = k_{non}/(k_{cat}/K_m)$) for the complex between the enzyme and the altered substrate in the transition state (Radzicka & Wolfenden, 1995a; Wolfenden, 1972; Wolfenden, 1976). The free energy of activation for the nonenzymatic racemization of TFL (ΔG_{non}) under assay conditions, at 25 °C, is equal to 33 (± 4) kcal/mol which corresponds to a nonenzymatic rate constant of $\sim \times 10^{-12}$ s^{-1} (Nagar *et al*., 2011). Comparison of k_{non} with the turnover number for the MR-catalyzed racemization of (*S*)-TFL ($k_{cat} = 2.5$ s^{-1}) suggests a rate enhancement of (6.3×10^{11})-fold at pH 7.5 and 25 ° C.

Comparison of k_{non} with the efficiency of MR-catalyzed racemization of (*S*)-TFL

(k_{cat}/K_m = 1.4 × 10^3 $M^{-1}s^{-1}$) indicates that the upper limit for K_{tx} is ~ 3 × 10^{-15} M. Hence, MR stabilizes the altered TFL in the transition state (ΔG_{tx}) by at least 20 kcal/mol **(Figure 2.7 B)**. This is slightly less than the transition state stabilization of 26 kcal/mol afforded by MR when mandelate is the substrate **(Figure 2.7 A)** (Bearne & Wolfenden, 1997). Interestingly, the free energy of activation at 25 °C for the nonenzymatic racemization of mandelate (34.6 ± 0.9 kcal/mol, (Bearne & Wolfenden, 1997)) is experimentally equal to the free energy of activation for the nonenzymatic racemization of TFL. Even though the barriers for abstraction of the α-proton in the absence of the enzyme are essentially equivalent for mandelate and TFL, such is not the case for bound mandelate and TFL since their k_{cat} values differ by ~318-fold. The acidifying effect of the phenyl ring of mandelate arises from both polar (inductive) effects and conjugation (Lowry & Richardson, 1981). Since MR stabilizes the transition state for racemization of mandelate more effectively than it stabilizes the transition state for racemization of TFL by ~ 6 kcal/mol, MR must interact with the phenyl ring of mandelate in the transition state to stabilize the negative charge more effectively through conjugation than can be achieved through inductive effects alone. For the enzymatic reaction, as opposed to the racemization of mandelate in solution, the binding of mandelate within the active site can enhance the acidity of the α-proton by enforcing a conformation of the phenyl ring that ensures efficient conjugation **(Figure 2.2)**. Such is not the case for TFL. Furthermore, MR may enhance conjugation through cation-π interaction as suggested by previous findings from the Bearne lab that MR binds the phenyl ring of transition state analogues with an affinity that exceeds that predicted based on hydrophobic effects alone by ~72-fold (St. Maurice & Bearne, 2004). Although such interactions may also play a role in the

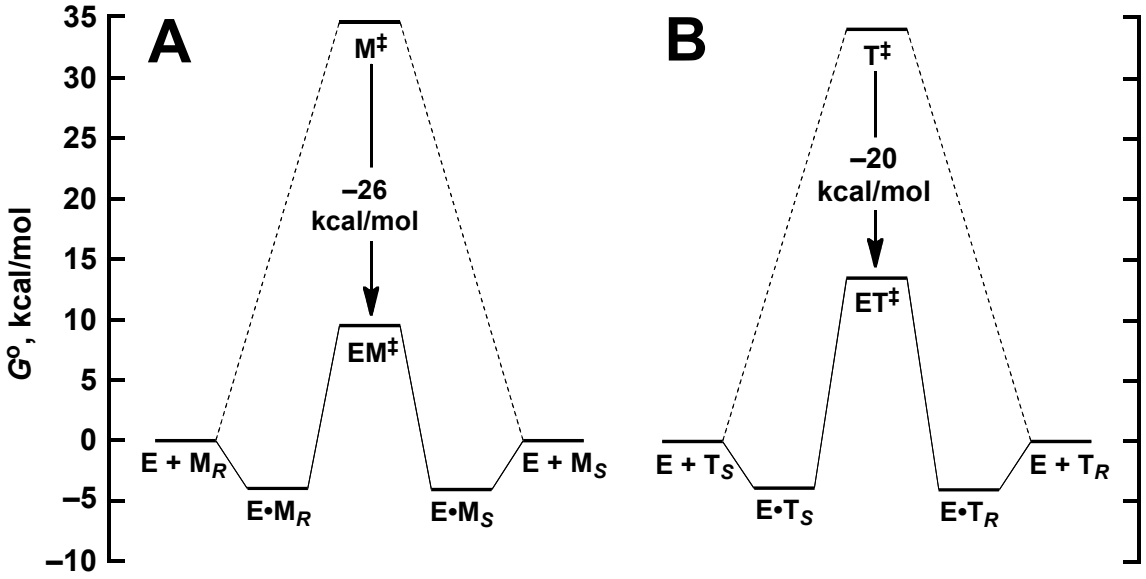

Figure 2.7 Reaction coordinate diagram for MR-catalyzed racemization of (A) (*R*)-mandelate (M_R) and (*S*)-mandelate (M_S) and (B) (*S*)-TFL (T_S) and (*R*)-TFL (T_R). The free energy profiles are derived using the kinetic parameters given in Table 2.1. $T^{‡}$ and $M^{‡}$ represent the altered TFL and mandelate in the transition state, respectively, in the absence of enzyme. $ET^{‡}$ and $EM^{‡}$ represent the corresponding enzyme–substrate complexes in the transition state. The black arrows show the extent of transition state stabilization. (Values are calculated for a standard state of 1 M.)

enhanced ground state binding of TFL, the binding affinity of TFL only exceeds that predicted based on hydrophobic effects alone by ≤ 10-fold (*vide supra*). The enzyme's propensity to stabilize conjugation in the transition state is further illustrated by the fact that the value of k_{cat} for MR-catalyzed racemization of vinylglycolate **(Figure 2.1)** is only reduced about 4-fold, relative to the value of k_{cat} for mandelate (Li *et al*., 1995).

When mandelate is the substrate, both the chemical (proton abstraction) and product release steps are partially rate-determining as indicated by the partial viscosity dependence of MR catalysis reported previously (St. Maurice & Bearne, 2002). Similar is the case with racemization of vinylglycolate. For this minimal substrate of MR, the primary kinetic isotope effect (KIE) ~4 suggested that proton abstraction is partially rate-limiting (Li *et al*., 1995). Because MR is not as proficient at stabilizing the altered TFL in the transition state as it is at stabilizing the altered mandelate in the transition state, the viscosity dependence of MR catalysis with (*S*)-TFL as the substrate, using sucrose as the viscosogen, was examined **(Table 2.2 and Figure 2.6)**. Indeed, no dependence on the microviscosity of the solvent was observed, consistent with the chemical step being rate-limiting (Brouwer & Kirsch, 1982). In this scenario, the observed rate constant, k_{cat} is equal to the rate constant for the chemical step (k_2) and thus calculation of K_{tx} ($K_{tx} = k_{non}/(k_{cat}/K_m)$) using k_{cat} provides a good approximation of TS stabilization (Wolfenden, 1972).

Thus, studies in this chapter have demonstrated that MR does not exhibit an absolute requirement for substrates having β,γ-unsaturation. The minimal substrate model of MR suggested by Felfer *et al*. (2005) should therefore be extended. Replacement of the phenyl ring of mandelate by the electron-withdrawing trifluoromethyl group is sufficient

to permit MR to catalyze the racemization of TFL. However, MR catalyzes the racemization of this "activated" substrate with reduced catalytic proficiency relative to that observed for the racemization of substrates possessing β,γ-unsaturation.

CHAPTER 3

INHIBITION OF MR BY FLUORINATED GROUND STATE AND TRANSITION STATE/INTERMEDIATE ANALOGUES

Reproduced in part with permission from – Nagar, M., Lietzan, A. D., St. Maurice, M., and Bearne, S. L. (2014) Potent Inhibition of Mandelate Racemase by a Fluorinated Substrate-Product Analogue with a Novel Binding Mode. Biochemistry ***53****, 1169–1178.*

3.1 INTRODUCTION

As demonstrated in the previous chapter, enantiomers of 3,3,3-trifluorolactate (TFL) also serve as substrates of MR (Nagar *et al*., 2011). Although k_{cat} for this substrate was reduced by ~100-fold relative to mandelate as a substrate, the binding affinity (K_m) for (*S*)- and (*R*)-TFL is similar to that observed for (*R*)- and (*S*)-mandelate **(Table 2.1)**. That MR exhibited such high binding affinity for TFL was unexpected considering that MR binds lactate with low affinity ($K_i \approx 30$ mM, (St. Maurice & Bearne, 2004)). Indeed, the rather high binding affinity that MR exhibits for TFL exceeds that expected on the basis of hydrophobic effects alone (Nagar *et al*., 2011). Therefore, the binding advantage offered by the trifluoromethyl group could be exploited to design fluorinated ground state and transition state (TS) analogue inhibitors of MR.

Studies on MR (Siddiqi *et al*., 2005), glutamate racemase (Pal & Bearne, 2014), serine racemase, and proline racemase (Harty *et al*., 2014) in the Bearne lab have revealed that mimicking the structure of both substrate enantiomers (i.e., a substrate-product analogue) could serve as a useful strategy for designing and developing inhibitors of racemases. For example, benzilate ($K_i = 0.67$ mM, (Siddiqi *et al*., 2005)), the substrate-product analogue of mandelate is believed to bind such that the two phenyl rings occupy

both the *R*- and *S*- binding pockets that normally bind the phenyl rings of (*R*)- and (*S*)-mandelate, respectively (Nagar *et al*., 2014; Siddiqi *et al*., 2005) **(Figure 3.1)**. This ligand binds with an affinity that is similar to that exhibited for mandelate. Since TFL is also a substrate for MR, replacing the α-H of TFL with a $-CF_3$ group could furnish an inhibitor of MR in a fashion similar to benzilate **(Figure 3.2)**.

An alternative strategy for developing an inhibitor of MR would be to design a TS analogue based on the MR-catalyzed racemization of TFL. Generally, TS analogues are more potent inhibitors (Radzicka & Wolfenden, 1995b; Wolfenden, 1972; Wolfenden, 1976) compared to substrate-product analogues, which mimic the ground state. In fact, α-hydroxybenzylphosphonate (α-HBP) (St. Maurice & Bearne, 2000), a phosphonate-containing analogue of mandelate that mimicks the dianionic character of the *aci*-carboxylate intermediate has been shown to bind MR ~100-fold more tightly than mandelate (substrate) and benzilate (substrate-product analogue). As the racemization of TFL and mandelate is expected to proceed by a similar mechanism, a TS analogue inhibitor of MR might be designed by replacing the carboxylate of TFL with a phosphonate moiety **(Figure 3.2)**.

The present chapter describes the competitive inhibition of MR by the substrate-product analogue 3,3,3-trifluoro-2-hydroxy-2-(trifluoromethyl)propanoate (TFHTP) and the corresponding non-fluorinated analogue α-hydroxyisobutyrate, and by the TS/intermediate analogues (*R*,*S*)-2,2,2-trifluro-1-hydroxyethylphophonate (TFHEP) and the corresponding non-fluorinated (*R*,*S*)-1-hydroxyethylphophonate (1-HEP). Surprisingly, TFHTP is a potent inhibitor that binds MR ~25-times more tightly than TFHEP. The x-ray crystal structure of MR with bound TFHTP, solved in the St. Maurice

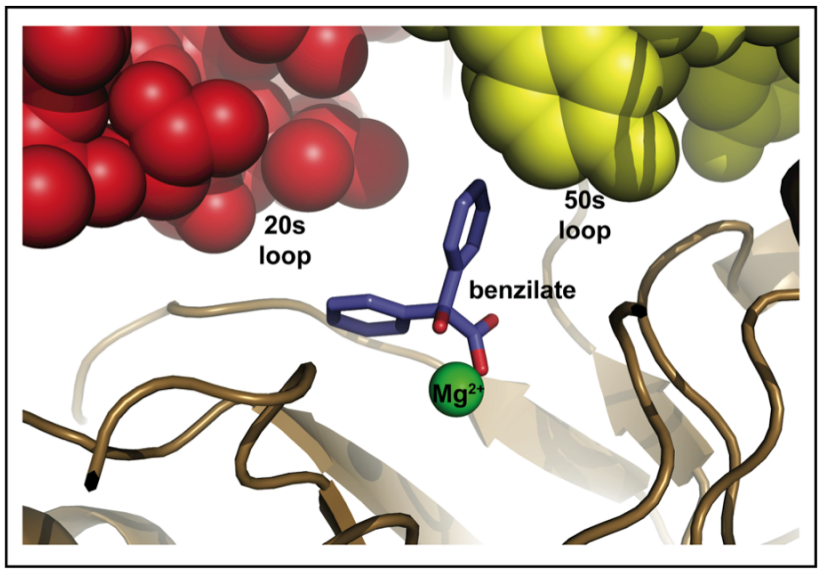

Figure 3.1 Active-site view of C92S/C264S/K166C-MR with bound benzilate [PDB entry 4HNC (Nagar *et al*., 2014)]. Phenyl rings of bound benzilate (purple) interact with hydrophobic pocket. Residues of the putative *R*-pocket (red) and *S*-pocket (yellow) are shown in space filling representation. Mg^{2+} ion is shown in green.

Figure 3.2 Inhibitor design based on the various substrates of MR

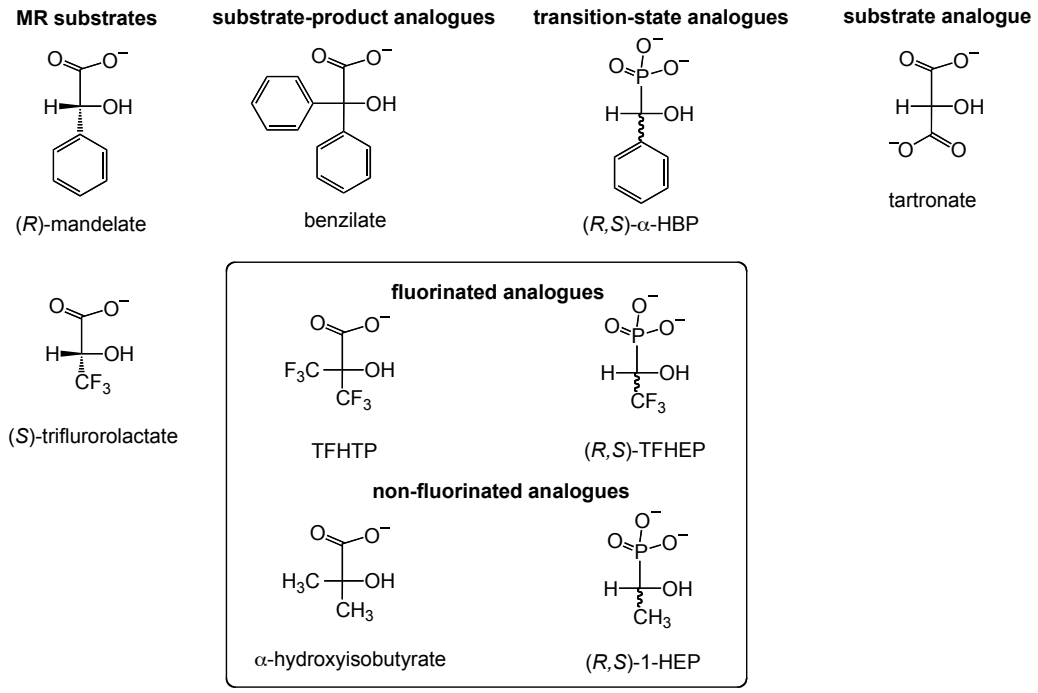

laboratory (Department of Biological Sciences, Marquette University, Wisconsin, USA), reveals that the higher binding affinity of TFHTP arises, in part, due to a novel binding orientation in which the carboxylate group forms a salt bridge between the Brønsted acid-base catalysts His 297 and Lys 166. Recognizing this novel-binding mode, tartronic acid (an analogue of mandelate in which phenyl ring is replaced by a carboxylate group, **Figure 3.2**) is predicted and shown to be a competitive inhibitor of MR.

3.2 MATERIALS AND METHODS

3.2.1 General

(*R*)-Mandelic acid, α-hydroxyisobutyric acid, 3,3,3-trifluoro-2-hydroxy-2-(trifluoromethyl)propanoic acid, and all other reagents, unless mentioned otherwise, were purchased from Sigma-Aldrich Canada Ltd. (Oakville, ON, Canada). Tartronic acid was purchased from Alfa Aesar (Ward Hill, MA). (*R,S*)-TFHEP was prepared from diethyl 1-hydroxy-2,2,2-trifluroethylphophonate by Dr. S. L. Bearne (Nagar *et al*., 2014) using a procedure similar to that described by Freeman *et al*. (1991). NMR analyses were conducted at the Nuclear Magnetic Resonance Research Resource (NMR-3) using either a Brüker/Tecmag AC-250 spectrometer, a Brüker AV-300 spectrometer, or a Brüker AV-500 spectrometer. Chemical shifts (δ) for proton (^{1}H), carbon (^{13}C), and phosphorus (^{31}P) spectra are reported in ppm. The deuterium signal was used to lock the spectrophotometer frequency for ^{1}H and ^{13}C NMR and used as the reference, while for ^{31}P NMR, 80% phosphoric acid was used as an external reference. High resolution electrospray ionization (ESI) mass spectra (MS) were collected using a Brüker microTOF Focus orthogonal ESI-TOF mass spectrometer instrument operating in either positive or negative ion mode. Circular dichroism (CD) assays were conducted using a JASCO J-810 spectropolarimeter (Jasco Inc., Easton, MD) with a jacketed cell holder. Melting points are uncorrected.

3.2.2 Synthesis of (*R,S*)-1-Hydroxyethylphosphonate

Dimethyl 1-hydroxyethyl-phosphonate was synthesized as described previously (Chen *et al*., 2006). Dimethyl phosphite (1.10 g, 10 mmol) and acetaldehyde (0.44 g, 10

mmol) were stirred together for 10 min at room temperature, followed by addition of potassium fluoride and basic alumina (1:1 mass ratio, 3 g each). After stirring the mixture for another 30 min, methylene chloride (15 mL) was added and the resulting suspension was filtered. From the filtrate, methylene chloride was evaporated under reduced pressure leaving 0.68 g of dimethyl 1-hydroxyethylphosphonate as a viscous yellow liquid. The methyl groups were removed from dimethyl 1-hydroxyethylphosphonate by treatment with trimethylsilylbromide using a procedure similar to that described by Freeman *et al*. (Freeman *et al*., 1991) Dimethyl 1-hydroxyethylphosphonate (0.49 g, 3.2 mmol) was dissolved in dry acetonitrile (10 mL) and trimethylsilylbromide (2.26 mL, 17.5 mmol, 5.0 equiv.) was added dropwise to the solution. The solution was refluxed for 1 h under an atmosphere of argon, and the solvent was removed using rotary evaporation under reduced pressure to yield a slightly yellow liquid. Dioxane (3.4 mL), water (3.4 mL), and cyclohexylamine (1.6 mL) were added, and the solution was stirred for 1 h at room temperature. After removal of the solvent using rotary evaporation, a slightly yellow liquid was obtained. This was dissolved in water (16 mL) and then acetone (150–250 mL) was added until the cyclohexylamine salt formed as a white precipitate. After cooling overnight at 4 °C, the precipitate was collected using suction filtration. The cyclohexylamine salt was then converted to the sodium salt by passing it through a column containing AG 50W-X8 (Na^+-form). Fractions containing phosphonate were pooled and lyophilized to obtain the sodium salt of 1-hydroxyethylphosphonate as a white powder (0.224 g, 41%): mp 223–225 °C; ^{1}H NMR (D_2O, 500 MHz) δ 1.23 (dd, $^3J_{H,H}$ = 7.1 Hz, $^3J_{H,P}$ = 15.9 Hz, 3H, CH_3), 3.74 (dq, $^3J_{H,H}$ = 7.1 Hz, $^2J_{H,P}$ = 5.9 Hz, 1H, OC*H*P); ^{13}C NMR (D_2O, 126 MHz, ^{1}H-decoupled) δ 17.10 (CH_3), 64.72 (d, $^1J_{C,P}$ = 157.9

Hz, O*C*HP); ^{31}P NMR (D_2O, 202 MHz, ^{1}H-decoupled) δ 20.94; ^{31}P NMR (D_2O, 202 MHz, ^{1}H-coupled,) δ 20.94 (dq, $^2J_{H,P}$ = 5.91 Hz, $^3J_{H,P}$ = 15.90 Hz). HRMS (ESI^+) m/z calculated for $C_2H_6Na_2O_4P$ $[M+H]^+$: 170.9799, found 170.9800.

3.2.3 Concentration Correction for TFHEP and 1-HEP

^{1}H NMR spectroscopy was used to correct for the presence of waters of hydration and sodium ion stoichiometry, and thereby permit accurate estimation of the concentration of TFHEP and 1-HEP in solution. Equimolar solutions (20 mM based on the theoretical molecular weight) of 1-HEP (170.01 g/mol) or TFHEP (223.98 g/mol) and sodium acetate were prepared in 5 mL of D_2O. ^{1}H NMR spectra for these solutions were obtained and integrated signal intensities corresponding to the α-H and α-CH_3 of 1-HEP, and the α-H of TFHEP, were determined and compared to the signal intensities of the methyl protons of the sodium acetate internal standard. The actual concentrations of 1-HEP and TFHEP were then calculated from the ratio of the signal intensities and known concentration of sodium acetate.

3.2.4 Expression and Purification of MR

Recombinant wild-type MR from *Pseudomonas putida* was over-expressed in and purified from *E. coli* BL21(DE3) cells transformed with the pET-52b(+)-wtMR, as described in Chapter 2 (section 2.2.2).

3.2.5 MR Inhibition Kinetics

MR activity was assayed using a CD-based assay by following the change in ellipticity of mandelate at 262 nm with a 1-cm light path (unless otherwise indicated) as described by Sharp *et al*. (1979). Inhibition experiments with TFHEP, 1-HEP, TFHTP, tartronate, and α-hydroxyisobutyrate were conducted at 25 °C in Na^+-HEPES buffer (0.1 M, pH 7.5) containing $MgCl_2$ (3.3 mM) and BSA (0.005%). The concentration of (*R*)-mandelate in the assay mixture ranged from 0.25–20.0 mM. The concentrations of the inhibitor and MR used, respectively, were: TFHEP (0.81, 1.62, & 3.24 mM; 150.72 ng/mL; using a cuvette with a 0.5-cm light-path for 3.24 mM TFHEP), 1-HEP (16.37, 32.74, & 65.49 mM; 122.4 ng/mL; using a cuvette with a 0.5-cm light-path), TFHTP (0.02, 0.05, & 0.10 mM; 129.8 ng/mL), tartronate (0.75, 1.50, & 3.00 mM; 131.45 ng/mL), and α-hydroxyisobutyrate (3.5, 7.0, & 14.0 mM; 141.55 ng/mL; using a cuvette with a 0.5-cm light-path).

The apparent kinetic constants V_{max} and K_m were determined by fitting equation 3.1 to the initial velocity data using nonlinear regression analysis and the program KaleidaGraph v. 4.02 from Synergy Software (Reading, PA). Competitive inhibition constants (K_i) were determined from plots of the apparent K_m/V_{max} values versus inhibitor concentration in accord with equation 3.2 (Segel, 1975). All kinetic parameters were determined in triplicate and average values are reported. The reported errors are standard deviations. The concentration of MR was determined from its absorbance at 280 nm using an extinction coefficient of 53 400 M^{-1} cm^{-1}, which was calculated using the ProtParam tool available on the ExPASy server (http://web.expasy.org/protparam) (Gasteiger *et al*., 2003).

$$v_i = \frac{V_{\max}[\mathrm{S}]}{K_{\mathrm{m}} + [\mathrm{S}]} \tag{3.1}$$

$$v_i = \frac{V_{\max}[\mathrm{S}]}{K_{\mathrm{m}}(1 + \frac{[\mathrm{I}]}{K_{\mathrm{i}}}) + [\mathrm{S}]} \tag{3.2}$$

3.3 RESULTS

Both TFHTP and TFHEP, and their corresponding non-fluorinated analogues α-hydroxybutyrate and 1-HEP respectively, were found to be competitive inhibitors of MR **(Figures 3.3, 3.4, 3.5,** & **3.6)**. Surprisingly, MR bound TFHTP with an affinity (K_i = 27 ± 4 μM) that exceeded that exhibited for mandelate and TFL by ~54-fold **(Table 3.1)**. However, MR showed low affinity for the corresponding non-fluorinated analogue, α-hydroxyisobutyrate (K_i = 5.5 ± 0.6 mM), indicating that the presence of the six fluorine atoms increased the binding affinity by ~200-fold. The TS/intermediate analogue of TFL, i.e., (*R*,*S*)-TFHEP (K_i = 0.67 ± 0.12 mM), bound MR with an affinity that is 60-fold greater than that exhibited for the corresponding non-fluorinated analogue, (*R*,*S*)-1-HEP (K_i = 40.2 ± 4.8 mM). Interestingly, the substrate-product analogue of TFA, TFHTP showed ~60-fold higher binding affinity compared to TFHEP. In addition, tartronate, a mandelate analogue that bears a polar carboxylate group in place of the nonpolar phenyl ring, was also a competitive inhibitor of MR **(Figure 3.7)** that bound MR with a binding affinity (K_i = 1.8 ± 0.1 mM) that was similar to that observed for the substrates mandelate and TFL **(Table 3.1)**.

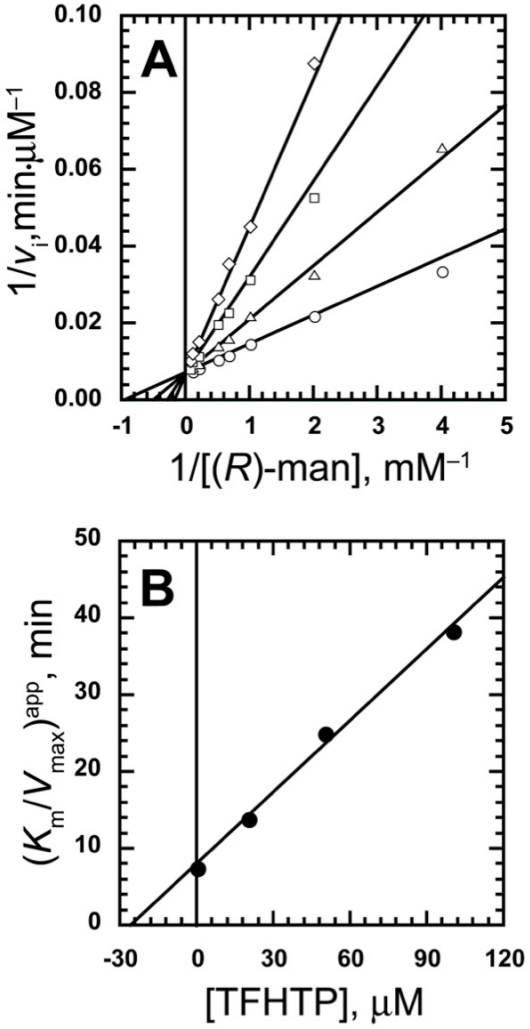

Figure 3.3 Inhibition of MR by (*R*,*S*)-2,2,2-trifluoro-1-hydroxyethylphosphonate (TFHTP). (A) A representative Lineweaver-Burk plot showing competitive inhibition of MR by TFHTP. Assays were conducted as described in section 3.2.5 with the concentration of (*R*)-mandelate ((*R*)-man) ranging between 0.25–10.0 mM, and concentrations of TFHTP equal to 0 μM (○), 20 μM (△), 50 μM (□), and 100 μM (◇). (B) A representative replot of the apparent K_m/V_{max} values (obtained by fitting equation 3.1 to the initial velocity data) as a function of TFHTP concentration. The negative of the x-intercept yields the K_i value (equation 3.2). The average value of $K_i = 27 \pm 4$ μM.

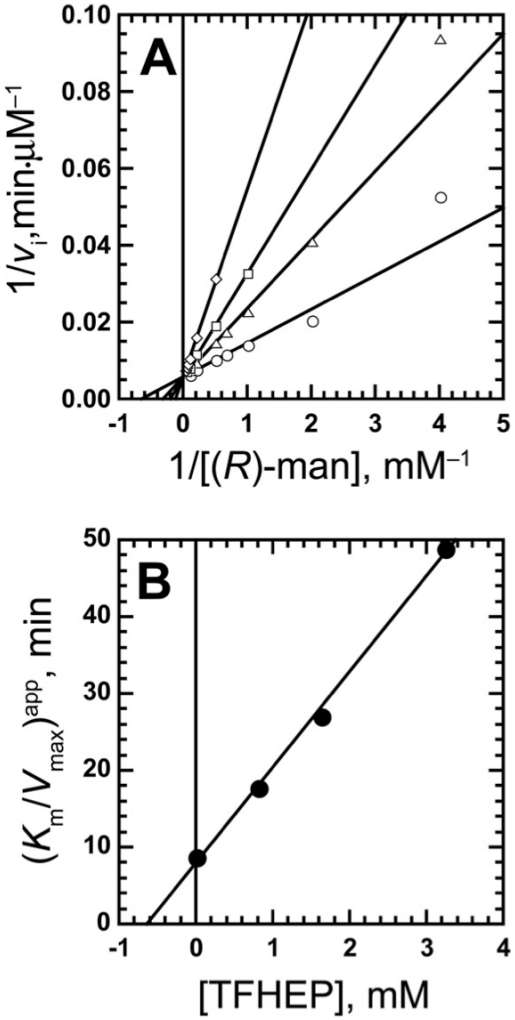

Figure 3.4 Inhibition of MR by (*R*,*S*)-2,2,2-trifluoro-1-hydroxyethylphosphonate (TFHEP). (A) A representative Lineweaver-Burk plot showing competitive inhibition of MR by TFHEP. Assays were conducted as described in section 3.2.5 with the concentration of (*R*)-mandelate ((*R*)-man) ranging between 0.25–10.0 mM, and concentrations of TFHEP equal to 0 mM (○), 0.81 mM (△), 1.62 mM (□), and 3.24 mM (◇). (B) A representative replot of the apparent K_m/V_{max} values (obtained by fitting equation 3.1 to the initial velocity data) as a function of TFHEP concentration. The negative of the x-intercept yields the K_i value (equation 3.2). The average value of K_i = 0.67 ± 0.13 mM

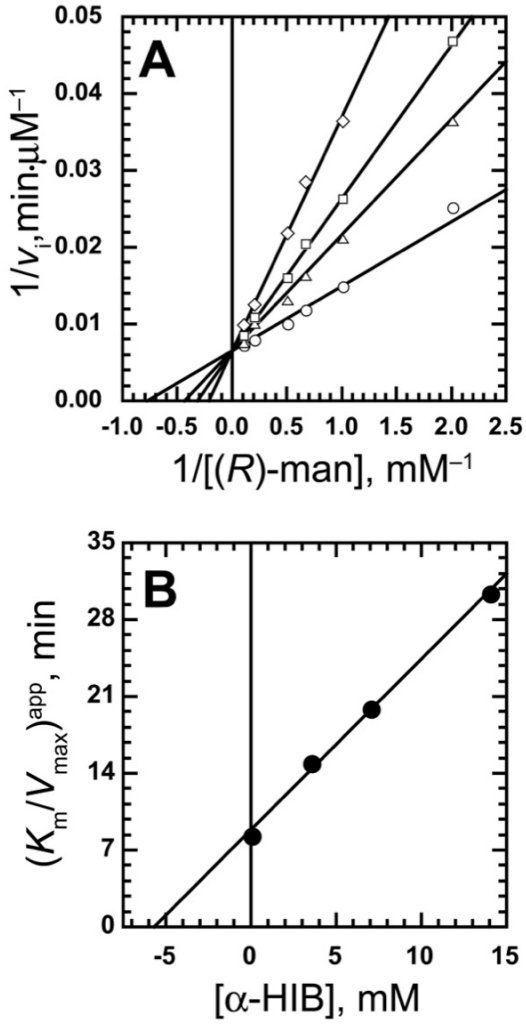

Figure 3.5 Inhibition of MR by α-hydroxyisobutyrate (α-HIB). (A) A representative Lineweaver-Burk plot showing competitive inhibition of MR by α-HIB. Assays were conducted as described in section 3.2.5 with the concentration of (*R*)-mandelate ((*R*)-man) ranging between 0.5–10.0 mM, and concentrations of α-HIB equal to 0 mM (○), 3.5 mM (△), 7.0 mM (□), and 14.0 mM (◇). (B) A representative replot of the apparent K_m/V_{max} values (obtained by fitting equation 3.1 to the initial velocity data) as a function of α-HIB concentration. The negative of the x-intercept yields the K_i value (equation 3.2). The average value of $K_i = 5.5 \pm 0.6$ mM.

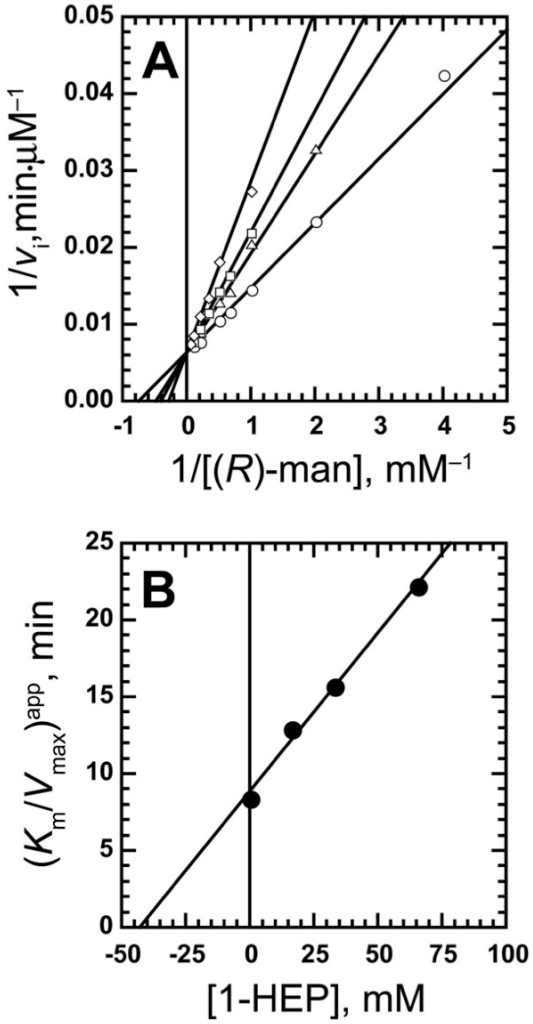

Figure 3.6 Inhibition of MR by (*R*,*S*)-1-hydroxyethylphosphonate (1-HEP). (A) A representative Lineweaver-Burk plot showing competitive inhibition of MR by 1-HEP. Assays were conducted as described in section 3.2.5 with the concentration of (*R*)-mandelate ((*R*)-man) ranging between 0.25–10.0 mM, and concentrations of 1-HEP equal to 0 mM (○), 16.37 mM (△), 32.74 mM (□), and 65.49 mM (◇). (B) A representative replot of the apparent K_m/V_{max} values (obtained by fitting equation 3.1 to the initial velocity data) as a function of 1-HEP concentration. The negative of the x-intercept yields the K_i value (equation 3.2). The average value of K_i = 40.2 ± 4.8 mM

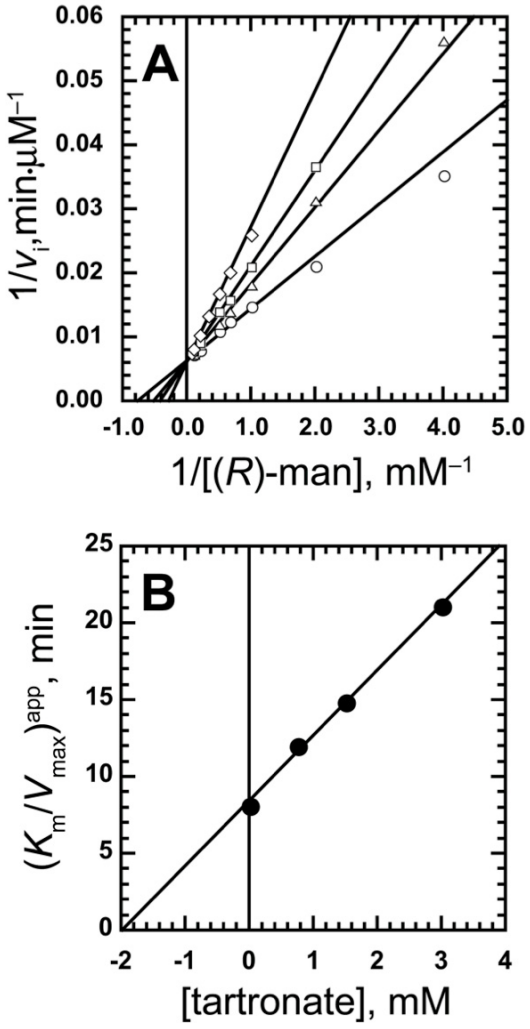

Figure 3.7 Inhibition of MR by tartronate. (A) A representative Lineweaver-Burk plot showing competitive inhibition of MR by tartronate. Assays were conducted as described in section 3.2.5 with the concentration of (*R*)-mandelate ((*R*)-man) ranging between 0.25–10.0 mM, and concentrations of tartronate equal to 0 mM (○), 0.75 mM (△), 1.5 mM (□), and 3.0 mM (◇). (B) A representative replot of the apparent K_m/V_{max} values (obtained by fitting equation 3.1 to the initial velocity data) as a function of tartronate concentration. The negative of the x-intercept yields the K_i value (equation 3.2). The average value of $K_i = 1.8 \pm 0.1$ mM.

Table 3.1 Binding constants for substrates, ground state analogues, and transition state/intermediate analogues

$R^1R^2R^3COH$				
R^1	**R^2**	**R^3**	**Ligand**	**K_i (mM)** [a]
Substrates/substrate analogues				
$-C_6H_5$	–H	$-COO^-$	(*R*)-mandelate	1.2 (± 0.2)[b]
			(*S*)-mandelate	1.0 (± 0.1)[b]
$-CF_3$	–H	$-COO^-$	(*R*)-trifluorolactate ((*R*)-TFL)	1.2 (± 0.2)[b]
			(*S*)-trifluorolactate ((*S*)-TFL)	1.74 ± (0.08)[b]
$-COO^-$	–H	$-COO^-$	tartronate	1.8 ± (0.1)
$-CH_3$	–H	$-COO^-$	(*R*)-lactate	32.0 ± (1.4)[c]
			(*S*)-lactate	26.1 ± (3.1)[c]
Substrate-product analogues				
$-C_6H_5$	$-C_6H_5$	$-COO^-$	benzilate	0.67 ± (0.12)[d]
$-CF_3$	$-CF_3$	$-COO^-$	3,3,3-trifluoro-2-hydroxy-2-(trifluoromethyl)propanoate (TFHTP)	0.027 ± (0.004)
$-CH_3$	$-CH_3$	$-COO^-$	α-hydroxyisobutyrate	5.5 (± 0.6)
Transition state/ intermediate analogues				
$-C_6H_5$	–H	$-PO_3^{2-}$	(*R*,*S*)-α-hydroxybenzylphosphonate	0.0047 ± (0.0007)[e]
$-CF_3$	–H	$-PO_3^{2-}$	(*R*,*S*)-2,2,2-trifluoro-1-hydroxyethylphosphonate (TFHEP)	0.67 (± 0.13)
$-CH_3$	–H	$-PO_3^{2-}$	(*R*,*S*)-1-hydroxyethylphosphonate (1-HEP)	40.2 (± 4.8)

[a] Unless indicated otherwise, values are competitive inhibition constants. Values are means of triplicate trials and reported errors are the standard deviations.
[b] K_m values from Chapter 2.
[c] From reference (St. Maurice *et al*., 2004).
[d] From reference (Siddiqi *et al*., 2005).
[e] From reference (St. Maurice *et al*., 2000).

3.4 DISCUSSION

3.4.1 Inhibition of MR by Ground State Analogues

MR binds the enantiomers of mandelate and TFL with similar affinities **(Table 3.1)**. However, the enzyme binds the enantiomers of lactate with approximately 26-fold less affinity than it exhibits for mandelate and TFL **(Table 3.1)**. This observation indicates that the trifluoromethyl group on the glycolate moiety contributes an additional ~2 kcal/mol to the free energy of binding relative to the methyl group. Based on the similar binding affinities that MR exhibits for mandelate and TFL, it appears that the binding determinants within the hydrophobic pocket of MR's active site bind the phenyl ring of mandelate and the trifluoromethyl group of TFL with approximately equal affinity. Since MR binds the substrate-product analogue benzilate with an affinity that is similar to that exhibited for mandelate (Siddiqi *et al*., 2005), one would expect that MR to bind TFHTP with similar affinity. However, the presence of two trifluoromethyl groups in TFHTP enhanced the binding affinity by ~66-fold relative to benzilate. Thus, TFHTP is the most potent ground state analogue inhibitor **(Table 3.1)** of MR reported to-date. Since the binding affinity of MR for TFHTP is only slightly less than that reported for the most potent TS/intermediate analogues (*R*,*S*)-α-hydroxybenzylphosphonate (K_i = 4.7 μM), benzohydroxamate (BzH, K_i = 9.3 μM) (St. Maurice & Bearne, 2000), *N*-hydroxyformanilide (K_i = 2.8 μM) and cupferron (CfN, K_i = 2.7 μM) (Bourque *et al*., 2007), the x-ray crystal structure of the MR-TFHTP complex was determined.

The x-ray crystal structure of the MR-TFHTP complex solved by our collaborators Dr. St. Maurice and Adam Lietzan revealed an unexpected binding orientation. Rather than binding in the expected "catalytic" or "productive" orientation,

i.e., with the glycolate moiety chelating the Mg^{2+} ion as observed previously in the complexes of MR with (*S*)-mandelate and (*S*)-atrolactate **(Chapter 2, Figure 2.2)** (Kallarakal *et al*., 1995; Landro *et al*., 1994; Mitra *et al*., 1995; Schafer *et al*., 1996), TFHTP interacts indirectly with the active site Mg^{2+} through a bridging water molecule **(Figure 3.8 A)**. The surprisingly high binding affinity of TFHTP must, therefore, arise for reasons other than its ability to chelate the active site metal ion. First, the two trifluoromethyl groups are intimately packed within the hydrophobic pocket, packing against residues of the closed active site flap (Leu 18, Val 22, Thr 24, and Val 29), residues within the α/β-barrel (Phe 52 and Tyr 54), Leu 298 (on a loop between the strand β10 and α-helix8), residues at the end of the β 11 strand (Leu 319 and Leu 321), and Leu 93 from the adjacent monomer within the dimer (**Figure 3.8 A)**. Second, the carboxylate group is locked in place by several H-bonds **(Figure 3.8 B)**. Asn 197 and Lys 166 form H-bonds ~3.2 Å in length to one oxygen of the carboxylate. Nε2 of His 297 interacts with the other oxygen of the carboxylate group via an H-bond of 2.6 Å, and Glu 317 interacts with the same carboxylate oxygen via a bridging water molecule (not shown). Thus, rather than chelating the Mg^{2+} ion, the carboxylate of TFHTP forms a bridge between the two active site Brønsted acid-base catalysts His 297 and Lys 166. As a consequence of TFHTP's binding orientation, the carboxylate group assumes a binding conformation such that the plane of the carboxylate group is roughly perpendicular to the orientation of the hydroxamate moiety of BzH **(Figure 3.8 B)**. In addition, Nε2 of His 297 interacts with the α-OH group of TFHTP via an H-bond of 3.3 Å. Considering that the pK_a of the hydroxyl group of TFHTP should be markedly reduced relative to that of

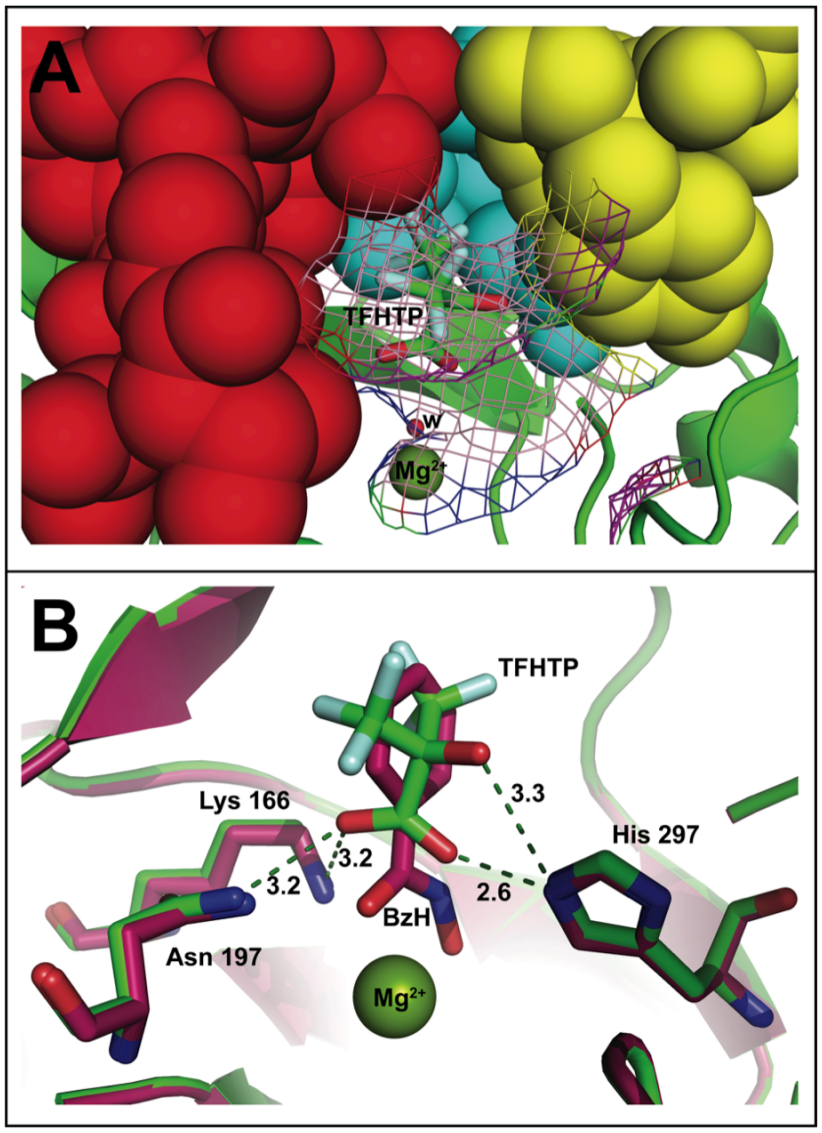

Figure 3.8 Binding orientation of TFHTP within the active-site of MR. (A) Tight packing of the trifluoromethyl groups of TFHTP [PDB entry 4FP1 (Nagar *et al*., 2014)] within the hydrophobic cavity of the active site of MR. Residues of the *R*-pocket (red), *S*-pocket (yellow), Leu 319 and Leu 321 (cyan) are shown in space filling representation. Leu 93 from adjacent monomer is shown as mesh (light pink). (B) Superpositioned structures of the MR complexes with bound TFHTP (green) and benzohydroxamate [BzH, magenta; PDB entry 3UXK (Lietzan *et al*., 2012)]. The Mg^{2+} ion is shown in space-filling representation, while the ligands and Asn 197, His 297, and Lys 166 are shown in stick representation. Putative hydrogen bonds are shown as dashes, and the measurements are in Å.

aliphatic alcohols (pK_a values are 17.1 for 2-propanol (Murto, 1964) and 9.3 for 1,1,1,3,3,3-hexafluoro-2-propanol (Dyatkin *et al.*, 1965), bearing in mind that a hydrophobic environment may increase the pK_a from that expected in aqueous solution), it is plausible that the enhanced binding of TFHTP may also arise, in part, from the transfer of the proton from the hydroxyl group to His 297. Such a scenario is reminiscent of the time-of-flight neutron structure of the D-xylose isomerase–product complex reported by Langan and coworkers in which O5 of D-xylulose was not protonated but formed an H-bond (3.07 Å) with a doubly protonated His residue (Kovalevsky *et al.*, 2008). Hence, it is the effect of the optimal hydrophobic packing interactions that pulls the trifluoromethyl groups of TFHTP toward the active site flap, the steric bulk of the trifluoromethyl groups that resides outside the plane of the phenyl ring of BzH, and the bridging interactions between the active site bases that produce the higher binding affinity of TFHTP.

Recognizing that positioning a carboxylate between the active site Brønsted acid-base catalysts could enhance the binding affinity of a ligand, tartronate was investigated as an inhibitor of MR. Tartronate was found to be a competitive inhibitor of MR **(Figure 3.7)** and bound with an affinity 15- to 18-fold greater than lactate **(Table 3.1)**, revealing that the carboxylate group contributes an additional 1.7 kcal/mol in binding energy relative to the methyl group. This observation suggests that, like TFHTP, the higher affinity of MR for tartronate relative to lactate could arise, in part, through interaction of the carboxylate with the active site Brønsted acid-base catalysts. Indeed, the x-ray crystal structure of MR-tartonate complex, solved by Dr. St. Maurice and Adam Lietzan, revealed that tartronate bound in the “catalytic” or “productive” orientation and that the

second carboxylate group does indeed bridge the two active site Brønsted acid-base catalysts **(Figure 3.9)**.

3.4.2 Inhibition of MR by Transition State Analogues

Previous studies have demonstrated that (*R*,*S*)-α-hydroxybenzylphosphonate is a potent inhibitor of MR (St. Maurice & Bearne, 2000). Therefore, inhibition of MR by (*R*,*S*)-TFHEP, an analogue of the putative *aci*-carboxylate intermediate formed during the racemization of trifluorolactate, was explored. Interestingly, MR bound (*R*,*S*)-TFHEP with an affinity (K_i = 0.67 mM) that was only about 3-fold greater than the affinity exhibited for TFL (K_m ~1.8 mM) **(Table 3.1)**, in contrast to the ~230-fold higher affinity exhibited for (*R*,*S*)-α-hydroxybenzylphosphonate relative to mandelate (K_m ~1.1 mM). Although it appears that, in this case, the trifluoromethyl group does not make a significant contribution to enhanced binding affinity, such is not the case. First, the overall binding affinity of TFHEP is expected to be less relative to α-hydroxybenzylphosphonate because of the lower transition state stabilization energy afforded by MR during the racemization of the corresponding fluorinated substrate. The transition state stabilization afforded by MR when mandelate is the substrate is –26 kcal/mol (Bearne & Wolfenden, 1997) while the transition state stabilization is reduced to –20 kcal/mol when TFL is the substrate (Chapter 2; Nagar *et al*., 2011) Consequently, one would expect MR to bind a TS/intermediate analogue based on the structure of the *aci*-carboxylate of TFL with approximately 2.5×10^4-fold less binding affinity than it would bind the corresponding TS/intermediate analogue based on the structure of the *aci*-carboxylate of mandelate. The observed reduction in binding affinity for (*R*,*S*)-TFHEP

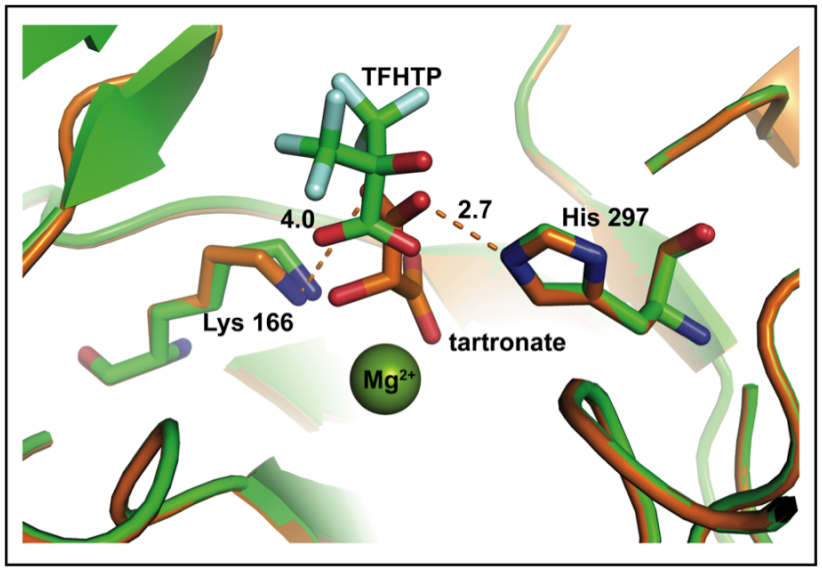

Figure 3.9 Active-site view of MR showing the superposition of the structures of the MR complexes with bound tartronate [orange; PDB entry 4M6U (Nagar *et al.*, 2014)] and TFHTP [green; PDB entry 4FP1 (Nagar *et al.*, 2014)]. The Mg^{2+} ion is shown in space-filling representation, while the ligands and His 297, and Lys 166 are shown in stick representation. Putative hydrogen bonds are shown as dashes, and the measurements are in Å.

(K_i = 0.67 mM), relative to (*R*,*S*)-α-hydroxybenzylphosphonate (K_i = 4.7 μM), is in accord with this expectation, although the magnitude of the reduction in binding affinity (~143-fold) is certainly much less than expected. Second, the non-fluorinated analogue of (*R*,*S*)-TFHEP, i.e., (*R*,*S*)-1-HEP, exhibited a 60-fold lower binding affinity than that observed for the corresponding fluorinated TS/intermediate analogue. Thus, the presence of the trifluoromethyl group in the phosphonate-based TS/intermediate analogue does enhance binding over that observed for the corresponding non-fluorinated analogue. Such enhanced binding arising from substitution of a trifluoromethyl group for a methyl group is not unexpected. For example, α-methylacyl-CoA racemase binds the α-methyl group of ligands at a hydrophobic pocket within the active site of the enzyme (Bhaumik *et al*., 2007; Sharma *et al*., 2012), and replacement of the α-methyl group in α-methylmyristoyl-CoA with an α-trifluoromethyl group leads to a 152-fold greater binding affinity (Carnell *et al*., 2007).

In a nutshell, the observations in the present chapter suggest that enhanced binding interactions occur within the hydrophobic pocket of MR when a trifluoromethyl group is present on a ligand and that inhibitors may also be designed by capitalizing on the interactions with the active site Brønsted acid-base catalysts. Consequently, this inhibitor design strategy should allow for the development of inhibitors of other enzymes of the enolase superfamily, especially those in the MR sub-group (Babbitt *et al*., 1996; Gerlt *et al*., 2012; Gerlt *et al*., 2005), to explore the role of Brønsted acid-base catalysts as binding determinants.

CHAPTER 4

IRREVERSIBLE INHIBITION OF MR BY 3-HYDROXYPYRUVATE VIA A SCHIFF-BASE MECHANISM

Reproduced in part with permission from – Nagar, M., Wyatt, B. N., St. Maurice, M., and Bearne, S. L. (2015) Inactivation of Mandelate Racemase by 3-Hydroxypyruvate Reveals a Potential Mechanistic Link between Enzyme Superfamilies. Biochemistry ***54****, 2747–2757. Copyright 2015 American Chemical Society.*

4.1 INTRODUCTION

MR is a well-characterized member of the enolase superfamily. Members of this mechanistically diverse superfamily share a common partial reaction, i.e., the Mg^{2+}-assisted general-base-catalyzed enolization of a carbon acid substrate generating an *aci*-carboxylate intermediate **(Scheme 4.1)** (Babbitt *et al*., 1996; Babbitt *et al*., 1995). MR, a highly proficient enzyme, can discriminate between the substrate in ground state and the altered substrate in TS, binding the latter with an association constant of ~5×10^{18} M^{-1} (Bearne & Wolfenden, 1997). Consequently, the ligands that share geometric and electronic features with the *aci*-carboxylate intermediate, such as benzohydroxamate (BzH, K_i = 11.7 μM) (Bourque & Bearne, 2008), cupferron (CfN, K_i = 2.7 μM), *N*-hydroxyformanimide (K_i = 2.8 μM) (Bourque *et al*., 2007), and (*R*,*S*)-α-hydroxybenzylphosphonate (K_i = 4.7 μM) (St. Maurice & Bearne, 2000) are the best known reversible inhibitors of MR. In Chapter 3, I showed that a substrate-product analogue, 3,3,3-trifluro-2-hydroxy-2-(trifluromethyl)-propionate (TFHTP, K_i = 27 μM), has an affinity similar to that of these TS analogues (Nagar *et al*., 2014). Part of the higher than expected binding affinity of TFHTP is attributed to the salt bridge interactions between the carboxylate of TFHTP and the active site Brønsted acid-base

Scheme 4.1 Partial reaction mechanism of members of enolase superfamily

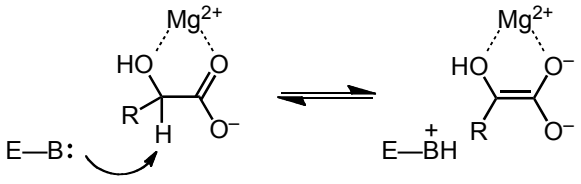

catalysts Lys 166 and His 297 (Nagar *et al*., 2014). Recognizing that active site bases can be exploited as binding determinants, I showed that tartronate (K_i = 1.8 mM) is also a reversible competitive inhibitor for MR (Chapter 3).

In order to better understand and to exploit the role of the Brønsted acid-base catalysts as binding determinants, the α-keto acids 3-hydroxypyruvate (3-HP), 3-fluoroypyruvate (3-FP), pyruvate, and mesoxalate were investigated as potential inhibitors for MR **(Figure 4.1)**. This chapter describes the competitive inhibition of MR by mesoxalate and 3-FP, both of which bind MR 10–15-fold more tightly than pyruvate, consistent with earlier observations that suggest that binding of a ligand could be enhanced by promoting H-bonding interactions between the ligand and the Brønsted acid**-**base catalysts (Chapters 2 & 3). In addition, surprisingly, 3-HP shows mechanism-based inhibition of MR that involves formation of covalent adduct with Lys 166 via a Schiff-base intermediate. Such a reaction mechanism is characteristic of class I aldolases and the *N*-acetylneuraminate lyase (NAL) superfamily but unprecedented in the enolase superfamily. Therefore, this study provides mechanistic evidence that supports the sequence and structure-based hypothesis that the metal-dependent enolase superfamily might have evolved from a Schiff-base-forming progenitor of the aldolases.

Figure 4.1 Various α-keto acid analogues of tartronate

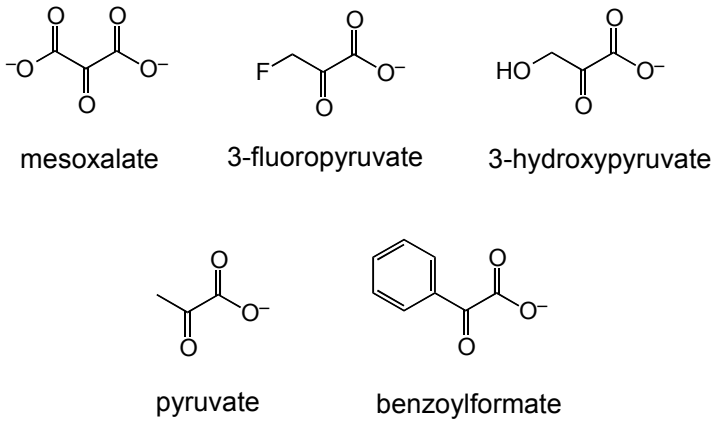

4.2 MATERIALS AND METHODS

4.2.1 General

(*R*)-Mandelic acid, lithium 3-hydroxypyruvate (3-HP), sodium 3-fluoropyruvate (3-FP), sodium mesoxalate monohydrate, benzoylformic acid, sodium pyruvate, benzohydroxamic acid (BzH) and all other reagents, unless mentioned otherwise, were purchased from Sigma-Aldrich Canada Ltd. (Oakville, ON, Canada). Circular dichroism (CD) assays were conducted using a JASCO J-810 spectropolarimeter (Jasco Inc., Easton, MD) with a jacketed cell holder. LC-MS/MS was performed using a nano flow HPLC system (Ultimate3000, Dionex, Idstein, Germany) interfaced to a hybrid ion trap-orbitrap high-resolution tandem mass spectrometer (VelosPro, Thermo Scientific) operated in data dependent acquisition (DDA) mode.

4.2.2 Concentration Correction for 3-Hydroxypyruvate

The extent of hydration in the commercially available 3-HP ($C_3H_3O_4Li \bullet xH_2O$, formula weight 109.99 g/mol) was determined by elemental analysis (Canadian Microanalytical Services Inc., BC, Canada) to get an accurate estimation of the concentration of the 3-HP in solution. Based on the presence of 26.13% carbon and 3.63% hydrogen in the sample, the calculated molecular weight of 3-HP was 137.89 g/mol which corresponds to $C_3H_3O_4Li \cdot \sim 1.5\ H_2O$.

4.2.3 Site-Directed Mutagenesis

The pET52b(+)-wtMR plasmid was used as a template to create the H297N-MR mutant by performing polymerase chain reaction (PCR)-based site-directed mutagenesis

using the QuikChange Site-directed Mutagenesis Kit (Stratgene, La Jolla, CA) and following the protocols described by the manufacturer. PCR reactions were conducted using *Pfu*Turbo DNA polymerase (Bio Basic Inc., Markham, ON). The forward (F) and reverse (R) synthetic deoxyoligonucleotide primers used to construct the mutants were 5′-CCAATGTCCAGC**A**AC<u></u>CTGTTCCAAGAAATCAGC-3′ (F) and 5′-GCTGATTTCTT GGAACAGGT**T**GCTGGACATTGG-3′ (R), repectively. The codons specifying the relevant amino acid are underlined and the altered bases are shown in bold. Potential mutant plasmids were used to transform competent *E. coli* DH5α cells. These DH5α cells were used for plasmid maintenance and for all sequencing reactions. The mutant open reading frame sequence was confirmed using commercial automated sequencing (Robarts Research Institute, London, ON) to ensure that no other alterations of the nucleotide sequence had been introduced.

4.2.4 Expression and Purification of MR

Recombinant variants of MR (wtMR and H297N-MR) from *Pseudomonas putida* were over-expressed in and purified from *E. coli* BL21(DE3) cells transformed with the pET-52b(+)-wtMR and pET-52b(+)-H297N-MR plasmid, respectively, as described in Chapter 2 (section 2.2.2).

4.2.5 Screening for Time-Dependent Inhibition by α-Keto Acids

wtMR (32.7 nM) was incubated at 25 °C with each α-carbonyl inhibitor [pyruvate (10 μM), mesoxalate (10 μM), benzoylformate (10 μM), 3-FP and 3-HP (8 μM)] in Na^+-HEPES buffer (0.1 M, pH 7.5) containing $MgCl_2$ (3.3 mM) and BSA (0.005%) for 0, 6,

12, 18 and 24 min. At each time point, 200 μL of enzyme-inhibitor mixture was added to assay buffer containing (*R*)-mandelate to determine MR activity (final concentrations of MR, α-carbonyl inhibitor, and (*R*)-mandelate in a 2.0 mL assay mixture were 3.3 nM, 1 μM (except that for 3-HP, which was 8 μM) and 10 mM, respectively). Simultaneously, a control containing wtMR (32.7 nM) in assay buffer and no α-carbonyl compound was also incubated at 25 °C for 0 and 30 min to determine the rate of loss of MR activity due to incubation during the course of inhibition assay. Similar inhibition experiments were conducted using a greater concentration of α-carbonyl inhibitors (2 mM, expect for 3-HP) for 0 and 10 min (final concentrations of MR, α-carbonyl inhibitor, and (*R*)-mandelate in the assay mixture (2.0 mL) were 3.3 nM, 0.2 mM, and 10 mM, respectively). The residual MR activity was measured using a CD-based assay (Sharp *et al*., 1979) by following the change in ellipticity of mandelate at 262 nm for 3 min with a 1-cm path-length cuvette (except for the residual activity in presence of benzoylformate (0.2 mM), which was measured using a 0.5-cm path-length cuvette).

4.2.6 Inhibition of MR by Mesoxalate and 3-Fluoropyruvate

Inhibition experiments with mesoxalate and 3-FP were conducted in Na^+-HEPES buffer (0.1 M, pH 7.5) containing $MgCl_2$ (3.3 mM) and BSA (0.005%) using (*R*)-mandelate (0.25–10.0 mM) as the substrate. The concentrations of mesoxalate and MR in the final assay mixture (2.0 mL) were 1.0, 2.0, & 4.0 mM; and 2.99 nM, respectively, while the concentrations of 3-FP and MR were 0.75, 1.5, & 3.0 mM; and 2.84 nM, respectively. Competitive inhibition constants (K_i) were determined as described in

Section 3.2.5 (Chapter 3). All kinetic parameters were determined in triplicate, and average values are reported. The reported errors are standard deviations.

4.2.7 Inhibition of MR by 3-Hydroxypyruvate

The kinetic parameters for the time-dependent inhibition of MR by 3-HP were determined by incubating wtMR (32.7 nM) with various concentrations of 3-HP (0, 3.99, 7.98, 11.96, and 15.95 μM) at 25 °C for 0, 6, 12, 18, and 24 min. At each time point, an aliquot (200 μL) of the MR-3-HP mix was added to the assay mixture containing (*R*)-mandelate as the substrate to determine the remaining MR activity. The final concentrations of MR (3.3 nM), 3-HP (0, 0.39, 0.79, 1.19 and 1.59 μM), and (*R*)-mandelate (10 mM) in the 2.0 mL assay mixture were as indicated. MR activity was measured as described above. Analysis of the inactivation of MR activity was conducted using **Scheme 4.2**.

Scheme 4.2

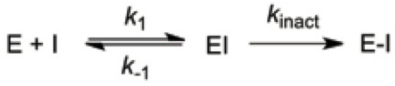

The observed pseudo-first-order rate constant for the inactivation of MR (k_{obs}) at each inhibitor concentration was determined by fitting the linearized form of equation 4.1, i.e., equation 4.2 to the data for loss in MR activity as a function of time. The k_{obs} values were re-plotted against 3-HP concentration to determine k_{inact}/K_I using equation 4.3 which reduces to equation 4.4 when $K_i >> [I]$ (Copeland, 2000). The rate constant k_{inact} corresponds to the maximal rate of enzyme inactivation and K_I is defined as the apparent

concentration of inhibitor at which rate of inactivation of enzyme is half of the maximum value (i.e., $k_{inact}/2$).

$$\frac{v_i}{v_o} = e^{-k_{obs}t} \tag{4.1}$$

$$\ln\ (\%\ activity) = 4.605 - k_{obs}t \tag{4.2}$$

$$k_{obs} = \frac{k_{inact}\ [\mathrm{I}]}{K_{\mathrm{I}} + [\mathrm{I}]} \tag{4.3}$$

$$k_{obs} = \frac{k_{inact}}{K_{\mathrm{I}}}\ [\mathrm{I}] \tag{4.4}$$

To test the irreversibility of inhibition, MR (32.7 nM) that had been completely inhibited by 3-HP (15.95 μM) was dialyzed for 4 h and 10.5 h at 4 °C against HEPES assay buffer (pH 7.5). After dialysis, the remaining activity of dialyzed MR was compared with the activity of the control to determine the extent of MR reactivation.

Inhibition of MR with 3-HP in presence of the reversible competitive inhibitor, benzohydroxamate (BzH): MR (32.7 nM) was incubated with 3-HP (15.95 μM) in the presence of BzH (0, 5, 10, and 20 μM) at 25 °C. At various time points (0, 6, 12, 18, and 24 min), 200 μL of the MR-3-HP mixture were added to the assay mixture containing (*R*)-mandelate as a substrate to determine the residual MR activity [final concentrations of MR (3.3 nM), 3-HP (1.59 μM), BzH (0, 0.5, 1.0, and 2.0 μM), and (*R*)-mandelate (10 mM)] in a 2.0 mL assay mixture were as indicated. MR activity was measured as described above. The observed rate constant for the inactivation of MR (k_{obs}) by 3-HP (15.95 mM) in presence of various concentrations of BzH were determined by fitting equation 4.2 to the data for loss in MR activity as a function of time.

4.2.8 Analysis of Inactivated MR using Mass Spectrometry

wtMR (0.7 mg/mL) and H297N-MR (0.98 mg/mL) were incubated with 3-HP (5 mM) at 25 °C until the residual wtMR activity was undetectable using the CD assay [final concentrations of MR (327 nM) and (*R*)-mandelate (10 mM) were as indicated]. The control sample, i.e., wtMR in assay buffer, was incubated for the same time period as the inhibition reaction. After complete inhibition of wtMR by 3-HP, each reaction mix (20 μL) was subjected to electrophoresis using a 12% SDS-polyacrylamide gel.

In-gel digestions: Protein bands corresponding to MR and H297N-MR were excised form gel and rinsed twice with deionized water (300 μL). The bands were further cut into cubes (~1 mm^3) and processed using an automated system for protein in-gel digestions (Investigator Progest, Genomic Solutions, MI, USA). Briefly, the protein in gel bands were reduced with dithiothreitol (DTT, 10 mM), carboxamidomethylated with iodoacetamide (100 mM), and finally digested with trypsin (Promega, Madison, WI) for 12 h at 37 °C. The peptides were extracted from the gel pieces following three 20 min incubations with acetonitrile-formic acid-LC-MS grade water (50:5:45, v/v/v, 30 μL) with gentle agitation. The extracts were pooled together and dried using a vacuum concentrator (Speed Vac Concentrator, SPD 111V-230, Thermo Electron Corporation, Asheville, NC, USA) and finally resuspended in acetonitrile-formic acid-LC-MS grade water (3:0.5:96.5, v/v/v, 15 μL).

LC-ESI-MS/MS and data analysis: LC-MS/MS was performed using a nano flow HPLC system (Ultimate3000, Dionex, Idstein, Germany) interfaced to a hybrid ion trap-orbitrap high resolution tandem mass spectrometer (VelosPro, Thermo Scientific) operated in data dependent acquisition (DDA) mode. The samples (1 μL each) were injected onto a

capillary column (C18 Onyx Monolithic, 0.10 x 150 mm Phenomenex) at a flow rate of 300 nL/min. Samples were sprayed at 1.6 kV using fused silica non-coated emitters (20-μm ID with 10-μm ID tip PicoTip Emitter from New Objective). Chromatographic separation was carried out using a linear gradient from 3% B to 35% B over 30 min, then increasing to 95% B over 5 min (A: 0.1% formic acid in water, B: 0.1% formic acid in acetonitrile). The raw files were acquired (Xcalibur, Thermo Fisher) and exported to Proteome Discoverer v1.4 (Thermo Fisher) software for peptide and protein identification using Sequest database search algorithm. Carbamidomethyl cysteine and oxidized methionines were selected as static and dynamic modifications, respectively. Peptide to spectrum match (PSM) validation was done using high confidence XCorr threshold values of 1.9, 2.3, and 2.6 for double, triple, and higher charged precursors.

Analysis of H297N-MR-3-HP complex reduced with $NaCNBH_3$: H297N-MR (0.98 mg/mL) was incubated with 3-HP (5 mM) at 25 °C for 30 min. After 30 min, $NaCNBH_3$ (50 mM) was added to the reaction mixture (pH was adjusted to 7.0) followed by incubation for another 30 min. Finally, the reaction mix (20 μL) was analyzed by electrophoresis using a 12% SDS-polyacrylamide gel followed by mass spectrometry analysis as described above.

4.3 RESULTS

4.3.1 Inhibition of MR with α-Keto Acids

Initial screening of various α-keto acids showed interesting results. Surprisingly, 3-HP (8 μM) inhibited MR in a time-dependent manner while all of the other α-keto acids (10 μM), pyruvate, mesoxalate, 3-FP, and benzoylformate, did not show time-

dependent inhibition at the indicated concentrations **(Figure 4.2 A)** or at higher concentrations, i.e., at 2 mM **(Figure 4.3 B)**.

Mesoxalate and 3-FP were found to be reversible competitive inhibitors **(Figures 4.3 A & 4.4 A)** of MR with respect to (*R*)-mandelate at pH 7.5. MR bound both mesoxalate (K_i = 1.75 ± 0.28 mM) **(Table 4.1, Figure 4.3 B)** and 3-FP (K_i = 1.26 ± 0.11 mM) **(Table 4.1, Figure 4.4 B)** with ~15-fold higher affinity than that estimated for pyruvate (K_i ~20 mM, value calculated based on 40% inhibition by 25 mM pyruvate and considering it to be a competitive inhibitor) **(Table 4.1)**, suggesting enhanced interactions of the COO^- and CH_2F groups with MR compared to the CH_3 group, respectively.

The observed time-dependent inhibition of MR with 3-HP **(Figures 4.1 A & 4.5 A)** could be either due to tight binding or irreversible binding. Extensive dialysis of 3-HP-inhibited MR against assay buffer for 10.5 h did not recover any significant activity compared to the activity of the untreated enzyme, suggesting formation of covalent adduct between 3-HP and MR. To further characterize the inactivation reaction, the inhibition kinetics were examined in detail. The observed pseudo-first-order rate constants for formation of the inactivated enzyme, k_{obs}, were determined at various concentrations of 3-HP **(Figure 4.5 A)**. Generally, plotting k_{obs} values against inhibitor concentration and fitting the data to equation 4.3 to yields a rectangular-hyperbola, which gives values for the maximal rate of inactivation (k_{inact}) and the overall binding affinity (K_I) (Copeland, 2000). However, saturation was not observed at 3-HP concentrations ≤16 μM, and at higher concentrations of 3-HP, accurate determination of k_{obs} values was hampered due to the rapid loss in MR activity (relative to the assay duration 3 min). Consequently, individual values for the maximal rate of inactivation (k_{inact}) and K_I could

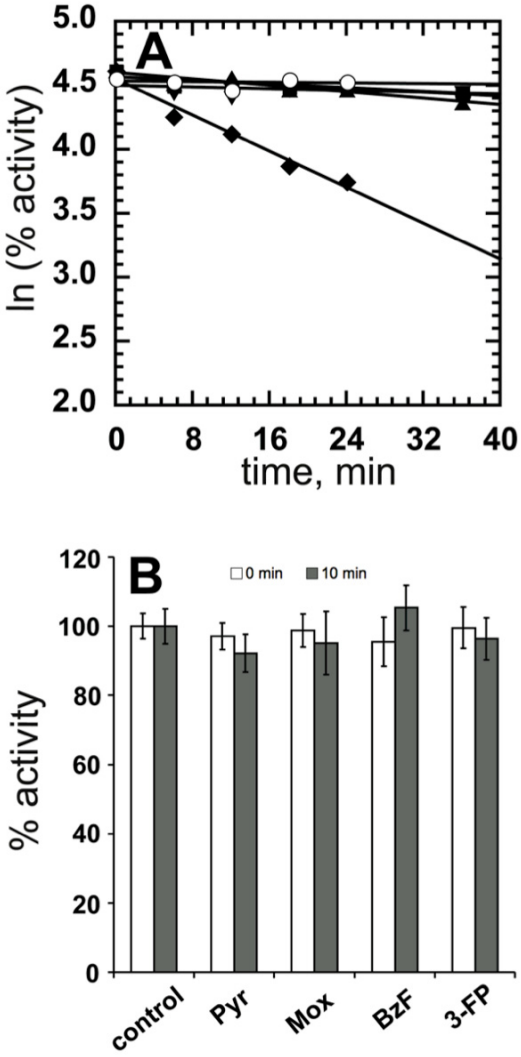

Figure 4.2 Screening for time-dependent inhibition of MR by various α-keto acids. (A) MR (32.7 nM) incubated with 3-HP (8.0 μM, ◆), mesoxalate (10 μM, ▼), 3-FP (10 μM, ○), pyruvate (10 μM, ■), benzoylformate (10 μM, ▲), or without inhibitor (●) at 25 °C. The initial rates were measured at the indicated time points. Refer to the Material and Methods for details. (B) MR (32.7 nM) incubated with buffer (control) or with α-keto acids (2 mM) – pyruvate (Pyr), mesoxalate (Mox), benzoylformate (BzF) or 3-FP. The initial rates were measured at 0 and 10 min.

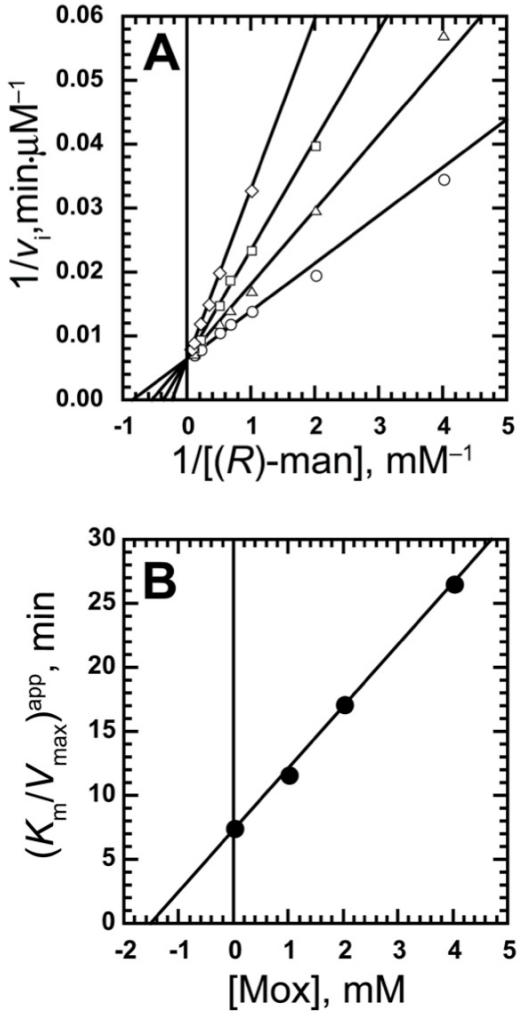

Figure 4.3 Inhibition of MR by mesoxalate. (A) A representative Lineweaver-Burk plot showing competitive inhibition of MR by mesoxalate (Mox). Assays were conducted as described in section 4.2.6 with the concentration of (*R*)-mandelate ((*R*)-man) ranging between 0.25–10.0 mM, and concentrations of mesoxalate equal to 0 mM (○), 1.0 mM (△), 2.0 mM (□), and 4.0 mM (◇). (B) A representative replot of the apparent K_m/V_{max} values (obtained by fitting the equation 3.1 to the initial velocity data) as a function of Mox concentration. The negative of the x-intercept yields the K_i value (equation 3.2, Chapter 3). The average K_i value = 1.75 ± 0.28 mM.

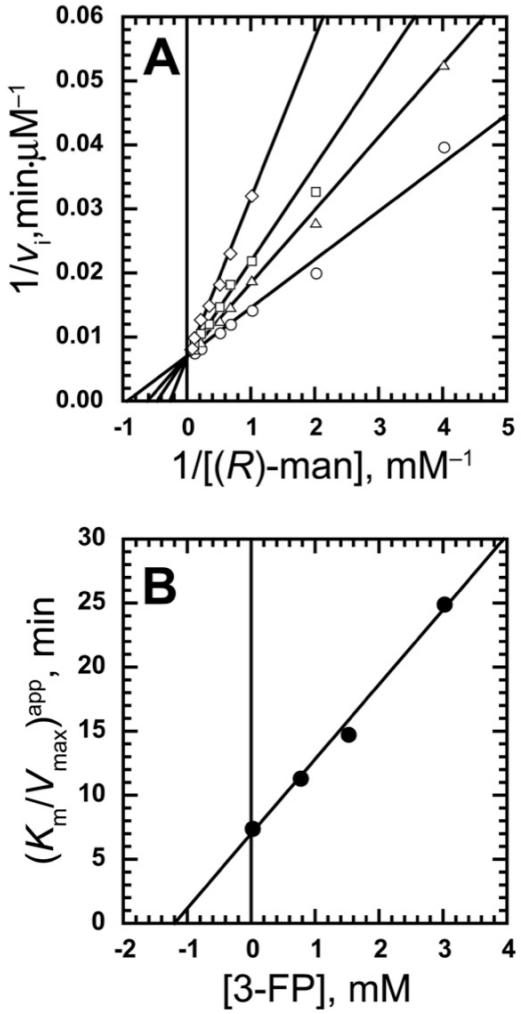

Figure 4.4 Inhibition of MR by 3-fluropyruvate. (A) A representative Lineweaver-Burk plot showing competitive inhibition of MR by 3-FP. Assays were conducted as described in section 4.2.6 with the concentration of (*R*)-mandelate ((*R*)-man) ranging between 0.25–10.0 mM, and concentrations of 3-FP equal to 0 mM (○), 0.75 mM (△), 1.5 mM (□), and 3.0 mM (◇). (B) A representative replot of the apparent K_m/V_{max} values (obtained by fitting equation 3.1 to the initial velocity data) as a function of 3-FP concentration. The negative of the x-intercept yields the K_i value (equation 3.2, Chapter 3). The average K_i value = 1.27 ± 0.11 mM.

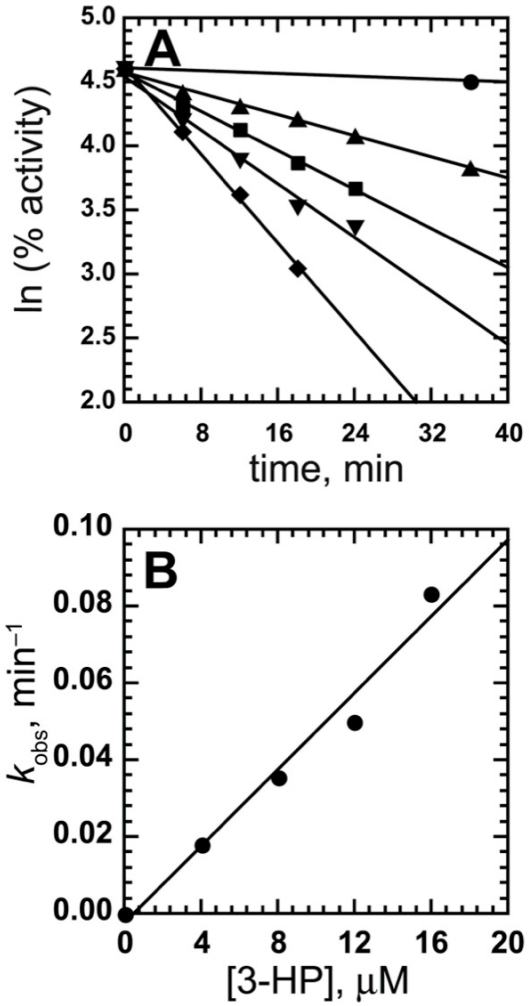

Figure 4.5 Time-dependent inhibition of MR by 3-hydroxypyruvate. (A) MR (32.7 nM) was incubated with various concentrations of 3-HP: 0 μM (●), 4.0 μM (▲), 8.0 μM (■), 12.0 μM (▼), and 16.0 μM (◆) at 25 °C and the initial rates were measured at the indicated time points. The slope yields the observed pseudo first-order rate constants (k_{obs}). Refer to the Material and Methods for details. (B) A plot of the observed pseudo first-order rate constant (k_{obs}) for inactivation as a function of 3-HP concentration. The slope, which is the apparent second-order rate constant for inactivation (k_{inact}/K_I), yielded a value of 83.0 ± 7.7 $M^{-1}s^{-1}$.

Table 4.1 Summary of inhibition of MR by various α-keto acids

α-keto acid	mode of inhibition	K_i (mM)	K_{inact}/K_I ($M^{-1}s^{-1}$)
mesoxalate	Competitive/reversible	1.75 ± 0.28	-
3-FP	Competitive/reversible	1.27 ± 0.11	-
pyruvate[a]	Competitive/reversible	~20	-
3-HP	Competitive/irreversible	-	83.0 ± 7.7

[a] Assuming pyruvate as a competitive inhibitor, K_i was calculated based on 40% inhibition of MR activity by 25 mM of pyruvate using (*R*)-mandelate (1.0 mM) as the substrate (K_m $^{(R)\text{-mandelate}}$ = 1.2 mM).

not be calculated. Instead, the first-order rate constants (k_{obs}) for the time-dependent inhibition of MR by 3-HP exhibited a linear dependence on the concentration of 3-HP **(Figure 4.5 B)**, suggesting that the kinetic mechanism for inactivation could be either a one-step or a two-step mechanism in which initial non-covalent weak binding of 3-HP is followed by formation of a covalent bond (i.e., [inhibitor] <<< K_I and equation 4.3 reduces to equation 4.4) (Copeland, 2000; Kitz & Wilson, 1962). The slope of the plot of k_{obs} versus [3-HP] yielded an apparent second-order rate constant for inactivation (k_{inact}/K_I) with a value of 83.0 ± 7.7 $M^{-1}s^{-1}$ **(Figure 4.5 B)**, which corresponds to the inhibition efficiency of a covalent inhibitor. The observed rate of inactivation (k_{obs}) of MR by 3-HP was reduced in presence of the reversible competitive inhibitor, benzohydroxamate (BzH, K_i = 11.7 μM) **(Figure 4.6)**, suggesting a competition between both ligands for the same site. Therefore, 3-HP appears to enter and bind at the active site to inhibit MR irreversibly.

4.3.2 Analysis of Inactivated MR using Mass Spectrometry

In order to identify the residue(s) modified upon inactivation of MR by 3-HP, unmodified MR (control-MR) and 3-HP-modified MR (3-HP-MR) samples were analyzed using LC-MS/MS. For both the control-MR and the 3-HP-MR, ≥95% sequence coverage was obtained. MS analysis revealed identical peptides in both control-MR and 3-HP-MR samples, except for the TKIGYPALDQDLAVVR fragment (TK-peptide, residue 165–180). The TK-peptide from the 3-HP-MR sample gave two *m/z* peaks: one peak corresponding to an unmodified peptide (MH^+, *m/z* = 1758.97) was observed in the control-MR, suggesting either that MR was partially modified or some modification was

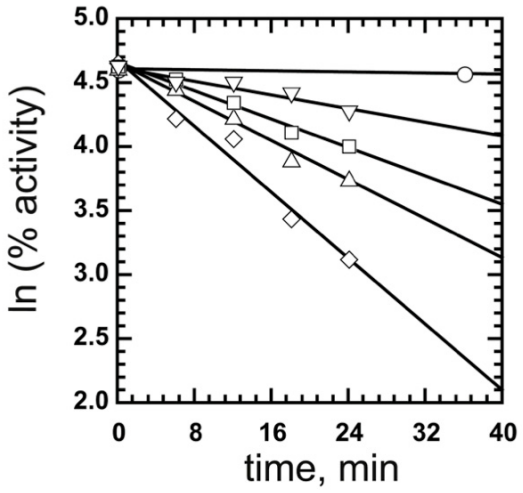

Figure 4.6 Protection of MR against 3-HP-dependent inactivation by BzH. MR (32.7 nM) incubated with 3-HP (16.0 μM) in presence of various concentrations of BzH: 0 μM (◇), 5 μM (△), 10 μM (□), and 20 μM (▽) at 25 °C and the initial rates were measured at the indicated time points. The value for the control reaction (loss in activity due to incubation conditions in absence of 3-HP) is shown (○). The slope yields the observed pseudo first-order rate constants (k_{obs}), which are decreasing with increasing concentrations of BzH. Refer to the Material and Methods for details.

reversed during sample preparation, and another peak corresponding to a modified TK-peptide (MH^+, m/z = 1844.98), suggesting that covalent modification by 3-HP adds 86 Da to the peptide. Internal fragmentation of the triply charged modified TK-peptide (monoisotopic, m/z = 615.66 Da) and unmodified TK-peptide (monoisotopic, m/z = 586.99 Da) precursors showed a mass increment of 86 Da between b_2-ions of the modified (316.34 Da) **(Figure 4.7 B)** and the unmodified (230.27 Da) peptides **(Figure 4.7 A)**, suggesting modification of either Thr 165 or Lys 166. But the possibility of Thr 165 being modified is low because (a) all available x-ray structures of MR shows that the side-chain of Thr 165 is directed away from the active site, and (b) chemically it is not easy to explain any adduct between 3-HP and the threonine side chain that could increase the mass of b_2-ion by 86 Da. Therefore, Lys 166 was most likely modified by 3-HP. The remaining b- and y-ions correspond well with the sequence. MS/MS analysis of the TK-peptide from H297N-MR incubated with 3-HP alone did not show any modification indicating a possible role of His 297 in the irreversible inactivation. However, MS/MS analysis of the TK-peptide from H297N-MR incubated with 3-HP in presence of $NaCNBH_3$ showed a mass increase of 88 Da between b_2-ions of the modified (318.14 Da) **(Figure 4.8)** and the unmodified (230.27 Da) peptides **(Figure 4.7 A)**.

4.4 DISCUSSION

In order to better understand and to exploit the role of Brønsted acid-base catalysts as binding determinants, the α-keto acids 3-HP, 3-FP, and mesoxalate were explored as inhibitors for MR.

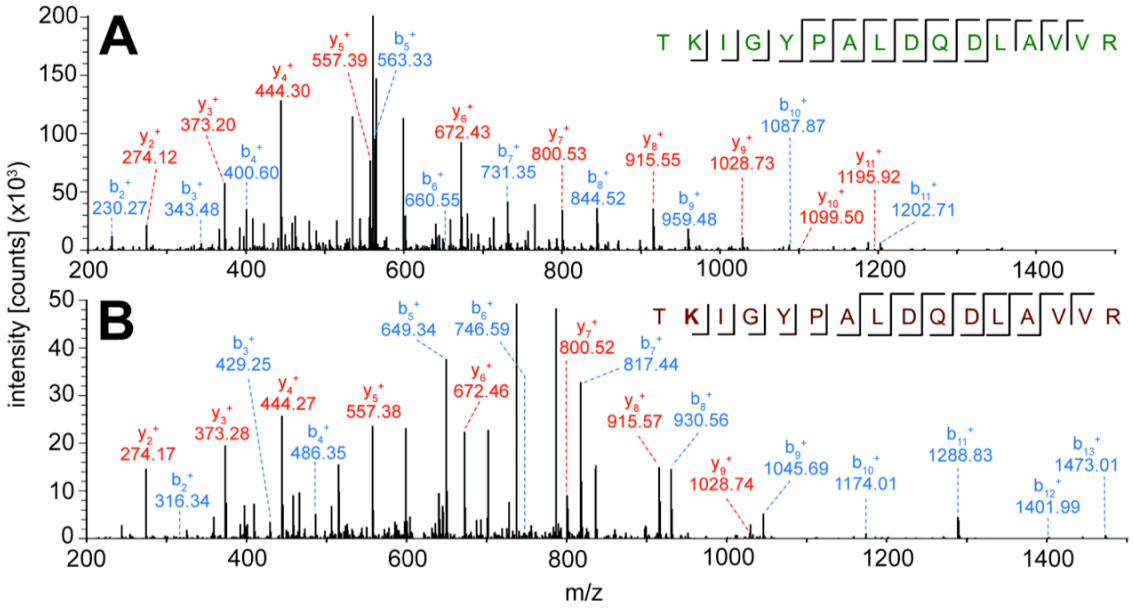

Figure 4.7 Analysis of inactivation of MR by 3-HP using mass spectrometry. MS/MS analysis of the triply charged ion of the TK-peptide from untreated wtMR (due to one missed cleavage site) (A; *m/z* = 586.995; MH^+ = 1758.971 Da) and 3-HP-treated wtMR (B; *m/z* = 615.664; MH^+ = 1844.976 Da) reveals the modification of the tryptic peptide by an 86 Da adduct. The increase in mass of the b_2^+ ion by 86 Da suggested modification of Lys 166 (shown as bold in B).

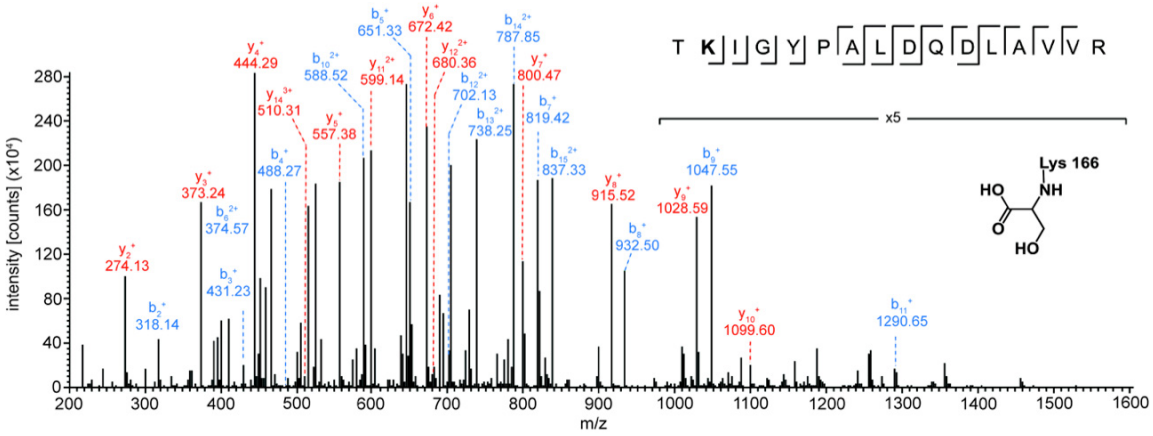

Figure 4.8 Analysis of inactivation of H297N-MR by 3-HP in presence of $NaCNBH_3$ using mass spectrometry. MS/MS analysis of the triply charged ion of the TK-peptide from H297N-MR treated with 3-HP in presence of $NaCNBH_3$ (m/z = 616.329; MH^+ = 1846.97 Da) reveals the modification of Lys 166. The increased mass of b_2^+ ion by 88 Da is consistent with the reduction of a Schiff-base as shown in the inset. See Discussion for further details.

4.4.1 Inhibition of MR by α-Keto Acids

The α-keto acids can exist as hydrates to varying degrees depending upon the electron withdrawing or donating nature of the group adjacent to the α-carbonyl (Cooper & Redfield, 1975). Since, hydration could change the hybridization of the α-C from sp^2 to sp^3, it could affect the binding of α-keto acids within the active site. However, pyruvate, which exists as keto form (> 92%) at pH 6.8 (Cooper & Redfield, 1975; Meany, 2007), exhibited a binding affinity (K_i ~20 mM) similar to that observed for lactate (K_i = 30 mM (St. Maurice & Bearne, 2004)), which is consistent with previous studies in which replacing the α-hydroxyl group with an α-carbonyl group did not show any effect on the binding of ground state analogues, e.g., MR showed similar binding affinities for benzoylformate (mostly exist as keto form (>99 %) due to resonance stabilization (Malpica & Calzadila, 2005)) and mandelate (benzoylformate, K_i = 0.65 mM; and (*R*)-mandelate, K_m = 0.81 mM (St. Maurice & Bearne, 2000)). These observations suggest that the sp^2 carbon of the α-carbonyl is not a good mimic of sp^2-α-C of the *aci*-carboxylate intermediate formed during MR catalysis and that the π-electron density should spread between α-carbon and the carboxylate carbon for better binding. This feature of MR catalysis will be explored in more detail in Chapter 6. Therefore, the low affinity MR exhibits for pyruvate and lactate (*cf*. tartronate, K_i = 1.8 mM (Nagar *et al*., 2014)) could be explained by the absence of the salt bridge between these ligands and the Brønsted acid-base catalysts relative to tartronate, and/or decreased hydrophobic interactions between the methyl group and the hydrophobic pocket within the active site, relative to the trifluoromethyl group of trifluorolactate or the phenyl group of mandelate.

An α-keto group flanked by electron withdrawing groups is prone to nucleophilic attack by water and thus more hydrated (Cooper & Redfield, 1975). Both mesoxalate (100% hydrated (Urbanskya & Bashe, 2000)) and 3-FP (> 90% hydrated (Goldstein *et al*., 1978; Hurley *et al*., 1979; Parisi & Abeles, 1992)) exist as *gem*-diols in solution, but within the active site, metal coordination could lead to the dehydration of mesoxalate and 3-FP *gem*-diols to yield the corresponding keto form (Pocker & Meany, 1970). Mesoxalate, a structural analogue of tartronate that has an α-carbonyl group instead of a hydroxyl group bound MR with an affinity (K_i = 1.75 mM) similar to tartronate (K_i 1.8 mM (Nagar *et al*., 2014)), suggesting that both ligands share a similar binding orientation in which the second carboxylate group forms a salt bridge with the Brønsted acid-base catalysts and therefore compensates for the loss of hydrophobic interactions. Similarly, the enhanced binding of 3-FP compared to pyruvate could be attributed to either dipolar interactions (rather than true hydrogen bonds (Dunitz & Taylor, 1997; Olsen *et al*., 2004)) with the Brønsted acid-base catalysts or enhanced hydrophobic interactions.

4.4.2 Inactivation of MR by 3-Hydroxypyruvate

Based on inhibition kinetics and mass spectrometry, 3-HP most likely covalently modifies the active site base Lys 166 such that the resulting adduct has a molecular weight of 86 Da. Two possible mechanisms could be envisioned to account for this increased residue mass **(Scheme 4.3)**. One of the possible mechanisms involves reversible formation of a C_α-Schiff-base (imine, EI) between the ε-amino group of Lys 166 and the α-carbonyl of 3-HP. Subsequent deprotonation of the β-C of the C_α-Schiff-base (presumably by His 297) would yield an enol, which could tautomerize to yield the

Scheme 4.3 Proposed reaction mechanisms that account for the increased mass of MR (by 86 Da) due to inactivation by 3-HP

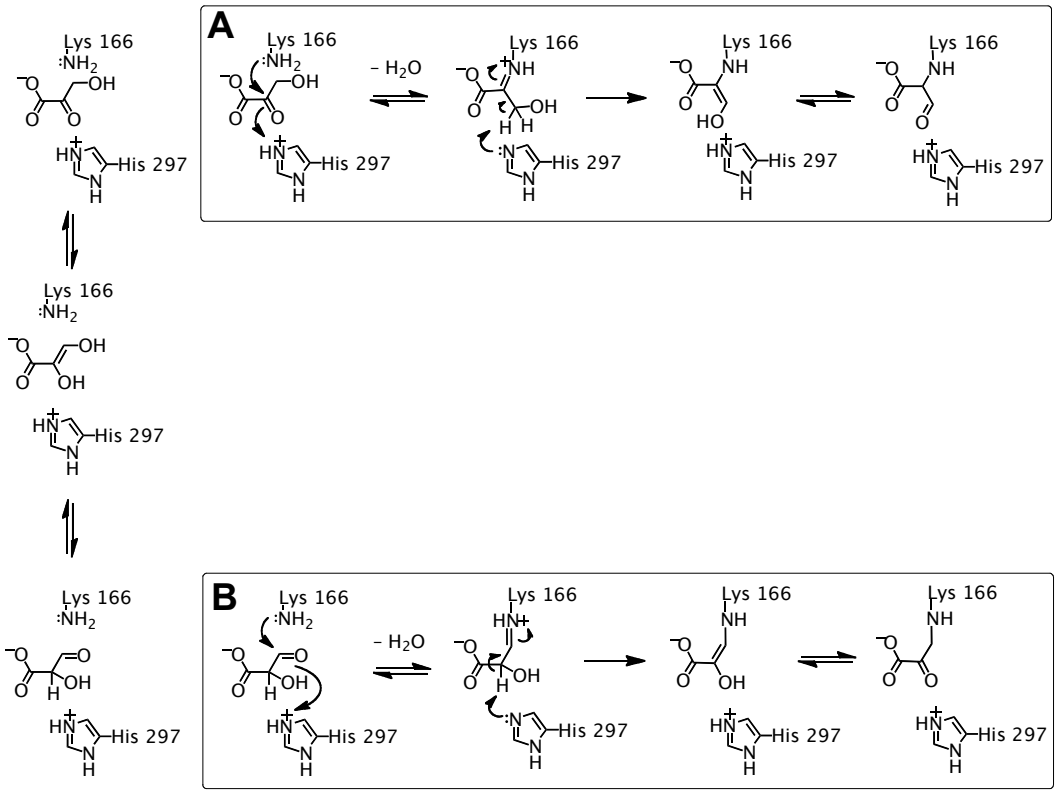

covalent aldehyde adduct (86 Da) **(Scheme 4.3 A)**. Alternatively, the presence of Mg^{2+} in the active site could promote tautomerism of 3-HP to tartronate semialdehyde (Hedrick & Sallach, 1961) and in that case, there would be reversible formation of a C_{β}-Schiff-base between the ε-amino group of Lys 166 and the β-carbonyl of tartronate semialdehyde **(Scheme 4.3 B)**. Subsequent deprotonation at α-C (again presumably by His 297) would yield an enol, which could tautomerize to yield the covalent α-keto adduct (86 Da). However, the ^{1}H NMR spectrum of 3-HP (in D_2O) incubated with $MgCl_2$ (~5 mM) for 4 h did not show conversion of 3-HP to tartronate semialdehyde (i.e., there were no signals for either the aldehyde proton or the α-proton) **(Figure 4.9)**. Therefore, the inactivation by 3-HP would most likely proceed via a mechanism shown in **Scheme 4.3 A**. Indeed, the x-ray crystal structure of MR inactivated by 3-HP (MR–3-HP complex, PDB entry as 4X2P (Nagar *et al*., 2015), solved by Dr. Martin St. Maurice and Brittney Wyatt), confirmed that Lys 166 attacks at the α-carbon of the 3-HP **(Figure 4.10)**. The absence of an 86 Da adduct in H297N-MR treated with 3-HP suggests that His 297 is required for inactivation while the increased mass of 88 Da for the TK-peptide from H297N-MR treated with 3-HP in presence of $NaCNBH_3$ **(Figure 4.8)** is consistent with reduction of the Schiff-base. These observations are in accord with the proposed inactivation mechanism via C_{α}-Schiff-base **(Scheme 4.3 A)**. Although the lithium salt of 3-HP exists as the hydrate (*gem*-diol form) in solution (Bellamy & Williams, 1958; Cooper *et al*., 1983; Dickens & Williamson, 1958), formation of the Schiff-base suggests that 3-HP must be present as the keto form (i.e., dehydrated) within the active site which is not surprising since divalent metal ion coordination could facilitate dehydration of the *gem*-

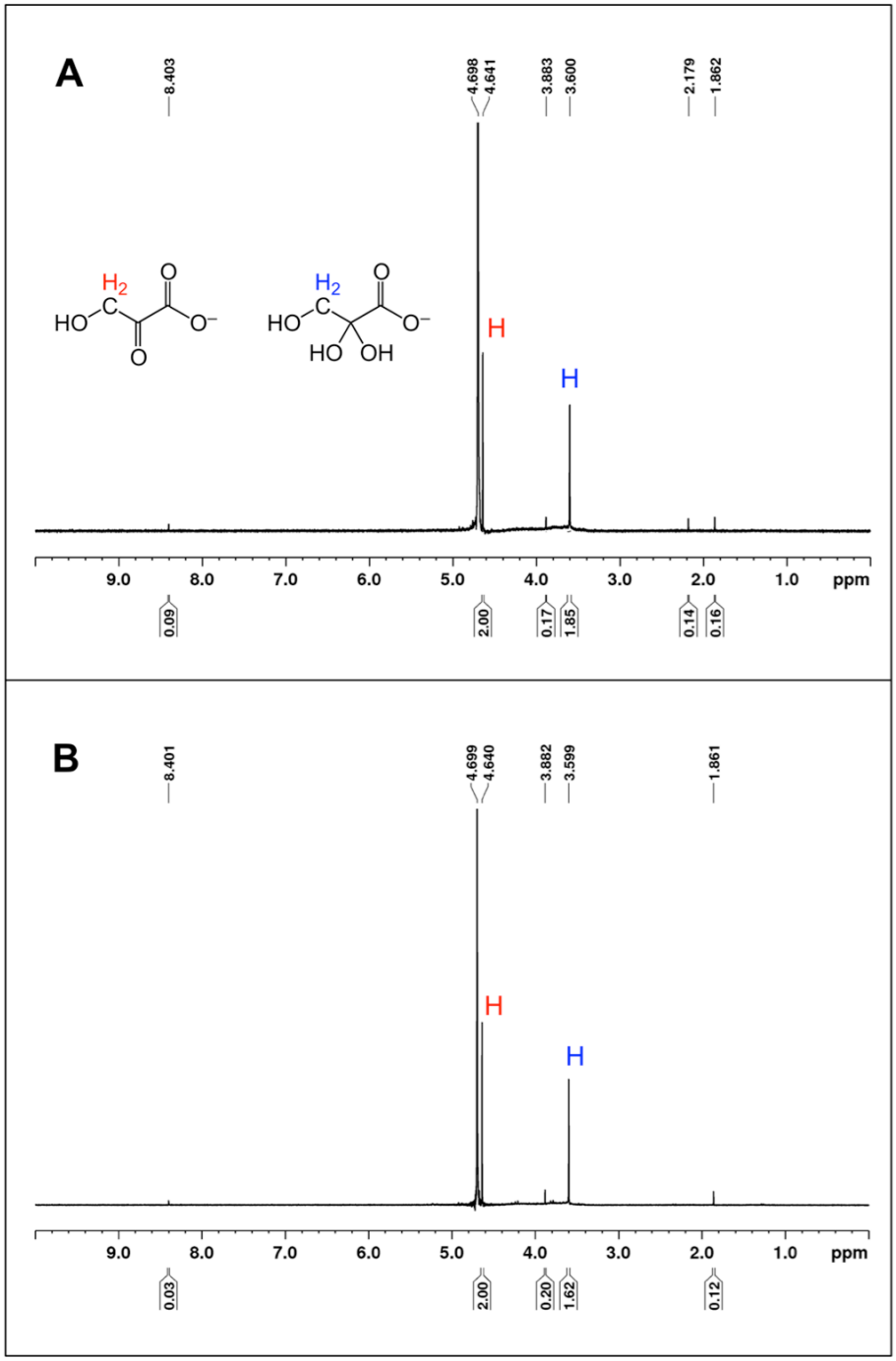

Figure 4.9 ^{1}H NMR spectra of 3-hydroxypyruvate in D_2O containing $MgCl_2$ (5 mM) (pH ~7.0) at 0 h (A) and 4 h (B). The signals from the β-protons of 3-HP (4.64 ppm; 2H, s) and its hydrate in *gem*-diol form (3.60 ppm; 2H, s) (refer inset for structures) are shown as red and blue, respectively. The integrals from each peak are shown below the x-axis. Peak at 4.69 ppm corresponds to the HOD signal. All other minor signals likely arise from the impurities present in the commercial sample. The spectra were obtained using 300 MHz Brüker AV-300 spectrometer.

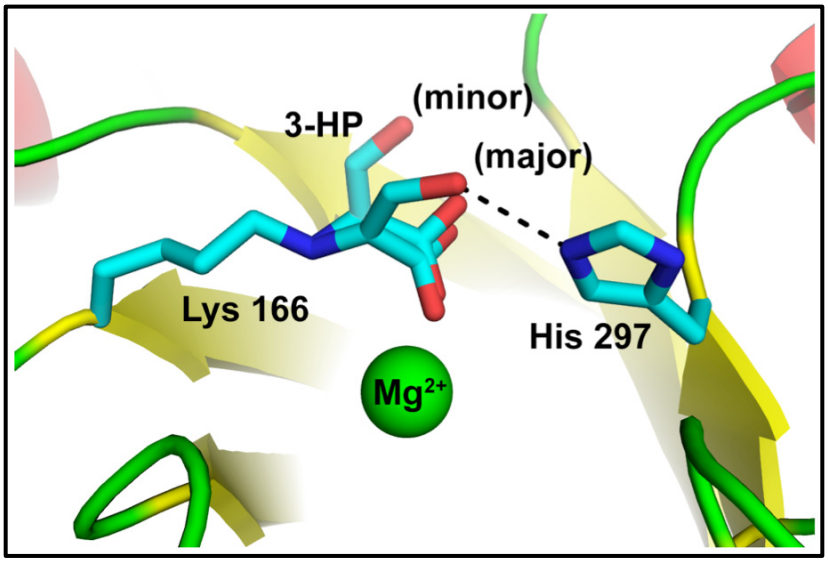

Figure 4.10 View of the active site of the x-ray structure of MR–3-HP complex [PDB entry 4X2P (Nagar *et al.*, 2015)] showing major (70%) and minor (30%) conformations of 3-HP adduct with Lys 166. The bond between the ε-amino of Lys 166 and the α-C of 3-HP is consistent with the mechanism shown in Scheme 4.3 A.

diol form (Pocker & Meany, 1970). Whether the product adduct exists as the aldehyde or enol is not known; however, the enol (enolate) may be preferred since enolase, which has similar active site architecture, is strongly inhibited by the enolate of D-tartronate semialdehyde phosphate (Lane & Hurst, 1974; Spring & Wold, 1971). Certainly, the active site of MR is optimized to stabilize the enolate in accord with its ability to catalyze racemization.

3-HP is a known irreversible inhibitor of members of the *N*-acetylneuraminate lyase (NAL)-superfamily. This superfamily includes NAL, dihydrodipicolinate synthase (DHDPS), trans-*o*-hydroxybenzylidene-pyruvate hydratase-aldolase, and D-4-deoxy-5-oxoglucarate dehydratases (Babbitt & Gerlt, 1997; Gerlt & Babbitt, 2009; Lawrence *et al*., 1997), which have been included within the class I aldolases (Nagano *et al*., 2002) by the SCOP database based on their Schiff-base chemistry and common $(\alpha/\beta)_8$-fold (or TIM barrel). 3-HP inactivates NAL from *Clostridium fringens* (DeVries & Binkley, 1972) and *E. coli* (Lawrence *et al*., 1997), and DHDPS from *E. coli* (Dobson *et al*., 2008) via a mechanism similar to that shown in **Scheme 4.3 A**. In fact, the x-ray crystal structure of the covalently modified NAL (Lawrence *et al*., 1997) and DHDPS (Dobson *et al*., 2008) enzymes revealed the presence of an aldehyde/enol-lysine adduct identical to the one proposed in **Scheme 4.3 A**. In spite of the similar mechanism of inactivation by 3-HP, the apparent second-order rate constant (k_{inact}/K_I) for the inactivation of wtMR is ~138 times greater than that observed for inactivation of DHDPS (0.56 $M^{-1}s^{-1}$, (Dobson *et al*., 2008)). This difference in rate constants could be due to the high proficiency of MR to stabilize the enolic intermediate during racemization.

4.4.3 Mechanistic Link Between Enzyme Superfamilies

Based on sequence, structure, and function comparisons, many of the enzymes that share $(\alpha/\beta)_8$-fold (or TIM barrel) topology, including class I aldolases, class II aldolases, and enzymes from enolase and NAL superfamilies, show links of common ancestry (i.e., are believed to have arisen via divergent evolution from a common or limited number of progenitor enzymes) (Copley & Bork, 2000; Gerlt & Raushel, 2003; Nagano *et al*., 2002). Allen and coworkers conducted a comparison of the primary and secondary structures of class I aldolases and members of the NAL superfamily and concluded that these enzymes are related by divergent evolution from a common ancestor and could all be included in a large superfamily utilizing Schiff-base chemistry **(Scheme 4.4)** (Choi *et al*., 2006). Although the reaction mechanisms of the two classes of aldolases are totally different **(Scheme 4.4)**, the ancestral aldolase "stepping-stone progenitor" has been proposed to be a Schiff-base-forming enzyme which evolved into the metal-dependent class II aldolase (Copley & Bork, 2000; Nagano *et al*., 2002). Since there is a clear mechanistic link between class II aldolases and the metal-dependent enolase superfamily (Rakus *et al*., 2008), i.e., the formation of a 'masked' carbanionic intermediate **(Scheme 4.1 & 4.4)**, the irreversible inhibition of MR by 3-HP via a Schiff-base mechanism strongly suggests that the enolase superfamily might have evolved from the same common ancestor that evolved into the class I & class II aldolases. Thus, this study provides a mechanistic evidence to support the divergent evolution of TIM $(\alpha/\beta)_8$ barrel families suggested on the basis of sequence and structure.

Scheme 4.4 Partial reaction mechanisms of aldolases and members of the NAL superfamily

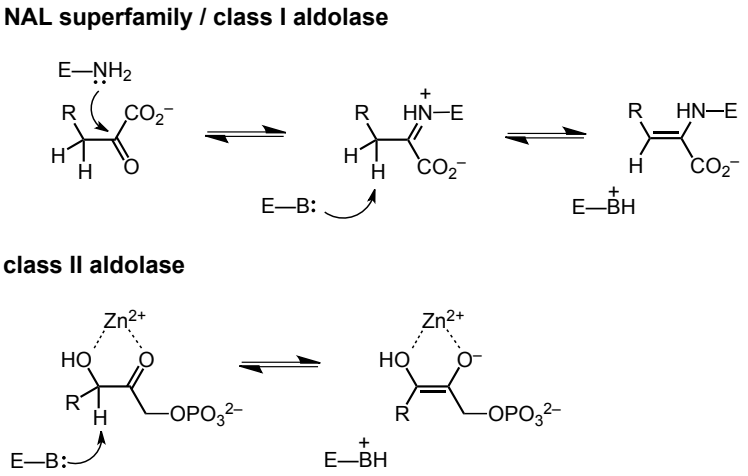

CHAPTER 5

ROLE OF TYR 54 IN MR CATALYSIS

*Reproduced in part with permission from – Lietzan, A. D., Nagar, M., Pellmann, E. A., Bourque, J. R., Bearne, S. L., and St. Maurice, M. (2012) Structure of Mandelate Racemase with Bound Intermediate Analogues Benzohydroxamate and Cupferron. Biochemistry **51**, 1160-1170. Copyright 2012 American Chemical Society.*

5.1 INTRODUCTION

MR is very proficient at discriminating between the substrate in the ground state and the altered substrate in the transition state, binding the latter species with an association constant equal to 5×10^{18} M^{-1} and stabilizing the transition state of the reaction by 26 kcal/mol (Bearne & Wolfenden, 1997; St. Maurice & Bearne, 2002). Various electrostatic and H-bonding interactions including interactions of the Asn 197 (St. Maurice & Bearne, 2000) and Glu 317 (Landro *et al*., 1994; Mitra *et al*., 1995) side chains with the α-hydroxyl group and carboxylate group of the substrate, respectively, and chelation of Mg^{2+} by the α-hydroxyl group and one of the carboxylate oxygens of the substrate (Cleland *et al*., 1998; Neidhart *et al*., 1991) have been shown to stabilize the transition state. In addition to these interactions, hydrophobic effects also contribute to TS stabilization by MR (St. Maurice & Bearne, 2004), suggesting a possible role for hydrophobic cavity residues in specifically stabilizing the altered substrate in the TS.

Comparison of the crystal structures of MR bound with the transition state analogues BzH and cupferron (CfN) to the MR structure with bound (*S*)-atrolactate, a substrate analogue, showed overall constriction of the active site, including the hydrophobic pocket (Lietzan *et al*., 2012). Despite the overall constriction of the active site, no major changes in the positions of hydrophobic amino acid side chains located in

the hydrophobic cavity could be confidently identified in the structures of MR with either bound CfN or BzH at 2.2-Å resolution (Lietzan *et al*., 2012). However, Tyr 54, which is part of the 50s loop of the *S*-specific pocket (Siddiqi *et al*., 2005), does appear to change its orientation slightly in the intermediate-bound state **(Figure 5.1)**, moving closer to the phenyl ring of BzH and CfN, thereby raising the possibility that it may interact with the phenyl ring of the *aci*-carboxylate intermediate during catalysis.

In this chapter, construction and characterization of the Y54F and Y54L mutants of MR is discussed in order to explore the role of Tyr 54 in both ground state binding and transition state stabilization. Similar kinetic parameters of Y54F, Y54L, and wtMR indicate that the role of Tyr 54 in MR catalysis is relatively minor. Therefore, it appears that alterations in the active site architecture of MR that contribute to discrimination between the ground state and the altered substrate in TS are extremely subtle.

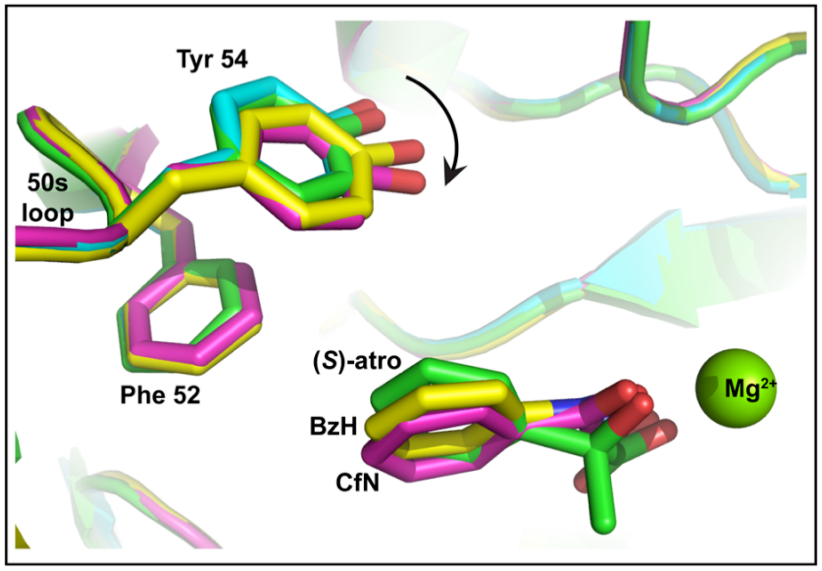

Figure 5.1 Side-chain movements of Tyr 54 associated with ligand binding. Structural overlay of the ligand-free MR [cyan; PDB entry 2MNR (Neidhart *et al*., 1991)], the MR–(*S*)-atrolactate complex [green; PDB entry 1MDR (Landro *et al*., 1994)], the MR–BzH complex [yellow; PDB entry 3UXK (Lietzan *et al*., 2012)], and the MR–CfN complex [magenta; PDB entry 3UXL (Lietzan *et al*., 2012)] reveals that there is not any significant change in active site structure including the hydrophobic pocket. The only exception is the side chain of Tyr 54 that moves closer to the intermediate analogues, suggesting a possible role for this residue in TS stabilization.

5.2 MATERIALS AND METHODS

5.2.1 General

(*R*)- and (*S*)-Mandelic acid, benzohydroxamic acid, and all other reagents, unless mentioned otherwise, were purchased from Sigma-Aldrich Canada Ltd. (Oakville, ON). Circular dichroism (CD) assays and spectral measurements were conducted using a JASCO J-810 spectropolarimeter. DNA oligonucleotide primers were obtained from Integrated DNA Technologies (Coralville, IA, USA) and restriction endonucleases were purchased from New England Biolabs (Ipswich, MA, USA)

5.2.2 Site-Directed Mutagenesis

To create the Y54F and Y54L MR variants, the pET-52b(+)-wtMR plasmid was used as the template for polymerase chain reaction-based site-directed mutagenesis using the QuikChange Site-Directed Mutagenesis Kit (Stratagene, La Jolla, CA) and following the protocols described by the manufacturer. The forward (F) and reverse (R) synthetic deoxyoligonucleotide primers used to incorporate the desired mutation into the ORFs encoding the Y54F- and Y54L-MR were as follows: 5′-CCATTCCTACCTGTTCGC A**TT**CACCCCCGTTGCG-3′ (F, Y54F), 5′-CGCAACGGGGGT**GA**ATGCGAACAGGT AGGAATGG-3′ (R, Y54F), 5′- CCATTCCTACCTGTTCGCA**CTC**ACCCCCGTTGCG -3′ (F, Y54L), 5′-CGCAACGGGGGT**GAG**TGCGAACAGGTAGGAATGG-3′ (R, Y54L). The codons specifying the relevant amino acids are underlined, and the altered bases are shown in boldface. After site-directed mutagenesis, mutant plasmids were used to transform competent *E. coli* DH5α cells for plasmid maintenance. Each mutant ORF was sequenced using commercial automated DNA sequencing (Robarts Research

Institute, London, ON) to ensure that no other alterations in the nucleotide sequence had been introduced. *E. coli* BL21(DE3) cells were used as the host for target gene expression, and the overproduced StrepII-tagged mutant MRs were purified as described below.

5.2.3 Expression and Purification of MR

Recombinant wild-type MR from *Pseudomonas putida* and other MR variants (Y54F & Y54L) were over-expressed and purified according to the protocol mentioned in section 2.2.2. Upon elution, the enzyme was dialyzed against storage buffer [HEPES buffer (100 mM, pH 7.5) containing $MgCl_2$ (3.3 mM), NaCl (200 mM), and glycerol (10%, v/v)] and stored at –20 °C. The purity of the enzyme preparations was assessed using SDS-PAGE (12% acrylamide) with staining by Coomassie blue R-250.

5.2.4 Kinetic Characterization of Y54F- and Y54L-MR

MR activity was assayed using a CD-based assay by following the change in ellipticity of mandelate at 262 nm with a 1-cm light path (unless otherwise indicated) as described by Sharp *et al*. (1979). All assays were conducted at 25 °C in Na^+-HEPES buffer (0.1 M, pH 7.5) containing $MgCl_2$ (3.3 mM) and bovine serum albumin (BSA, 0.005%). The concentrations of (*R*)- and (*S*)-mandelate for assays of both mutant MR enzymes ranged between 0.25–10.0 mM. The concentrations of variant MRs (Y54F and Y54L) were determined from their absorbance at 280 nm using an extinction coefficient of 51 910 M^{-1} cm^{-1} that was calculated using the ProtParam tool available on the ExPASy server (Gasteiger *et al*., 2003).

5.2.5 Inhibition by Benzohydroxamate

Inhibition experiments with BzH were conducted in Na^+-HEPES buffer (0.1 M, pH 7.5) containing $MgCl_2$ (3.3 mM) and using (*R*)-mandelate (0.5–20.0 mM) as the substrate. Assay details have been described in the above section. For the inhibition experiments, the following concentrations of the mutant enzymes and BzH were used: 158 ng/mL and 10, 20, 30, and 40 μM, respectively, for Y54F; 321 ng/mL and 25, 50, and 75 μM, respectively, for Y54L (using a cuvette with a 0.5-cm light-path). Competitive inhibition constants (K_i) were determined as described in Chapter 3. All kinetic parameters were determined in triplicate and average values are reported. The reported errors are the standard deviations.

5.3 RESULTS

To assess the role of Tyr 54 in MR catalysis, the Y54F- and Y54L-MR mutants were created using site-directed mutagenesis and the impact of these mutations on the interconversion of (*R*)- and (*S*)-mandelate was studied. Introduction of phenylalanine (Y54F) did not affect the binding (K_m) of either (*R*)- or (*S*)-mandelate but replacement of Tyr 54 with leucine slightly reduced the affinity of the enzyme for both substrates by ~2-fold **(Table 5.1)**. Similarly, the mutations had little impact on catalysis. The values of k_{cat} (in both the (*R*) → (*S*) and (*S*) → (*R*) reaction directions) were reduced by ~1.7-fold and ~2.5-fold (*cf.* wtMR) due to the Y54F and Y54L mutations, respectively **(Table 5.1)**, confirming that groups with higher hydrophobicity provide slightly better TS stabilization. These results are consistent with the binding affinity of Y54F- and Y54L-

Table 5.1 Kinetic parameters and competitive inhibition constants for the inhibition of MR variants by benzohydroxamate

enzyme	substrate	K_m (mM)	k_{cat} (s^{-1})	k_{cat}/K_m ($M^{-1}s^{-1}$)	K_i (μM)
wtMR	(*R*)-mandelate	1.2 ± 0.2	792 ± 19	6.5 (± 0.8) × 10^5	11.7 ± 1.2[a]
	(*S*)-mandelate	1.0 ± 0.1	637 ± 31	6.2 (± 0.8) × 10^5	
Y54F	(*R*)-mandelate	1.02 ± 0.06	456 ± 16	4.5 (± 0.3) × 10^5	13.0 ± 1.1
	(*S*)-mandelate	0.90 ± 0.08	397 ± 21	4.4 (± 0.5) × 10^5	
Y54L	(*R*)-mandelate	2.0 ± 0.2	253 ± 4	1.3 (± 0.1) × 10^5	25.7 ± 1.9
	(*S*)-mandelate	2.3 ± 0.3	301 ± 9	1.3 (± 0.2) × 10^5	

[a]Value is from Bourque *et al*. (2008)

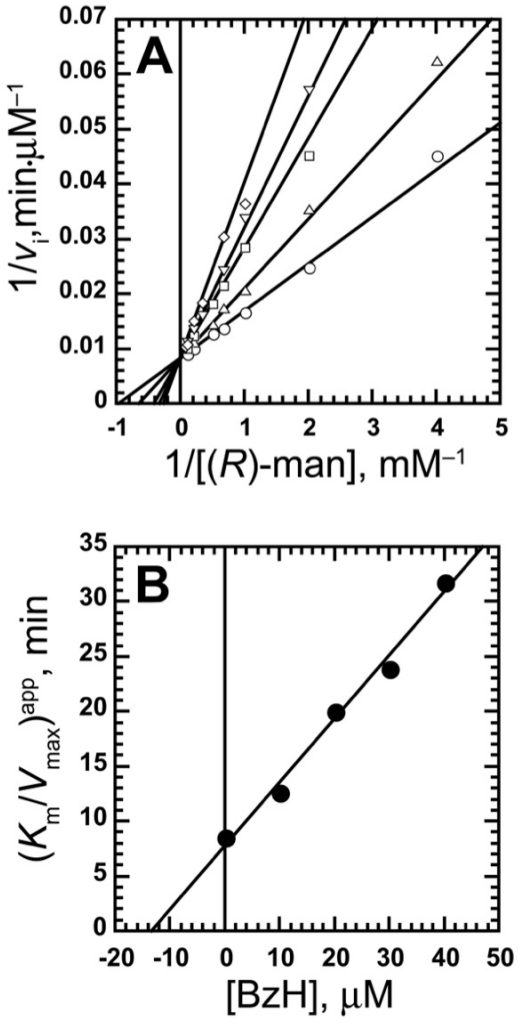

Figure 5.2 Inhibition of Y54F-MR by BzH. (A) A representative Lineweaver-Burk plot showing competitive inhibition of Y54F-MR by BzH. Assays were conducted as described in section 5.2.5 with the concentration of (*R*)-mandelate ((*R*)-man) ranging between 0.25–10 mM, and concentrations of BzH equal to 0 μM (○), 10 μM (△), 20 μM (□), 30 μM (▽), and 40 μM (◇). (B) A representative replot of the apparent K_m/V_{max} values (obtained by fitting equation 3.1 to the initial velocity data) as a function of BzH concentration. The negative of the x-intercept yields the K_i value (equation 3.2, Chapter 3). The average value of K_i = 13.0 ± 1.1 μM.

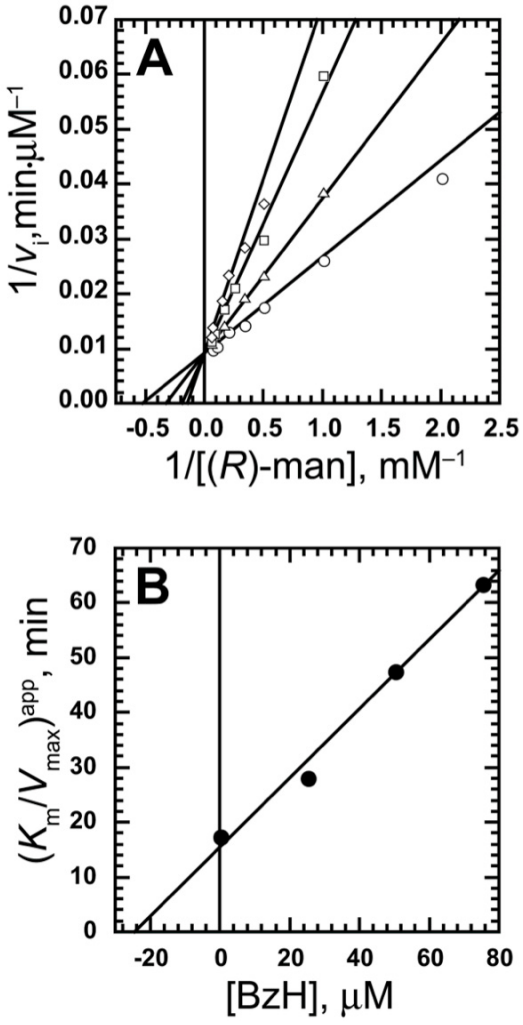

Figure 5.3 Inhibition of Y54L-MR by BzH. (A) A representative Lineweaver-Burk plot showing competitive inhibition Y54L-MR by BzH. Assays were conducted as described in section 5.2.5 with the concentration of (*R*)-mandelate ((*R*)-man) ranging between 0.5–10 mM, and concentrations of BzH equal to 0 μM (○), 25 μM (△), 50 μM (□), and 75 μM (◇). (B) A representative replot of the apparent K_m/V_{max} values (obtained by fitting equation 3.1 to the initial velocity data) as a function of BzH concentration. The negative of the x-intercept yields the K_i value (equation 3.2, Chapter 3). The average value of K_i = 25.7 ± 1.9 μM.

MR mutants for the transition state analogue inhibitor BzH. Inhibition studies of these mutants with BzH **(Figure 5.2** & **5.3)** revealed that Y54F-MR and wtMR both bound BzH with similar affinity, which is 2.2-fold better than that measured for Y54L-MR **(Table 5.1).**

5.4 DISCUSSION

Analysis of the structures of MR with bound substrate analogues and transition state analogues indicated a possible role of Tyr 54 in MR catalysis (Lietzan *et al*., 2012). The *p*-hydroxyl group of tyrosine could interact with the phenyl ring of substrate via weak H-bond interactions (Nallini *et al*., 2004; Schaefer *et al*., 1984). Therefore, to assess whether the hydroxyl and/or aromatic ring of the Tyr 54 side chain play a role in MR catalysis, Y54F- and Y54L-MR mutants were created. Relative to the kinetic parameters for wtMR, the Y54F mutation had negligible effects on the binding affinity for substrate (K_m), turnover (k_{cat}), and catalytic efficiency (k_{cat}/K_m) when either (*R*)- or (*S*)-mandelate was the substrate. In addition, the binding affinity of BzH was not altered significantly for this mutant **(Table 5.1)**. Hence, interactions with the hydroxyl group of Tyr 54 do not play a significant role in TS stabilization.

If the aromatic ring of Tyr 54 plays a specific role in TS stabilization, then the Y54L mutation should exhibit a much more significant effect on k_{cat}/K_m than on K_m for (*R*)- and (*S*)-mandelate. Conversely, if Tyr 54 contributes generally to the packing of the hydrophobic cavity, the Y54L mutation is expected to have an effect on both substrate binding [manifested in K_m for (*R*)- and (*S*)-mandelate, because $K_m = K_s$ for MR (St. Maurice & Bearne, 2002)] and TS stabilization (manifested in k_{cat}/K_m). The Y54L

mutation results in only a ~2-fold increase in K_m over that of the wild-type enzyme but a 5-fold decrease in k_{cat}/K_m when either (*R*)- or (*S*)-mandelate is the substrate **(Table 5.1)**. This drop in catalytic efficiency corresponds to ~0.9 kcal/mol loss in TS stabilization, which indicates that Tyr 54 plays a relatively minor role in TS stabilization. Interestingly, the effect of the Y54L mutation on the steady state kinetic parameters is much smaller than the effect observed upon mutation of several other hydrophobic pocket residues (Bourque & Bearne, 2008; Siddiqi *et al*., 2005). Thus, the motion of the Tyr 54 side chain during the MR catalysis is likely a consequence of altered packing rearrangements due to reduction in cavity volume of the hydrophobic pocket (Lietzan *et al*., 2012) rather than a result of a specific role for Tyr 54 in TS stabilization.

CHAPTER 6

AN ADDITIONAL ROLE OF THE BRØNSTED ACID-BASE CATALYSTS OF MR

6.1 INTRODUCTION

MR catalyzes the Mg^{2+}-dependent 1,1-proton transfer that interconverts the enantiomers of mandelate via highly unstable *aci*-carboxylate intermediate using a two-base mechanism (Gerlt, 1998). When MR converts (*S*)- to (*R*)-mandelate, His 297 acts as a Brønsted acid (pK_a~6) and Lys 166 acts as a Brønsted base (pK_a~10). In the opposite direction, the roles and pK_a values of His 297 and Lys 166 are interchanged (Kallarakal *et al*., 1995; Landro *et al*., 1994; Powers *et al*., 1991) (**Scheme 6.1**). MR is an extremely proficient enzyme and can discriminate between the substrate in the ground state and the altered substrate in the transition state (TS), binding the latter species with an association constant equal to 5×10^{18} M^{-1} corresponding to stabilization of the TS by 26 kcal/mol (Bearne & Wolfenden, 1997; St. Maurice & Bearne, 2002). Extensive studies on MR have revealed various electrostatic interactions that facilitate stabilization of the altered substrate in TS, for example, Glu 317 acts as a general acid catalyst (Mitra *et al*., 1995), Lys 164 interacts with the carboxyl group of mandelate (Neidhart *et al*., 1991), and Asn 197 interacts with the α-hydroxyl of mandelate (St. Maurice & Bearne, 2000).

Studies from the Bearne Lab have shown that BzH (K_i = 9.3 mM (St. Maurice & Bearne, 2000)) is a potent reversible competitive inhibitor of MR and is a reasonable mimic of the TS and/or intermediate (Lietzan *et al*., 2012). St. Maurice & Bearne (2004) studied the binding of a series of intermediate analogues (BzH analogues bearing

Scheme 6.1 MR-catalyzed reaction with possible cation-π/NH-π interactions

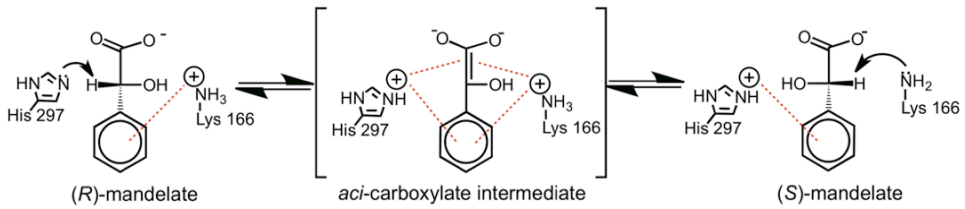

different alkyl groups in place of the phenyl group) within the hydrophobic cavity to evaluate the role of hydrophobic interactions in stabilizing altered substrate in the TS, and demonstrated that the free energy of binding is directly proportional to the hydrophobicity of the group replacing phenyl ring. Surprisingly, MR exhibited greater binding affinity for BzH than predicted solely on the basis of hydrophobic interactions (St. Maurice & Bearne, 2004). The crystal structure of MR complexed with BzH reveals that the Brønsted acid/base catalysts, Lys 166 and His 297, are located equidistant from the α-carbon of BzH (Lietzan *et al*., 2012). The distances from the ζN of Lys 166 to the center of phenyl ring and the C=N bond of hydroxamate moiety are 4.8 and 3.0 Å, respectively, while the distances from the ε^2N of the imidazole ring of His 297 to the center of the phenyl ring and the C=N bond of the hydroxamate moiety are 4.5 and 3.1 Å, respectively **(Figure 6.1)**. These distances are well within the reported range (3.4–6 Å) for cation-π interactions (specifically known as NH-π interactions if the amino group of a lysine, arginine, asparagine, glutamine, and histidine side chain contain a δ(+) charge rather than a full formal positive charge) observed in a number of high-resolution protein structures (Burley & Petsko, 1986; Mitchell *et al*., 1994; Scrutton & Raine, 1996; Zacharias & Dougherty, 2002). Therefore, it is important to realize that the side chains of Lys 166 and His 297 could interact with the π-electron cloud of the ligand to stabilize the TS. Similarly, the crystal structure of MR complexed with (*S*)-atrolactate, a substrate analogue, shows that the phenyl ring is inclined towards the His 297, and the positive charge on this Brønsted acid could aid in substrate binding. In short, cation-π/NH-π interactions could play a role in the substrate binding in ground state as well as in stabilizing the altered substrate in the TS **(Scheme 6.1)**.

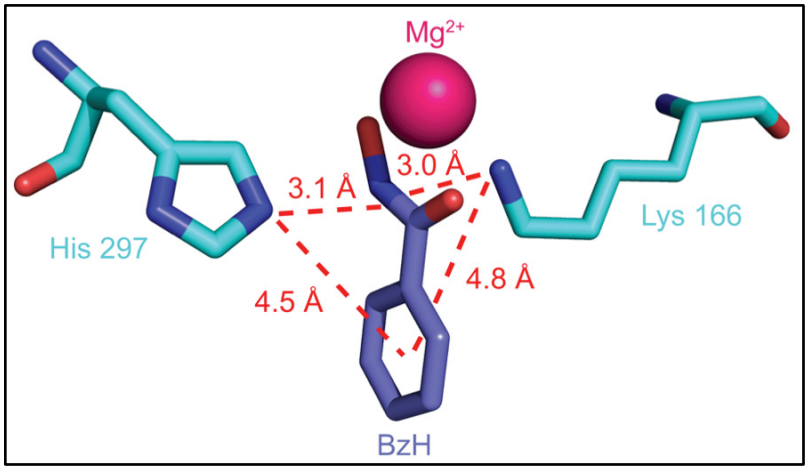

Figure 6.1 Active site of MR with bound BzH [PDB entry 3UXK (Lietzan *et al.*, 2012)] showing distances between the Brønsted acid-base catalysts and the hydroxamate moiety and the phenyl ring.

In the present chapter, binding interactions between the active-site bases Lys 166 and His 297, and the substrate or TS/intermediate analogues were analyzed using site-directed mutagenesis and isothermal titration calorimetry (ITC). Binding affinities of wtMR and various MR variants (i.e., K166C, K166M, H297N, and K166M/H297N MR mutants) with TS analogues (BzH and cyclohexanecarbohydroxymate (CHCHA)) and substrate analogues ((*R*)- and (*S*)-atrolactate) were measured using ITC **(Figure 6.2)**. The implications of changes in thermodynamic parameters are discussed in terms of electrostatic interactions that might participate in ligand binding. Thermodynamic analysis of the binding of wtMR to BzH revealed an entropy-driven interaction with a negative ΔC_p (heat capacity change), which is consistent with increased hydrophobic interactions. Furthermore, comparison of the binding affinities of the MR variants for BzH, (*R*)-atrolactate, and (*S*)-atrolactate also indicated that electrostatic interactions occur between the conjugate acids of Lys 166/His 297 and the aromatic ring. However, CHCHA, which lacks an aromatic ring, showed a similar trend in altered binding affinities as BzH, suggesting that the active site Brønsted acid catalysts not only interact with phenyl ring but also interact with the π-system of hydroxamate moiety. Overall, the results reveal that the conjugate acids of His 297 and Lys 166 interact with the π-system of the phenyl ring during substrate binding; in addition, they (predominantly Lys 166) also likely interact with the enolate moiety of the *aci*-carboxylate intermediate (and TS). Therefore, Lys 166 and His 297 play a dual role; they can act as Brønsted acid/base catalysts and can provide stabilization for the delocalized negative charge of the carbanionic intermediate/TS.

Figure 6.2 Ligands used for ITC studies

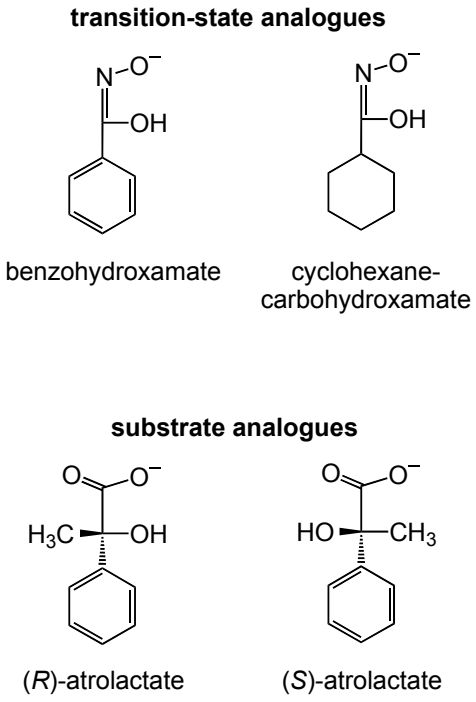

6.2 MATERIALS AND METHODS

6.2.1 General

Benzohydroxamate, and all other reagents, unless mentioned otherwise, were purchased from Sigma-Aldrich Canada Ltd. (Oakville, ON, Canada). (*R*)- and (*S*)-Atrolactic acid were purchased from Alfa Aesar (Heysham, Lancashire, UK). Cyclohexanecarbohydroxamic acid (CHCHA) was previously synthesized in the Bearne lab (St. Maurice & Bearne, 2004). All reagents were of highest quality available, and were used without purification. DNA oligonucleotide primers were obtained from Integrated DNA Technologies (Coralville, IA, USA) and restriction endonucleases were purchased from New England Biolabs (Ipswich, MA, USA). Binding studies were conducted using a VP-ITC MicroCalorimeter (MicroCal, Inc., Northampton, MA). Circular dichroism (CD) spectral measurements were conducted using a JASCO J-810 spectropolarimeter (Jasco Inc., Easton, MI).

6.2.2 Site-Directed Mutagenesis

The MR variants K166M, K166C, H297N, and K166M/H297N were created using site-directed mutagenesis. For the K166M and H297N MR variants, the pET-52b(+)-wtMR plasmid was used as the template for polymerase chain reaction-based site-directed mutagenesis using the QuikChange Site-Directed Mutagenesis Kit (Stratagene, La Jolla, CA) and following the protocols described by the manufacturer. The forward (F) and reverse (R) synthetic deoxyoligonucleotide primers used to incorporate the desired mutation into the ORFs encoding the K166M, K166C, and H297N MR variants were as follows: 5′-GCGGTTAAGACCA**T**GATCGGCTATCCGGC-3′ (F, K166M), 5′-

GCCGGATAGCCGATC**A**TGGTCTTAACCGC-3′ (R, K166M), 5′-GCGGTTAAGAC C**TGC**ATCGGCTATCCGGC-3′ (F, K166C), 5′-GCCGGATAGCCGAT**GCA**GGTCT TAACCGC-3′ (R, K166C), 5′-CCAATGTCCAGC**A**ACCTGTTCCAAGAAATCAGC-3′ (F, H297N), 5′-GCTGATTTCTTGGAACAGGT**T**GCTGGACATTGG-3′ (R, H297N). The modified codons are underlined and the altered bases are shown in boldface. The double mutant K166M/H297N-MR was created by using pET-52b(+)-H297N-MR as the template, and the forward and reverse K166M primers. After site-directed mutagenesis, mutant plasmids were used to transform competent *E. coli* DH5α cells for plasmid maintenance. Each mutant ORF was sequenced using commercial automated DNA sequencing (Robarts Research Institute, London, ON) to ensure that no other alterations in the nucleotide sequence had been introduced.

6.2.3 Expression and Purification of MR

StrepII-tagged recombinant variants of MR (wtMR, K166M-MR, K166C-MR, H297N-MR and K166M/H297N-MR) were over-expressed in and purified from *E. coli* BL21(DE3) cells, as described in Chapter 2 (Section 2.2.2). The protein concentration was determined by the intrinsic enzyme absorbance at 280 nm using an extinction coefficient $\varepsilon = 53400\ M^{-1}\ cm^{-1}$ for all MR variants which was estimated using ProtParam program from ExPasy (Gasteiger *et al*., 2005).

6.2.4 Circular Dichroism Spectroscopy

The effects of mutations on the secondary structure of MR variants were evaluated using circular dichroism (CD) spectroscopy. WtMR, K166M-MR, and H297N-

MR were dialyzed against potassium phosphate buffer (10 mM, pH 7.4). The samples were adjusted to give a protein concentration of 160 μg/mL. CD spectra were obtained using using 0.1-cm quartz cuvette. MR samples and buffer were scanned from 190 to 260 nm in 1 nm increments at 25 °C. Three consecutive scans were done and data were averaged for each sample. The buffer spectrum was subtracted from each MR variant spectra before analyzing CD data using DICHROWEB http://dichroweb.cryst.bbk.ac.uk/html/home.shtml (Whitmore & Wallace, 2004, 2008).

6.2.5 Isothermal Titration Calorimetry Studies

Ligand solutions of TS analogues (BzH and CHCHA) and substrate analogues ((*R*)- and (*S*)-atrolactic acid) were prepared in the final dialysis buffer to eliminate heat signals that could arise from buffer mismatch. The enzyme and ligand solutions were degassed (Microcal Thermovac) for 15 min, before loading into the sample cell (1.46 mL) and injection syringe (297 μL), respectively. The stirred-cell contained MR variants at a typical concentration of 30–77 μM and the injection syringe contained various concentrations of BzH (0.55–40 mM), CHCHA (2 -10 mM), (*R*)-atrolactate (7.5–25 mM) or (*S*)-atrolactate (2–20 mM), depending upon the experiment. Titrations of BzH and CHCHA into solutions containing MR variants were conducted at 15 °C while the titrations using (*R*)- and (*S*)-atrolactate as the ligands were conducted at 20 °C. For most of the titration experiments, a total of 21–25 injections of 6–10 μL were made at 240 s intervals. The heat released due to the initial injection (typically 2–4 μL) was excluded from data analyses to minimize the effect of titrant diffusion from the syringe tip during the equilibration process. As a control, ligand titrations were also conducted with the

sample cell containing only buffer to correct for the heats of dilution and mixing. The dilution isotherm of each ligand was subtracted from the appropriate binding isotherm prior to curve fitting. Binding affinities, ΔH, and ΔS of binding of the MR variants to the TS and substrate analogues were obtained by fitting the calorimetric data to a single-site model using the Origin 7.0 software (OriginLab, Northampton, MA) with the stoichiometry parameter *n* fixed at 1.0.

Determination of the binding affinity for a low-affinity ligand-enzyme system using competition-based ITC. The thermodynamic parameters for the binding of H297N-MR to (*S*)-atrolactate, a low-affinity ligand (designated L_2), were determined by the following ITC experiments. First, the H297N-MR was titrated with BzH, a high-affinity, competitive ligand (L_1) that occupies the same binding site as the low-affinity ligand. This yields the binding affinity (K_1) for L_1. Second, BzH was titrated into a solution containing H297N-MR (36.9 μM) saturated with (*S*)-atrolactate (20 mM) (L_{2sat}) to obtain the apparent binding affinity (K_{app}). Equation 6.1 correlates the binding affinity for the (*S*)-atrolactate (K_2) with K_{app}, and therefore, K_2 can be calculated according to equation 6.2 (Zhang & Zhang, 1998) .

$$K_{\text{app}} = \frac{K_1}{1 + K_2 \cdot \text{L}_{\text{2sat}}} \tag{6.1}$$

$$K_2 = \left(\frac{K_1}{K_{\text{app}}} - 1\right) \cdot \frac{1}{\text{L}_{\text{2sat}}} \tag{6.2}$$

Similar experiments were carried out to determine the binding affinity of K166M for (*R*)-atrolactate. For this particular mutant, (*S*)-atrolactate was used as a high affinity competitive ligand (see results). In this case, (*S*)-atrolactate was titrated into a solution

containing K166M-MR (67.2 μM) and (*R*)-atrolactate (20 mM) to obtain the apparent binding affinity (K_{app}). In competitive ITC experiments, the high affinity ligand was also titrated into the sample cell containing only the low affinity ligand in buffer to correct for the heat of dilution and mixing.

6.2.6 Determination of Heat Capacity Change for wtMR upon Binding of BzH

Titrations were carried out at four different temperatures (10, 15, 20, and 25 °C) to determine the heat capacity change (ΔC_p) of wtMR binding to BzH. The enthalpies of binding (ΔH) were plotted as a function of temperature and the slope of this linear plot is the heat capacity change accompanying BzH binding.

6.3 RESULTS

The structures of the various ligands that were used in this study are shown in **Figure 6.2** and the representative calorimetric titrations are shown in **Figures 6.3**, and **6.6–6.9**. In an ITC plot, each peak in the binding isotherm (top panels) is a single injection of ligand and the positive deflections from the baseline indicate that heat was absorbed while negative deflections indicate that heat was released. The enthalpy change accompanying each injection was plotted versus the [ligand]/[MR] molar ratio (bottom panels). The shape of a titration curve depends on the *c* value (i.e., the ratio of total analyte concentration in the ITC sample cell to the K_d value when the binding stoichiometry is 1:1) (Aitken *et al*., 2001; Broecker *et al*., 2011; Wiseman *et al*., 1989). High *c* values yield a sigmoidal curve; however, in order to accurately estimate parameters like K_d, ΔH, and *n* (stoichiometry number), the experimental range of the *c*

values must be 1–1000 (Wiseman *et al*., 1989), e.g., **Figure 6.9 B**. At low *c* values (< 1, typical for ligands with millimolar K_d values), the titration curve does not appear sigmoidal, e.g., **Figure 6.6 D** and a strong correlation between ΔH and *n* makes it difficult to accurately determine both of these simultaneously (Tellinghuisen, 2005). In order to increase the *c* value, i.e., to obtain a sigmoidal curve for a weak binding interaction, the enzyme concentration in the ITC sample cell should be in the millimolar range. This strategy could not be used for MR because of its tendency to precipitate at concentrations greater than 90 μM when stirred constantly during the ITC experiment. However, even at very low *c* values (i.e., 10^{-2}–10^{-3}), K_d can be calculated accurately with prior knowledge of binding stoichiometry, i.e., by fixing the value of *n* (Tellinghuisen, 2008; Turnbull & Daranas, 2003). Analysis of x-ray crystal structures of MR bound with substrate analogues, substrate-product analogues, and intermediate analogues confirms that a single molecule of ligand occupies a single active site per monomer (Landro *et al*., 1994; Lietzan *et al*., 2012; Nagar *et al*., 2014; Schafer *et al*., 1996). Therefore, while fitting raw ITC data using Origin, the value of *n* was set at 1.0 to determine reliable binding constants.

6.3.1 Heat Capacity Change for wtMR upon Binding of BzH

The change in heat capacity (ΔC_P) is defined as the dependence of the enthalpy change on temperature **(**equation 6.3**)** (Olsson *et al.*, 2008; Talhout *et al.*, 2003).

$$\Delta C_P = \frac{\delta \Delta H}{\delta T} \tag{6.3}$$

The thermodynamic parameters for wtMR binding BzH were measured at temperatures ranging from 10 to 25 °C **(Figure 6.3)** and the results are listed in **Table 6.1**. Within this temperature range, ΔH was linearly dependent on temperature **(Figure 6.4)** and the ΔC_P was determined to be –358 ± 3 cal/(mol•K). Change in heat capacity has been strongly linked to changes in both biomolecular and solvent hydrogen bonding (Olsson *et al.*, 2008). A negative ΔC_P value indicates that enhanced hydrophobic interactions may arise from removal of a non-polar surface from the solvent or the exclusion of bulk water from the enzyme active site (Guan *et al.*, 2011; Myslinski *et al.*, 2011; Parker *et al.*, 1999) upon BzH binding.

6.3.2 ITC Binding Study with BzH and CHCHA

As discussed above, the thermodynamic parameters for wtMR binding BzH were calculated at temperatures ranging from 10 to 25 °C. At 15 °C, the binding isotherms showed the highest heat signals with the lowest signal-to-noise ratio (*cf*. heat signals at 20 and 25 °C) **(Figure 6.3)** and therefore this temperature was selected for further studies. To assess the interaction of the Brønsted acid/base catalysts with the π-system of the phenyl ring in the TS, the binding of BzH and CHCHA (an analogue of BzH that bears a cyclohexyl group in place of the aromatic ring) were compared. BzH and CHCHA were titrated into solutions of various MR variants: wtMR, K166C, K166M, H297N, and K166M/H297N. Comparison of the CD spectra of wtMR, K166M and H297N suggests that mutations did not introduce any significant changes in the secondary structure **(Figure 6.5)**. Representative ITC plots for binding of BzH and CHCHA to the MR variants are shown in **Figure 6.6 A–E** and **Figure 6.7 A–C**, respectively, and the

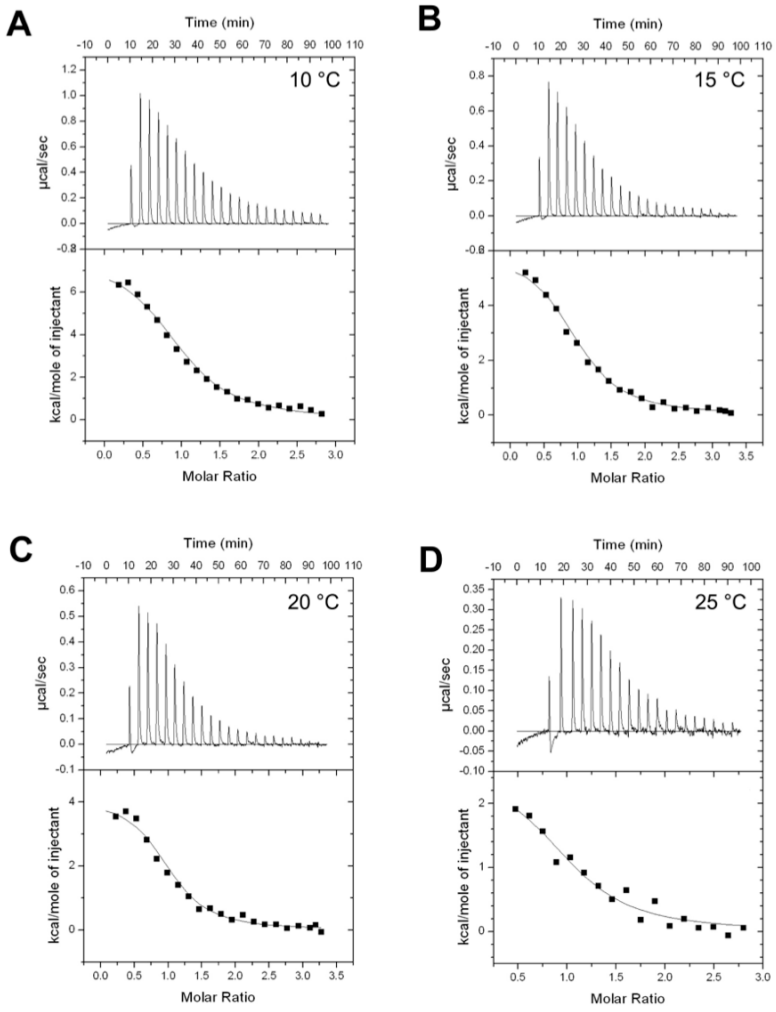

Figure 6.3 Representative ITC data for wtMR binding BzH at various temperatures. Isothermal calorimetry titration of (A) wtMR (31.82 μM) with BzH (0.55 mM, 10 μL per injection) at 10 °C, (B) wtMR (26.03 μM) with BzH (0.55 mM, 10 μL per injection) at 15 °C, (C) wtMR (26.03 μM) with BzH (0.55 mM, 10 μL per injection) at 20 °C, and (D) wtMR (28.97 μM) with BzH (0.55 mM, 10 μL per injection) at 25 °C. In each case (top panel), the first injection was 5 μL, and was omitted in the calculation of the thermodynamic parameters. The molar ratio is [BzH]/[wtMR].

Table 6.1 Thermodynamic parameters for wtMR binding BzH at various temperatures

Temp (°C)	K_d (μM)	Δ*G* (kcal/mol)	Δ*H* (kcal/mol)	TΔ*S* (kcal/mol)
10	5.25 ± 0.13	–6.82 ± 0.01	7.69 ± 0.04	14.51 ± 0.03
15	3.68 ± 0.10	–7.15 ± 0.02	5.89 ± 0.08	13.05 ± 0.08
20	2.90 ± 0.40	–7.42 ± 0.08	4.06 ± 0.07	11.49 ± 0.12
25	3.34 ± 1.07	–7.49 ± 0.22	2.33 ± 0.27	9.82 ± 0.06

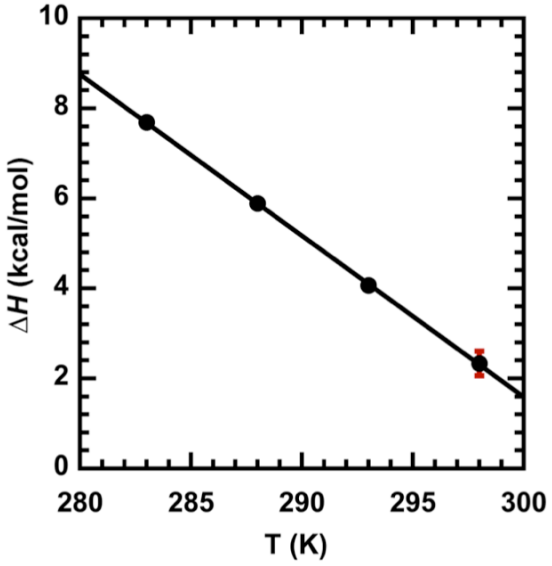

Figure 6.4 Heat capacity change accompanying wtMR binding of BzH. The binding enthalpy for BzH was measured at temperatures from 10 to 25 °C. ΔC_P (slope) = –358 ± 3 cal/(mol•K).

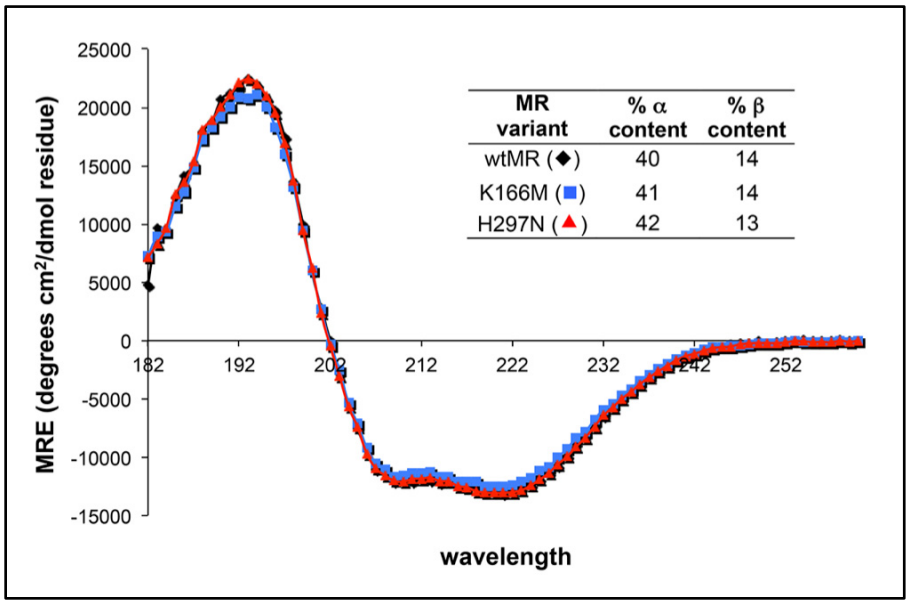

Figure 6.5 Far UV-CD spectra of wtMR, K166M-MR, and H297N-MR. The samples (160 μg/mL) were prepared in potassium phosphate buffer (10 mM, pH 7.4). α-Helical and β-strand content in each variant (inset) were determined by analyzing CD data using DICROWEB (Whitmore & Wallace, 2004, 2008).

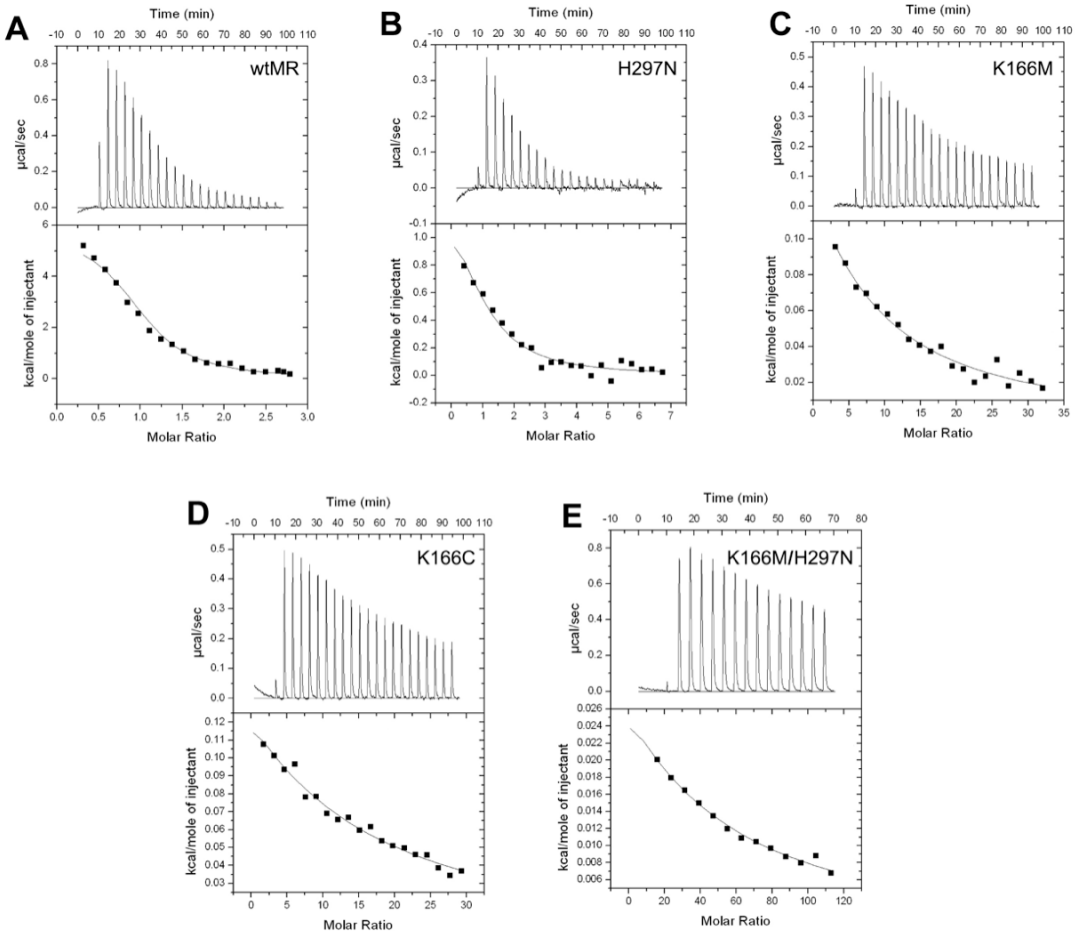

Figure 6.6 Representative ITC data for various MR variants binding BzH at 15 °C. Isothermal calorimetry titration of (A) wtMR (30.62 μM) with BzH (0.55 mM, 10 μL per injection), (B) H297N-MR (38.57 μM) with BzH (2.75 mM, 6 μL per injection), (C) K166M-MR (75.28 μM) with BzH (15.0 mM, 10 μL per injection), (D) K166C-MR (73.10 μM) with BzH (15.0 mM, 10 μL per injection), and (E) K166M/H297N-MR (56.96 μM) with BzH (40.0 mM, 15 μL per injection). In each case (top panel), the first injection was 2 μL except for in (A) which had a 5 μL injection, and these first injections were omitted for calculation of the thermodynamic parameters. The molar ratio is [BzH]/[MR variant].

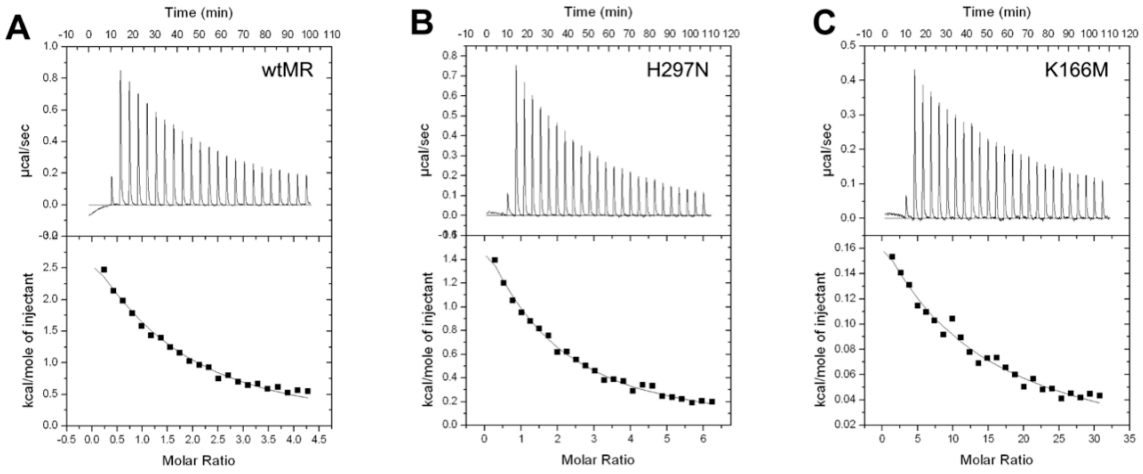

Figure 6.7 Representative ITC data for various MR variants binding CHCHA at 15 °C. Isothermal calorimetry titration of (A) wtMR (46.32 μM) with CHCHA (2.0 mM, 6 μL per injection), (B) H297N-MR (59.47 μM) with CHCHA (2.0 mM, 10 μL per injection), and (C) K166M-MR (60.29 μM) with CHCHA (10.0 mM, 10 μL per injection). The first injection in each case (top panel) was 2 μL, and was omitted for calculation of the thermodynamic parameters. The molar ratio is [CHCHA]/[MR variant].

Table 6.2 Thermodynamic parameters for the various MR variants binding the TS analogues BzH and CHCHA at 15 °C

MR variant	K_d (μM)	Δ*G* (kcal/mol)	Δ*H* (kcal/mol)	TΔ*S* (kcal/mol)
	BzH			
wtMR	3.7 ± 0.1	–7.15 ± 0.01	5.90 ± 0.08	13.05 ± 0.08
H297N	28.5 ± 2.9	–5.98 ± 0.06	1.62 ± 0.04	7.60 ± 0.03
K166M	1640 ± 90	–3.67 ± 0.02	2.85 ± 0.2	6.52 ± 0.19
K166C	3100 ± 265	–3.31 ± 0.04	4.94 ± 0.4	8.26 ± 0.35
K166M/H297N	8449 ± 910	–2.74 ± 0.06	2.85 ± 0.2	6.28 ± 0.27
	CHCHA			
wtMR	98.9 ± 10.4	–5.28 ± 0.06	7.94 ± 0.3	13.22 ± 0.30
H297N	156 ± 10	–5.02 ± 0.04	5.2 ± 0.2	10.23 ± 0.16
K166M	2020 ± 89	–3.54 ± 0.02	5.5 ± 0.2	9.09 ± 0.19

thermodynamic parameters are listed in **Table 6.2**.

6.3.3 ITC Binding Study with (*R*)- and (*S*)-Atrolactate

To investigate the interaction between the active site Brønsted acid/base catalysts and the phenyl ring of the substrate, (*R*)-atrolactate was titrated into solutions of wtMR **(Figure 6.8 A)** and H297N-MR **(Figure 6.8 B)**, and (*S*)-atrolactate was titrated into solutions of wtMR **(Figure 6.9 A)**, K166M **(Figure 6.9 B)**, and K166M/H297N **(Figure 6.9 D)** at 20 °C. The thermodynamic parameters are listed in **Table 6.3**. The K_d values for wtMR binding (*R*)- and (*S*)-atrolactate are 259 μM and 557 μM, respectively, and are in reasonable agreement with the previously reported binding affinities ((*R*)-atrolactate, K_i = 410 μM (Landro *et al*., 1994) and 950 μM (St. Maurice & Bearne, 2000); and (*S*)-atrolactate, K_i = 150 μM (Landro *et al*., 1994)) determined from inhibition studies using the CD assay. Direct titration of (*R*)-atrolactate and (*S*)-atrolactate into K166M-MR and H297N-MR, respectively, failed to yield any heat signals, suggesting very weak binding interactions. To overcome this problem, a displacement titration or competition-based method was used to the determine dissociation constant (Zhang & Zhang, 1998). BzH, a high affinity ligand for H297N-MR (K_d = 28.5 μM, **Table 6.2**) was titrated into the solution containing H297N-MR and (*S*)-atrolactate **(Figure 6.9 C)** to determine the K_d value of H297N-MR binding (*S*)-atrolactate (K_d = 36.6 mM, **Table 6.3**). Similarly, to estimate the K_d value of K166M-MR binding (*R*)-atrolactate, (*S*)-atrolactate was used as a primary ligand because of the unexpectedly high binding affinity of K166M-MR for this ligand (K_d = 3.94 μM, **Table 6.3**). Unfortunately, this experiment did not show any decrease in the binding affinity of K166M-MR for (*S*)-atrolactate in presence of (*R*)-

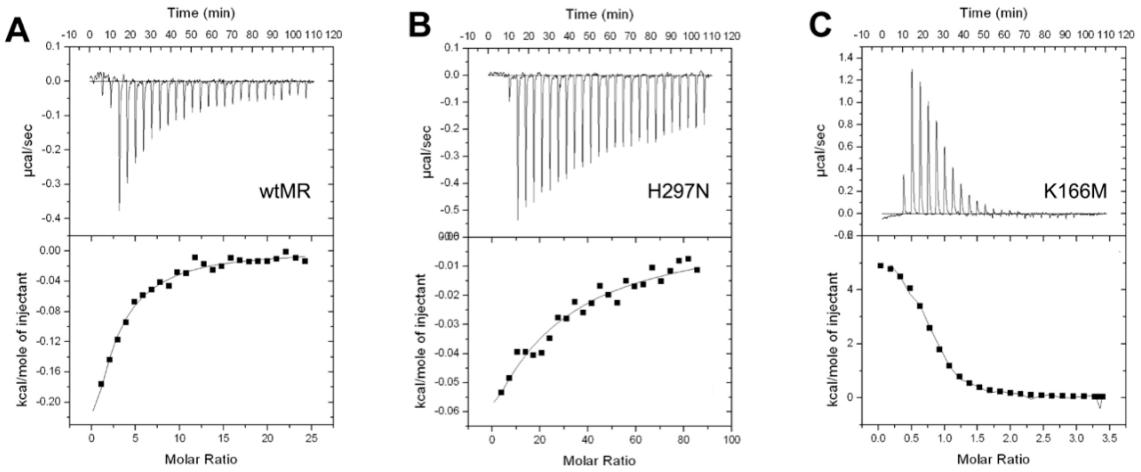

Figure 6.8 Representative ITC data for various MR variants binding (*R*)-atrolactate at 20 °C. Isothermal calorimetry titration of (A) wtMR (57.30 μM) with (*R*)-atrolactate (7.5 mM, 10 μL per injection), (B) H297N-MR (54.12 μM) with (*R*)-atrolactate (25.0 mM, 10 μL per injection), and (C) K166M-MR (62.17 μM) in (*R*)-atrolactate (20.0 mM) with (*S*)-atrolactate (1.6 mM, 8 μL per injection). The first injection in each case (top panel) was 2 μL, and was omitted when calculating the thermodynamic parameters. The molar ratio is [(*R*)-atrolactate]/[MR variant].

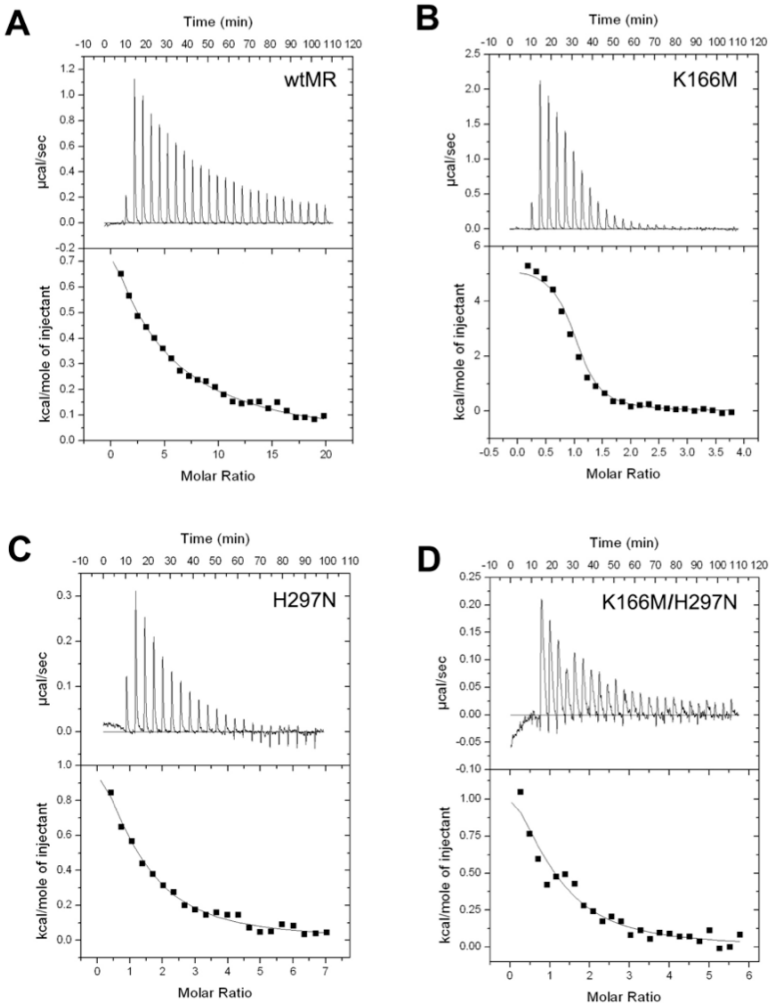

Figure 6.9 Representative ITC data for various MR variants binding (*S*)-atrolactate at 20 °C. Isothermal calorimetry titration of (A) wtMR (55.45 μM) with (*S*)-atrolactate (7.5 mM, 8 μL per injection), (B) K166M-MR (77.45 μM) with (*S*)-atrolactate (2.0 mM, 8 μL per injection), (C) H297N-MR (36.90 μM) and (*S*)-atrolactate (20 mM) solution with BzH (2.75 mM, 6 μL per injection)[§], (D) K166M/H297N-MR (64.23 μM) with (*S*)-atrolactate (2 mM, 10 μL per injection). The first injection in each case (top panels) was 2 μL, and was omitted when calculating the thermodynamic parameters. The molar ratio is [(*S*)-atrolactate]/[MR variant]. [§] This titration was performed at 15 °C

Table 6.3 Thermodynamic parameters for the various MR variants binding the substrate analogues (*R*)- and (*S*)-atrolactate at 20 °C

MR variant	K_d (μM)	Δ*G* (kcal/mol)	Δ*H* (kcal/mol)	TΔ*S* (kcal/mol)
	(*R*)-atrolactate			
wtMR	259 ± 24	–4.80 ± 0.06	–1.29 ± 0.04	3.51 ± 0.08
H297N	3996 ± 104	–3.22 ± 0.01	–4.97 ± 0.90	–1.75 ± 0.93
K166M	≥ 40000[a]	≥ -1.87[a]	-	-
	(*S*)-atrolactate			
wtMR	557 ± 25	–4.36 ± 0.02	7.85 ± 0.18	12.21 ± 0.16
H297N	36645 ± 6375[b]	–1.90 ± 0.10[b]	-	-
K166M	3.94 ± 0.10	–7.24 ± 0.01	5.22 ± 0.06	12.46 ± 0.68
K166M/H297N	51 ± 7	–5.75 ± 0.08	2.23 ± 0.50	7.98 ± 0.43

[a] No binding was observed even with competition-based ITC (with (*S*)-atrolactate as high affinity ligand) at 20 °C . Therefore, the given value is an estimate based on the binding affinity of H297N-MR for (*S*)-atrolactate.

[b] Determined using the competition-based ITC (with BzH as high affinity ligand) at 15 °C.

atrolactate (20 mM) **(Figure 6.8 C)**. Possibly, (*R*)-atrolactate (20 mM) failed to saturate K166M-MR, which is the basic requirement of competition-based binding experiment. Higher concentrations of (*R*)-atrolactate (>20 mM) in the enzyme solution could not be used because of its low solubility at concentrations >40 mM in the stock solutions. Therefore, the true K_d value could not be determined. Based on the binding affinity of H297N-MR for (*S*)-atrolactate, a lower limit for the dissociation constant for K166M-MR binding (*R*)-atrolactate was estimated to be ≥40 mM **(Table 6.3).**

6.4 DISCUSSION

6.4.1 Binding of Transition State/Intermediate Analogues

The energetics of wtMR binding BzH and CHCHA showed that the free energy of binding (ΔG_{BzH} = –7.15 and ΔG_{CHCHA} = –5.28 kcal/mol) is dominated by entropy (with $T\Delta S$ values of –13.05 kcal/mol (BzH) and –13.22 kcal/mol (CHCHA), respectively, at 15 °C) **(Figure 6.10)**. Therefore, intermediate analogues with hydrophobic substituents showed favorable entropic partitioning from the aqueous solvent to the relatively hydrophobic active site of MR. This observation is in accord with the negative ΔC_p value **(Figure 6.4)** that suggests that release of water or formation of an increased system of hydrophobic interactions accompany BzH binding (Guan *et al.*, 2011; Myslinski *et al.*, 2011; Parker *et al.*, 1999). These results are in agreement with previous studies that suggested that hydrophobic interactions play an important role of in MR catalysis (St. Maurice & Bearne, 2004). The crystal structure of wtMR with bound BzH **(Figure 1.4)** also shows that the phenyl group binds in the hydrophobic pocket lined by residues from

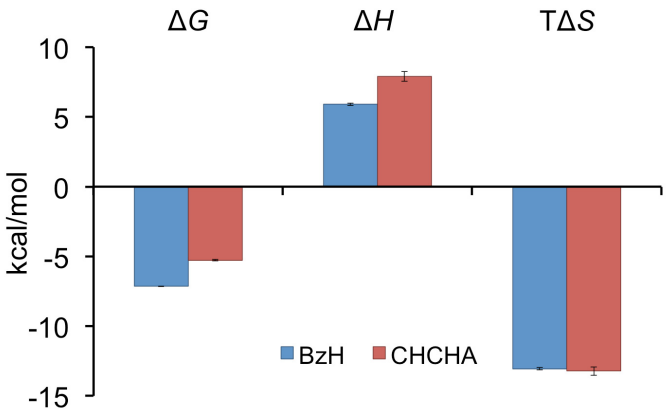

Figure 6.10 Thermodynamic parameters for wtMR binding the intermediate/TS analogues BzH and CHCHA at 15 °C. The binding of both ligands is driven by entropy with considerable enthalpic penalty.

the N-terminal domain (Leu 18, Val 22, Val29, Phe 52, and Tyr 54), the barrel domain (Leu 298, Leu 319, and Leu 321), and Leu 93 from the adjoining monomeric unit (Lietzan *et al.*, 2012). Expulsion of water from the active site upon BzH binding could account for the favorable entropy term. In addition, binding of BzH induces a conformational change, i.e., closure of 20s loop that prevents access of solvent into the active site (Lietzan *et al.*, 2012), which is also consistent with an entropy-driven binding process.

In order to estimate the contribution of cation-π/NH-π interactions in stabilizing the TS/intermediate, the ability of various MR mutants to bind the intermediate analogues BzH and CHCHA (which lacks aromatic π electrons), were compared. The $\Delta\Delta G$ values accompanying the binding of H297N-MR and K166M-MR with CHCHA (relative to wtMR) were –0.26 kcal/mol and –1.74 kcal/mol, respectively, suggesting that the overall contribution of cation-π/NH-π interactions of Lys 166 and His 297 with the hydroxamate moiety is –2.0 kcal/mol **(Figure 6.11)**. However, the $\Delta\Delta G$ values accompanying H297N-MR and K166M-MR binding BzH (relative to wtMR) were –1.17 kcal/mol and –3.48 kcal/mol, respectively, suggesting that the overall contribution of cation-π/NH-π interactions of Lys 166 and His 297 with both the hydroxamate moiety and the phenyl ring is –4.65 kcal/mol. This additivity of functional group contributions is in accord with the observation that $\Delta\Delta G$ = –4.41 kcal/mol for binding of the double mutant K166M/H297N-MR with BzH **(Table 6.2)**. The contribution of the individual cation-π/NH-π interactions between Lys 166 and His 296, and the phenyl ring of BzH can be calculated by taking difference of $\Delta\Delta G$ values for the binding of H297N-MR with BzH and CHCHA (i.e., 1.17 – 0.26 = 0.96 kcal/mol), and of K166M-MR with BzH (3.48 –

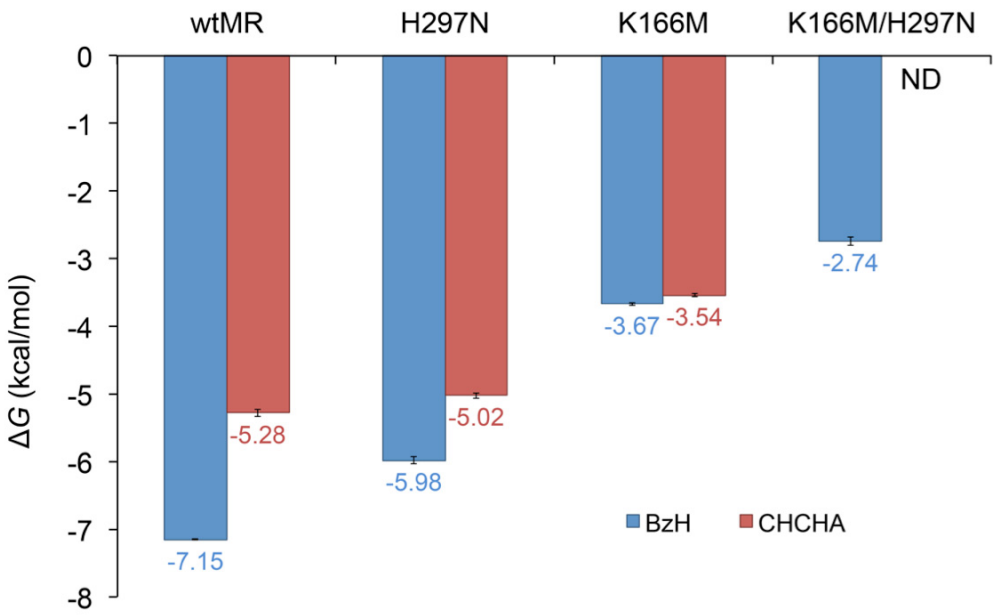

Figure 6.11 Free energy changes for various MR mutants binding the TS/intermediate analogues BzH and CHCHA at 15 °C. ND denotes not determined.

1.74 = 1.74 kcal/mol). It has been reported that the K166M mutation might alter the active site structure based on its inability to catalyze elimination of bromide ion from (*R*,*S*)-*p*-(bromomethyl)mandelate (Kallarakal *et al*., 1995). Although the CD spectrum did not suggest any major perturbation in secondary structure of K166M-MR **(Figure 6.5)**, ITC studies with this mutant were also validated by conducting K166C-MR binding studies with BzH **(Figure 6.6 D)** as K166C mutation does not appear to change the architecture of the active site (Nagar *et al*., 2014) (**Figure 7.11**, Chapter 7). This mutant exhibited similar free energy changes accompanying BzH binding, i.e., $\Delta G_{K166M} \approx \Delta G_{K166C}$ **(Table 6.2)**. Overall, both Lys 166 and His 297 enhance binding of the TS/intermediate analogues, but the contribution to the free energy of binding ($\Delta\Delta G$) is ~3 times more for Lys 166 compared to His 297. This difference could arise if His 297 is not protonated during BzH binding. During MR catalysis, both His 297 and Lys 166 are expected to exist as their positively charged conjugate acids when the intermediate is formed (**Scheme 6.1**), and therefore, the contribution of both residues towards stabilization of the *aci*-carboxylate intermediate might be expected to be equal.

Similar cation-π interactions have been reported in *o*-succinylbenzoate synthase (OSBS) from *Escherichia coli*. For this member of the enolase superfamily, Lys 235 is involved in cation-π interaction with the cyclohexadienyl moiety of 2-succinyl-6-hydroxy-2,4-cyclohexadiene-1-carboxylate (SHCHC), suggesting that Lys 235 stabilizes the enediolate anion intermediate (Klenchin *et al*., 2003). Although the crystal structure of OSBS with bound SHCHC shows that the α-carbon is sandwiched between the ε-ammonium groups of Lys 133 (Brønsted acid/base catalyst) at the end of second β-strand and Lys 235 at the end of sixth β-strand (Klenchin *et al*., 2003), the authors did not note

the potential role of Lys 133 in stabilizing the enediolate anion intermediate. Based on the studies presented in this chapter, both lysine residues could contribute to the stabilization of intermediate/TS during OSBS catalysis via cation-π interactions.

6.4.2 Binding of Ground State/Substrate Analogues

The x-ray crystal structure of MR with bound (*S*)-atrolactate shows that the phenyl group of this substrate analogue occupies the *S*-binding pocket and is inclined towards the Brønsted acid His 297 (Landro *et al*., 1994). Such a binding mode suggests that cation-π/NH-π interactions between this Brønsted acid and the aromatic ring (and/or carboxyl group) of the substrate could contribute to substrate binding. In order to evaluate these interactions, the thermodynamics accompanying the binding of K166M and H297N-MR with the ground state analogues (*R*)- and (*S*)-atrolactate were examined.

The ITC data reveals that mutation of the Brønsted base (i.e., Lys 166 when the (*S*)-enantiomer binds and His 297 when the (*R*)-enantiomer binds) did not have significant adverse effects on binding **(Figure 6.12)**. In fact, the K166M mutation showed a positive impact on (*S*)-atrolactate binding, with the observed binding affinity increasing by ~140-fold, equivalent to $\Delta\Delta G$ = –2.88 kcal/mol relative to wtMR **(Figure 6.12)**. This unexpected increase in binding affinity could arise from enhanced hydrophobic interactions between the methionine side chain and the α-CH_3 and the phenyl ring of (*S*)-atrolactate or from CH-π interactions. CH-π interactions are considered 'borderline' cases of nonconventional hydrogen bonds (Kadam *et al*., 2013; Plevin *et al*., 2010) where the phenyl ring acts as an H-bond acceptor (Levitt & Perutz, 1988). These interactions could be strong when the CH bond points directly at the center

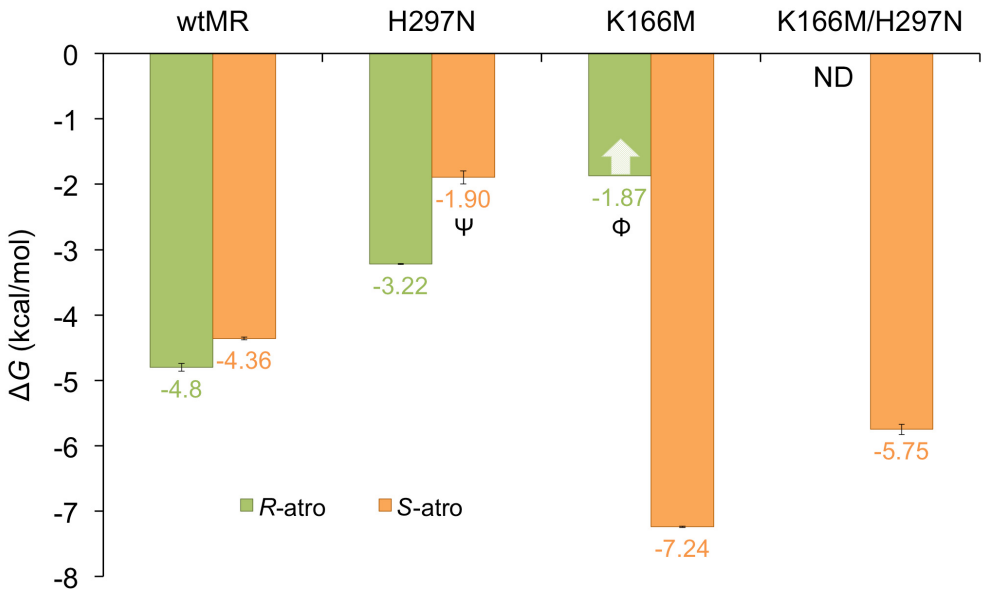

Figure 6.12 Free energy changes for various MR mutants binding substrate analogues (*R*)-atrolactate and (*S*)-atrolactate at 20 °C. [Ψ] Competition-based method (using BzH as high affinity ligand) was used to determine binding affinity at 15 °C. [Φ] No binding was observed with the competition-based method (using (*S*)-atrolactate as high affinity ligand) due to low solubility of (*R*)-atrolactate, and therefore, the lower limit (indicated by an arrow) is reported. ND denotes not determined.

of the aromatic ring of the ligand (Tsuzuki *et al*., 2006; Tsuzuki *et al*., 2000) and the distance is between 2.53–2.75 Å (Kadam *et al*., 2013). Such CH-π interactions are observed in complexes of (a) aromatic galactosides with Lectin Lec A from *Pseudomonas aeruginosa* (Kadam *et al*., 2013), and (b) sialoadhesin with sialic acid-based inhibitors (Zaccai *et al*., 2003), where CH groups from His 50 and Val 109 stack against the π-face of the aromatic group of the ligand.

In contrast, mutation of the Brønsted acid (i.e., Lys 166 when the (*R*)-enantiomer binds and His 297 when the (*S*)-enantiomer binds) has a drastic effect on the binding of the respective enantiomers of atrolactate **(Figure 6.12).** Despite of exceptional binding affinity of K166M-MR for (*S*)-atrolactate, the K166M/H297N double mutation decreased the binding of (*S*)-atrolactate ~12-fold relative to K166M **(Table 6.3)**, indicating that the H297N mutation disrupts interaction between Brønsted acid and (*S*)-atrolactate. Given these points and assuming that the Brønsted bases His 297 and Lys 166 exist as their conjugate acids when (*R*)- and (*S*)-atrolactate bind, respectively, the positive charge on Lys 166 and His 297 could contribute to substrate binding by favorable cation-π /NH-π interactions. Indeed, mutation of Lys 166 to arginine (predominantly positively changed at physiological pH (Guillén Schlippe & Hedstrom, 2005)) did not reduce affinity of MR for the substrate ((*R*)-mandelate, K_m^{wtMR} = 0.34 mM, K_m^{K166R} = 0.59 mM) (Kallarakal *et al*., 1995). Although cation-π/NH-π interactions between a positively charged side chain and the substrate have been suggested for another enzyme in the enolase superfamily, e.g., interaction between Arg 54 and the Phe side chain of the dipeptide substrate in Ala-Glu epimerase from *Bacillus subtilis* (Kalyanaraman *et al*., 2008), the contribution of the Brønsted acid catalysts to substrate binding appears to be unique for MR.

Analysis of the free energy of binding for ground state analogues suggests that the contribution of His 297 (–2.46 kcal/mol) towards binding of (*S*)-atrolactate is ~2-fold more than its contribution for BzH binding (–1.17 kcal/mol). This observation indicates that His 297 could be positively charged upon binding of (*S*)-atrolactate (as it likely is upon binding (*S*)-mandelate) but neutral upon binding of the TS analogue BzH. On the other hand, Lys 166 might be positive charged in both cases as suggested by the similar contributions observed for BzH (–3.48 kcal/mol) and (*R*)-atrolactate (–2.93 kcal/mol) binding. The slightly higher contribution towards BzH binding supports enhanced cation-π/NH-π interactions during TS/intermediate stabilization.

Overall, the removal of the formal positive charge by mutating the Brønsted acid-base catalysts leads to a loss in binding affinity for both substrate analogues and TS/intermediate analogues, suggesting the presence of cation-π/NH-π interactions between the conjugate acids of His 297 and Lys 166 and the π system of the phenyl ring as well as the enolate moiety of the TS/intermediate. Anslyn and coworkers have proposed that many enzymes such as citrate synthase, 4-chlorobenzoyl-CoA dehydrogenase, and triosephosphate isomerase could use cation-π/NH-π interactions to activate their carbon acid substrate (i.e., reduce pK_a of the α-carbon) through electrophilic coordination directed towards π-bond of carbonyl group (Houk *et al*., 2008). This coordination destabilizes the α-C–H bond via backside coordination while enhancing the stability of the emerging delocalized π-electron density on the enolate (Houk *et al*., 2006). Likewise, in MR, these cation-π/NH-π interactions could facilitate reduction of the pK_a of the α-carbon of mandelate, in addition to other catalytic mechanisms such as the formation of low barrier hydrogen bonds (Cleland & Kreevoy, 1994; Gerlt &

Gassman, 1993a) and/or metal coordination (Guthrie & Kluger, 1993; Warshel, 1998) that are at play during the catalysis by this proficient enzyme. Therefore, Lys 166 and His 297 appear to play a dual role in MR catalysis – general acid/base catalysis and electrostatic stabilization of the TS/intermediate.

CHAPTER 7

INVESTIGATION OF THE PROTONATION STATE OF LYS 166 USING ^{15}N NMR SPECTROSCOPY

7.1 INTRODUCTION

MR employs a two-base mechanism to catalyze the Mg^{2+}-dependent 1,1-proton transfer reaction that interconverts the enantiomers of mandelate (Gerlt, 1998). Lys 166 acts as a Brønsted base to abstract the α-H from (*S*)-mandelate to generate the *aci*-carboxylate intermediate, which gets reprotonated from the opposite side by His 297, a Brønsted acid, to yield (*R*)-mandelate. In the opposite direction, the roles and pK_a values of His 297 and Lys 166 are interchanged (Kallarakal *et al*., 1995; Landro *et al*., 1994; Powers *et al*., 1991) **(Scheme 6.1)**. In other words, the positive charge of Lys 166 or His 297 depends on the ligand that occupies the active site. In Chapter 3, I suggested that the higher than expected binding affinity of THTPA and tartronic acid arose because of salt bridge formation between Lys 166 and the carboxylate group of these ligands (Nagar *et al*., 2014). Similarly, the second carboxylate group of mesoxalate, an analogue of tartronic acid that binds MR with similar affinity (Chapter 4), could be involved in a salt bridge with Lys 166. These interactions require that Lys 166 is protonated, which is consistent with the normal pK_a value of this residue. On the other hand, irreversible inactivation of MR by 3-HP via a Schiff-base mechanism indicates that at least for a portion of time Lys 166 exists in its deprotonated form. Binding of 3-HP may also depress the pK_a of Lys 166 so that it behaves as a nucleophile to form a Schiff base with this keto acid (Chapter 4). ITC binding studies in Chapter 6 also suggest that the

protonation state of Lys 166 depends on the bound ligand. For example, Lys 166 is most likely positively charged when TS analogues like BzH and CHCHA occupy the active site. Binding studies with substrate analogues suggest that Lys 166 could be positively charged when (*R*)-atrolactate is bound and neutral when (*S*)-atrolactate is present in active site, consistent with the MR mechanism. Together, these studies suggest that the ionization of Lys 166, and hence its pK_a, reflect its participation in general acid-base and nucleophilic catalysis, salt-bridges, H-bonding or other kinds of electrostatic interactions (Poon *et al*., 2006; Zhang & Vogel, 1993). Therefore, it is important to determine the true ionization state of Lys 166 in the presence of various ligands.

Unfortunately, there is no neutron diffraction or atomic resolution x-ray diffraction data available for MR allowing for direct determination of protonation state of Lys 166. Indirect methods such as construction of pH-rate profiles have been used to determine the pK_a values of the Brønsted acid-base catalysts (Lys 166 and His 297) (Kallarakal *et al*., 1995; Landro *et al*., 1991), but the protonation equilibria of specific lysine side chain amines (i.e., intrinsic pK_a) can be better studied using NMR spectroscopy (McIntosh *et al*., 1996; Poon *et al*., 2006) because chemical shifts can be assigned to individual nuclei of specific residues. In addition, the direction and magnitude of the chemical shift are indicative of particular interactions as well as the protonation state (Song *et al*., 2003).

In this chapter, it is shown that Lys 166, a Brønsted acid-base catalyst, can be successfully replaced by a non-natural lysine analogue, thialysine, using site-directed mutagenesis combined with chemical modification using ethylenimine. Isoelectric focusing (IEF) is used for the quantification of thiol modification. Kinetic parameters of this thialysine-MR variant, determined in both the (*R*) → (*S*) and (*S*) → (*R*) reaction

directions, demonstrate activation of the catalytically inactive C92S/C264S/K166C triple mutant upon aminoethylation. The pK_a values of thialysine in both directions are determined by kinetic analysis of pH-rate data. The relative kinetic parameters of the thialysine-MR variant are independent of the microviscosity of the solvent, suggesting that the chemical step is rate-limiting for this variant. An optimized method of chemical modification is used to prepare an ^{15}N-thialysine-MR variant, but due to its unstable nature at higher concentrations, the ^{15}N-thialysine-MR variant was not amenable to NMR spectroscopy studies. As an alternate, ^{15}N NMR spectroscopy studies were conducted using uniformly labeled ^{15}N-MR variants in the presence of the transition state analogue BzH and the ground state analogues (*R*)- and (*S*)-atrolactate. However the ^{15}N NMR spectroscopy data are inconclusive as there are signals that could arise from either Lys 166 or Lys 164 and therefore further investigation is required.

7.2 MATERIALS AND METHODS

7.2.1 General

All reagents, unless mentioned otherwise, were purchased from Sigma-Aldrich Canada Ltd. (Oakville, ON). (*R*)- and (*S*)-Atrolactic acid were purchased from Alfa Aesar (Heysham, Lancashire, UK). Unlabeled ethylenimine was purchased from Chem Service (West Chester, PA), and ^{15}N-ethylenimine was synthesized by Dr. Palash Bhar (unpublished data, Bearne Lab) following published protocols (Li & Gershon, 2006; Philippossian *et al*., 1989; Wystrach *et al*., 1955). All reagents were of highest quality available, and were used without further purification. ^{15}N-NH_4Cl was purchased from Cambridge Isotope Laboratories (Tewksbury, Mass.). Immobiline Dry strips, and the Ettan IPGphor II isoelectric focusing system were purchased from Amersham Biosciences (Baie d'Urfé, QC). Amicon centrifugal filter devices (10 kDa molecular weight cut off) were purchased from Millipore (Billerica, MA). NMR data were collected on a Bruker Avance III 700 MHz NMR spectrometer equipped with a broadband (BBO) probe tuned to ^{15}N and located at the National Research Council, Halifax, NS.

7.2.2 Site-Directed Mutagenesis

Various MR variants, C264S, C92S/C264S-MR, C92S/C264S/K166C-MR, and K164C-MR, were created. The triple mutant MR (tmMR), C92S/C264S/K166C-MR, was constructed by performing three rounds of polymerase chain reaction-based site-directed mutagenesis using the QuikChange Site-Directed Mutagenesis Kit (Stratgene, La Jolla, CA) and following the protocols described by the manufacturer. The pET52b(+)-wtMR plasmid was used as a template to create the C264S-MR and K164C-MR mutant plasmid.

The former plasmid was used as a template to create the C92S/C264S-MR (double-mutant, dmMR) plasmid. Finally, the K166C mutation was introduced in dmMR plasmid to generate tmMR. Reactions were conducted using Pfu Turbo DNA polymerase (Bio Basic Inc., Markham, ON). The forward (F) and reverse (R) synthetic deoxyoligonucleotide primers used to construct the mutants were 5′-CGCAAAACG CTTC**A**GCCTGGCAGGTTATACGGG-3′ (F, C92S), 5′-CCCGTATAACCTGCCAG GC**T**GAAGCGTTTTGCG-3′ (R, C92S), 5′-GCATTGAGCATCGGTGCA**AG**CCGGTT GGCTATGCC-3′ (F, C264S), 5′-GGCATAGCCAACCG**GCT**TGCACCGATGCTCAA TGC-3′ (R, C264S), 5′-GCGG TTAAGACC**TGC**ATCGGCTATCCGGC-3′ (F, K166C), 5′-GCCGGATAGCCGAT**GCA**GGTCTTAACCGC-3′ (R, K166C), 5′-GGATTCCGG GCGGTT**TGC**ACCAAGATCGGC-3′ (F, K164C), and 5′-GCCGATCTTGGT**GCA**AA CCGCCCGGAATCC-3′ (R, K164C). The codons specifying the relevant modified amino acids are underlined, and the altered bases are shown in boldface. After site-directed mutagenesis, mutant plasmids were used to transform competent *E. coli* DH5α cells for plasmid maintenance. Each mutant ORF was sequenced using commercial automated DNA sequencing (Robarts Research Institute, London, ON) to ensure that no other alterations in the nucleotide sequence had been introduced. *E. coli* BL21(DE3) cells were used as the host for target gene expression, and the overproduced StrepII-tagged mutant MRs were purified as described previously.

7.2.3 Chemical Modification of Cys 166 of tmMR to Thialysine or ζ-^{15}N-Thialysine

Chemical modification of Cys 166 in tmMR was performed under denaturing conditions using ethylenimine. The aminoethylation reaction was started by adding

tmMR (1.2 mg/mL) into Na^+-HEPES buffer (0.1 M, pH 8.5) containing $MgCl_2$ (3.3 mM) and urea (6 M), followed by addition of ethylenimine (168 mM). This reaction mixture (10 mL) was incubated for 12–14 h with minimal stirring at 25 °C and then dialyzed overnight against assay buffer (~1.0 L) in a gradient manner as described previously (Kohyama *et al*., 2010) followed by dialysis (2 × 500 mL) for 8 h. The resulting aminoethylated tmMR from now on will be referred as tmMR-thiaLys. A similar method of chemical modification with a few variations was used to create ζ-^{15}N-tmMR-thiaLys for NMR spectroscopy studies. In this case, ^{15}N-labeled ethylenimine was used for aminoethylation and refolding was performed using direct dilution method in a stepwise manner, i.e., assay buffer was added directly into the reaction mixture (10 mL) using a peristaltic pump (Amersham Biosciences) such that the urea concentration reduced to 4 M in the first step (flow rate, ~5 mL/h) and to 2 M in the second step (flow rate, ~10 mL/h). The resulting solution was dialyzed extensively against (3 × 1 L) MOPS buffer (25 mM, pH 7.5) containing NaCl (50 mM) and $MgCl_2$ (3.3 mM) for 18 h to remove the remaining urea. After dialysis (gradient or stepwise), misfolded or precipitated protein was removed by ultracentrifugation (110,000 ×*g*) at 4 °C for 20 min. The soluble fraction was aliquotted and stored at –20 °C until further characterization. The protein concentration was determined from the absorbance at 280 nm (ε_{280} = 53400 $M^{-1}cm^{-1}$).

7.2.4 Kinetic Characterization of dmMR and tmMR-thiaLys

The activity of the various MR variants was determined using a CD-based assay similar to that described by Sharp *et al*. (1979). All assays were conducted at 25 °C in Na^+-HEPES buffer (0.1 M, pH 7.5) containing $MgCl_2$ (3.3 mM) (i.e., assay buffer) and

BSA (0.005%). Initial velocities for inter-conversion of mandelate enantiomers were determined by following change in ellipticity at 262 nm, using a quartz cuvette with 1-cm light path. The concentrations of mandelate ranged from 0.25–18.00 mM. Substrate solutions were incubated at 25 °C prior to initiation of the reaction by addition of freshly thawed dmMR or tmMR-thiaLys stock to yield a final concentration of 0.16 and 2.5 μg/mL respectively. Kinetic parameters were determined as described in section 2.2.4 (Chapter 2).

pH study: The kinetic parameters, k_{cat} and k_{cat}/K_m, were determined in both reaction directions ((*R*) → (*S*) and (*S*) → (*R*)) for dmMR and tmMR-thiaLys variants over a pH range of 5.5–10 using various buffers (100 mM) containing $MgCl_2$ (3.3 mM) and BSA (0.005%), e.g., MES (pH 5.5, 6.0, and 6.5), PIPES (pH 6.5 and 7.0), HEPES (pH 7.0, 7.5, and 8.0), TAPS (pH 8.0, 8.5, and 9.0), and CHES (pH 9.0, 9.5, and 10.0). The enzyme concentrations and substrate concentrations used at each pH value are listed in **Table 7.1**. It was necessary to use different enzyme concentrations and substrate concentrations at higher pH values to facilitate measurement of the kinetic parameters. Equations 7.1 and 7.2 describe the pH-dependence of k_{cat} and k_{cat}/K_m, respectively. Equation 7.3 was fit to the pH-rate data (where y is either k_{cat} or k_{cat}/K_m) and analyzed using nonlinear regression with the KaleidaGraph v. 4.02 software from Synergy Software (Reading, PA).

$$(k_{cat})_{obs} = \frac{(k_{cat})_{max}}{1 + 10^{(pK_{a1} - pH)} + 10^{(pH - pK_{a2})}} \tag{7.1}$$

$$\left(\frac{k_{cat}}{K_m}\right)_{obs} = \frac{(k_{cat}/K_m)_{max}}{1 + 10^{(pK_{a1} - pH)} + 10^{(pH - pK_{a2})}} \tag{7.2}$$

Table 7.1 Concentration of enzymes and substrates used for pH studies

buffer	pH	tmMR-thiaLys			
		[E] (μM)	(*R*)-man (mM)	[E] (μM)	(*S*)-man (mM)
MES	5.5	0.0514	0.125–10	0.0490	1–18
	6.0	0.0514	0.125–10	0.0490	0.50–18
	6.5	0.0514	0.125–10	0.0490	0.50–18
PIPES	6.5	0.0514	0.25–10	0.0606	0.50–18
	7.0	0.0514	0.25–10	0.0606	1–18
HEPES	7.0	0.0514	0.25–15	0.0606	1–18
	7.5	0.0514	0.25–15	0.0606	1–18
	8.0	0.0514	0.25–15	0.0606	1–18
TAPS	8.0	0.0514	0.25–15	0.0593	1–18
	8.5	0.0514	0.5–15	0.0593	1–18
	9.0	0.0514	1–15	0.1542	7.5–120
CHES	9.0	0.1028	4–28	0.1542	7.5–120
	9.5	0.6170	15–90	0.6170	20–180
	10.0	0.9255	30–120	–	–
		dmMR			
MES	5.5	0.0038	0.10–5	0.0038	0.20–8
	6.0	0.0038	0.20–5	0.0038	0.20–8
	6.5	0.0038	0.5–10	0.0038	0.25–10
PIPES	6.5	0.0038	0.25–10	0.0038	0.25–15
	7.0	0.0038	0.25–15	0.0038	0.25–15
HEPES	7.0	0.0038	0.25–15	0.0038	0.25–10
	7.5	0.0038	0.25–15	0.0038	0.25–15
	8.0	0.0038	0.5–15	0.0038	0.50–15
TAPS	8.0	0.0102	1–20	0.0051	0.50–20
	8.5	0.0204	1.5–45	0.0051	0.5–30
	9.0	0.0191	2–60	0.0102	1–38
CHES	9.0	0.0191	2–60	0.0191	2–60
	9.5	0.0893	10–160	0.0893	10–160
	9.75	0.0893	10–160	0.0893	10–180
	10.0	0.1148	10–180	0.0893	1–180

$$\log y_{obs} = \log y_{max} - \log\left(1 + 10^{(pK_{a1} - pH)} + 10^{(pH - pK_{a2})}\right) \quad (7.3)$$

Viscosity study: The dependence of the dmMR- and tmMR-thiaLys-catalyzed racemization of (*R*)- and (*S*)-mandelate on the viscosity of the solution was evaluated as described previously (St. Maurice & Bearne, 2002) using sucrose as viscosogen (refer section 2.2.6 for details). Reaction mixtures were prepared in quartz cuvettes with a 0.5-cm light path. Typically, 400 μL of (*R*)-mandelate (0.25–15 mM) or (*S*)-mandelate (0.5–22.5 mM) in Na^+-HEPES buffer (0.1 M, pH 7.5) containing $MgCl_2$ (3.3 mM) was mixed with 500 μL of the viscosogen containing stock solution (prepared at twice the desired final concentration). The reaction was initiated by addition of the MR variant (final concentrations of dmMR and tmMR-thiaLys were 0.16 μg/mL and 2.12 μg/mL, respectively) in Na^+-HEPES buffer (0.1 M, pH 7.5) containing $MgCl_2$ (3.3 mM) and BSA (0.005%).

7.2.5 Quantification of the Extent of Modification using Isoelectric Focusing

The extent of covalent modification of Cys 166 with ethylenimine to yield thialysine in tmMR was quantified using isoelectric focusing (IEF). Samples (10 μL, containing ~10–20 μg protein) dissolved in rehydration IEF buffer solution (340 μL, containing urea (8 M), CHAPS (2%), IPG buffer (0.5%), and trace amounts of bromophenol blue G-250) were transferred (distributed evenly) into ceramic strip holders, followed by careful placement of the Immobiline Dry strip (18 cm) with a linear pH range (5.3–6.5) (GE Healthcare) while the gel side was facing down. The strip was then overlaid with DryStrip Cover fluid and allowed to rehydrate for 16 h at 20 °C before

IEF was conducted using Ettan IPGphor. The IEF voltage was applied in steps: 1) step and hold 500 V, 3 h; 2) gradient 1000 V, 2 h; 3) gradient 8000 V, 3 h; and 4) step and hold 8000 V, 8 h. Following the IEF run, the strips were rinsed with autoclaved double-distilled water to remove excess DryStrip Cover fluid and stained with either colloidal stain or Coomassie blue R-250 followed by destaining to visualize the bands. Quantification of the intensity of the bands for the tmMR-thiaLys sample was conducted using ImageJ software (Schneider *et al*., 2012).

7.2.6 Expression and Purification of Uniformly Labeled ^{15}N-MR Variants

Uniformly ^{15}N-labeled MR variants (wtMR, K166M-MR, and K164C-MR) were expressed in M9 minimal media (refer to **Table 7.2** for the detailed recipe of the M9 minimal media). M9 minimal media (25 mL) containing $^{15}NH_4Cl$ (1.0 g/L), glucose (4.0 g/L), and ampicillin (100 μg/mL) was inoculated with *E. coli* BL21 (DE3) cells containing the pET52b(+) plasmid bearing the desired MR variant ORF (25 μL of glycerol stock) and incubated overnight on a rotary shaker at 37 °C. This starter culture was transferred to fresh minimal media (1 L, composition as mentioned above) and allowed to grow until OD_{600} = 0.6–0.8 before induction with isopropyl-β-D-thiogalactopyranoside (IPTG, 1 mM). After 6 h, the cells were harvested by centrifugation (4000 rpm, 10 min, 4 °C) and stored at –80 °C until further processing. Refer section 2.2.4 for purification of MR variants. After purification using FPLC, the MR variants were dialyzed against MOPS buffer (25 mM, pH 7.5) containing $MgCl_2$ (3.3 mM) and NaCl (50 mM) and aliquots (1.5–2.0 mL) were stored at –20 °C.

Table 7.2 Composition of minimal media
This recipe is a modification of M9 minimal media (Sambrook *et al*., 1989)

minimal media contents	**1 liter**	**25 mL**
[a]M9-N	1 L	25 mL
[b]1000× micronutrients	1 mL	25 μL
1 M $MgSO_4$	2 mL	50 μL
1M $CaCl_2$	100 μL	2.5 μL
10 mM $FeSO_4$ (freshly made, 2.78 mg/mL)	100 μL	2.5 μL
40% glucose	10 mL	250 μL
10% $^{15}NH_4Cl$	10 mL	250 μL
ampicillin	2 mL	50 μL
[a]M9-N media		
Na_2HPO_4	6.0 g	150 mg
KH_2PO_4	3.0 g	75 mg
NaCl	0.5 g	12.5 mg
pH adjusted to 7.5 using NaOH		
[b]1000× micronutrients (Neidhardt *et al*., 1974)		
	amount (mg)/10 mL	[b]volume (μL) to be added and make up the total volume 100 mL of micronutrient stock
$(NH_4)_6(Mo_7O_{24})$	124	30
H_3BO_3	25	1000
$CaCl_2$	24	300
$CuSO_4$	25	100
$MnCl_2 \cdot 4H_2O$	20	800
$ZnCl_2$	14	100

7.2.7 ^{15}N NMR Spectroscopic Study

Frozen aliquots of uniformly labeled ^{15}N-MR variants were thawed and concentrated 6–10-fold (~350 μM). Samples with ligands were prepared by mixing equal volumes of thawed aliquots of the MR variants and the ligand solution (at 2.25× the concentration needed in the NMR tube, i.e., saturating concentration), and then concentrated (~12–20-fold) using ultra centrifugal filters (10 kDa molecular weight cut off (Millipore, Billerica, MA)) to achieve the desired protein concentration, i.e., ~350 μM. Deuterium oxide (60 μL) was added to the ^{15}N-labeled MR variant sample (540 μL) before transferring the sample into an NMR tube. Final concentrations of ligands in the NMR tube were as follows: BzH, 2.25 mM with wtMR and K164C-MR[a] and 18 mM with K166M-MR; (*R*)- and (*S*)-atrolactate, 10.25 mM in each case with wtMR. Data were collected at 15 °C on a Bruker Avance III 700 MHz NMR spectrometer equipped with a 5 mm broadband (BBO) probe tuned to ^{15}N. A 1-D-pulse program (zgpg) was used with a single 90° nitrogen pulse using power-gated proton decoupling (Culp *et al*., 1989; Inbar & Lapidot, 1988). A total of 16, 000 scans were collected over 9 h with a recycle delay of 1 s. The reported ^{15}N chemical shifts are in ppm and relative to anhydrous liquid ^{15}N-NH_3.

[a] Note on K164C-MR: Kinetic studies showed that K1664C-MR was catalytically inactive (no activity at 1 μM *cf*. wtMR concentration in normal assay (3 nM)). Therefore, the binding affinity of K164C-MR for BzH was determined using ITC (refer to Chapter 6 Material and Methods section) to estimate the saturating concentrations of BzH required for the NMR spectroscopic study. K164C-MR bound BzH with an affinity (K_d) of 94.6 μM **(Figure 7.1)**, ~25-fold weaker than wtMR binds BzH (K_d = 3.7 μM). Interestingly, the binding affinity of K164C-MR for BzH was ~25-fold tighter than the binding affinities of K166M- and K166C-MR for BzH, suggesting that Lys 166, which is likely protonated in absence of the neighboring Lys 164, is crucial for binding.

.

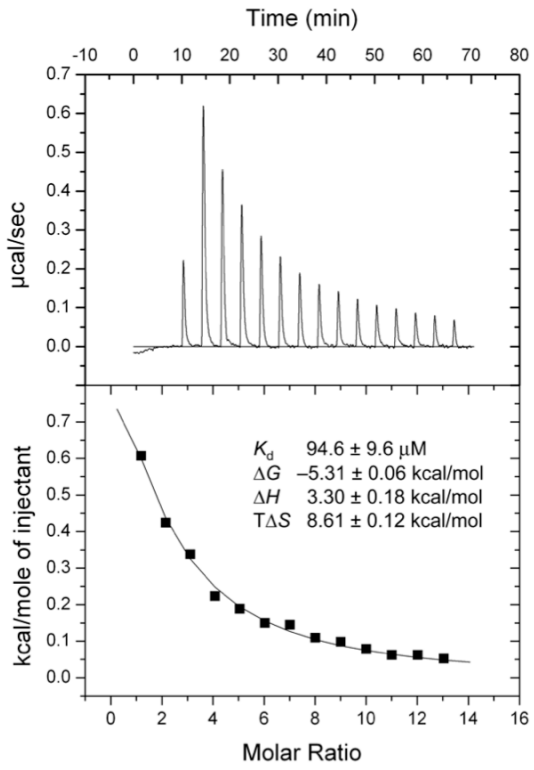

Figure 7.1 Representative ITC data for K164C-MR binding BzH. Isothermal calorimetry titration of K164C-MR (29.77 µM, in titration cell) with BzH (5 mM, in syringe, 8 µL per injection) at 15 °C. The first injection was 2 µL, and was omitted when calculating thermodynamic parameters. The dissociation constant and the thermodynamic parameters shown in the lower panel are the average of 3 experiments.

7.3 RESULTS

7.3.1 Kinetic Characterization of dmMR and tmMR-thiaLys

Site-directed mutagenesis and chemical modification were used in a stepwise strategy to replace Lys 166 with an isosteric thialysine residue. First, Cys 92 and Cys 264 in wtMR were replaced by serine residues using SDM to create a double mutant C92/264S-MR (dmMR) to avoid aminoethylation of these residues during chemical modification. All kinetic parameters of dmMR were similar to wtMR **(Table 7.3)** suggesting neither of these cysteine residues is critical for catalysis. Finally, Lys 166 of dmMR was replaced by Cys to create the triple mutant MR (tmMR). This mutant was inactive even when assayed at high concentrations (~7 μM, *cf.* [wtMR] = 3 nM) **(Table 7.3)**. Aminoethylation of Cys 166 of tmMR using ethylenimine under denaturing conditions, followed by refolding, activated the inactive enzyme due to formation of thialysine at position 166 in the active site, now referred as tmMR-thiaLys. The aminoethylation reaction under denaturing conditions (in the presence of 6 M urea) yielded more active tmMR-thiaLys ($(V_{max}/[E]_T)^{R\text{-man}}$ = 17.1 μM/min; $(V_{max}/[E]_T)^{S\text{-man}}$ = 38.5 μM/min) than when the reaction was conducted under native conditions ($(V_{max}/[E]_T)^{R\text{-man}}$ = 6.8 μM/min; $(V_{max}/[E]_T)^{S\text{-man}}$ = 16.7 μM/min), likely due to greater accessibility of the Cys 166 side-chain under denaturing conditions. Therefore, in spite of low refolding yields (~10–25%; unaffected by the method of dilution used for refolding), the aminoethylation reaction was conducted under denaturing conditions. Kinetic

Table 7.3 Kinetic parameters for the racemization of mandelate catalyzed by dmMR and tmMR-thiaLys

MR	(*R*) → (*S*)-mandelate		
	k_{cat} (s^{-1})	K_m (mM)	k_{cat}/K_m ($M^{-1}s^{-1}$)
wtMR	791 ± 43	1.21 ± 0.18	6.5 (± 0.8) × 10^5
dmMR[a]	469 ± 45	1.32 ± 0.00	3.6 (± 0.3) × 10^5
tmMR[b]	-	-	-
tmMR-thiaLys[a]	25 ± 2	0.99 ± 0.10	2.5 (± 0.3) × 10^4
tmMR-thiaLys[a,c]	75 ± 7		7.6 (± 1.0) × 10^4
	(*S*) → (*R*)-mandelate		
wtMR	637 ± 19	1.02 ± 0.10	6.2 (± 0.8) × 10^5
dmMR[a]	682 ± 33	1.98 ± 0.08	3.5 (± 0.2) × 10^5
tmMR[b]	-	-	-
tmMR-thiaLys[a]	79 ± 1	3.79 ± 0.20	2.1 (± 0.1) × 10^4
tmMR-thiaLys[a,c]	237 ± 2		6.3 (± 0.3) × 10^4

[a] Average of two independent experiments,

[b] No activity was observed at ~6.7 μM of tmMR

[c] Corrected values based on the observed % aminoethylation of tmMR using IEF

characterization of tmMR-thiaLys showed a 10–20-fold reduction in both the catalytic efficiency (k_{cat}/K_m) and turnover (k_{cat}) in both reaction directions relative to wtMR and dmMR **(Table 7.3)**, but the binding affinity (K_m) for the substrates was not significantly altered **(Table 7.3)**.

7.3.2 Quantification of the Extent of Modification using Isoelectric Focusing

The pI values for wtMR (5.77), dmMR (5.77), and tmMR (5.66), as indicated, were determined using the ProtParam tool on the ExPASy server (Gasteiger *et al*., 2005). Hence the pI value for tmMR-thiaLys is also expected to be within this range. Therefore, an IEF gel strip with a pH range of 5.3 to 6.5 was used to separate modified tmMR from the unmodified triple mutant. As expected, wtMR (strip 1) and dmMR (strip 2) showed major (intense) bands at the same distances from the anode (indicated as '+' in **Figure 7.2**), consistent with their similar pI values, while tmMR (strip 3) migrated closer to the anode due to its lower pI value **(Figure 7.2)**. In addition, there were minor (less intense) bands in all preparations. The tmMR-thiaLys sample also produced three bands on the IEF gel **(Figure 7.2)**, but analysis using ImageJ (Schneider *et al*., 2012) suggested similar intensities of all three bands. Considering that all three bands move together as a result of their altered pI value upon modification (bands in strip 4 of **Figure 7.2** corresponds to: (a) unmodified tmMR (≥ 95%), (b) unmodified tmMR (≥ 95%), and (c) modified tmMR (starting from anode)), the extent of modification could be estimated as ≥ 33%. Therefore, k_{cat} values for tmMR-thiaLys were corrected by multiplying observed k_{cat} values by 3 **(Table 7.3)** (i.e., $[E]_T^{obs}/3$).

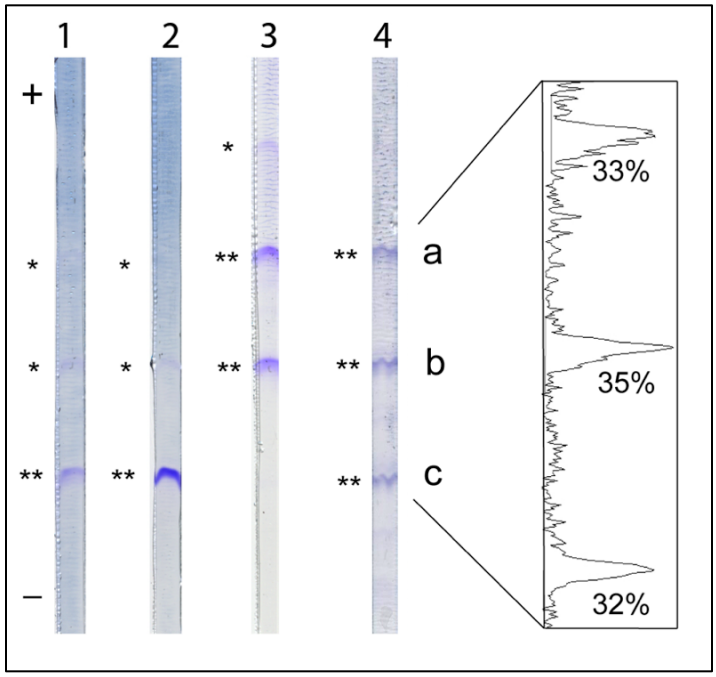

Figure 7.2 Isoelectric focusing of various MR variants under denaturing conditions. Strip 1 contains wtMR; strip 2, dmMR; strip 3, tmMR; and strip 4, tmMR treated with ethylenimine, i.e., tmMR-thiaLys. Inset shows densitometric analysis of strip 4 using ImageJ and the indicated peak areas (~15–20% error). The anodic (low pH) and cathodic (high pH) ends of the IEF gel strips are indicated as (+) and (–), respectively. The major and minor bands are indicated as (**) and (*), respectively.

7.3.3 Effect of pH on dmMR and tmMR-thiaLys Activity

The effect of pH on the kinetic parameters, k_{cat} and k_{cat}/K_m, of dmMR and tmMR-thiaLys were studied using (*R*)- and (*S*)-mandelate as substrates. In both the (*R*)→(*S*) and (*S*)→(*R*) reaction directions, the dependence of k_{cat} on pH yielded bell-shaped curves with limiting slopes of unity on the ascending and descending limbs. Such a pH-dependence indicates the presence of two ionizable groups. The pK_a of the ascending limb (pK_{a1}) could be assigned to deprotonation of the conjugate acid of the Brønsted base that abstracts the α-proton from the carbon acid substrate (Kallarakal *et al*., 1995; Landro *et al*., 1991; Schafer *et al*., 1996). That said, pK_{a1} in the k_{cat}-pH profiles of dmMR and tmMR-thiaLys, when (*R*)-mandelate was used as substrate **(Figure 7.3 A and 7.5 A)**, corresponds to the pK_a of His 297 (5.98 ± 0.04 and 5.50 ± 0.06) in the respective ES complexes. In the opposite direction, i.e., when (*S*)-mandelate is the substrate **(Figure 7.4 A and 7.6 A)**, pK_{a1} corresponds to the pK_a of Lys 166 (6.20 ± 0.05) and thiaLys 166 (5.77 ± 0.02) in the dmMR- and tmMR-thiaLys-(*S*)-mandelate complexes, respectively. Although controversial, the pK_a of the descending limb (pK_{a2}) could be assigned to the deprotonation of the Brønsted acid catalyst that donates a proton to the *aci*-carboxylate intermediate (Kallarakal *et al*., 1995; Landro *et al*., 1991). Thus, pK_{a2} in the k_{cat}-pH profiles of dmMR and tmMR-thiaLys **(Figure 7.3 A & 7.5 A)** suggest pK_a values for Lys (10.15 ± 0.08) and thialysine (9.81 ± 0.05) as indicated in dmMR- and tmMR-thiaLys-(*R*)-mandelate complexes, respectively. However, in the (*S*)→(*R*) reaction direction, pK_{a2} in the k_{cat}-pH profiles of dmMR corresponds to the pK_a of His 297 (10.23 ± 0.16) **(Figure 7.4 A)**. Unfortunately, the pK_a value of His 297 in the tmMR-thiaLys-(*R*)-mandelate complex could not be estimated due to the absence of a descending limb **(Figure 7.6 A)**.

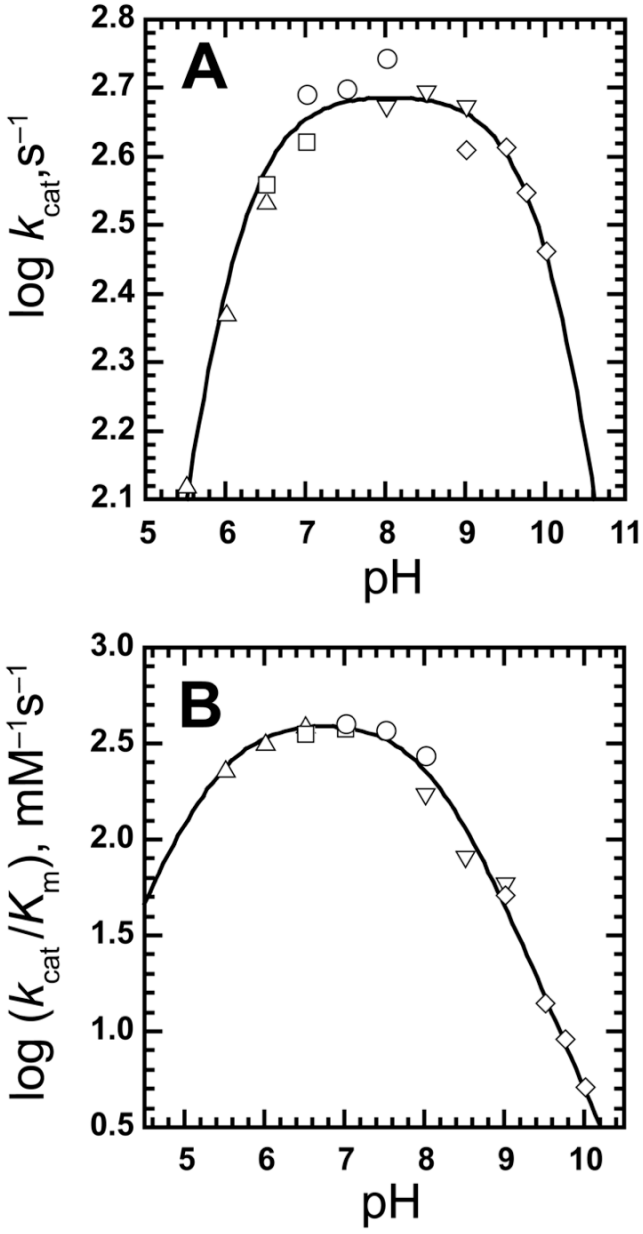

Figure 7.3 pH-rate profiles for the racemization of (*R*)-mandelate catalyzed by dmMR. (A) pH dependence of log k_{cat} showing pK_{a1} = 5.98 ± 0.04, pK_{a2} = 10.15 ± 0.08, and log $(k_{cat})_{max}$ = 2.69 ± 0.01 (B) pH dependence of log (k_{cat}/K_m) showing pK_{a1} = 5.41 ± 0.20, pK_{a2} = 8.08 ± 0.06, and log $(k_{cat}/K_m)_{max}$ = 2.63 ± 0.04. The buffers used were MES (△; pH 5.5, 6.0, and 6.5), PIPES (□; pH 6.5 and 7.0), HEPES (○; pH 7.0, 7.5, and 8.0), TAPS (▽; pH 8.0, 8.5, and 9.0), and CHES (◇; pH 9.0, 9.5, and 10.0).

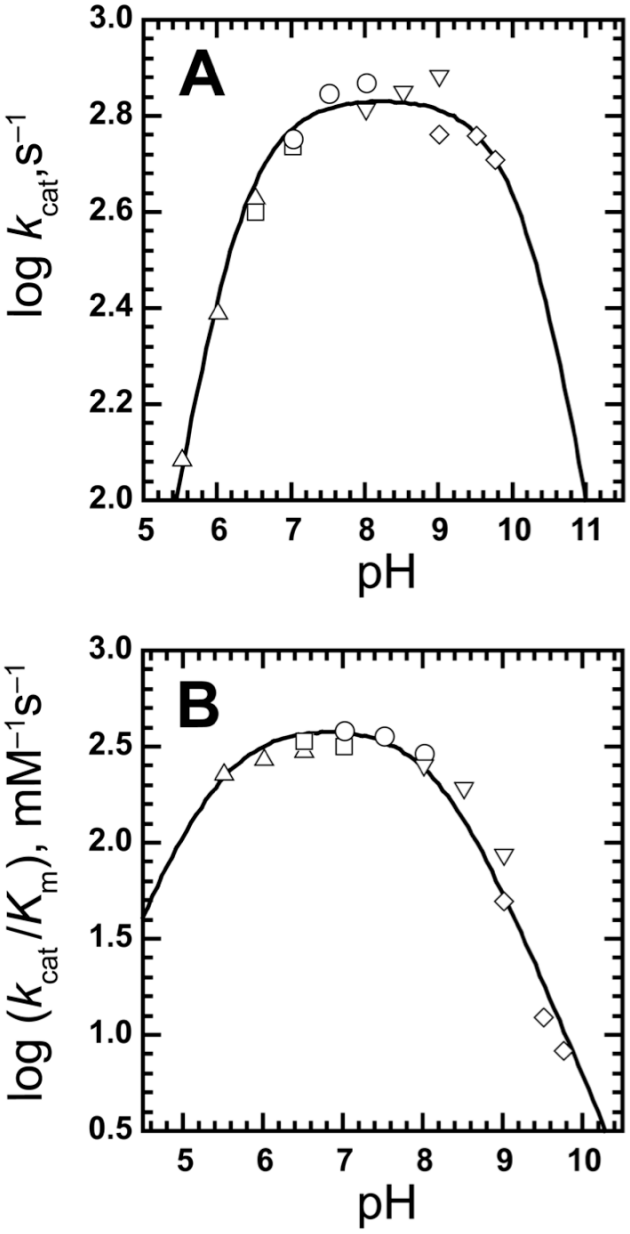

Figure 7.4 pH-rate profiles for the racemization of (*S*)-mandelate catalyzed by dmMR. (A) pH dependence of log k_{cat} showing pK_{a1} = 6.20 ± 0.05, pK_{a2} = 10.23 ± 0.16, and log $(k_{cat})_{max}$ = 2.84 ± 0.02 (B) pH dependence of log (k_{cat}/K_m) showing pK_{a1} = 5.45 ± 0.27, pK_{a2} = 8.19 ± 0.08, and log $(k_{cat}/K_m)_{max}$ = 2.61 ± 0.05. The buffers used were MES (△; pH 5.5, 6.0, and 6.5), PIPES (□; pH 6.5 and 7.0), HEPES (○; pH 7.0, 7.5, and 8.0), TAPS (▽; pH 8.0, 8.5, and 9.0), and CHES (◇; pH 9.0, 9.5, and 9.75).

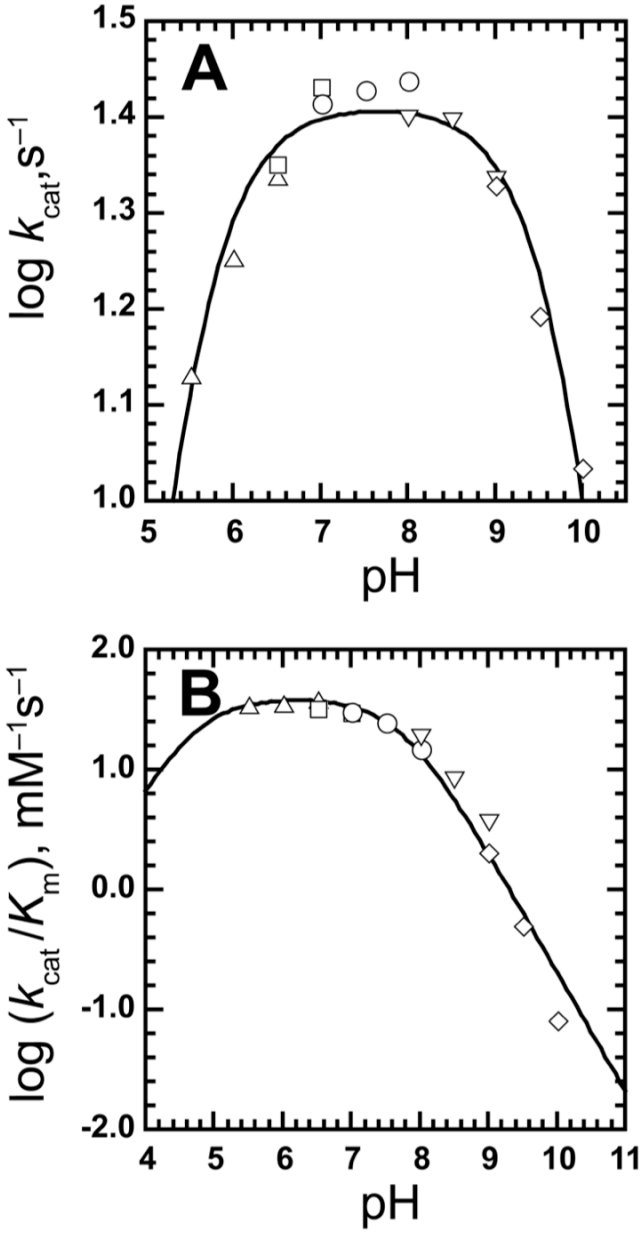

Figure 7.5 pH-rate profiles for the racemization of (*R*)-mandelate catalyzed by tmMR-thiaLys. (A) pH dependence of log k_{cat} showing pK_{a1} = 5.50 ± 0.06, pK_{a2} = 9.81 ± 0.05, and log $(k_{cat})_{max}$ = 1.41 ± 0.01 (B) pH dependence of log (k_{cat}/K_m) showing pK_{a1} = 4.70 ± 1.47, pK_{a2} = 7.72 ± 0.13 and log $(k_{cat}/K_m)_{max}$ = 1.60 ± 0.09. The buffers used were MES (△; pH 5.5, 6.0, and 6.5), PIPES (□; pH 6.5 and 7.0), HEPES (○; pH 7.0, 7.5, and 8.0), TAPS (▽; pH 8.0, 8.5, and 9.0), and CHES (◇; pH 9.0, 9.5, and 10.0).

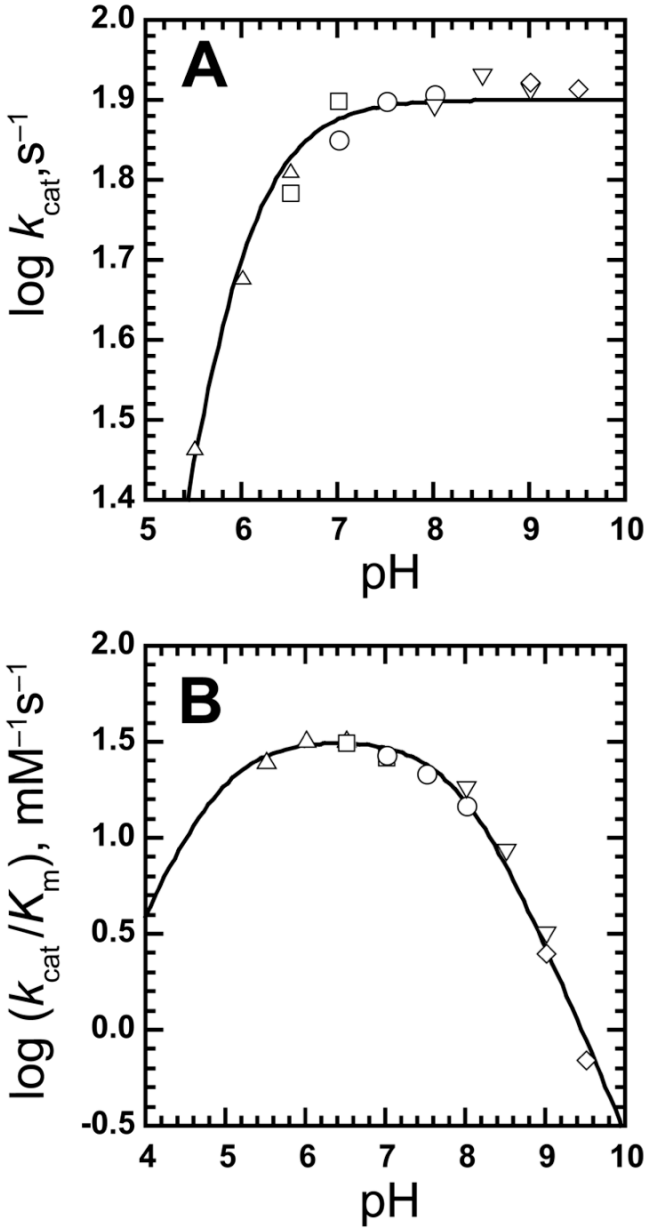

Figure 7.6 pH-rate profiles for the racemization of (*S*)-mandelate catalyzed by tmMR-thiaLys. (A) pH dependence of log k_{cat} showing pK_{a1} = 5.77 ± 0.02 and log $(k_{cat})_{max}$ = 1.9 ± 0.09 (B) pH dependence of log (k_{cat}/K_m) showing pK_{a1} = 4.87 ± 0.36, pK_{a2} = 7.95 ± 0.05, and log $(k_{cat}/K_m)_{max}$ = 1.52 ± 0.03. The buffers used were MES (△; pH 5.5, 6.0, and 6.5), PIPES (□; pH 6.5 and 7.0), HEPES (○; pH 7.0, 7.5, and 8.0), TAPS (▽; pH 8.0, 8.5, and 9.0), and CHES (◇; pH 9.0, and 9.5).

Table 7.4 Effect of pH on the kinetic parameters for the racemization of (*R*)- and (*S*)-mandelate catalyzed by dmMR and tmMR-thiaLys [a]

buffer	pH	dmMR			
		(*R*) → (*S*)		(*S*) → (*R*)	
		k_{cat}, s^{-1}	K_m, mM	k_{cat}, s^{-1}	K_m, mM
MES	5.5	133.1	0.56	123.6	0.52
	6.0	237.2	0.73	249.3	0.88
	6.5	344.7	0.86	432.3	1.39
PIPES	6.5	363.7	1.01	401.0	1.16
	7.0	420.5	1.09	548.8	1.70
HEPES	7.0	493.1	1.20	569.7	1.47
	7.5	501.4	1.32	705.8	1.92
	8.0	556.5	1.99	745.3	2.50
TAPS	8.0	470.3	2.77	646.1	2.58
	8.5	492.8	6.20	702.5	3.68
	9.0	469.7	8.09	761.6	8.90
CHES	9.0	409.0	7.90	581.0	11.48
	9.5	413.1	28.90	575.3	45.69
	9.75	354.5	38.67	512.8	60.63
	10.0	291.0	55.96	508.3	78.57
		tmMR-thiaLys			
MES	5.5	13.5	0.38	29.3	1.14
	6.0	18.0	0.50	47.8	1.45
	6.5	21.8	0.56	65.0	1.95
PIPES	6.5	22.4	0.69	60.9	1.92
	7.0	27.0	0.89	79.3	2.99
HEPES	7.0	26.0	0.85	71.1	2.59
	7.5	26.8	1.06	79.6	3.65
	8.0	27.4	1.80	80.9	5.40
TAPS	8.0	25.1	1.31	77.9	4.33
	8.5	24.9	2.97	85.0	9.98
	9.0	21.7	5.91	81.6	25.68
CHES	9.0	21.3	10.51	83.9	33.02
	9.5	15.6	30.92	82.2	116.03
	10.0	10.8	133.53	–	–

[a] estimated errors on k_{cat} and K_m values are 5% and 10%, respectively

Considering the pH-profile for wtMR in the (*S*)→(*R*) reaction direction (Landro *et al*., 1991), where k_{cat} shows a plateau up to at least pH 9.5, the missing descending limb for tmMR-thiaLys is most probably a result of inability to assay the enzyme at pH > 9.5.

The plots of log (k_{cat}/K_m) vs. pH for dmMR and tmMR-thiaLys also showed bell-shaped dependencies on pH in both the (*R*)→(*S*) and (*S*)→(*R*) reaction directions **(Figures 7.3–7.6 B)**. In general, such cases suggest the presence of two ionizable groups on the free enzyme or the free substrate. But for both dmMR and tmMR-thiaLys, both ionizations are likely to be associated with the free MR variants because there are no ionizable groups on the mandelate with pK_a values in range of 5.5–10 (pK_a mandelate = ~29; (Renaud & Fox, 1988)). In the (*R*)→(*S*) reaction direction, the calculated pK_{a1} ~5 and pK_{a2} ~8 values could be assigned to His 297 and Lys 166, while in the (*S*)→(*R*) reaction direction, the pK_a values would be reversed. Surprisingly, the pK_a values for free MR variants were slightly perturbed (especially pK_{a2}) compared to the pK_a values of these residues in the dmMR- and tmMR-thiaLys-substrate complexes (pK_{a1} ~6 and pK_{a2} ~10), which could be attributed to change in microenvironment upon substrate binding.

7.3.4 Effect of Viscosity on dmMR and tmMR-thiaLys Activity

The kinetic parameters for the racemization of mandelate catalyzed by wtMR showed partial viscosity dependence (St. Maurice & Bearne, 2002), suggesting that the chemical step, as well as substrate association and/or product dissociation, are partially rate-limiting (Brouwer & Kirsch, 1982), a characteristic of highly proficient enzymes. Although the catalytic efficiency of dmMR was only reduced ~2-fold relative to wtMR, the value of k_{cat}/K_m for tmMR-thiaLys was reduced by ~ 30-fold **(Table 7.3)**. Therefore,

the effect of solvent viscosity on the steady-state kinetic parameters of tmMR-thiaLys and dmMR (as a control) in both reaction directions with either (*R*)- or (*S*)-mandelate as the substrate was examined using sucrose as a viscosogen **(Table 7.5 & 7.6)**. The relative kinetic parameters (i.e., $k_{cat}^{o}/k_{cat}^{\eta}$ and $(k_{cat}/K_m)^{o}/(k_{cat}/K_m)^{\eta}$) of both MR variants in the (*R*)→(*S*) reaction direction **(Figure 7.7)**, and in the (*S*)→(*R*) reaction direction **(Figure 7.8)** did not show any significant dependence of on the microviscosity of the solvent. These results suggested that viscosity dependent processes such as substrate binding and/or product release were no longer rate-limiting; instead, the chemical step is fully rate-limiting in the reaction catalyzed by tmMR-thiaLys and dmMR.

7.3.5 ^{15}N NMR Spectroscopic Study

Power-gated proton decoupled 1-D ^{15}N NMR (Culp *et al*., 1989; Inbar & Lapidot, 1988) was used in an attempt to study the change in pK_a of Lys 166 upon ligand binding. But, instead of specifically labeled tmMR-^{15}N-thiaLys, uniformly ^{15}N-labeled MR variants (wtMR, K166M-MR, and K164C-MR) were used because tmMR-^{15}N-thiaLys (~300–400 μM) precipitated within 1 h after concentration.

The power-gated proton-decoupled ^{15}N NMR spectrum of ^{15}N-enriched MR variants showed signal inversion **(Figure 7.9 & 7.10)** due to a negative nuclear Overhauser enhancement (NOE). The extent of negative NOE, i.e., signal intensity depends on the protonation state of the nitrogen, therefore, nitrogen not attached to a proton does not appear in the spectra (Culp *et al*., 1989). NMR spectra of ^{15}N-wtMR showed 5 low intensity signals at 31.25, 31.75, 33.25, 33.75, and 34.5 ppm, corresponding to ζN of 5 Lys residues, and one large, broad signal at 32–33 ppm that

Table 7.5 Effect of viscosity on the kinetic parameters for the racemization of (*R*)- and (*S*)-mandelate catalyzed by dmMR [a]

sucrose (%)	η/η°	(*R*) → (*S*)			
		k_{cat} (s^{-1})	K_m (mM)	$k_{cat}^\circ/k_{cat}^\eta$	$(k_{cat}/K_m)^\circ/(k_{cat}/K_m)^\eta$
0.00	1.00	437.50	1.31	1.00	1.00
10.0	1.32	419.05	1.25	1.04	0.99
20.0	1.88	442.66	1.39	0.99	1.04
27.5	2.48	539.17	1.33	0.81	0.82
32.5	3.06	508.32	1.41	0.86	0.92
35.0	3.42	472.98	1.17	0.92	0.83
		(*S*) → (*R*)			
0.00	1.00	659.13	2.03	1.00	1.00
10.0	1.32	642.22	1.71	1.03	0.86
20.0	1.88	651.24	1.81	1.01	0.90
27.5	2.48	644.84	2.07	1.02	1.04
32.5	3.06	613.42	1.68	1.07	0.89
35.0	3.42	542.18	1.29	1.22	0.77

[a] estimated errors on k_{cat}, K_m, $(k_{cat}^\circ/k_{cat}^\eta)$, and $((k_{cat}/K_m)^\circ/(k_{cat}/K_m)^\eta)$ values are 5%, 10%, 15–20%, and 15–20%, respectively

Table 7.6 Effect of viscosity on the kinetic parameters for the racemization of (*R*)- and (*S*)-mandelate by tmMR-thiaLys

sucrose (%)	η/η°	(*R*) → (*S*)			
		k_{cat} (s^{-1})	K_m (mM)	$k_{cat}^\circ/k_{cat}^\eta$	$(k_{cat}/K_m)^\circ/(k_{cat}/K_m)^\eta$
0.00	1.00	23.46	0.92	1.00	1.00
10.0	1.32	25.97	0.99	0.90	0.97
20.0	1.88	29.39	1.08	0.80	0.94
27.5	2.48	33.31	1.27	0.70	0.98
32.5	3.06	36.00	1.33	0.65	0.94
35.0	3.42	25.00	1.19	0.63	0.82
		(*S*) → (*R*)			
0.00	1.00	78.76	3.94	1.00	1.00
10.0	1.32	86.67	4.87	0.91	1.13
20.0	1.88	79.36	4.02	0.99	1.01
27.5	2.48	80.24	4.03	0.98	1.00
32.5	3.06	72.75	3.07	1.08	0.84
35.0	3.42	72.85	3.10	1.08	0.85

[a] estimated errors on k_{cat}, K_m, $(k_{cat}^\circ/k_{cat}^\eta)$, and $((k_{cat}/K_m)^\circ/(k_{cat}/K_m)^\eta)$ values are 5%, 10%, 15–20%, and 15–20%, respectively

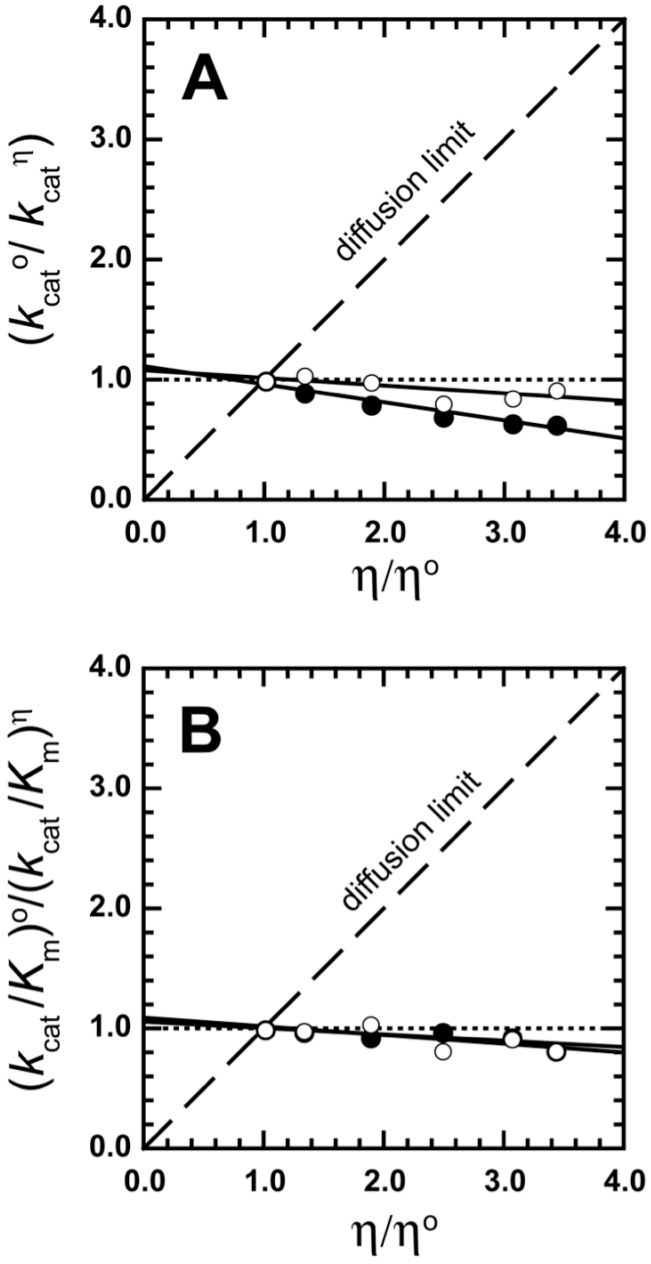

Figure 7.7 Dependence of the relative kinetic parameters for the racemization of (*R*)-mandelate catalyzed by dmMR (○) and tmMR-thiaLys (●) on solvent viscosity. (A) relative k_{cat} (i.e., $k_{cat}^{o}/k_{cat}^{\eta}$) and (B) relative k_{cat}/K_m (i.e., $(k_{cat}/K_m)^{o}/(k_{cat}/K_m)^{\eta}$) values were determined at varying values of η_{rel} using sucrose as the viscosogen. The values of used η_{rel} were from St. Maurice & Bearne (2002). The long dashed line (slope = 1) corresponds to the situation when the rate of the reaction is fully limited by diffusion.

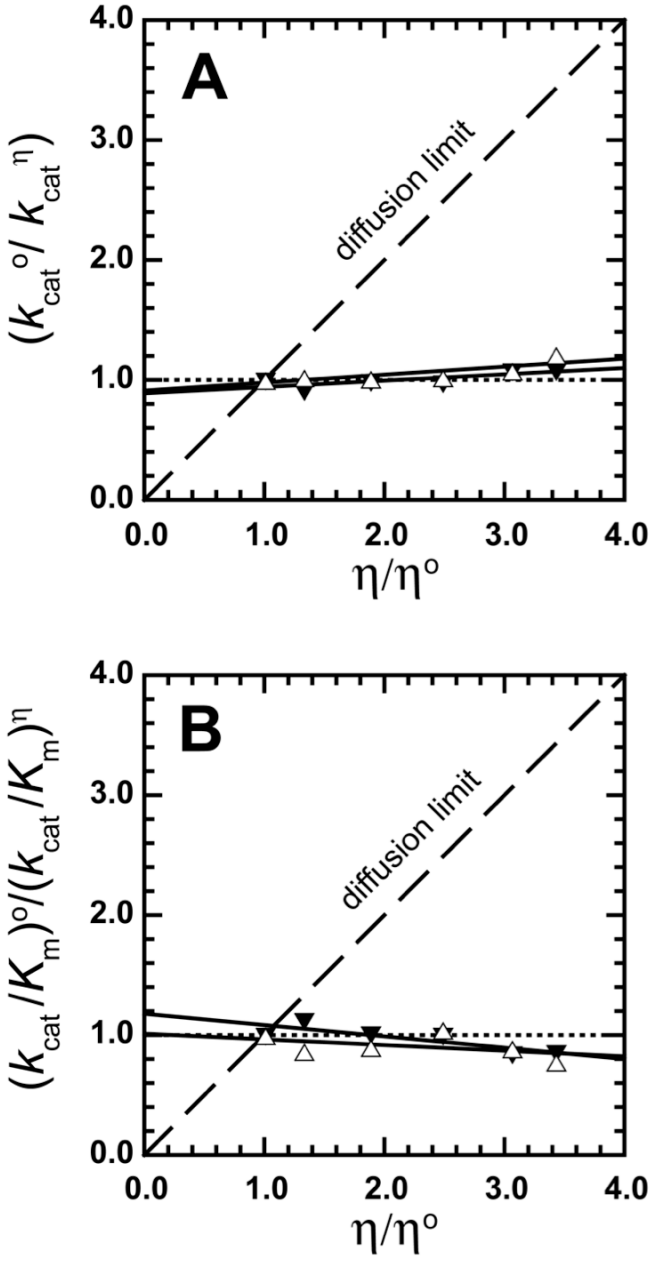

Figure 7.8 Dependence of the relative kinetic parameters for the racemization of (*S*)-mandelate catalyzed by dmMR (△) and tmMR-thiaLys (▼). (A) relative k_{cat} (i.e., $k_{cat}^{o}/k_{cat}^{\eta}$) and (B) relative k_{cat}/K_m (i.e., $(k_{cat}/K_m)^{o}/(k_{cat}/K_m)^{\eta}$) values were determined at varying values of η_{rel} using sucrose as the viscosogen. The values of used η_{rel} were from St. Maurice & Bearne (2002). The long dashed line (slope = 1) corresponds to the situation when the rate of the reaction is fully limited by diffusion.

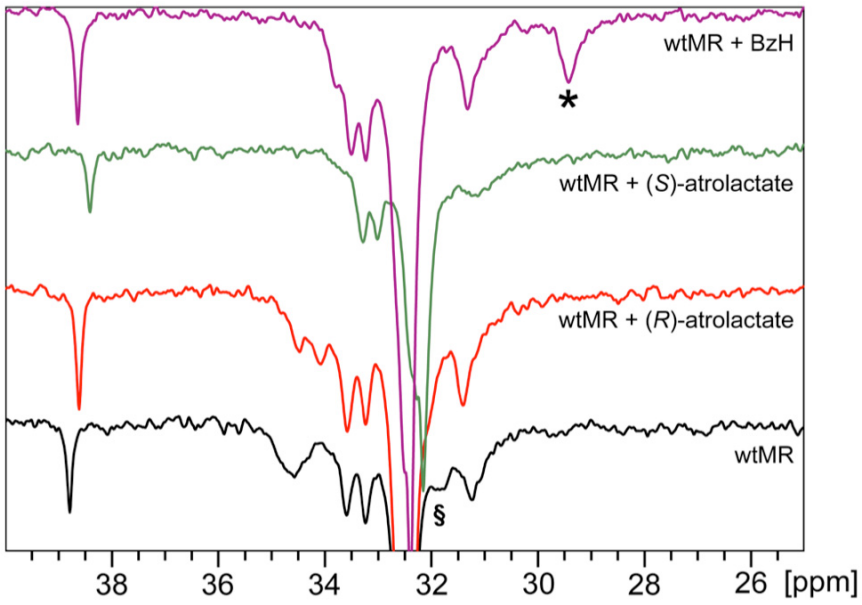

Figure 7.9 1-D ^{15}N NMR spectra of [ζ^{15}N]-lysines of wtMR in presence of various ligands at pH 7.5. Final concentration of ^{15}N-wtMR in each case was ~350 μM, and the concentrations of (*R*)-atrolactate, (*S*)-atrolactate, and BzH were, 10.25, 10.25, and 2.25 mM, respectively. Spectra were collected at 15 °C on a Bruker Avance III 700 MHz NMR spectrometer equipped with a 5 mm broadband (BBO) probe tuned to ^{15}N. *Indicates unique signal observed in presence of BzH. §Denotes possible assignment of Lys 166.

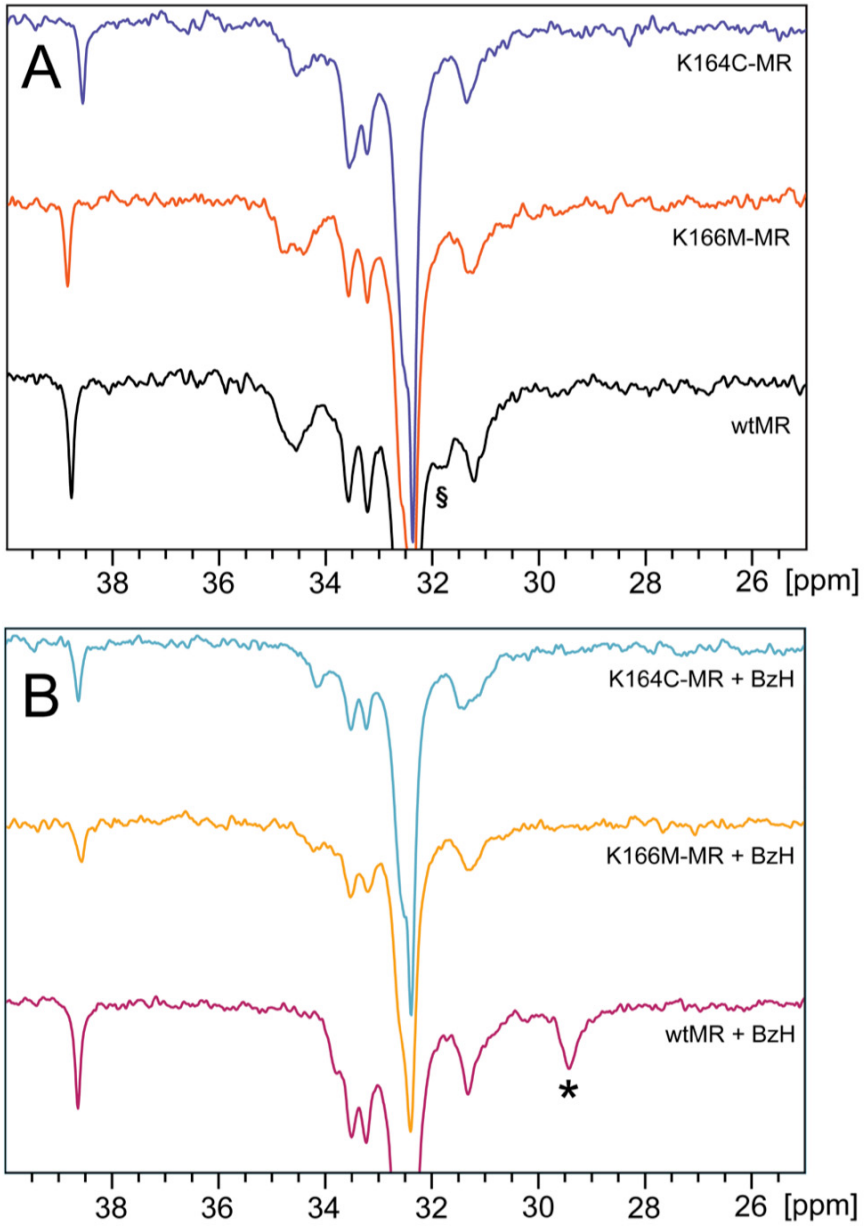

Figure 7.10 1-D ^{15}N NMR spectra of [ζ^{15}N]-lysines of wtMR, K166M-MR, and K164C-MR at pH 7.5. (A) ^{15}N-wtMR, ^{15}N-K166M-MR, and ^{15}N-K164C-MR (~350 μM in each case) without any ligand. (B) ^{15}N-wtMR, ^{15}N-K166M-MR, and ^{15}N-K164C-MR (~350 μM in each case) with BzH (2.25, 18.0, and 2.25 mM, respectively). Spectra were collected at 15 °C on a Bruker Avance III 700 MHz NMR spectrometer equipped with a 5 mm broadband (BBO) probe tuned to ^{15}N. *Indicates unique signal not observed in mutants in presence of BzH. §Denotes possible assignment of Lys 166.

corresponds to the remaining 10 of the total 15 Lys residues in wtMR **(Figure 7.9)**. The signal at ~38.5 ppm likely corresponds to the positively charged N-terminus of the protein (Platzer *et al*., 2014) and is present in all spectra **(Figure 7.9 & 7.10)**. The NMR spectra of ^{15}N-wtMR in presence of various ligands **(Figure 7.9)** showed two prominent changes: first, an upfield shift of the signal at 34.5 ppm in the presence of (*S*)-atrolactate and BzH; and second, the appearance of a new signal at 29.5 ppm only in presence of BzH. These signals could correspond to Lys residues present at the active site, i.e., Lys 164 and/or Lys 166, because ligand binding is more likely to modulate the pK_a of these residues. In order to tease out which signals might correspond to Lys 164 and Lys 166, the K164C- and K166M-MR mutants were created. Comparison of the NMR spectra of ^{15}N-K164C-MR, ^{15}N-K164C-MR, and ^{15}N-wtMR showed no major changes and thus the signal at 34.25 ppm could not be assigned to either Lys 164 or Lys 166 **(Figure 7.10 A)**. However, close examination of the ^{15}N-wtMR NMR spectra showed one minor signal at 31.75 ppm that could be assigned to Lys 166 because it was absent in the ^{15}N-K166M-MR NMR spectrum **(Figure 7.10 A)**. This signal was also absent in the ^{15}N-K164C-MR NMR spectrum, which is in agreement with the above assignment because the Lys 166 signal should shift downfield (into the broad central signal) in the absence of Lys 164 due to protonation. Examination of the wtMR NMR spectra in the presence of various ligands **(Figure 7.9)** also provides support for assignment of this signal to Lys 166. NMR spectra of ^{15}N-wtMR in the presence of (*R*)-atrolactate and BzH did not contain a signal at 31.75 ppm, consistent with the signal arising from Lys 166 because in the presence of these ligands, Lys 166 is expected to be positively charged, i.e., pK_a of lysine is expected to increase, and the signal would move into the broad central signal. In the presence of (*S*)-

atrolactate, the putative Lys 166 signal (31.75 ppm, wtMR spectra) is expected to move upfield and could merge into the signal at 31.5 ppm. Indeed, the broad signal at 31.25 ppm in the ^{15}N-wtMR-(*S*)-atrolactate NMR spectrum (otherwise sharp in all cases) suggests such merging of signals. Overall, the signal at 31.75 ppm in the ^{15}N-wtMR NMR spectra could correspond to Lys 166, but further investigation is required to confirm this assignment.

To investigate the source of the signal at 29.5 ppm in the ^{15}N-wtMR-BzH NMR spectrum, the NMR spectra of ^{15}N-K164C- and ^{15}N-K166M-MR were collected in the presence of BzH **(Figure 7.10 B)**. Interestingly, neither of the NMR spectra showed a signal at 29.5 ppm. In the ^{15}N-wtMR-BzH NMR spectrum, this signal does not likely arise from Lys166 because, most probably, this residue is charged, yet the signal is located upfield with a chemical shift more characteristic of an uncharged Lys residue. Even if one considers that Lys166 might be uncharged upon BzH binding (in contrast to conclusions from the ITC studies in Chapter 6), then this signal would be expected to be observed in the ^{15}N-wtMR-(*S*)-atrolactate NMR spectrum **(Figure 7.9)**, but it is not detected. Within the active site of MR, a positively charged Lys 166 could depress the pK_a of the adjacent Lys 164 (i.e., favor deprotonation of Lys 164), therefore, one might assign the signal at 29.5 ppm to Lys 164 in ^{15}N-wtMR-BzH spectrum, which is consistent with the absence of that signal in the ^{15}N-K164C-MR-BzH NMR spectrum. But the absence of a signal at 29.5 ppm in ^{15}N-wtMR-(*R*)-atrolactate NMR spectrum **(Figure 7.9)** does not agree with this assignment. Over all, the data are inconclusive, and it is not yet possible to assign the signal at 29.5 ppm to either Lys 166 or Lys 164.

7.4 DISCUSSION

MR modulates the pK_a of the Brønsted acid-base catalysts to catalyze the inter-conversion of mandelate enantiomers, e.g., when (*S*)-mandelate is substrate, Lys 166 acts as base (pK_a of conjugate acid of the Brønsted base is ~6.5) and when (*R*)-mandelate is used as substrate, Lys 166 acts as Brønsted acid (pK_a ~10.5) (Kallarakal *et al*., 1995; Landro *et al*., 1994; Powers *et al*., 1991). Since the role depends on the ionization state or pK_a, it is important to determine the microscopic pK_a of the ε-amino group of Lys 166 *in situ*. ^{15}N NMR spectroscopy is one of the most suitable and commonly employed methods to obtain site-specific information on the ionization state of lysine side chains (André *et al*., 2007; McIntosh *et al*., 1996). Therefore, to study the protonation state of Lys 166, NMR spectroscopic studies were attempted using two approaches: first, using specifically labeled Lys 166 (^{15}N-thialysine); and second, using uniformly labeled ^{15}N-MR variants.

Site-directed mutagenesis and chemical modification have been used in combination to replace lysine with thialysine in many enzyme systems such as ribulosebisphosphate carboxylase (Smith & Hartman, 1988), aspartate aminotransferase (Gloss & Kirsch, 1995; Kim *et al*., 1994), acetoacetate decarboxylase (Highbarger *et al*., 1996), fructose 1,6-bisphosphate aldolase (Hopkins *et al*., 2002), and *N*-acetylneuraminic acid lyase (Timms *et al*., 2013). The methodology is straightforward, e.g., replacing the amino acid at the desired position with cysteine and then converting this cysteine to a thialysine by either direct aminoethylation of the cysteine using bromoethylamine (Gloss & Kirsch, 1995; Highbarger *et al*., 1996; Hopkins *et al*., 2002; Olucha *et al*., 2012; Smith & Hartman, 1988), or *N*-(β-iodoethyl)trifluoroacetamide (Bhattacharyya *et al*., 2007;

Sakai, 2005; Schwartz *et al*., 1980) or ethylenimine/aziridine (Hopkins *et al*., 2005; Li & Gershon, 2006; Raftery & Cole, 1966; Yoshimura *et al*., 1990), or indirectly via a dihydroalanine variant using 2,5-dibromo-1,6-hexadiamide and 2-aminoethanethiol (Timms *et al*., 2013). For MR, this methodology required replacement of both Cys 92 and Cys 264 by serines (dmMR) before changing Lys 166 to a Cys residue to create tmMR. Conversion of Cys 92 and Cys 264 to serines was not detrimental to activity, with the kinetic parameters of dmMR being very similar to those of wtMR **(Table 7.3)**, suggesting that neither of these cysteine residues is critical for catalysis. However, in the absence of the essential Lys 166, tmMR was completely inactive **(Table 7.3)**. The crystal structure of tmMR with bound benzilate (Nagar *et al*., 2014) showed that the overall structure, including the active site architecture, is largely unperturbed **(Figure 7.11)**. Preliminary modification of tmMR using ethylenimine/aziridine and bromoethylamine suggested that the former reagent is the better aminoethylating reagent. This is not surprising because ethylenimine is inherently more reactive due to internal bond strain (Hopkins *et al*., 2005; Li & Gershon, 2006). Several different experimental conditions were tried before aminoethylation of tmMR using ethylenimine under denaturing conditions, followed by refolding was selected. This approach afforded active tmMR-thiaLys. The extent of aminoethylation was estimated using IEF after unsuccessful attempts using Ellman's reagent (5,5′-dithiobis-(2-nitrobenzoic acid)) (Ellman, 1959; Riener *et al*., 2002), and 4,4′-dithiodipyridine (error > 25%) (Hansen *et al*., 2007). Hartman and co-workers used IEF to quantify the extent of aminoethylation in ribulosebisphosphate carboxylase (Lorimer & Hartman, 1988; Smith & Hartman, 1988). Although IEF indicated that tmMR-thiaLys focused at the same points as wtMR **(Figure 7.2)**, the presence of

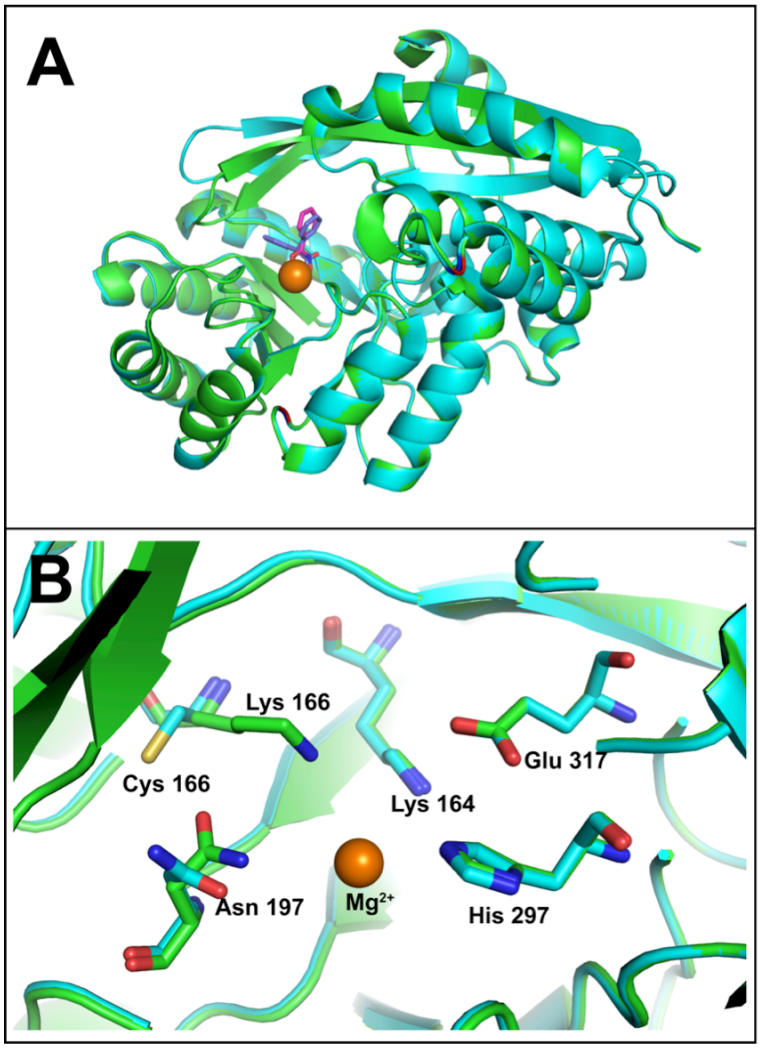

Figure 7.11 Structural comparison of the tmMR–benzilate and wtMR–BzH complexes. (A) Overlay of the x-ray crystal structure of a monomer of the wtMR–BzH [cyan; PDB entry 3UXK (Lietzan *et al*., 2012)] and tmMR–benzilate complexes [green; PDB entry 4HNC (Nagar *et al*., 2014) indicates that replacement of Cys 92 and Cys 264 (shown in magenta) by Ser residues (shown as purple) had no appreciable impact on the over all structure. Although the 20s loop of the N-terminal capping domain is not closed, this seems to be a ligand binding related issue rather than a mutational impact. (B) Active-site view of the wtMR–BzH and tmMR–benzilate complexes (ligands not shown) shows that replacement of Lys 166 with Cys did not change the active site architecture except for the movement of Asn 197 to accommodate the phenyl rings of the "bulky" benzilate (ligand not shown).

multiple bands in both the wtMR and tmMR IEF gel strips hampered accurate quantification **(Figure 7.2)**. All 3 bands in each strip corresponded to an intact MR monomer on a 2-D gel (not shown); therefore, these multiple bands could not arise due to proteolysis of the sample during IEF. However, such multiple bands could be a result of: (a) subtle post-translational modifications, e.g., phosphorylation of serines and threonines that usually induce an acidic shift of the pI (Zhu *et al*., 2005), or (b) complexation with carrier ampholytes (Frater, 1970; Guengerich, 1979), or (c) electrolytic reduction of the MR samples induced by high salt concentrations during IEF (Lee & Chang, 2009). Densitometric analysis of the bands in the aminoethylated-tmMR containing strip using ImageJ (Schneider *et al*., 2012) suggested that ≥ 33% modification had occurred and, therefore, k_{cat} values for tmMR-thiaLys were adjusted accordingly **(Table 7.3)**. Although kinetic characterization of tmMR-thiaLys showed a 5–10-fold reduction in catalytic efficiency (k_{cat}/K_m) and k_{cat} in both reaction directions relative to wtMR and dmMR **(Table 7.3)**, thialysine is still a reasonable replacement of lysine 166 because the catalytic efficiency of this MR variant is 100-times better than MR with an arginine substituted at position 166 (Kallarakal *et al*., 1995). The similar binding affinity (K_m) of wtMR and tmMR-thiaLys for (*R*)-mandelate **(Table 7.3)** is also consistent with the interpretations from the ITC studies that suggested the importance of Lys 166 in substrate binding (Chapter 6).

The pH-dependence of k_{cat} and k_{cat}/K_m of tmMR-thiaLys catalysis **(Figure 7.5 & 7.6)** showed that the pK_a of thialysine when acting as a Brønsted base (*S* → *R*) is ~5.8, and ~9.8 when thialysine acts as a Brønsted acid (*R* → *S*). These values are similar to the pK_a values of the Lys 166 in dmMR (~6.2, *S* → *R*; and ~10.1, *R* → *S*) **(Figure 7.4 & 7.5)**

and with those reported for Lys 166 in wtMR (~6.5, $S \rightarrow R$; and ~10.5, $R \rightarrow S$, (Landro *et al*., 1991)). The presence of sulfur in the thialysine side chain should lower the pK_a by 1 unit relative to Lys (Hermann & Lemke, 1968; Li & Gershon, 2006). In the present study, the difference was merely ~0.3, which is within the errors associated with the kinetic data. Therefore, thialysine is an ideal candidate to replace lysine, and tmMR-ThiaLys could be used for studying the pK_a shift accompanying substrate binding. Interestingly, the K_m value showed a direct dependence on pH **(Table 7.3)**. At high pH, when both Brønsted acid-base catalysts are expected be uncharged/deprotonated, the substrate binding affinity of both dmMR and tmMR-thiaLys drastically decreased suggesting that positive a charge on the Brønsted acid-base catalyst is important for substrate binding. This observation is in accord with the conclusions drawn from the ITC studies (Chapter 6).

The kinetic parameters for the racemization of mandelate catalyzed by tmMR-thiaLys did not show any significant dependence on the microviscosity of the solvent **(Figure 7.7** & **7.8,** and **Table 7.6)**, suggesting that the chemical step is fully rate-limiting. This result is in contrast to wtMR, which shows a partial viscosity dependence (St. Maurice & Bearne, 2002) indicating that the chemical step along with substrate association and/or product dissociation is partially rate-limiting (Brouwer & Kirsch, 1982). Surprisingly, the kinetic parameters for dmMR, which has a similar catalytic efficiency to wtMR were also independent of microviscosity **(Figure 7.7** & **7.8**, and **Table 7.5)**. Therefore, the behavior of tmMR-thiaLys might not only be attributed to replacement of Lys 166 with thialysine, but also could arise from very minor structural changes due to Cys mutations. Although the x-ray crystal structure of tmMR did not show any observable change in structure

(Figure 7.11), it is possible that subtle structural changes could have caused the change in the rate-limiting step.

One of the goals of developing a method to prepare tmMR-thiaLys and its kinetic characterization was to make tmMR-^{15}N-thiaLys to study the protonation state/pK_a of the side chain of residue 166 using NMR. Unfortunately, tmMR-^{15}N-thiaLys precipitated at the concentration required for NMR spectroscopy. As an alternate, uniformly labeled ^{15}N-MR variants were used for the NMR spectroscopy study. ^{1}H–^{15}N heteronuclear correlation spectroscopy is a commonly used NMR technique to study the ionization of the ε-amino group of the lysine side chain in a protein. For MR, being an octamer in solution (monomeric molecular weight ~40 kDa), such studies are problematic due to the slow tumbling of the enzyme in solution, leading to rapid decay of the NMR signal and a low signal to noise ratio. Therefore, ^{15}N NMR spectra of Lys residues of the enriched ^{15}N-MR variants, in presence of various ligands, were collected using power-gated proton decoupled 1-D ^{15}N NMR with full NOE to enhance nitrogen signals (Inbar & Lapidot, 1988; Lorimer & Hartman, 1988). 1-D ^{15}N NMR experiments have been used to determine pK_a of histidine in Rieske protein from *Thermus thermophilus* (Lin *et al*., 2006) and of proline in 4-oxalocrotonate tautomerase (Stivers *et al*., 1996). In a typical ^{15}N NMR spectrum, signals from the lysine side-chain ζ-^{15}N appear between 34 and 25 ppm (André *et al*., 2007; Esadze *et al*., 2011; Iwahara *et al*., 2007; Poon *et al*., 2006), in its protonated (NH_3^+) and deprotonated (NH_2) states (Poon *et al*., 2006), respectively. This pattern of chemical shifts can be explained by the increased electron density at the ^{15}N nucleus because of deprotonation of the amine, which increases local diamagnetism, hence causing an upfield shift of the signal (Zhu *et al*., 1995). Due to the presence of 15

Lys residues in wtMR, most of the signals overlap at 32.5 ppm, making the 1-D spectra difficult to analyze and not particularly informative. Most of the NMR spectra look alike, except for the spectrum of wtMR-(*S*)-atrolactate, which lacked a signal at 33.5 ppm, and the spectrum of wtMR-BzH, which also lacked a signal at 33.5 ppm but showed a new prominent signal at 29.5 ppm **(Figure 7.9 & 7.10)**. Both of these signals could not be conclusively assigned to any of the active site Lys residues. However, close inspection of the NMR spectra of wtMR, K166M-MR, and K166C-MR indicated that a signal at 31.75 ppm could correspond to Lys 166. Although this signal shifts as expected due to the binding of various ligands, further investigation is required for definitive assignment. In addition, a circumstantial case can be made that the signal at 29.5 ppm may arise from Lys 164; however, again, additional investigation is required before a definitive assignment can be made.

Overall, the work in this chapter shows that Lys 166, a Brønsted acid-base catalyst, can be successfully replaced by the non-natural analogue thialysine. The overlap of NMR signals present in the spectra of uniformly labeled ^{15}N-MR variants could be avoided by using ^{15}N-thialysine. Hence, conditions to enhance the yield of tmMR-^{15}N-thialysine after modification, e.g., aminoethylation under either native conditions, or denaturing conditions using guanidine hydrochloride (Maxwell *et al*., 2003) should be explored. In addition, conditions to prevent precipitation at higher concentrations (Yamaguchi & Miyazaki, 2014) should be sought. Although addition of glycerol (Gekko & Timasheff, 1981; Vagenende *et al*., 2009) and other sugars (Bondos & Bicknell, 2003; Kaushik & Bhat, 2003) could stabilize the protein at higher concentrations, increased viscosity due to the presence of these agents could be problematic for NMR studies. Alternatively,

combinations of arginine and glutamic acid could be explored to prevent tmMR-^{15}N-thiaLys aggregation, which has been shown suitable for solution state studies of isotopically labeled proteins using NMR spectroscopy (Golovanov *et al*., 2004; Schneider *et al*., 2011; Shukla & Trout, 2011). Although the mechanism of action of these reagents is not fully understood, it is believed that the presence of arginine and glutamic acid around proteins leads to enhanced crowding that diminishes protein-protein interactions (Shukla & Trout, 2011).

CHAPTER 8

CONCLUSION

MR-catalyzed racemization of (*R*)- and (*S*)-trifluorolactate (TFL) demonstrates that β,γ-unsaturation is not an absolute requirement in MR substrates, and the minimal substrate model of MR proposed by Felfer *et al*. (2005) should therefore be extended. The reduced catalytic efficiency of MR with TFL (*cf*. mandelate) and the microviscosity-independent kinetic parameters suggests that the chemical step is fully rate-limiting when TFL is the substrate. The TS of MR-catalyzed racemization of mandelate is better stabilized, by ~6 kcal/mol, compared to the TS of MR-catalyzed racemization of TFL. This demonstrates that the inductive effects due to the presence of electron withdrawing trifluoromethyl group are sufficient for catalysis; however, β,γ-unsaturation in the substrates, e.g., mandelate and vinylglycolate, provides additional stabilization to the enolic intermediate via conjugation/resonance. Although, MR showed similar binding affinity for mandelate and TFL, the binding affinity of TFL is higher than expected considering the hydrophobicity of the trifluoromethyl group. Therefore, stable fluorinated ground state and TS analogues inhibitors were designed to exploit the advantage offered by the trifluoromethyl group.

3,3,3-Trifluoro-2-hydroxy-2-(trifluoromethyl)-propanoate (TFHTP), a substrate-product analogue of TFL, is a potent competitive inhibitor of MR that has an astounding binding affinity that is ~50-fold higher than that observed for the substrates, TFL and mandelate, and similar to that observed for the TS analogue inhibitors. The x-ray crystal structure of the MR–TFHTP complex solved at 1.68-Å resolution by St. Maurice and

Lietzan (2014) shows a novel TFHTP-binding mode within the active site that could explain the high affinity of TFHTP. Unlike the normal binding mode, in which the glycolate moiety of the ligand chelates the active site Mg^{2+}, the carboxylate of TFHTP "hangs" above the Mg^{2+} due to the close packing of trifluoromethyl groups of TFHTP against the 20s loop of the capping domain and bridges the two active site Brønsted acid-base catalysts Lys 166 and His 297 via salt-bridge interactions. Recognizing that positioning a carboxylate between the Brønsted acid-base catalysts could yield an inhibitor, tartronate was identified as competitive inhibitor of MR that bound MR in the normal binding mode with its second carboxylate interacting with Brønsted acid-base catalysts. These studies opened new frontiers to design inhibitors of MR by exploiting Brønsted acid-base catalysts as binding determinants. A similar strategy could be used to develop inhibitors for the other members of enolase superfamily especially those belong to MR-subgroup such as L-talarate/galactarate dehydratase (Yew *et al*., 2007) and D-tartrate dehydratase (Yew *et al*., 2006).

With that discovered, α-keto acids such as mesoxalate and 3-hydroxypyruvate (tartronate analogues), and 3-fluoropyruvate were identified as inhibitors of MR. Mesoxalate is a reversible competitive inhibitor that binds MR with similar affinity to that observed for tartronate. Surprisingly, 3-hydroxypyruvate (3-HP) is an irreversible, time-dependent inhibitor. Protection studies using BzH; trypsinolysis and ESI-MS/MS analyses; and, x-ray crystallographic studies revealed that 3-HP undergoes Schiff-base formation with Lys 166 at the active site, followed by formation of an aldehyde/enol(ate) adduct. Such a reaction is unprecedented in the enolase superfamily. Therefore, the ability of MR to form and deprotonate a Schiff-base intermediate furnishes a previously

unrecognized potential mechanistic link to other α/β-barrel enzymes utilizing Schiff-base chemistry, and is in accord with the sequence- and structure-based hypothesis that members of the metal-dependent enolase superfamily and the Schiff-base forming ***N***-acetylneuraminate lyase superfamily and aldolases share a common ancestor.

Salt-bridge interactions of TFHTP, irreversible inactivation by 3-HP, and enhanced binding of TFL and 3-FP to MR that could arise due to weak polar H-bonding with Lys 166 and/or His 297, suggest that Brønsted acid-base catalysts can play a role in ligand binding. In fact, the x-ray crystal structure of the MR–BzH complex (Lietzan *et al*., 2012) also shows that the side chains of Lys 166, His 297 (which are equidistant from the α-carbon), and Tyr 54 are positioned in such a way that these residues can play a role in binding of this TS/intermediate analogue inhibitor. Kinetic and inhibition studies with Y54F and Y54L mutants revealed that the role of Tyr 54 in MR BzH binding is relatively minor. ITC studies using Lys 166 and/or His 297 mutants with substrate analogues revealed that the Brønsted acid-base catalysts interact with the phenyl ring of substrates while studies with the TS/intermediate analogue inhibitors BzH and CHCHA revealed that the Brønsted acid-base catalysts, especially Lys 166, also interact with the hydroxamate moiety in addition to the phenyl ring of BzH, possibly via cation-π/NH-π interactions. ^{15}N NMR spectroscopy studies could provide insight into the protonation state of Lys 166, but unfortunately the data acquired to date are inconclusive and further investigation is required.

In summary, the work in this thesis redefines the minimal substrate requirements for MR, suggests an unprecedented potential mechanistic link between α/β-barrel containing enzyme superfamilies, and has led to the identification of the Brønsted acid-

base catalysts as binding determinants that can stabilize the enolate moiety of the altered substrate in TS, a role that has been overlooked in this proficient enzyme.

REFERENCES

Aitken, S. M., Turnbull, J. L., Percival, M. D., and English, A. M. (2001) Thermodynamic analysis of the binding of aromatic hydroxamic acid analogues to ferric horseradish peroxidase. *Biochemistry* **40**, 13980–13989.

Alberg, D. G., Lauhon, C. T., Nyfeler, R., Faessler, A., and Bartlett, P. A. (1992) Inhibition of 5-enolpyruvoylshikimate 3-phosphate (EPSP) synthase by analogs of the tetrahedral intermediate and of EPSP. *J. Am. Chem. Soc.* **114**, 3535–3546.

Amyes, T. L., and Richard, J. P. (2013) Specificity in transition state binding: the Pauling model revisited. *Biochemistry* **52**, 2021–2035.

André, I., Linse, S., and Mulder, F. A. (2007) Residue-specific pK_a determination of lysine and arginine side chains by indirect ^{15}N and ^{13}C NMR spectroscopy: application to apo calmodulin. *J. Am. Chem. Soc.* **129**, 15805–15813.

Ash, E. L., Sudmeier, J. L., De Fabo, E. C., and Bachovchin, W. W. (1997) A low-barrier hydrogen bond in the catalytic triad of serine proteases? Theory versus experiment. *Science* **278**, 1128–1132.

Babbitt, P. C., and Gerlt, J. A. (1997) Understanding enzyme superfamilies. Chemistry as the fundamental determinant in the evolution of new catalytic activities. *J. Biol. Chem.* **272**, 30591–30594.

Babbitt, P. C., Hasson, M. S., Wedekind, J. E., Palmer, D. R., Barrett, W. C., Reed, G. H., Rayment, I., Ringe, D., Kenyon, G. L., and Gerlt, J. A. (1996) The enolase superfamily: a general strategy for enzyme-catalyzed abstraction of the α-protons of carboxylic acids. *Biochemistry* **35**, 16489–16501.

Babbitt, P. C., Mrachko, G. T., Hasson, M. S., Huisman, G. W., Kolter, R., Ringe, D., Petsko, G. A., Kenyon, G. L., and Gerlt, J. A. (1995) A functionally diverse enzyme superfamily that abstracts the alpha protons of carboxylic acids. *Science* **267**, 1159–1161.

Banner, D. W., Bloomer, A. C., Petsko, G. A., Phillips, D. C., Pogson, C. I., Wilson, I. A., Corran, P. H., Furth, A. J., Milman, J. D., Offord, R. E., Priddle, J. D., and Waley, S. G. (1975) Structure of chicken muscle triose phosphate isomerase determined crystallographically at 2.5 angstrom resolution using amino acid sequence data. *Nature* **255**, 609–614.

Barbour, J. B., and Karty, J. M. (2004) Resonance energies of the allyl cation and allyl anion: contribution by resonance and inductive effects toward the acidity and hydride abstraction enthalpy of propene. *J. Org. Chem.* **69**, 648–654.

Bartlett, P. A., and Marlowe, C. K. (1983) Phosphonamidates as transition-state analogue inhibitors of thermolysin. *Biochemistry* **22**, 4618–4624.

Bazelyansky, M., Robey, E., and Kirsch, J. F. (1986) Fractional diffusion-limited component of reactions catalyzed by acetylcholinesterase. *Biochemistry* **25**, 125–130.

Bearne, S. L., and Kluger, R. (1992) Phosphoenol acetylphosphonates: substrate analogues as inhibitors of phosphoenolpyruvate enzymes. *Bioorg. Chem.* **20**, 135–147.

Bearne, S. L., St. Maurice, M., and Vaughan, M. D. (1999) An assay for mandelate racemase using high-performance liquid chromatography. *Anal. Biochem.* **269**, 332–336.

Bearne, S. L., and Wolfenden, R. (1997) Mandelate racemase in pieces: effective concentrations of enzyme functional groups in the transition state. *Biochemistry* **36**, 1646–1656.

Bégué, J. P., and Bonnet-Delpon, D. (2008) *Bioorganic and Medicinal Chemistry of Fluorine*, John Wiley & Sons, Inc., Hoboken, NJ.

Bellamy, L. J., and Williams, R. L. (1958) The infrared spectra of hydroxypyruvic acid and related compounds. *Biochem. J.* **68**, 81–84.

Berkowitz, D. B., Karukurichi, K. R., de la Salud-Bea, R., Nelson, D. L., and McCune, C. D. (2008) Use of fluorinated functionality in enzyme inhibitor development: mechanistic and analytical advantages. *J. Fluor. Chem.* **129**, 731–742.

Bhat, S. G., and Vaidyanathan, C. S. (1976) Involvement of 4-hydroxymandelic acid in the degradation of mandelic acid by *Pseudomonas convexa*. *J. Bacteriol.* **127**, 1108–1118.

Bhattacharyya, J., Shipova, E. V., Santhoshkumar, P., Sharma, K. K., and Ortwerth, B. J. (2007) Effect of a single AGE modification on the structure and chaperone activity of human αB-crystallin. *Biochemistry* **46**, 14682–14692.

Bhaumik, P., Schmitz, W., Hassinen, A., Hiltunen, J. K., Conzelmann, E., and Wierenga, R. K. (2007) The catalysis of the 1,1-proton transfer by α-methyl-acyl-CoA racemase is coupled to a movement of the fatty acyl moiety over a hydrophobic, methionine-rich surface. *J. Mol. Biol.* **367**, 1145–1161.

Biffinger, J. C., Kim, H. W., and DiMagno, S. G. (2004) The polar hydrophobicity of fluorinated compounds. *ChemBioChem* **5**, 622–627.

Blacklow, S. C., Raines, R. T., Lim, W. A., Zamore, P. D., and Knowles, J. R. (1988) Triosephosphate isomerase catalysis is diffusion controlled. *Biochemistry* **27**, 1158–1167.

Bondos, S. E., and Bicknell, A. (2003) Detection and prevention of protein aggregation before, during, and after purification. *Anal. Biochem.* **316**, 223–231.

Bourque, J. R., and Bearne, S. L. (2008) Mutational analysis of the active site flap (20s loop) of mandelate racemase. *Biochemistry* **47**, 566–578.

Bourque, J. R., Burley, R. K., and Bearne, S. L. (2007) Intermediate analogue inhibitors of mandelate racemase: *N*-hydroxyformanilide and cupferron. *Bioorg. Med. Chem. Lett.* **17**, 105–108.

Broecker, J., Vargas, C., and Keller, S. (2011) Revisiting the optimal *c* value for isothermal titration calorimetry. *Anal. Biochem.* **418**, 307–309.

Brouwer, A. C., and Kirsch, J. F. (1982) Investigation of diffusion-limited rates of chymotrypsin reactions by viscosity variation. *Biochemistry* **21**, 1302–1307.

Burgi, H. B., Dunitz, J. D., and Shefter, E. (1973) Geometrical reaction coordinates. II. Nucleophilic addition to a carbonyl group. *J. Am. Chem. Soc.* **95**, 5065–5067.

Burley, R. K., and Bearne, S. L. (2005) Inhibition of mandelate racemase by the substrate-intermediate-product analogue 1,1-diphenyl-1-hydroxymethylphosphonate. *Bioorg. Med. Chem. Lett.* **15**, 4342–4344.

Burley, S. K., and Petsko, G. A. (1986) Amino-aromatic interactions in proteins. *FEBS letters* **203**, 139–143.

Byers, L. D. (1978) Binding of reactive intermediate analogs to enzymes. *J. Theor. Biol.* **74**, 501–512.

Cardinale, G. J., and Abeles, R. H. (1968) Purification and mechanism of action of proline racemase. *Biochemistry* **7**, 3970–3978.

Carnell, A. J., Hale, I., Denis, S., Wanders, R. J., Isaacs, W. B., Wilson, B. A., and Ferdinandusse, S. (2007) Design, synthesis, and in vitro testing of α-methylacyl-CoA racemase inhibitors. *J. Med. Chem.* **50**, 2700–2707.

Chen, T., Shen, P., Li, Y., and He, H. (2006) The synthesis and herbicidal evaluation of fluorine-containing phenoxyacetoxyalkyl-phosphonate derivatives. *Phosphorus, Sulfur Silicon Relat. Elem.* **181**, 2135–2145.

Chiang, Y., and Kresge, A. J. (1991) Enols and other reactive species. *Science* **253**, 395–400.

Chiang, Y., Kresge, A. J., Popik, V. V., and Schepp, N. P. (1997) The mandelic acid keto–enol system in aqueous solution. Generation of the enol by hydration of phenylhydroxyketene and phenylcarboxycarbene. *J. Am. Chem. Soc.* **119**, 10203–10212.

Chiang, Y., Kresge, A. J., Pruszynski, P., Schepp, N. P., and Wirz, J. (1990) The enol of mandelic acid, detection, acidity in aqueous solution, and estimation of the keto-enol equilibrium constant and carbon acidity of mandelic Acid. *Angew. Chem. Int. Ed. Engl.* **29**, 792–794.

Choi, K. H., Lai, V., Foster, C. E., Morris, A. J., Tolan, D. R., and Allen, K. N. (2006) New superfamily members identified for Schiff-base enzymes based on verification of catalytically essential residues. *Biochemistry* **45**, 8546–8555.

Cleland, W. W., Frey, P. A., and Gerlt, J. A. (1998) The low barrier hydrogen bond in enzymatic catalysis. *J. Biol. Chem.* **273**, 25529–25532.

Cleland, W. W., and Kreevoy, M. M. (1994) Low-barrier hydrogen bonds and enzymic catalysis. *Science* **264**, 1887–1890.

Cooper, A. J. L., Ginos, J. Z., and Meister, A. (1983) Synthesis and properties of the α-keto acids. *Chem. Rev.* **83**, 321–358.

Cooper, A. J. L., and Redfield, A. G. (1975) Proton magnetic resonance studies of α-keto acids. *J. Biol. Chem.* **250**, 527–532.

Copeland, R. A. (2000) Time dependent inhibition, in *Enzymes: a practical introduction to structure, mechanism, and data analysis* (Copeland, R. A., Ed.), pp 318–349, John Wiley & Sons, Inc., New York.

Copley, R. R., and Bork, P. (2000) Homology among $(\alpha\beta)_8$ barrels: implications for the evolution of metabolic pathways. *J. Mol. Biol.* **303**, 627–641.

Culp, S. J., Cho, B. P., Kadlubar, F. F., and Evans, F. E. (1989) Structural and conformational analyses of 8-hydroxy-2'-deoxyguanosine. *Chem. Res. Toxicol.* **2**, 416–422.

Cummings, J. A., Vetting, M., Ghodge, S. V., Xu, C., Hillerich, B., Seidel, R. D., Almo, S. C., and Raushel, F. M. (2014) Prospecting for unannotated enzymes: discovery of a 3',5'-nucleotide bisphosphate phosphatase within the amidohydrolase superfamily. *Biochemistry* **53**, 591–600.

DeVries, G. H., and Binkley, S. B. (1972) 3-Hydroxy-*N*-acetylneuraminic acid: synthesis and inhibitory properties. *Arch. Biochem. Biophys.* **151**, 243–250.

Dickens, F., and Williamson, D. H. (1958) The preparation and properties of lithium hydroxypyruvate and hydroxypyruvic acid. *Biochem. J.* **68**, 74–84.

Dobson, R. C., Griffin, M. D., Devenish, S. R., Pearce, F. G., Hutton, C. A., Gerrard, J. A., Jameson, G. B., and Perugini, M. A. (2008) Conserved main-chain peptide distortions: a proposed role for Ile203 in catalysis by dihydrodipicolinate synthase. *Protein. Sci.* **17**, 2080–2090.

Dunitz, J. D. (2004) Organic fluorine: odd man out. *ChemBioChem* **5**, 614-621.

Dunitz, J. D., and Taylor, R. (1997) Organic fluorine hardly ever accepts hydrogen bonds. *Chem. Eur. J.* **3**, 89–98.

Dyatkin, B. L., Mochalina, E. P., and Knunyants, I. L. (1965) The acidic properties of fluorine-containing alcohols, hydroxylamines and oximes. *Tetrahedron* **21**, 2991–2995.

Edwards, D. R., Lohman, D. C., and Wolfenden, R. (2012) Catalytic proficiency: the extreme case of S–O cleaving sulfatases. *J. Am. Chem. Soc.* **134**, 525–531.

Ellman, G. L. (1959) Tissue sulfhydryl groups. *Arch. Biochem. Biophys.* **82**, 70–77.

Esadze, A., Li, D. W., Wang, T., Bruschweiler, R., and Iwahara, J. (2011) Dynamics of lysine side-chain amino groups in a protein studied by heteronuclear ^{1}H–^{15}N NMR spectroscopy. *J. Am. Chem. Soc.* **133**, 909–919.

Fee, J. A., Hegeman, G. D., and Kenyon, G. L. (1974) Mandelate racemase from *Pseudomonas putida*. Subunit composition and absolute divalent metal ion requirement. *Biochemistry* **13**, 2528–2532.

Felfer, U., Goriup, M., Koegl, M. F., Wagner, U., Larissegger-Schnell, B., Faber, K., and Kroutil, W. (2005) The substrate spectrum of mandelate racemase: minimum structural requirements for substrates and substrate model. *Adv. Synth. & Catal.* **347**, 951-961.

Felfer, U., Strauss, U. T., Kroutil, W., Fabian, W. M. F., and Faber, K. (2001) Substrate spectrum of mandelate racemase: Part 2. (Hetero)-aryl-substituted mandelate derivatives and modulation of activity. *J. Mol. Catal. B: Enzym.* **15**, 213-222.

Fischer, F. R., Schweizer, W. B., and Diederich, F. (2007) Molecular torsion balances: evidence for favorable orthogonal dipolar interactions between organic fluorine and amide groups. *Angew. Chem. Int. Ed. Engl.* **46**, 8270–8273.

Flexser, L. A., Hammett, L. P., and Dingwall, A. (1935) The determination of ionization by ultraviolet spectrophotometry: its validity and its application to the measurement of the strength of very weak bases. *J. Am. Chem. Soc.* **57**, 2103–2115.

Frater, R. (1970) Behavior of ampholines during isoelectric focusing. *Anal. Biochem.* **38**, 536–538.

Freeman, S., Irwin, W. J., and Schwalbe, C. H. (1991) Synthesis and hydrolysis studies of phosphonopyruvate. *J. Chem. Soc., Perkin Trans.* **2**, 263–267.

Frey, P. A., Whitt, S. A., and Tobin, J. B. (1994) A low-barrier hydrogen bond in the catalytic triad of serine proteases. *Science* **264**, 1927–1930.

Frick, L., Yang, C., Marquez, V. E., and Wolfenden, R. (1989) Binding of pyrimidin-2-one ribonucleoside by cytidine deaminase as the transition-state analogue 3,4-dihydrouridine and the contribution of the 4-hydroxyl group to its binding affinity. *Biochemistry* **28**, 9423–9430.

Fuchigami, T., and Nakagawa, Y. (1987) Electrolytic transformation of fluoroorganic compounds. 2. Generation and alkylation of a stable (trifluoromethyl)malonic ester enolate using an electrogenerated base. *J. Org. Chem.* **52**, 5276–5277.

Garcia-Viloca, M., Gonzalez-Lafont, A., and Lluch, J. M. (2001) A QM/MM study of the racemization of vinylglycolate catalyzed by mandelate racemase enzyme. *J. Am. Chem. Soc.* **123**, 709–721.

Gasteiger, E., Gattiker, A., Hoogland, C., Ivanyi, I., Appel, R. D., and Bairoch, A. (2003) ExPASy: The proteomics server for in-depth protein knowledge and analysis. *Nucleic Acids Res.* **31**, 3784–3788.

Gasteiger, E., Hoogland, C., Gattiker, A., Duvaud, S., Wilkins, M. R., Appel, R. D., and Bairoch, A. (2005) Protein identification and analysis tools on the ExPASy server, in *The Proteomics Protocols Handbook* (Walker, J. M., Ed.), pp 571–607, Humana Press.

Gekko, K., and Timasheff, S. N. (1981) Mechanism of protein stabilization by glycerol: preferential hydration in glycerol-water mixtures. *Biochemistry* **20**, 4667–4676.

Gerlt, J. A. (1998) Understanding the mechanism and rates of enzyme-catalyzed proton transfer reactions to and from carbon, in *Bioorganic Chemistry: Peptides and Proteins* (Hecht, S. M., Ed.), pp 279–311, Oxford University Press, New York.

Gerlt, J. A. (2007) Enzymatic catalysis of proton transfer at carbon atoms, in *Hydrogen Transfer Reactions* (Hynes, J. T., Klinman, J. P., Limbach, H. H. & Schwen, R. L., Eds.), pp 1107–1137, Wiley-VCH.

Gerlt, J. A., and Babbitt, P. C. (2009) Enzyme (re)design: lessons from natural evolution and computation. *Curr. Opin. Struct. Biol.* **13**, 10–18.

Gerlt, J. A., Babbitt, P. C., Jacobson, M. P., and Almo, S. C. (2012) Divergent evolution in enolase superfamily: strategies for assigning functions. *J. Biol. Chem.* **287**, 29–34.

Gerlt, J. A., Babbitt, P. C., and Rayment, I. (2005) Divergent evolution in the enolase superfamily: the interplay of mechanism and specificity. *Arch. Biochem. Biophys.* **433**, 59–70.

Gerlt, J. A., and Gassman, P. G. (1992) Understanding enzyme-catalyzed proton abstraction from carbon acids: details of stepwise mechanisms for β-elimination reactions. *J. Am. Chem. Soc.* **114**, 5928–5934.

Gerlt, J. A., and Gassman, P. G. (1993a) An explanation for rapid enzyme-catalyzed proton abstraction from carbon acids: importance of late transition states in concerted mechanisms. *J. Am. Chem. Soc.* **115**, 11552–11568.

Gerlt, J. A., and Gassman, P. G. (1993b) Understanding the rates of certain enzyme-catalyzed reactions: proton abstraction from carbon acids, acyl-transfer reactions, and displacement reactions of phosphodiesters. *Biochemistry* **32**, 11943–11952.

Gerlt, J. A., Kozarich, J. W., Kenyon, G. L., and Gassman, P. G. (1991) Electrophilic catalysis can explain the unexpected acidity of carbon acids in enzyme-catalyzed reactions. *J. Am. Chem. Soc.* **113**, 9667–9669.

Gerlt, J. A., and Raushel, F. M. (2003) Evolution of function in $(\beta/\alpha)_8$-barrel enzymes. *Curr. Opin. Struct. Biol.* **7**, 252–264.

Gloss, L. M., and Kirsch, J. F. (1995) Decreasing the basicity of the active site base, Lys-258, of *Escherichia coli* aspartate aminotransferase by replacement with γ-thialysine. *Biochemistry* **34**, 3990–3998.

Goldstein, J. A., Cheung, Y.-F., Marletta, M. A., and Walsh, C. (1978) Fluorinated substrate analogs as stereochemical probes of enzymic reaction mechanisms. *Biochemistry* **17**, 5567–5575.

Golovanov, A. P., Hautbergue, G. M., Wilson, S. A., and Lian, L. Y. (2004) A simple method for improving protein solubility and long-term stability. *J. Am. Chem. Soc.* **126**, 8933–8939.

Götzö, S. P., and Seebach, D. (1996) Preparation of (*R*)- and (*S*)-3-hydroxy-2-(trifluoromethyl)propionic acid by resolution with (*R*,*R*)- and (*S*,*S*)-2-amino-1-phenylpropane-1,3-diol. *Chimia* **50**, 20–23.

Graham, J. D., Buytendyk, A. M., Wang, D., Bowen, K. H., and Collins, K. D. (2013) Strong, low-barrier hydrogen bonds may be available to enzymes. *Biochemistry* **53**, 344–349.

Groninger-Poe, F. P., Bouvier, J. T., Vetting, M. W., Kalyanaraman, C., Kumar, R., Almo, S. C., Jacobson, M. P., and Gerlt, J. A. (2014) Evolution of enzymatic activities in the enolase superfamily: galactarate dehydratase III from *Agrobacterium tumefaciens* C58. *Biochemistry* **53**, 4192–4203.

Gu, J., and Yu, H. (2012) The role of residue S139 of mandelate racemase: synergistic effect of S139 and E317 on transition state stabilization. *J. Biomol. Struct. Dyn.* **30**, 585–593.

Guan, R., Ho, M. C., Brenowitz, M., Tyler, P. C., Evans, G. B., Almo, S. C., and Schramm, V. L. (2011) Entropy-driven binding of picomolar transition state analogue inhibitors to human 5'-methylthioadenosine phosphorylase. *Biochemistry* **50**, 10408–10417.

Guengerich, F. P. (1979) Artifacts in isoelectric focusing of the microsomal enzymes cytochrome P-450 and NADPH-cytochrome P-450 reductase. *Biochim. Biophys. Acta*. **577**, 132–141.

Guillén Schlippe, Y. V., and Hedstrom, L. (2005) A twisted base? The role of arginine in enzyme-catalyzed proton abstractions. *Arch. Biochem. Biophys*. **433**, 266–278.

Gulick, A. M., Hubbard, B. K., Gerlt, J. A., and Rayment, I. (2000) Evolution of enzymatic activities in the enolase superfamily: crystallographic and mutagenesis studies of the reaction catalyzed by D-glucarate dehydratase from *Escherichia coli*. *Biochemistry* **39**, 4590–4602.

Gunsalus, C. F., Stanier, R. Y., and Gunsalus, I. C. (1953a) The enzymatic conversion of mandelic acid to benzoic acid. III. Fractionation and properties of the soluble enzymes. *J. Bacteriol*. **66**, 548–553.

Gunsalus, I. C., Gunsalus, C. F., and Stanier, R. Y. (1953b) The enzymatic conversion of mandelic acid to benzoic acid. I. Gross fractionation of the system into soluble and particulate components. *J. Bacteriol*. **66**, 538–542.

Guthrie, J. P. (1996) Short strong hydrogen bonds: can they explain enzymic catalysis? *Chem. Biol*. **3**, 163–170.

Guthrie, J. P., and Kluger, R. (1993) Electrostatic stabilization can explain the unexpected acidity of carbon acids in enzyme-catalyzed reactions. *J. Am. Chem. Soc*. **115**, 11569–11572.

Hansch, C., and Leo, A. (1979) *Substituent Constants for Correlation Analysis in Chemistry and Biology*, John Wiley &Sons, New York.

Hansen, R. E., Ostergaard, H., Norgaard, P., and Winther, J. R. (2007) Quantification of protein thiols and dithiols in the picomolar range using sodium borohydride and 4,4'-dithiodipyridine. *Anal. Biochem*. **363**, 77–82.

Hardy, L. W., and Kirsch, J. F. (1984) Diffusion-limited component of reactions catalyzed by *Bacillus cereus* β-lactamase I. *Biochemistry* **23**, 1275–1282.

Harty, M., Nagar, M., Atkinson, L., Legay, C. M., Derksen, D. J., and Bearne, S. L. (2014) Inhibition of serine and proline racemases by substrate-product analogues. *Bioorg. Med. Chem. Lett*. **24**, 390–393.

Hasson, M. S., Schlichting, I., Moulai, J., Taylor, K., Barrett, W., Kenyon, G. L., Babbitt, P. C., Gerlt, J. A., Petsko, G. A., and Ringe, D. (1998) Evolution of an enzyme active site: the structure of a new crystal form of muconate lactonizing enzyme compared with mandelate racemase and enolase. *Proc. Natl. Acad. Sci. USA* **95**, 10396–10401.

Hedrick, J. L., and Sallach, H. J. (1961) The metabolism of hydroxypyruvate: I. The non-enzymatic decarboxylation and autooxidation of hydroxypyruvate. *J. Biol. Chem.* **236**, 1867–1871.

Hegeman, G. D. (1966a) Synthesis of the enzymes of the mandelate pathway by *Pseudomonas putida*. I. Synthesis of enzymes by the wild type. *J. Bacteriol.* **91**, 1140–1154.

Hegeman, G. D. (1966b) Synthesis of the enzymes of the mandelate pathway by *Pseudomonas putida*. III. Isolation and properties of constitutive mutants. *J. Bacteriol.* **91**, 1161–1167.

Hegeman, G. D. (1970) Mandelate racemase (*Pseudomonas putida*), in *Methods Enzymol.* (Herbert Tabor, C. W. T., Ed.)Vol. Volume 17, Part A, pp 670–674, Academic Press.

Hegeman, G. D., Rosenberg, E. Y., and Kenyon, G. L. (1970) Mandelic acid racemase from *Pseudomonas putida*. Purification and properties of the enzyme. *Biochemistry* **9**, 4029–4036.

Hermann, P., and Lemke, K. (1968) Ionization constants and stability constants of the copper(II)-complexes of some amino acids and their sulfur-containing analogs. *Hoppe-Seylers Z. Physiol. Chem.* **349**, 390–394.

Highbarger, L. A., Gerlt, J. A., and Kenyon, G. L. (1996) Mechanism of the reaction catalyzed by acetoacetate decarboxylase. Importance of lysine 116 in determining the pK_a of active-site lysine 115. *Biochemistry* **35**, 41–46.

Hopkins, C. E., Hernandez, G., Lee, J. P., and Tolan, D. R. (2005) Aminoethylation in model peptides reveals conditions for maximizing thiol specificity. *Arch. Biochem. Biophys.* **443**, 1–10.

Hopkins, C. E., O'Connor, P. B., Allen, K. N., Costello, C. E., and Tolan, D. R. (2002) Chemical-modification rescue assessed by mass spectrometry demonstrates that γ -thialysine yields the same activity as lysine in aldolase. *Prot. Sci.* **11**, 1591–1599.

Houk, R. J., Monzingo, A., and Anslyn, E. V. (2008) Electrophilic coordination catalysis: a summary of previous thought and a new angle of analysis. *Acc. Chem. Res.* **41**, 401–410.

Houk, R. J. T., Anslyn, E. V., and Stanton, J. F. (2006) Carbonyl coordination chemistry from a new angle: a computational study of α-carbon acidity based on electrophile coordination geometry. *Org. Lett.* **8**, 3461–3463.

Hurley, T. J., Carrell, H. L., Gupta, R. K., Schwartz, J., and Glusker, J. P. (1979) The structure of sodium β-fluoropyruvate: a *gem*-diol. *Arch. Biochem. Biophys.* **193**, 478–486.

Inbar, L., and Lapidot, A. (1988) The structure and biosynthesis of new tetrahydropyrimidine derivatives in actinomycin D producer *Streptomyces parvulus*. Use of ^{13}C- and ^{15}N-labeled L-glutamate and ^{13}C and ^{15}N NMR spectroscopy. *J. Biol. Chem.* **263**, 16014–16022.

Ishida, T. (2006) Low-barrier hydrogen bond hypothesis in the catalytic triad residue of serine proteases: correlation between structural rearrangement and chemical shifts in the acylation process. *Biochemistry* **45**, 5413–5420.

Ishikita, H., and Saito, K. (2014) Proton transfer reactions and hydrogen-bond networks in protein environments. *J. R. Soc. Interface* **11**.

Itoh, Y., Yamanaka, M., and Mikami, K. (2003) Dipole interaction-controlled stereoselectivity in aldol reaction of α-CF_3 enolate with fluoral. *Org. Lett.* **5**, 4807–4809.

Iwahara, J., Jung, Y. S., and Clore, G. M. (2007) Heteronuclear NMR spectroscopy for lysine NH_3 groups in proteins: unique effect of water exchange on ^{15}N transverse relaxation. *J. Am. Chem. Soc.* **129**, 2971–2980.

Jencks, W. P., and Regenstein, J. (1968) Ionization constants of acids and bases, in *Handbook of Biochemistry* (Sober, H. A., Ed.), pp J150–J189, The Chemical RubberCo., Cleveland, OH.

Kadam, R. U., Garg, D., Schwartz, J., Visini, R., Sattler, M., Stocker, A., Darbre, T., and Reymond, J. L. (2013) CH-π "T-shape" interaction with histidine explains binding of aromatic galactosides to *Pseudomonas aeruginosa* lectin LecA. *ACS Chem. Biol.* **8**, 1925–1930.

Kallarakal, A. T., Mitra, B., Kozarich, J. W., Gerlt, J. A., Clifton, J. G., Petsko, G. A., and Kenyon, G. L. (1995) Mechanism of the reaction catalyzed by mandelate racemase: structure and mechanistic properties of the K166R mutant. *Biochemistry* **34**, 2788–2797.

Kalyanaraman, C., Imker, H. J., Fedorov, A. A., Fedorov, E. V., Glasner, M. E., Babbitt, P. C., Almo, S. C., Gerlt, J. A., and Jacobson, M. P. (2008) Discovery of a dipeptide epimerase enzymatic function guided by homology modeling and virtual screening. *Structure* **16**, 1668–1677.

Kati, W. M., and Wolfenden, R. (1989) Major enhancement of the affinity of an enzyme for a transition-state analog by a single hydroxyl group. *Science* **243**, 1591–1593.

Kaushik, J. K., and Bhat, R. (2003) Why is trehalose an exceptional protein stabilizer? An analysis of the thermal stability of proteins in the presence of the compatible osmolyte trehalose. *J. Biol. Chem.* **278**, 26458–26465.

Kenyon, G. L., and Hegeman, G. D. (1970) Mandelic acid racemase from *Pseudomonas putida*. Evidence favoring a carbanion intermediate in the mechanism of action. *Biochemistry* **9**, 4036–4043.

Kenyon, G. L., and Hegeman, G. D. (1979) Mandelate racemase. *Adv. Enzymol. Relat. Areas Mol. Biol.* **50**, 325–360.

Kim, D. W., Yoshimura, T., Esaki, N., Satoh, E., and Soda, K. (1994) Studies of the active-site lysyl residue of thermostable aspartate aminotransferase: combination of site-directed mutagenesis and chemical modification. *J. Biochem.* **115**, 93–97.

Kim, H. W., Rossi, P., Shoemaker, R. K., and DiMagno, S. G. (1998) Structure and transport properties of a novel, heavily fluorinated carbohydrate analogue. *J. Am. Chem. Soc.* **120**, 9082–9083.

Kitz, R., and Wilson, I. B. (1962) Esters of methanesulfonic acid as irreversible inhibitors of acetylcholinesterase. *J. Biol. Chem.* **237**, 3245–3249.

Klenchin, V. A., Taylor Ringia, E. A., Gerlt, J. A., and Rayment, I. (2003) Evolution of enzymatic activity in the enolase superfamily: structural and mutagenic studies of the mechanism of the reaction catalyzed by *o*-succinylbenzoate synthase from *Escherichia coli*. *Biochemistry* **42**, 14427–14433.

Kohyama, K., Matsumoto, T., and Imoto, T. (2010) Refolding of an unstable lysozyme by gradient removal of a solubilizer and gradient addition of a stabilizer. *J. Biochem.* **147**, 427–431.

Kovalevsky, A. Y., Katz, A. K., Carrell, H. L., Hanson, L., Mustyakimov, M., Fisher, S. Z., Coates, L., Schoenborn, B. P., Bunick, G. J., Glusker, J. P., and Langan, P. (2008) Hydrogen location in stages of an enzyme-catalyzed reaction: time-of-flight neutron structure of D-xylose isomerase with bound D-xylulose. *Biochemistry* **47**, 7595–7597.

Landro, J. A., Gerlt, J. A., Kozarich, J. W., Koo, C. W., Shah, V. J., Kenyon, G. L., Neidhart, D. J., Fujita, S., and Petsko, G. A. (1994) The role of lysine 166 in the mechanism of mandelate racemase from *Pseudomonas putida*: mechanistic and crystallographic evidence for stereospecific alkylation by (*R*)-α-phenylglycidate. *Biochemistry* **33**, 635–643.

Landro, J. A., Kallarakal, A. T., Ransom, S. C., Gerlt, J. A., Kozarich, J. W., Neidhart, D. J., and Kenyon, G. L. (1991) Mechanism of the reaction catalyzed by mandelate racemase. 3. Asymmetry in reactions catalyzed by the H297N mutant. *Biochemistry* **30**, 9274–9281.

Landro, J. A., Kenyon, G. L., and Kozarich, J. W. (1992) Mechanism-based inactivation of mandelate racemase by propargylglycolate. *Bioorg. Med. Chem. Lett.* **2**, 1411–1418.

Lane, R. H., and Hurst, J. K. (1974) Intermediates in enolase-catalyzed reactions. *Biochemistry* **13**, 3292–3297.

Lawrence, M. C., Barbosa, J. A., Smith, B. J., Hall, N. E., Pilling, P. A., Ooi, H. C., and Marcuccio, S. M. (1997) Structure and mechanism of a sub-family of enzymes related to *N*-acetylneuraminate lyase. *J. Mol. Biol.* **266**, 381–399.

Lee, D. Y., and Chang, G. D. (2009) Electrolytic reduction: modification of proteins occurring in isoelectric focusing electrophoresis and in electrolytic reactions in the presence of high salts. *Anal. Chem.* **81**, 3957–3964.

Levitt, M., and Perutz, M. F. (1988) Aromatic rings acts as hydrogen bond acceptors. *J. Mol. Biol.* **201**, 751–754.

Li, C., and Gershon, P. D. (2006) pK_a of the mRNA cap-specific 2'-*O*-methyltransferase catalytic lysine by HSQC NMR detection of a two-carbon probe. *Biochemistry* **45**, 907–917.

Li, R., Powers, V. M., Kozarich, J. W., and Kenyon, G. L. (1995) Racemization of vinylglycolate catalyzed by mandelate racemase. *J. Org. Chem.* **60**, 3347–3351.

Lienhard, G. E. (1973) Enzymatic catalysis and transition-state theory. *Science* **180**, 149–154.

Lietzan, A. D., Nagar, M., Pellmann, E. A., Bourque, J. R., Bearne, S. L., and St. Maurice, M. (2012) Structure of mandelate racemase with bound intermediate analogues benzohydroxamate and cupferron. *Biochemistry* **51**, 1160–1170.

Lin, D. T., Powers, V. M., Reynolds, L. J., Whitman, C. P., Kozarich, J. W., and Kenyon, G. L. (1988) Evidence for the generation of α-carboxy-α-hydroxy-*p*-xylylene from *p*-(bromomethyl)mandelate by mandelate racemase. *J. Am. Chem. Soc.* **110**, 323–324.

Lin, I. J., Chen, Y., Fee, J. A., Song, J., Westler, W. M., and Markley, J. L. (2006) Rieske protein from *Thermus thermophilus*: ^{15}N NMR titration study demonstrates the role of iron-ligated histidines in the pH dependence of the reduction potential. *J. Am. Chem. Soc.* **128**, 10672–10673.

Lolis, E., and Petsko, G. A. (1990) Transition-state analogues in protein crystallography: probes of the structural source of enzyme catalysis. *Annu. Rev. Biochem.* **59**, 597–630.

Lorimer, G. H., and Hartman, F. C. (1988) Evidence supporting lysine 166 of *Rhodospirillum rubrum* ribulosebisphosphate carboxylase as the essential base which initiates catalysis. *J. Biol. Chem.* **263**, 6468–6471.

Lowry, T. H., and Richardson, K. S. (1981) *Mechanism and Theory in Organic Chemistry* (2nd ed.), Harper & Row, New York.

Maggio, E. T., Kenyon, G. L., Mildvan, A. S., and Hegeman, G. D. (1975) Mandelate racemase from *Pseudomonas putida*. Magnetic resonance and kinetic studies of the mechanism of catalysis. *Biochemistry* **14**, 1131–1139.

Malpica, A., and Calzadila, M. (2005) Kinetics and mechanism of oxime formation from methyl benzoylformate. *J. Phys. Org. Chem.* **18**, 945–949.

Massiah, M. A., Viragh, C., Reddy, P. M., Kovach, I. M., Johnson, J., Rosenberry, T. L., and Mildvan, A. S. (2001) Short, strong hydrogen bonds at the active site of human acetylcholinesterase: proton NMR studies. *Biochemistry* **40**, 5682–5690.

Mattei, P., Kast, P., and Hilvert, D. (1999) *Bacillus subtilis* chorismate mutase is partially diffusion-controlled. *Eur. J. Biochem.* **261**, 25–32.

Maxwell, K. L., Bona, D., Liu, C., Arrowsmith, C. H., and Edwards, A. M. (2003) Refolding out of guanidine hydrochloride is an effective approach for high-throughput structural studies of small proteins. *Protein Sci.* **12**, 2073–2080.

McIntosh, L. P., Hand, G., Johnson, P. E., Joshi, M. D., Korner, M., Plesniak, L. A., Ziser, L., Wakarchuk, W. W., and Withers, S. G. (1996) The pK_a of the general acid/base carboxyl group of a glycosidase cycles during catalysis: a ^{13}C-NMR study of *Bacillus circulans* xylanase. *Biochemistry* **35**, 9958–9966.

Meany, J. E. (2007) Lactate dehydrogenase catalysis: roles of keto, hydrated, and enol pyruvate. *J. Chem. Edu.* **84**, 1520–1523.

Miller, B. G., and Wolfenden, R. (2002) Catalytic proficiency: the unusual case of OMP decarboxylase. *Annu. Rev. Biochem.* **71**, 847–885.

Mitchell, J. B., Nandi, C. L., McDonald, I. K., Thornton, J. M., and Price, S. L. (1994) Amino/aromatic interactions in proteins: is the evidence stacked against hydrogen bonding? *J. Mol. Biol.* **239**, 315–331.

Mitra, B., Kallarakal, A. T., Kozarich, J. W., Gerlt, J. A., Clifton, J. G., Petsko, G. A., and Kenyon, G. L. (1995) Mechanism of the reaction catalyzed by mandelate racemase: importance of electrophilic catalysis by glutamic acid 317. *Biochemistry* **34**, 2777–2787.

Murto, J. (1964) Nucleophilic reactivity of alkoxide ions toward 2,4-dinitrofluorobenzene and the acidity of alcohols. *Acta. Chem. Scand.* **18**, 1043–1053.

Myslinski, J. M., DeLorbe, J. E., Clements, J. H., and Martin, S. F. (2011) Protein-ligand interactions: thermodynamic effects associated with increasing nonpolar surface area. *J. Am. Chem. Soc.* **133**, 18518–18521.

Nadal-Ferret, M., Gelabert, R., Moreno, M., and Lluch, J. M. (2014) Are there really low-barrier hydrogen bonds in proteins? The case of photoactive yellow protein. *J. Am. Chem. Soc.* **136**, 3542–3552.

Nagano, N., Orengo, C. A., and Thornton, J. M. (2002) One fold with many functions: the evolutionary relationships between TIM barrel families based on their sequences, structures and functions. *J. Mol. Biol.* **321**, 741–765.

Nagar, M., Lietzan, A. D., St Maurice, M., and Bearne, S. L. (2014) Potent inhibition of mandelate racemase by a fluorinated substrate-product analogue with a novel binding mode. *Biochemistry* **53**, 1169–1178.

Nagar, M., Narmandakh, A., Khalak, Y., and Bearne, S. L. (2011) Redefining the minimal substrate tolerance of mandelate racemase. Racemization of trifluorolactate. *Biochemistry* **50**, 8846–8852.

Nagar, M., Wyatt, B. N., St Maurice, M., and Bearne, S. L. (2015) Inactivation of mandelate racemase by 3-hydroxypyruvate reveals a potential mechanistic link between enzyme superfamilies. *Biochemistry* **54**, 2747-2757.

Nallini, A., Saraboji, K., and Ponnuswamy, M. N. (2004) A study of aromatic hydrogen bonds of peptides with aromatic amino acid side-chains. *Indian J. Biochem. Biophys.* **41**, 184–187.

Narmandakh, A., and Bearne, S. L. (2010) Purification of recombinant mandelate racemase: improved catalytic activity. *Protein Expr. Purif.* **69**, 39–46.

Neidhardt, F. C., Bloch, P. L., and Smith, D. F. (1974) Culture medium for enterobacteria. *J. Bacteriol.* **119**, 736–747.

Neidhart, D. J., Howell, P. L., Petsko, G. A., Powers, V. M., Li, R. S., Kenyon, G. L., and Gerlt, J. A. (1991) Mechanism of the reaction catalyzed by mandelate racemase. 2. Crystal structure of mandelate racemase at 2.5-Å resolution: identification of the active site and possible catalytic residues. *Biochemistry* **30**, 9264–9273.

Neidhart, D. J., Kenyon, G. L., Gerlt, J. A., and Petsko, G. A. (1990) Mandelate racemase and muconate lactonizing enzyme are mechanistically distinct and structurally homologous. *Nature* **347**, 692–694.

Neidhart, D. J., Powers, V. M., Kenyon, G. L., Tsou, A. Y., Ransom, S. C., Gerlt, J. A., and Petsko, G. A. (1988) Preliminary x-ray data on crystals of mandelate racemase. *J. Biol. Chem.* **263**, 9268–9270.

Olsen, J. A., Banner, D. W., Seiler, P., Wagner, B., Tschopp, T., Obst-Sander, U., Kansy, M., Muller, K., and Diederich, F. (2004) Fluorine interactions at the thrombin active site: protein backbone fragments H-C(α)-C=O comprise a favorable C-F environment and interactions of C-F with electrophiles. *ChemBioChem* **5**, 666-675.

Olsson, T. S., Williams, M. A., Pitt, W. R., and Ladbury, J. E. (2008) The thermodynamics of protein-ligand interaction and solvation: insights for ligand design. *J. Mol. Biol.* **384**, 1002–1017.

Olucha, J., Meneely, K. M., and Lamb, A. L. (2012) Modification of residue 42 of the active site loop with a lysine-mimetic side chain rescues isochorismate-pyruvate lyase activity in *Pseudomonas aeruginosa* PchB. *Biochemistry* **51**, 7525–7532.

Ornston, L. N. (1971) Regulation of catabolic pathways in *Pseudomonas*. *Bacteriol. Rev.* **35**, 87–116.

Pal, M., and Bearne, S. L. (2014) Inhibition of glutamate racemase by substrate-product analogues. *Bioorg. Med. Chem. Lett.* **24**, 1432–1436.

Parisi, M. F., and Abeles, R. H. (1992) Inhibition of chymotrypsin by fluorinated α-keto acid derivatives. *Biochemistry* **31**, 9429–9435.

Parker, M. H., Lunney, E. A., Ortwine, D. F., Pavlovsky, A. G., Humblet, C., and Brouillette, C. G. (1999) Analysis of the binding of hydroxamic acid and carboxylic acid inhibitors to the stromelysin-1 (matrix metalloproteinase-3) catalytic domain by isothermal titration calorimetry. *Biochemistry* **38**, 13592–13601.

Pauling, L. (1948) Nature of forces between large molecules of biological interest. *Nature* **161**, 707–709.

Paulini, R., Muller, K., and Diederich, F. (2005) Orthogonal multipolar interactions in structural chemistry and biology. *Angew. Chem. Int. Ed. Engl.* **44**, 1788–1805.

Pennacchio, A., Pucci, B., Secundo, F., La Cara, F., Rossi, M., and Raia, C. A. (2008) Purification and characterization of a novel recombinant highly enantioselective short-chain NAD(H)-dependent alcohol dehydrogenase from *Thermus thermophilus*. *Appl. Environ. Microbiol.* **74**, 3949–3958.

Philippossian, G., Welti, D. H., Fumeaux, R., Richli, U., and Anantharaman, K. (1989) Synthesis and NMR characterization of (^{15}N)taurine [2-(^{15}N)aminoethanesulfonic acid]. *J. Label. Compd. Radiopharm.* **27**, 1267–1273.

Phillips, M. A., Kaplan, A. P., Rutter, W. J., and Bartlett, P. A. (1992) Transition-state characterization: a new approach combining inhibitor analogues and variation in enzyme structure. *Biochemistry* **31**, 959–963.

Platzer, G., Okon, M., and McIntosh, L. P. (2014) pH-dependent random coil ^{1}H, ^{13}C, and ^{15}N chemical shifts of the ionizable amino acids: a guide for protein pK_a measurements. *J. Biomol. NMR* **60**, 109–129.

Plevin, M. J., Bryce, D. L., and Boisbouvier, J. (2010) Direct detection of CH/π interactions in proteins. *Nat. Chem.* **2**, 466–471.

Pocker, Y., and Janjic, N. (1987) Enzyme kinetics in solvents of increased viscosity. Dynamic aspects of carbonic anhydrase catalysis. *Biochemistry* **26**, 2597-2606.

Pocker, Y., and Meany, J. E. (1970) The reversible hydration of pyruvic acid. II. Metal ion and enzyme catalysis. *J. Phys. Chem.* **74**, 1486–1492.

Poon, D. K., Schubert, M., Au, J., Okon, M., Withers, S. G., and McIntosh, L. P. (2006) Unambiguous determination of the ionization state of a glycoside hydrolase active site lysine by ^{1}H–^{15}N heteronuclear correlation spectroscopy. *J. Am. Chem. Soc.* **128**, 15388–15389.

Powers, V. M., Koo, C. W., Kenyon, G. L., Gerlt, J. A., and Kozarich, J. W. (1991) Mechanism of the reaction catalyzed by mandelate racemase. 1. Chemical and kinetic evidence for a two-base mechanism. *Biochemistry* **30**, 9255–9263.

Radzicka, A., and Wolfenden, R. (1995a) A proficient enzyme. *Science* **267**, 90–93.

Radzicka, A., and Wolfenden, R. (1995b) Transition state and multisubstrate analog inhibitors. *Methods Enzymol.* **249**, 284–312.

Raftery, M. A., and Cole, R. D. (1966) On the aminoethylation of proteins. *J. Biol. Chem.* **241**, 3457–3461.

Rakus, J. F., Fedorov, A. A., Fedorov, E. V., Glasner, M. E., Hubbard, B. K., Delli, J. D., Babbitt, P. C., Almo, S. C., and Gerlt, J. A. (2008) Evolution of enzymatic activities in the enolase superfamily: L-rhamnonate dehydratase. *Biochemistry* **47**, 9944–9954.

Ransom, S. C., Gerlt, J. A., Powers, V. M., and Kenyon, G. L. (1988) Cloning, DNA sequence analysis, and expression in *Escherichia coli* of the gene for mandelate racemase from *Pseudomonas putida*. *Biochemistry* **27**, 540–545.

Reiner, A. M. (1971) Metabolism of benzoic acid by bacteria: 3,5-cyclohexadiene-1,2-diol-1-carboxylic acid is an intermediate in the formation of catechol. *J. Bacteriol.* **108**, 89–94.

Reiner, A. M., and Hegeman, G. D. (1971) Metabolism of benzoic acid by bacteria. Accumulation of (-)-3,5-cyclohexadiene-1,2-diol-1-carboxylic acid by mutant strain of *Alcaligenes eutrophus*. *Biochemistry* **10**, 2530–2536.

Renaud, P., and Fox, M. A. (1988) An electrochemical characterization of dianions: dilithiated carboxylic acids. *J. Am. Chem. Soc.* **110**, 5705–5709.

Richard, J. P., and Amyes, T. L. (2001) Proton transfer at carbon. *Curr. Opin. Struct. Biol.* **5**, 626–633.

Riener, C. K., Kada, G., and Gruber, H. J. (2002) Quick measurement of protein sulfhydryls with Ellman's reagent and with 4,4'-dithiodipyridine. *Anal. Bioanal. Chem.* **373**, 266–276.

Rose, I. A. (1966) Mechanisms of enzyme action. *Annu. Rev. Biochem.* **35**, 23–56.

Sakai, H. (2005) Mutagenesis of the active site lysine 221 of the pyruvate kinase from *Bacillus stearothermophilus*. *J. Biochem.* **137**, 141–145.

Sambrook, J., Fritsch, E. F., and Maniatis, T. (1989) *Molecular Cloning: A Laboratory Manual*, Cold Spring Harbor Laboratory Press, Plainview, NY.

Schaefer, T., Wildman, T. A., Sebastain, R., and McKinnon, D. M. (1984) The phenyl group as a hydrogen bond acceptor in 2-phenylphenol derivatives. Substituent comparisons. *Can. J. Chem.* **62**, 2692–2696.

Schafer, S. L., Barrett, W. C., Kallarakal, A. T., Mitra, B., Kozarich, J. W., Gerlt, J. A., Clifton, J. G., Petsko, G. A., and Kenyon, G. L. (1996) Mechanism of the reaction catalyzed by mandelate racemase: structure and mechanistic properties of the D270N mutant. *Biochemistry* **35**, 5662–5669.

Scheiner, S., and Kar, T. (1995) The nonexistence of specially stabilized hydrogen bonds in enzymes. *J. Am. Chem. Soc.* **117**, 6970–6975.

Schmidt, D. M., Mundorff, E. C., Dojka, M., Bermudez, E., Ness, J. E., Govindarajan, S., Babbitt, P. C., Minshull, J., and Gerlt, J. A. (2003) Evolutionary potential of $(\beta/\alpha)_8$-barrels: functional promiscuity produced by single substitutions in the enolase superfamily. *Biochemistry* **42**, 8387–8393.

Schneider, C. A., Rasband, W. S., and Eliceiri, K. W. (2012) NIH Image to ImageJ: 25 years of image analysis. *Nat. Meth.* **9**, 671–675.

Schneider, C. P., Shukla, D., and Trout, B. L. (2011) Arginine and the Hofmeister Series: the role of ion-ion interactions in protein aggregation suppression. *J. Phys. Chem. B* **115**, 7447–7458.

Schramm, V. L. (1998) Enzymatic transition states and transition state analog design. *Annu. Rev. Biochem.* **67**, 693–720.

Schramm, V. L. (2005) Enzymatic transition states and transition state analogues. *Curr. Opin. Struct. Biol.* **15**, 604–613.

Schramm, V. L. (2007) Enzymatic transition state theory and transition state analogue design. *J. Biol. Chem.* **282**, 28297–28300.

Schutz, C. N., and Warshel, A. (2004) The low barrier hydrogen bond (LBHB) proposal revisited: the case of the Asp – His pair in serine proteases. *Proteins: Struct., Funct., Bioinf.* **55**, 711–723.

Schwartz, S. D., and Schramm, V. L. (2009) Enzymatic transition states and dynamic motion in barrier crossing. *Nat. Chem. Biol.* **5**, 551–558.

Schwartz, W. E., Smith, P. K., and Royer, G. P. (1980) N-(β-Iodoethyl)trifluoroacetamide: a new reagent for the aminoethylation of thio groups in proteins. *Anal. Biochem.* **106**, 43–48.

Scrutton, N. S., and Raine, A. R. C. (1996) Cation-π bonding and amino-aromatic interactions in the biomolecular recognition of substituted ammonium ligands. *Biochem. J.* **319**, 1–8.

Seebach, D., Beck, A. K., and Renaud, P. (1986) Di- and trifluoro-substituted dilithium compounds for organic syntheses. *Angew. Chem. Int. Ed. Engl.* **25**, 98–99.

Segel, I. H. (1975) *Enzyme Kinetics*, John Wiley & Sons, Inc., New York.

Sharma, S., Bhaumik, P., Schmitz, W., Venkatesan, R., Hiltunen, J. K., Conzelmann, E., Juffer, A. H., and Wierenga, R. K. (2012) The enolization chemistry of a thioester-dependent racemase: the 1.4 Å crystal structure of a reaction intermediate complex characterized by detailed QM/MM calculations. *J. Phys. Chem. B* **116**, 3619–3629.

Sharp, T. R., Hegeman, G. D., and Kenyon, G. L. (1977) Mandelate racemase from *Pseudomonas putida*. Absence of detectable intermolecular proton transfer accompanying racemization. *Biochemistry* **16**, 1123–1128.

Sharp, T. R., Hegeman, G. D., and Kenyon, G. L. (1979) A direct kinetic assay for mandelate racemase using circular dichroic measurements. *Anal. Biochem.* **94**, 329–334.

Shukla, D., and Trout, B. L. (2011) Understanding the synergistic effect of arginine and glutamic acid mixtures on protein solubility. *J. Phys. Chem. B* **115**, 11831–11839.

Siddiqi, F., Bourque, J. R., Jiang, H., Gardner, M., St. Maurice, M., Blouin, C., and Bearne, S. L. (2005) Perturbing the hydrophobic pocket of mandelate racemase to probe phenyl motion during catalysis. *Biochemistry* **44**, 9013–9021.

Simopoulos, T. T., and Jencks, W. P. (1994) Alkaline phosphatase is an almost perfect enzyme. *Biochemistry* **33**, 10375–10380.

Smith, H. B., and Hartman, F. C. (1988) Restoration of activity to catalytically deficient mutants of ribulosebisphosphate carboxylase/oxygenase by aminoethylation. *J. Biol. Chem.* **263**, 4921–4925.

Snider, M. J., and Wolfenden, R. (2001) Site-bound water and the shortcomings of a less than perfect transition state analogue. *Biochemistry* **40**, 11364–11371.

Song, J., Laskowski, M., Jr., Qasim, M. A., and Markley, J. L. (2003) NMR determination of pK_a values for Asp, Glu, His, and Lys mutants at each variable contiguous enzyme-inhibitor contact position of the turkey ovomucoid third domain. *Biochemistry* **42**, 2847–2856.

Spring, T. G., and Wold, F. (1971) Two high-affinity enolase inhibitors. Reaction with enolases. *Biochemistry* **10**, 4655–4660.

St. Maurice, M. (2003) *The role of binding determinants in ground state and transition state stabilization by mandelate racemase*. (PhD Thesis), Dalhousie University, Halifax, Nova Scotia.

St. Maurice, M., and Bearne, S. L. (2000) Reaction intermediate analogues for mandelate racemase: interaction between Asn 197 and the α-hydroxyl of the substrate promotes catalysis. *Biochemistry* **39**, 13324–13335.

St. Maurice, M., and Bearne, S. L. (2002) Kinetics and thermodynamics of mandelate racemase catalysis. *Biochemistry* **41**, 4048–4058.

St. Maurice, M., and Bearne, S. L. (2004) Hydrophobic nature of the active site of mandelate racemase. *Biochemistry* **43**, 2524–2532.

Stanier, R. Y., Gunsalus, I. C., and Gunsalus, C. F. (1953) The enzymatic conversion of mandelic acid to benzoic acid. II. Properties of the particulate fractions. *J. Bacteriol.* **66**, 543–547.

Stecher, H., Hermetter, A., and Faber, K. (1998) Mandelate racemase assayed by polarimetry. *Biotechnol. Tech.* **12**, 257–261.

Stivers, J. T., Abeygunawardana, C., Mildvan, A. S., Hajipour, G., and Whitman, C. P. (1996) 4-Oxalocrotonate tautomerase: pH dependence of catalysis and pK_a values of active site residues. *Biochemistry* **35**, 814–823.

Stockbridge, R. B., and Wolfenden, R. (2009) The intrinsic reactivity of ATP and the catalytic proficiencies of kinases acting on glucose, *N*-acetylgalactosamine, and homoserine: a thermodynamic analysis. *J. Biol. Chem.* **284**, 22747–22757.

Stubbe, J., and Abeles, R. H. (1980) Mechanism of action of enolase: effect of the β-hydroxy group on the rate of dissociation of the α-carbon-hydrogen bond. *Biochemistry* **19**, 5505–5512.

Sweet, W. L., and Blanchard, J. S. (1990) Fumarase: viscosity dependence of the kinetic parameters. *Arch. Biochem. Biophys.* **277**, 196–202.

Talhout, R., Villa, A., Mark, A. E., and Engberts, J. B. (2003) Understanding binding affinity: a combined isothermal titration calorimetry/molecular dynamics study of the binding of a series of hydrophobically modified benzamidinium chloride inhibitors to trypsin. *J. Am. Chem. Soc.* **125**, 10570–10579.

Tanner, M. E. (2002) Understanding nature's strategies for enzyme-catalyzed racemization and epimerization. *Acc. Chem. Res.* **35**, 237–246.

Tellinghuisen, J. (2005) Optimizing experimental parameters in isothermal titration calorimetry. *J. Phys. Chem. B* **109**, 20027–20035.

Tellinghuisen, J. (2008) Isothermal titration calorimetry at very low *c*. *Anal. Biochem.* **373**, 395–397.

Thibblin, A., and Jencks, W. P. (1979) Unstable carbanions. General acid catalysis of the cleavage of 1-phenylcyclopropanol and 1-phenyl-2-arylcyclopropanol anions. *J. Am. Chem. Soc.* **101**, 4963–4973.

Timms, N., Windle, C. L., Polyakova, A., Ault, J. R., Trinh, C. H., Pearson, A. R., Nelson, A., and Berry, A. (2013) Structural insights into the recovery of aldolase activity in *N*-acetylneuraminic acid lyase by replacement of the catalytically active lysine with γ-thialysine by using a chemical mutagenesis strategy. *ChemBioChem* **14**, 474–481.

True, J. E., Thomas, T. D., Winter, R. W., and Gard, G. L. (2003) Electronegativities from core-ionization energies: electronegativities of SF_5 and CF_3. *Inorg. Chem.* **42**, 4437–4441.

Tsou, A. Y., Ransom, S. C., Gerlt, J. A., Buechter, D. D., Babbitt, P. C., and Kenyon, G. L. (1990) Mandelate pathway of *Pseudomonas putida*: sequence relationships involving mandelate racemase, (*S*)-mandelate dehydrogenase, and benzoylformate decarboxylase and expression of benzoylformate decarboxylase in *Escherichia coli*. *Biochemistry* **29**, 9856–9862.

Tsou, A. Y., Ransom, S. C., Gerlt, J. A., Powers, V. M., and Kenyon, G. L. (1989) Selection and characterization of a mutant of the cloned gene for mandelate racemase that confers resistance to an affinity label by greatly enhanced production of enzyme. *Biochemistry* **28**, 969–975.

Tsuzuki, S., Honda, K., Uchimaru, T., Mikami, M., and Fujii, A. (2006) Magnitude and directionality of the interaction energy of the aliphatic CH/π interaction: significant difference from hydrogen bond. *J. Phys. Chem. A* **110**, 10163–10168.

Tsuzuki, S., Honda, K., Uchimaru, T., Mikami, M., and Tanabe, K. (2000) Origin of the attraction and directionality of the NH/π interaction: comparison with OH/π and CH/π interactions. *J. Am. Chem. Soc.* **122**, 11450–11458.

Turnbull, W. B., and Daranas, A. H. (2003) On the value of *c*: can low affinity systems be studied by isothermal titration calorimetry? . *J. Am. Chem. Soc.* **125**, 14859–14866.

Uneyama, K., Katagiri, T., and Amii, H. (2008) α-Trifluoromethylated carbanion synthons. *Acc. Chem. Res.* **41**, 817–829.

Urbanskya, E. T., and Bashe, W. J. (2000) Comparative methodology in the determination of α-oxocarboxylates in aqueous solution. Ion chromatography versus gas chromatography after oximation, extraction and esterification. *J. Chromatogr. A* **867**, 143–149.

Vagenende, V., Yap, M. G., and Trout, B. L. (2009) Mechanisms of protein stabilization and prevention of protein aggregation by glycerol. *Biochemistry* **48**, 11084–11096.

Vick, J. E., and Gerlt, J. A. (2007) Evolutionary potential of $(\beta/\alpha)_8$-barrels: stepwise evolution of a "new" reaction in the enolase superfamily. *Biochemistry* **46**, 14589–14597.

Warshel, A. (1998) Electrostatic origin of the catalytic power of enzymes and the role of preorganized active sites. *J. Biol. Chem.* **273**, 27035–27038.

Warshel, A., Papazyan, A., and Kollman, P. A. (1995) On low-barrier hydrogen bonds and enzyme catalysis. *Science* **269**, 102–106.

Wedekind, J. E., Poyner, R. R., Reed, G. H., and Rayment, I. (1994) Chelation of serine 39 to Mg^{2+} latches a gate at the active site of enolase: structure of the bis(Mg^{2+}) complex of yeast enolase and the intermediate analog phosphonoacetohydroxamate at 2.1-Å resolution. *Biochemistry* **33**, 9333–9342.

Weil-Malherbe, H. (1966) Some properties of mandelate racemase from *Pseudomonas fluorescens*. *Biochem. J.* **101**, 169–175.

Wheelis, M. L., and Stanier, R. Y. (1970) The genetic control of dissimilatory pathways in *Pseudomonas putida*. *Genetics* **66**, 245–266.

Whitman, C. P., Hegeman, G. D., Cleland, W. W., and Kenyon, G. L. (1985) Symmetry and asymmetry in mandelate racemase catalysis. *Biochemistry* **24**, 3936–3942.

Whitmore, L., and Wallace, B. A. (2004) DICHROWEB: an online server for protein secondary structure analyses from circular dichroism spectroscopic data. *Nucleic Acids Res.* **32**, W668–673.

Whitmore, L., and Wallace, B. A. (2008) Protein secondary structure analyses from circular dichroism spectroscopy: methods and reference databases. *Biopolymers* **89**, 392–400.

Wichelecki, D. J., Balthazor, B. M., Chau, A. C., Vetting, M. W., Fedorov, A. A., Fedorov, E. V., Lukk, T., Patskovsky, Y. V., Stead, M. B., Hillerich, B. S., Seidel, R. D., Almo, S. C., and Gerlt, J. A. (2014) Discovery of function in the enolase superfamily: D-mannonate and D-gluconate dehydratases in the D-mannonate dehydratase subgroup. *Biochemistry* **53**, 2722–2731.

Wiseman, T., Williston, S., Brandts, J. F., and Lin, L.-N. (1989) Rapid measurement of binding constants and heats of binding using a new titration calorimeter. *Anal. Biochem.* **179**, 131–137.

Wolfenden, R. (1969) Transition state analogues for enzyme catalysis. *Nature* **223**, 704–705.

Wolfenden, R. (1972) Analog approaches to the structure of the transition state in enzyme reactions. *Acc. Chem. Res.* **5**, 10–18.

Wolfenden, R. (1976) Transition state analog inhibitors and enzyme catalysis. *Ann. Rev. Biophys. Bioeng.* **5**, 271–306.

Wystrach, V. P., Kaiser, D. W., and Schaefer, F. C. (1955) Preparation of ethylenimine and triethylenemelamine. *J. Am. Chem. Soc.* **77**, 5915–5918.

Yamaguchi, H., and Miyazaki, M. (2014) Refolding techniques for recovering biologically active recombinant proteins from inclusion bodies. *Biomolecules* **4**, 235–251.

Yamazaki, T., Taguchi, T., and Ojima, I. (2009) Unique properties of fluorine and their relevance to medicinal chemistry and chemical biology, in *Fluorine in Medicinal Chemistry and Chemical Biology* (Ojima, I., Ed.), pp 3–49, Wiley-Blackwell Publishing Ltd., Chichester, UK.

Yew, W. S., Fedorov, A. A., Fedorov, E. V., Almo, S. C., and Gerlt, J. A. (2007) Evolution of enzymatic activities in the enolase superfamily: L-talarate/galactarate dehydratase from *Salmonella typhimurium* LT2. *Biochemistry* **46**, 9564–9577.

Yew, W. S., Fedorov, A. A., Fedorov, E. V., Wood, B. M., Almo, S. C., and Gerlt, J. A. (2006) Evolution of enzymatic activities in the enolase superfamily: D-tartrate dehydratase from *Bradyrhizobium japonicum*. *Biochemistry* **45**, 14598–14608.

Yoshimura, T., Matsushima, Y., Tanizawa, K., Sung, M. H., Yamauchi, T., Wakayama, M., Esaki, N., and Soda, K. (1990) Substitution of S-(β-aminoethyl)-cysteine for active-site lysine of thermostable aspartate aminotransferase. *J. Biochem.* **108**, 699–700.

Zaccai, N. R., Maenaka, K., Maenaka, T., Crocker, P. R., Brossmer, R., Kelm, S., and Jones, E. Y. (2003) Structure-guided design of sialic acid-based siglec inhibitors and crystallographic analysis in complex with sialoadhesin. *Structure* **11**, 557–567.

Zacharias, N., and Dougherty, D. A. (2002) Cation-π interactions in ligand recognition and catalysis. *Trends Pharmacol. Sci.* **23**, 281–287.

Zhang, E., Hatada, M., Brewer, J. M., and Lebioda, L. (1994) Catalytic metal ion binding in enolase: the crystal structure of an enolase-Mn^{2+}-phosphonoacetohydroxamate complex at 2.4-Å resolution. *Biochemistry* **33**, 6295-6300.

Zhang, M., and Vogel, H. J. (1993) Determination of the side chain pK_a values of the lysine residues in calmodulin. *J. Biol. Chem.* **268**, 22420–22428.

Zhang, X., Kumar, R., Vetting, M. W., Zhao, S., Jacobson, M. P., Almo, S. C., and Gerlt, J. A. (2015) A unique *cis*-3-hydroxy-L-proline dehydratase in the enolase superfamily. *J. Am. Chem. Soc.* **137**, 1388–1391.

Zhang, Y.-L., and Zhang, Z.-Y. (1998) Low-affinity binding determined by titration calorimetry using a high-affinity coupling ligand: a thermodynamic study of ligand binding to protein tyrosine phosphatase 1B. *Anal. Biochem.* **261**, 139–148.

Zhao, S., Kumar, R., Sakai, A., Vetting, M. W., Wood, B. M., Brown, S., Bonanno, J. B., Hillerich, B. S., Seidel, R. D., Babbitt, P. C., Almo, S. C., Sweedler, J. V., Gerlt, J. A., Cronan, J. E., and Jacobson, M. P. (2013) Discovery of new enzymes and metabolic pathways by using structure and genome context. *Nature* **502**, 698–702.

Zhu, K., Zhao, J., Lubman, D. M., Miller, F. R., and Barder, T. J. (2005) Protein pI shifts due to posttranslational modifications in the separation and characterization of proteins. *Anal. Chem.* **77**, 2745–2755.

Zhu, L., Kemple, M. D., Yuan, P., and Prendergast, F. G. (1995) N-terminus and lysine side chain pK_a values of melittin in aqueous solutions and micellar dispersions measured by ^{15}N NMR. *Biochemistry* **34**, 13196–13202.

APPENDIX
Copyright permission letters

American Chemical Society's Policy on Theses and Dissertations

If your university requires you to obtain permission, you must use the RightsLink permission system.
See RightsLink instructions at
http://pubs.acs.org/page/copyright/permissions.html.

This is regarding request for permission to include **your** paper(s) or portions of text from **your** paper(s) in your thesis. Permission is now automatically granted; please pay special attention to the **implications** paragraph below. The Copyright Subcommittee of the Joint Board/Council Committees on Publications approved the following:

> Copyright permission for published and submitted material from theses and dissertations
> ACS extends blanket permission to students to include in their theses and dissertations their own articles, or portions thereof, that have been published in ACS journals or submitted to ACS journals for publication, provided that the ACS copyright credit line is noted on the appropriate page(s).
>
> Publishing **implications** of electronic publication of theses and dissertation material
> Students and their mentors should be aware that posting of theses and dissertation material on the Web prior to submission of material from that thesis or dissertation to an ACS journal may affect publication in that journal. Whether Web posting is considered prior publication may be evaluated on a case-by-case basis by the journal's editor. If an ACS journal editor considers Web posting to be "prior publication", the paper will not be accepted for publication in that journal. If you intend to submit your unpublished paper to ACS for publication, check with the appropriate editor prior to posting your manuscript electronically.

Reuse/Republication of the Entire Work in Theses or Collections: Authors may reuse all or part of the Submitted, Accepted or Published Work in a thesis or dissertation that the author writes and is required to submit to satisfy the criteria of degree-granting institutions. Such reuse is permitted subject to the ACS' "Ethical Guidelines to Publication of Chemical Research" (http://pubs.acs.org/page/policy/ethics/index.html); the author should secure written confirmation (via letter or email) from the respective ACS journal editor(s) to avoid potential conflicts with journal prior publication*/embargo policies. Appropriate citation of the Published Work must be made. If the thesis or dissertation to be

published is in electronic format, a direct link to the Published Work must also be included using the ACS Articles on Request author-directed link – see http://pubs.acs.org/page/policy/articlesonrequest/index.html

* Prior publication policies of ACS journals are posted on the ACS website at http://pubs.acs.org/page/policy/prior/index.html

If your paper has **not** yet been published by ACS, please print the following credit line on the first page of your article: "Reproduced (or 'Reproduced in part') with permission from [JOURNAL NAME], in press (or 'submitted for publication'). Unpublished work copyright [CURRENT YEAR] American Chemical Society." Include appropriate information.

If your paper has already been published by ACS and you want to include the text or portions of the text in your thesis/dissertation, please print the ACS copyright credit line on the first page of your article: "Reproduced (or 'Reproduced in part') with permission from [FULL REFERENCE CITATION.] Copyright [YEAR] American Chemical Society." Include appropriate information.

Submission to a Dissertation Distributor: If you plan to submit your thesis to UMI or to another dissertation distributor, you should not include the unpublished ACS paper in your thesis if the thesis will be disseminated electronically, until ACS has published your paper. After publication of the paper by ACS, you may release the entire thesis (**not the individual ACS article by itself**) for electronic dissemination through the distributor; ACS's copyright credit line should be printed on the first page of the ACS paper.